Digital Wave Corporation
13760 East Arapahoe Road
Centennial, CO 80112

Use of Modal Acoustic Emission (MAE) for life extension of civilian self-contained breathing apparatus (SCBA) DOT-CFFC cylinders

FINAL REPORT

Prepared for
Mark Toughiry
Office of Hazardous Materials Safety
Engineering and Research Division
Department of Transportation

Contract DTPH56-13-P-000029

Contents

Executive Summary

From the entirety of the physical testing contained within this research program, several important observations about the structural integrity of 100 randomly selected DOT-CFFC SCBA pressure cylinders owned and operated by civilian fire departments across the USA, which were past their allotted fifteen year service life were made. All 100 DOT-CFFC SCBA pressure cylinders were operated under DOT-SP 10915 or DOT-SP 10945, were of 30, 45, or 60 minute air volumes, and all had a service pressure of 4500 psi. No reduction in burst strength for cylinders at the end of their fifteen year service life or at the end of their fifteen year service life with an additional twenty years of simulated service was observed. Of the eighty-one DOT-CFFC cylinders that were burst test, seventy-eight of the cylinders met or exceeded the minimum required burst pressure of the DOT CFFC 5th Revision. Two of the three cylinders which did not meet the minimum required burst pressure were intentionally notched, while the third cylinder was as received. Furthermore, it was found that the stiffness of the carbon fiber composite overwrap was not compromised by fifteen years of service life, or fatigue cycling the cylinders to the maximum developed pressure during fast fill for an additional twenty years of service life.

The impact resistance, notch tolerance, and corrosion resistance of the DOT-CFFC design was evaluated, in which it was found that the DOT-CFFC design had no problem meeting and surpassing the requirements of the ISO 11119.2 testing requirements, or potential thirty-year life cylinders operated under newer DOT special permits (e.g., DOT-SP 13583 and DOT-SP 14232). No quantifiable effect on cylinder volume was observed in the physical testing conducted.

While the performance testing described in the preceding paragraphs is extremely important relative to proving that the composite material's properties are not being degraded from in service use or additional simulated life, it is not adequate to ensure the continued safe operation of DOT-CFFC SCBA pressure cylinders. The key component to this work was the use of Modal Acoustic Emission, and the ability to identify the various damage mechanisms that were occurring within the composite microstructure. Through the ability to identify and classify the various damage mechanisms that occur within composite materials, all three cylinders which burst below the minimum required burst pressure were identified and rejected by Modal Acoustic Emission, a claim that no other NDE technique could make. To emphasize this point, the percentage of the time that MAE properly identified the health of a DOT-CFFC cylinder (i.e., was the burst strength greater than or equal to the minimum required burst pressure) was compared to the currently used visual inspection and rejectable elastic expansion criteria. It was found that MAE properly identified 98.2% of all tested cylinders, while visual inspection and rejectable elastic expansion only properly identified cylinders 86.4% of the time. MAE properly identified all three DOT-CFFC cylinders which burst below the minimum required burst pressure, with the one improperly identified cylinder by means of MAE examination coming on a cylinder with artificial damage (i.e., notches) that burst within 700 psi of the minimum required burst pressure.

Moreover, through the use of Modal Acoustic Emission it was found that background energy oscillations occurred between 50 and 70% of the burst strength of the cylinder, with an average value of 60.7% and a standard deviation of 5.7%. Due to the consistent and repeatable nature of the onset of the background energy oscillations a confidence interval can be calculated for the burst pressure of a given cylinder, and cylinders which are identified as having too large of a probability of having an inadequate burst strength may be rejected. The ability of Modal Acoustic Emission to quantify the "effect of a defect" in the DOT-CFFC composite pressure cylinders (effectively facilitating a strength prediction) is a significant step forward in the nondestructive evaluation of composite pressure cylinders.

Through the testing and analysis performed in this research program, the ability to safely extend the life of civilian DOT-CFFC SCBA pressure cylinders appears to be possible through the use of Modal Acoustic Emission at the five year re-qualification intervals. The ability of Modal Acoustic Emission to properly identify cylinders with compromised burst strength enables degraded cylinders to be removed from service, while allowing cylinders which still meet the at manufacture requirements to continue in service. The granting of life extension to existing civilian DOT-CFFC SCBA pressure cylinders (which showed no degradation in material performance) would reduce budgetary burdens on civilian fire departments, as well as be beneficial to the environment by not tossing tens (potentially hundreds) of thousands of perfectly good cylinders into landfills.

List of Figures

1.0 Introduction

1.1 Objective

The purpose of this study was to evaluate the potential for extending the life of civilian DOT-CFFC carbon fiber composite overwrapped pressure cylinders that are at or near their allotted fifteen (15) year service life.

1.2 Background

In 1997 the Department of Transportation (DOT) issued the "DOT-CFFC Basic Requirements (first revision)" [1] which specified the design, construction, inspection, qualification, and usable service life of carbon fiber composite overwrapped pressure cylinders. All cylinders which were manufactured to the DOT-CFFC specifications by companies who were granted DOT exemptions (or special permits, e.g., DOT-SP 10915 and DOT-SP 10945) were limited to a service life of fifteen years. Originally, there was the potential for the manufacturing companies to attempt to extend the service life to thirty (30) years, however, no company (manufacturer or NDE) that attempted to gain life extension was granted this exemption by the Associate Administrator of the Pipeline and Hazardous Material Safety Administration (PHMSA).

More recently beginning around 2006, a few manufacturers of SCBA DOT-CFFC cylinders have designed and tested cylinders to ISO 11119.2 specifications which provides for a considerably longer service life than fifteen years [2]. Examples of such cylinders are manufactured and operated under DOT-SP 13583, and DOT-SP 14232; these cylinders again have the potential for thirty years of service life, provided that the cylinders physical characteristics meet the requirements set forth in the respective special permit. To date no cylinders have been granted a life extension, as no cylinder is old enough to have been subjected to the physical testing requirements that would grant the life extension.

In 2012 a research program executed by the Digital Wave Corporation which was funded by the United States Navy investigated the potential for developing a nondestructive testing procedure that would be capable of extending the life on DOT-CFFC and DOT-FRP1 cylinders [3]. In the research program 84 DOT-CFFC and FRP-1 cylinders that were at or approaching their fifteen year service life were subjected to the physical testing outlined in ISO 11119.2 [2]. In that work, all cylinders that were not intentionally damaged were found to meet or exceed the burst strength requirements of virgin cylinders. Further, it was shown through the use of Modal Acoustic Emission (MAE) that cylinders which were intentionally damaged and had compromised burst strengths could be unequivocally identified. In the research program, Digital Wave Corporation showed that they were able to predict the burst pressure of cylinders (within 10% of the actual value); such a predictive capability enables Digital Wave Corporation to identify cylinders which have compromised strength at the requalification test pressure, and eliminate the compromised cylinder from service. Finally, through residual stress measurement of the glass fiber composite overwrap and Classical Laminated Plate Theory (CLPT) calculations, it was shown that stress rupture of DOT-FRP1 cylinders was not an issue at the stress state within the fiber at the service pressure of DOT-FRP1 cylinders. This research program resulted in Digital Wave Corporation being awarded DOT-SP 15720, allowing for the life extension of Navy SCBA pressure cylinders manufactured under DOT-SP 7277, DOT-SP 10915, and DOT-SP 10945.

1.3 Technical Approach

The structural integrity of 100 randomly selected civilian owned and operated DOT-CFFC pressure cylinders which were past their allowed fifteen (15) year service life was evaluated through physical testing which is outlined in ISO 11119.2 [2]. Digital Wave Corporation gratefully acknowledges the donations of all of the civilian fire departments who donated cylinders to the research program. Table 1.1 provides the name of the contributing department, the Fire Chief of the department, and the number of cylinders donated. Physical testing included burst testing (ISO 11119.2, Section 8.5.4), cyclic hydrostatic pressurization to the maximum developed pressure during fast filling (ISO 11119.2, Section 8.5.5), notch tolerance (ISO 111119.2, Section 8.5.7), impact resistance (ISO 11119.2, Section 8.5.8), extreme impact resistance (DOT/DWC developed impact simulation), and corrosion resistance (ISO 11515, Section 8.5.17 [4]).

Table 1.1 Summary of fire departments, fire chiefs, and number of SCBA cylinders donated.

Location	Fire Chief	Number of Vessels Donated
FDNY	Battalion Chief William Mundy	100
Fairfax, VA	Fire Chief Dave Rohr	44
Coeur d'Alene, ID	Fire Chief Kenneth Gabriel	1
Caney, OK	Fire Chief Michael Harkey	3
SC	Fire Chief Shane Ray	1
Howard, PA	Fire Chief Doug Corman	36
Kennebunkport, ME	Fire Chief Allan Moir	12
Prince Georges County FD	Fire Chief Marc Bashoor	5
Beaufort, SC	Fire Chief Sammy Negron	1
Houston, TX	Fire Chief Terry Garrison	9
South Berwick, ME	Fire Chief George Gorman	19
Tucson, AZ	Fire Chief Michael B Fischback	3
Marina, CA	Fire Chief Harald Kelley	4
Sonora, CA	Fire Chief Mike Burrows	2
Cherry Hills, NJ	Fire Chief Patrick Kelly	20
Riverside, CA	Fire Chief Michael Esparza	28
Spirit Lake, ID	Fire Chief John DeBernardi	1
Oneonta Fire Department	Fire Chief Patrick Pidgeon	3
Aiken County Fire Dpartment	Fire Chief Fred Wilhite	6
Scott Fire Protection District	Fire Chief Ron Myers	1

Prior to and during physical testing of all SCBA cylinders, nondestructive evaluation techniques were utilized to evaluate the integrity of the cylinder. Prior to any physical testing, external and internal visual inspection of the cylinder was performed in accordance with CGA 6.2 [5]. During burst and cyclic fatigue testing, strain gages and pressure transducers were utilized to monitor the mechanical response of the cylinder. Finally, broadband MAE transducers were used to detect the stress waves which propagate due to local strain energy releases as the composite overwrap accumulates damage. The efficacy of MAE in evaluating the health of an SCBA cylinder was demonstrated in [3], thus a very similar approach was utilized in this work.

2.0 Definitions and Nomenclature

σ_{HOOP}: the hoop stress

σ_{AXIAL}: the axial stress

ε_{HOOP}: the hoop strain

ε_{AXIAL}: the axial strain

BEO: Background Energy Oscillation

BEOP: Background Energy Oscillation Pressure

M_R: the multiplicative factor of the background energy level rise above the quiescent level which indicates that a large amount of localized damage is occurring within the composite material

M_O: the multiplicative factor between neighboring maxima and minima of the calculated N point moving average from all background energy values that suggests that the composite pressure cylinder is progressing towards failure

R: cyclic fatigue stress ratio, equal to the minimum stress on a cycle divided by the maximum stress on a cycle.

3.0 Modal Acoustic Emission (MAE)

Modal acoustic emission (MAE) is a branch of Acoustic Emission (AE) that utilizes the capture of the high fidelity stress waves which propagate through a structure as strain energy releases occur due to highly localized damage mechanisms occurring. It has been shown through the use of four accept/reject criteria derived from MAE metrics that composite overwrapped pressure cylinders which have diminished strength may be identified [6-8]. The four criteria used in this report to evaluate the integrity of the SCBA cylinders are defined and explained in sections 3.4 - 3.7. All four criteria were evaluated during the end-of-life (EOL) burst test procedure (during the cycles up to and holding at test pressure, refer to Section 5.1 for details), while Background Energy Oscillation (BEO) was also evaluated on the burst ramp to develop a predictive capability on the burst pressure of the cylinder. The pressurization schedule described in ASME Section X [6] was used to evaluate the cylinders prior to the burst test, and is described in greater detail in Section 5.1.

3.1 Modal Acoustic Emission Instrumentation and Hardware

A key component to the Modal Acoustic Emission testing technique is the instrumentation used for high fidelity waveform transduction and recording. These two requirements were met using Digital Wave Corporations in-house MAE equipment. All equipment used in this study for MAE waveform recording and analysis met the requirements of ASME Section X and NB10-0601 [6, 7]. The hardware, software, and data acquisition system settings used during testing were as follows:

Hardware
Sensors: Digital Wave Corporation B1025
Preamplifiers: Digital Wave Corporation PA0
Signal Conditioning Unit: Digital Wave Corporation FM-1

Software
Data Acquisition and Analysis: Digital Wave Corporation WaveExplorer™

Data Acquisition System Trigger Settings
A/D Rate: 2 MHz
Total Trigger Gain: 48 dB
Total Waveform Gain: 42 dB
Bandpass trigger filter: 50-750 kHz
Point per waveform: 4096
Pre-trigger points: 1024

An important aspect of detecting modal acoustic emissions is properly acoustically coupling the broadband transducer to the surface in which the stress waves are propagating. To this end, sensors were coupled to the outer surface of the SCBA pressure cylinders using medium viscosity vacuum grease with a small amount of normal force, provided by rubber inner-tubes, used to insure consistency of acoustic coupling (Figure 3.1).

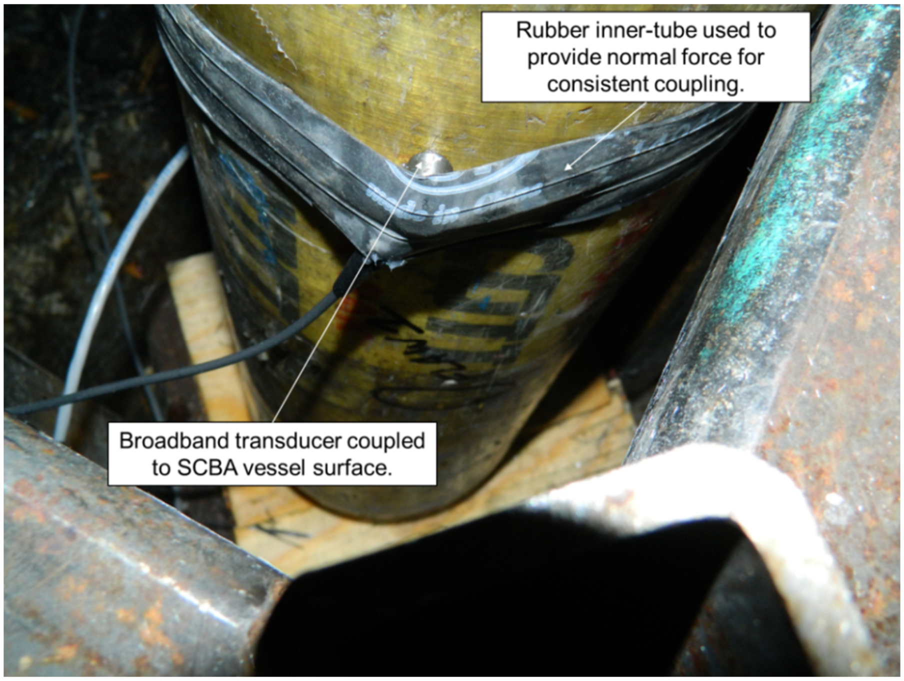

Figure 3.1 – Broadband MAE transducer acoustically coupled to an SCBA pressure cylinder.

3.2 Modal Acoustic Emission Spectral Analysis

Due to the large number of events that may be captured during MAE testing, a few metrics were used to identify the natural clustering in the frequency domain of source mechanisms. Specifically, the weighted peak frequency (WPF), and concept of partial power (PP) was used to identify natural clustering of the various damage mechanisms which occur within composite materials as they are subjected to a stress state. The weighted peak frequency is calculated by

$$WPF = \sqrt{\frac{f_{max} \cdot \int f \cdot \widehat{U}(f) df}{\int \widehat{U}(f) df}}, \quad (1)$$

while the partial power of the spectrum was defined as

$$PP = \frac{\int_{400\,kHz}^{800\,kHz} \widehat{U}(f) df}{\int_{0\,kHz}^{800\,kHz} \widehat{U}(f) df}. \quad (2)$$

In equations (1) and (2), $\widehat{U}(f)$ is the fast Fourier transform (FFT) of a given waveform $U(t)$, f is the frequency vector associated with the FFT of a waveform, and f_{MAX} is the frequency at which the maximum amplitude of the FFT was observed. The weighted peak frequency may be thought of as a scaled centroidal frequency, while the partial power of a spectrum describes how much high frequency content (> 400 kHz) was present in a given signal. Through these two metrics the natural clustering of MAE waveforms which are related to the various types of damage mechanisms can be observed in the frequency domain.

3.3 Sensor Calibrations

Two primary sensor calibrations are required in [6-8], which were also used in this study. First, to insure that a given transducer has an appropriate level of sensitivity to sense the out-of-plane surface motions that are generated by the propagating stress waves, an absolute calibration of the sensor is required. The absolute calibration of the B1025 transducers was accomplished using a heterodyne Michelson interferometer, following the approach of Wagner [9]. An example of the magnitude response of a B1025 (S/N R1384) is shown in Figure 3.2, from which it is clear that the response of the sensor is flat (within ± 6 dB) over a broad frequency range. The flatness of a sensor is a key component in the ability to identify the propagating plate wave modes, and thus perform MAE analyses.

The second calibration which is required in [6-8], is referred to as a Rolling Ball Impact (RBI) calibration [17]. The essence of the RBI calibration is to determine the conversion factor from mechanical energy to transduced electrical energy for a given sensor-system configuration. In the calibration a hardened steel ball rolls down an inclined plane and impacts the mid-plane of a 7075-T6 Aluminum plate having large lateral dimensions with the transducer under test mounted to the plate. The impact of the ball generates the fundamental extensional and flexural plate modes, as shown in Figure 3.3. The recorded energy of the first cycle of the transduced extensional mode is then compared to the known mechanical energy of the rolling ball [6], and a conversion factor for a given transducer is determined.

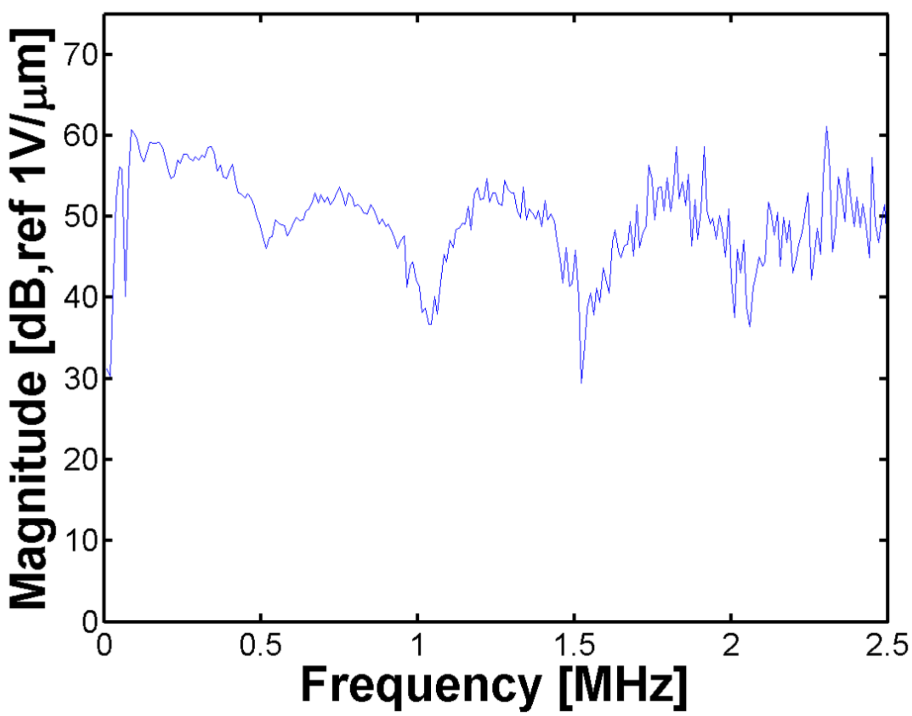

Figure 3.2 – Absolute magnitude response of a B1025 sensor (S/N: R1384)

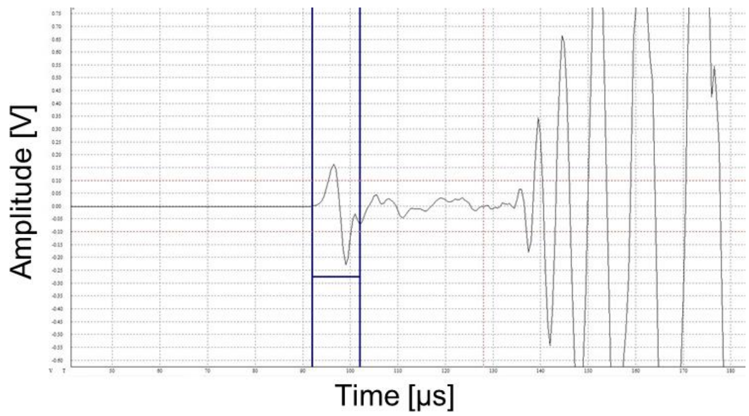

Figure 3.3 – Example of the waveform captured from a rolling ball impact calibration.

3.4 Stability

During the two holds at the test pressure of the cylinder, both the number of events and the cumulative energy from the events are partitioned into equally spaced bins for the entire hold time. Both metrics must be found to be exponentially decaying, with the requirements for the exponential decay rate parameter (B) and the goodness of fit (R^2) summarized in Table 3.1.

Table 3.1 – Summary of the requirements for stability curve fitting parameters.

Metric	Exponential Decay Parameter (B) Requirements	R^2 Requirement
Events	$-0.1 < B < -0.0001$	$R^2 \geq 0.80$
Energy	$-0.2 < B < -0.0001$	$R^2 \geq 0.80$

Typically, stability is a metric that is more applicable to cylinders that have just been manufactured, and is less applicable to cylinders that have experienced several cycles to operating and test pressure. Due to several cycles to operating and test pressure during the in-service life of the current SCBA cylinders, minimal new matrix cracking is taking place resulting in very few events occurring during the holds at test pressure; such observations are in good agreement with the Kaiser Effect. If not enough events occur during the holds at test pressure the composite is deemed to be stable due to a lack of emission, and is considered to meet the stability criteria.

3.5 Background Energy

The background energy is defined as the minimum value of energy of a windowed contiguous portion of a given waveform.

A rise in the background energy level above the quiescent level greater than a factor of M_R indicates that a large amount of localized damage is occurring.

An oscillation in an N point moving average of the background energy values on a given channel greater than a factor of M_O between the adjacent maximum background energy level to the minimum background energy level indicates that the composite pressure cylinder has begun progressing towards failure, and that the internal pressure within the cylinder should be reduced immediately. It has been shown in [3], and will be shown in this report, that an oscillation of the background energy of greater than two occurs on average at 60% of the burst strength of the SCBA pressure cylinder. Hence, by using the background energy oscillation metric, cylinders with burst strengths below a minimum value may be identified and removed from service.

Thus, any rise in the background energy level greater than M_R, or any oscillation in the background energy greater than M_O at or below the test pressure of a DOT-CFFC cylinder shall fail the cylinder under test.

3.6 Fiber bundle Fracture Energy

Fiber bundle fracture energy during the second pressurization cycle to test pressure shall be less than 2.7×10^{-16} J for carbon fiber composite cylinders. The burst strength of composite overwrapped pressure cylinders is known to be a fiber dominated property, thus by setting a criteria of only allowing ~6,000 filaments to fracture on a single event, a conservative restriction has been put in place to extend the life of a cylinder. Note that the energy conversion for wave transduction by the specific sensor must be accounted for using the Rolling Ball Impact calibration described in National Board Inspection Code NB10-0601 Supplement S9 [7]. An example calculation of the mechanical energy released from a single fiber fracture is provided in [7]. Further, NB10-0601 and DOT-SP 15720 provide the energy ratios in particular frequency bands used to determine if a fiber fracture has occurred.

3.7 Single MAE Event Energy

The energy of any single MAE event on the second test pressurization cycle shall be less than 2.7×10^{-14} J. Extremely large energy events are indicative that a significant stress concentrator exists in the structure that could compromise the cylinders structural integrity. See Section 3.6 regarding energy scaling for a given transducer and the necessity for the Rolling Ball Impact calibration.

4.0 Visual Inspections

All 100 cylinders that were used in this study were subjected to an external and internal visual inspection per CGA 6.2. Observations from the external and internal visual inspections are summarized in Table 4.1. From Table 4.1, it was observed that 83.0% of the cylinders that were subjected to the external visual inspection were found to have damage on the external portion of the DOT-CFFC cylinder no greater than level 2, as specified by [5]; at such a level, cylinders are eligible for re-working (if identified as having level 2 damage) and re-qualification. Further, as CGA 6.2 does not define acceptable limits on internal corrosion, or flaws in the aluminum liner, the applicable type of flaw was noted but not used to fail a cylinder. It is pointed out that 62.0% of the cylinders inspected in this study exhibited some form of pitting/corrosion of the aluminum liner. A vast majority of the cylinders which exhibited pitting and/or corrosion were also found to have visible water stains of the aluminum liner; this indicates that water had sat in cylinder for an extended period of time, most probably during the five year requalifications.

Table 4.1 – Summary of all visual inspections performed prior to physical testing.

Test	Location	DOT-SP	Time	Designation	SN	Mfg Date	Pressure	Internal Visual Inspection	External Visual Inspection	Visually Condemned [Y/N]
EOL Burst	FDNY	10945	60	ALT 604	3742	05/98	4500	Minor pitting on cylinder, good threads	L1 abrasions throughout, L2 cut/burn damage on cylinder near BD, L2 impact on BD	N
EOL Burst	FDNY	10945	45	ALT 695	4436	07/98	4500	Pitting throughout, good threads	L2 impacts on cylinder, L2 abrasions on PD, L3 impacts/chips on PD	Y
EOL Burst	FDNY	10945	60	ALT 604	4962	08/98	4500	Good liner, threads	L1/2 abrasions on BD, L2 impacts/abrasions on cylinder, L2 cut on PD	N
EOL Burst	FDNY	10945	45	ALT 695	3650	06/98	4500	Pitting throughout, good threads	L2 impacts/cuts and abrasions on BD, L3 impact/cut on BD near shoulder, L2 impacts/cuts throughout cylinder, L2 cuts on PD	Y
EOL Burst	FDNY	10945	45	ALT 695	4494	07/98	4500	Pitting throughout, good threads	L2 cut on PD, L2 cut on cylinder, L1 abrasions throughout, cosmetic matrix cracking on cylinder parallel to fibers, L2 cuts on cylinder, L2 impacts/cuts on BD	N
EOL Burst	Fairfax, VA	10915	45	OM	3915	08/98	4500	Good liner, threads	RW and L2 cuts on PD, L1 abrasions on BD	N
EOL Burst	Fairfax, VA	10915	45	OM	3990	08/98	4500	Pits on BD, good threads	RW and L2 impact on PD, L2 impact on cylinder, RW on BD (x2)	N
EOL Burst	Fairfax, VA	10915	45	OM	3934	08/98	4500	Good liner, threads	RW and visible delam on PD, RW on cylinder, L2 abrasions throughout	N
EOL Burst	Fairfax, VA	10915	45	OM	3941	08/98	4500	Good liner, threads	RW and L2 impact w/delam on PD, L2 abrasions on cylinder, RW on BD (x2), L1 abrasions throughout	N
EOL Burst	Fairfax, VA	10915	45	OM	3962	08/98	4500	Good liner, threads	RW and L2 impact with delam on PD, L2 impact on BD, L2 abrasions throughout	N
EOL Burst	Howard, PA	10945	30	ALT 639	14969	12/98	4500	Black/gray residue throughout	L2 cuts on PD, RW on BD	N
EOL Burst	Howard, PA	10945	30	ALT 639	17663	12/98	4500	Pitting throughout	L2 cuts on cylinder wall near PD, L2 cut on cylinder wall (1/2 way down), L2 cut on cylinder wall near BD	N
EOL Burst	Howard, PA	10945	30	ALT 639	18023	12/98	4500	Good liner, threads	L2 cut (x3) on cylinder near label, L2 on BD	N
EOL Burst	Howard, PA	10945	30	ALT 639	69216	10/00	4500	Good liner, threads	L2 on PD, and cylinder wall	N
EOL Burst	Howard, PA	10945	30	ALT 639	18629	01/99	4500	Pitting throughout	Large L2 abrasion on PD, L2 cut on BD	N
EOL Burst	South Berwick, ME	10915	30	IH	1740	06/98	4500	Pitting on BD and cylinder	L1 abrasions on cylinder	N
EOL Burst	South Berwick, ME	10915	30	IH	1855	06/98	4500	Good liner, threads	L2 cut on PD and cylinder (1/4 way down), L2 cut on cylinder near bottom	N
EOL Burst	South Berwick, ME	10915	30	IH	1763	06/98	4500	Slight pitting on BD	L2 cut on cylinder (2/3 down), L2 scratches on cyl near BD	N
EOL Burst	South Berwick, ME	10915	30	IH	1135	06/98	4500	Good liner, threads	L2 cut (x2) on BD	N
EOL Burst	South Berwick, ME	10915	30	IH	1929	06/98	4500	Good liner, threads	L2 on BD (x2)	N
EOL Burst	Kennebunkport, ME/Houston, TX	10945	60	ALT 604	6739	12/98	4500	Minor pitting throughout, good threads	L2 chips on PD, L2 chip on cylinder, L2 cut on cylinder, L2 chips on BD	N
EOL Burst	Kennebunkport, ME/Houston, TX	10945	30	ALT 639	17688	12/98	4500	Pitting on cylinder wall	L2 cut and L1 impact on BD	N
EOL Burst	Kennebunkport, ME/Houston, TX	10945	30	ALT 639	18862	01/99	4500	Minor pitting throughout, good threads	L2 cuts on BD	N
EOL Burst	Kennebunkport, ME/Houston, TX	10945	30	ALT 639	18507	01/99	4500	Good liner, threads	L2 abrasion on PD, L2 cut on BD	N
EOL Burst	Kennebunkport, ME/Houston, TX	10945	30	ALT 639	18793	01/99	4500	Good liner, threads	L2 cuts on cylinder wall	N
10k and Burst	FDNY	SCI	45	ALT 695	1700	03/98	4500	Pitting throughout, good threads	L3 impact/cut on cylinder, L2 abrasions throughout	Y
10k and Burst	FDNY	SCI	45	ALT695	6058	09/98	4500	Pitting throughout with brown discoloration, good threads	L2 cuts and L2 burn damage on BD, L2 cuts on cylinder, cosmetic matrix cracking of sacrificial layer, L2 cut and impact on PD	N
10k and Burst	FDNY	SCI	45	ALT695	5353	09/98	4500	Minor pitting throughout, good threads	L2 impacts/cuts on BD, L3 impact/cut on shoulder of BD, L2 impacts/cuts throughout cylinder, odd raised section on PD, L2 cut on cylinder near re-test sticker	Y
10k and Burst	FDNY	SCI	45	ALT695	4745	07/98	4500	Pitting throughout, good threads	L1 abrasions on PD, L2 cut and L2 abrasion on cylinder, L1 and L2 cuts and abrasions on BD	N
10k and Burst	FDNY	SCI	45	ALT695	1668	03/98	4500	Heavy pitting on throughout, brown discoloration, good threads	L2 cuts, abrasions, and impact on BD, L2 impacts and cuts on cylinder throughout, L3 cut on label, L2 cuts and abrasions on PD	Y
10k and Burst	Fairfax, VA	Luxfer	45	OM	3947	08/98	4500	Good liner, threads	L1 impact and abrasions on PD, L1 abrasions on cylinder and BD, L2 impact/chip on BD	N
10k and Burst	Fairfax, VA	Luxfer	45	OM	3950	08/98	4500	Good liner, threads	RW on PD, L2 impact/cut on BD, L2 impact on PD, L2 abrasion on cylinder	N
10k and Burst	Fairfax, VA	Luxfer	45	OM	3921	08/98	4500	Good liner, threads	L2 impact/cut on PD, resin crack RW on cylinder, L1 abrasions and L2 cut/delamination on BD	N
10k and Burst	Fairfax, VA	Luxfer	45	OM	3928	08/98	4500	Good liner, threads	L2 cuts on PD, RW on PD/cylinder, L1 abrasions on BD	N
10k and Burst	Fairfax, VA	Luxfer	45	OM	3913	08/98	4500	Good liner, threads	L2 impact/chip on BD and PD, L1 abrasions throughout	N
10k and Burst	South Berwick, ME	Luxfer	30	IH	1271	06/98	4500	Slight pitting on BD	L2 on cylinder	N
10k and Burst	South Berwick, ME	Luxfer	30	IH	2483	07/98	4500	Slight pitting on BD	L2 scribe on cylinder (red scribe marks)	N
10k and Burst	South Berwick, ME	Luxfer	30	IH	1748	06/98	4500	Slight pitting on BD	L1 cuts on PD, L2 cut on BD/cyl, L1 abrasions of BD	N
10k and Burst	South Berwick, ME	Luxfer	30	IH	1820	06/98	4500	Minor scuffing on threads, slight pitting on BD	L1 abrasion of BD and cylinder near BD	N
10k and Burst	South Berwick, ME	Luxfer	30	IH	1027	06/98	4500	Good liner, threads	L2 on PD, L2 xuts (x3) on BD	N
10k and Burst	Kennebunkport, ME	SCI	30	ALT639	18974	01/99	4500	Good liner, threads	L1 impact on BD	N
10k and Burst	Kennebunkport, ME	SCI	30	ALT639	18799	01/99	4500	Discoloration near BD	L1 abrasion on PD and cylinder, L2 cuts on BD	N
10k and Burst	Kennebunkport, ME	SCI	30	ALT639	18790	01/99	4500	Good liner, threads	Good	N
10k and Burst	Houston, TX	SCI	60	ALT695	1653	03/98	4500	Minor pitting on BD, good threads	L2 chips on PD. RW on cylinder, L2 chips on cylinder, L2 chips on BD	N
10k and Burst	Houston, TX	SCI	60	ALT604	4342	07/98	4500	Good liner, threads	L2 cuts on PD, L2 cuts on cylinder, L2 cuts and abrasions on BD	N
10k and Burst	Howard, PA	SCI	30	ALT639	39764	11/99	4500	Good liner, threads	L2 cuts (x2) on PD, RW on BD, L2 on BD	N
10k and Burst	Howard, PA	SCI	30	ALT639	18435	01/99	4500	Good liner, threads	L2 cut on PD, L2 cut on cylinder wall, L2 cut on BD	N
10k and Burst	Howard, PA	SCI	30	ALT639	39694	11/99	4500	Pitting throughout	L2 abrasion (x3) on PD, L2 cuts on bottom of cylinder wall	N
10k and Burst	Howard, PA	SCI	30	ALT639	18683	01/99	4500	Good liner, threads	L2 cut on cylinder near label	N
10k and Burst	Howard, PA	SCI	30	ALT639	18020	01/99	4500	Pitting on cylinder wall	L2 cuts (x2) on BD	N

Test	Location	DOT-SP	Time	Designation	SN	Mfg Date	Pressure	Internal Visual Inspection	External Visual Inspection	Visually Condemned [Y/N]
ISO Drop and Burst	FDNY	SCI	60	ALT 604	3567	05/98	4500	Good liner, threads	L2 abrasions throughout, L3 cut on BD	Y
ISO Drop and Burst	Fairfax, VA	Luxfer	45	OM	3983	08/98	4500	Significant pitting throughout, good threads	L2 impact and L2 cut on PD, RW on BD, L1 abrasions throughout	N
ISO Drop and Burst	South Berwick, ME	Luxfer	30	IH	2482	07/98	4500	Flaws/pits on BD, sidewall staining	L2 cuts on cylinder and BD	N
ISO Drop and Burst	Houston, TX	SCI	60	ALT604	4371	07/98	4500	Corrosion patches throughout	L2 cuts on PD, L2 abrasions on cylinder, L2 chips on BD	N
ISO Drop and Burst	Howard, PA	SCI	30	ALT639	18722	01/99	4500	Good liner, threads	L2 cut on PD, L1 impact on BD	N
ISO Drop, 10k cycle and burst	FDNY	SCI	60	ALT 604	6021	10/98	4500	Pitting throughout, good threads	L2 abrasions/wear throughout, L3 abrasions on bottom (wear), L3 cut on label, L2 cut on label, L3 cut on PD	Y
ISO Drop, 10k cycle and burst	Fairfax, VA	Luxfer	45	OM	3938	08/98	4500	Good liner, threads	L2 cuts on PD and BD, L2 impact on BD	N
ISO Drop, 10k cycle and burst	South Berwick, ME	Luxfer	30	IH	2036	06/98	4500	Pitting on BD	L3 on PD, L2 on cylinder wall	N
ISO Drop, 10k cycle and burst	Houston, TX	SCI	60	ALT604	5582	11/98	4500	Good liner, threads	L2 chip on PD, L2 abrasion on PD, L2 cut on wall, L2 chips/cuts on BD	N
ISO Drop, 10k cycle and burst	Howard, PA	SCI	30	ALT639	40157	12/99	4500	Minor pitting throughout, good threads	L1 scratches throughout	N
DOT Drop and Burst	FDNY	SCI	45	ALT 695	3794	06/98	4500	Pitting throughout, good threads	L2 cuts on PD, L1 abrasions on cylinder, L2 impact and L1 abrasions on BD	N
DOT Drop and Burst	Fairfax, VA	Luxfer	45	OM	3948	08/98	4500	Minor pitting ~2/3 down cylinder, good threads	L2 cuts on PD, L1 abrasions throughout	N
DOT Drop and Burst	Houston, TX	Luxfer	60	OP	11769	03/99	4500	Good liner, threads	L1 impact on PD, L2 cut on cylinder, L2 cuts on BD	N
DOT Drop and Burst	South Berwick, ME	Luxfer	30	IH	2533	07/98	4500	Slight pitting on BD	L2 cut on cyl/PD, L2 cut on cylinder	N
DOT Drop and Burst	Howard, PA	SCI	30	ALT639	18699	01/99	4500	Pitting on cylinder wall	L2 abrasions on cylinder wall, L2 cuts on BD	N
DOT Drop, 10k cycle and burst	FDNY	SCI	45	ALT 695	4638	07/98	4500	Pitting throughout, good threads	L1 abrasions on PD, L2 cut w/delam on cylinder, L2 abrasions/cuts/impacts on BD	N
DOT Drop, 10k cycle and burst	Fairfax, VA	Luxfer	45	OM	3975	08/98	4500	Minor pitting, good threads	L2 impact on PD (x2), L1 abrasions throughout, RW and L2 abrasions on BD	N
DOT Drop, 10k cycle and burst	Kennebunkport, ME	SCI	30	ALT639	17697	12/98	4500	Minor pitting on cylinder wall	L2 cuts on BD	N
DOT Drop, 10k cycle and burst	South Berwick, ME	Luxfer	30	IH	1854	06/98	4500	Good liner, threads	Possible burn marks on neck of threads, L2 cuts on PD, L2 on cylinder (2/3 down), L2 on BD	N
DOT Drop, 10k cycle and burst	Howard, PA	Luxfer	30	ALT639	18601	01/99	4500	Good liner, threads	L1 scratches on PD	N
EOL Burst w/ ISO Notch	FDNY	SCI	45	ALT695	3929	06/98	4500	Pitting throughout, good threads	Numerous L2 impacts/cuts on BD (w/delam), L3 impact/cut on shoulder near BD, L2 impacts/cuts and abrasions throughout cylinder, L3 impact/cut on cylinder left of label, L2 impacts and cuts on PD	Y
EOL Burst w/ ISO Notch	Fairfax, VA	Luxfer	45	OM	3984	08/98	4500	Minor pitting on BD, good threads	L1 abrasions on PD, L2 abrasion on cylinder, L2 abrasion and impact on BD	Y
EOL Burst w/ ISO Notch	Kennebunkport, ME	SCI	30	ALT639	17732	12/98	4500	Good liner, threads	L2 cuts on cylinder wall	Y
EOL Burst w/ ISO Notch	South Berwick, ME	Luxfer	30	IH	2554	07/98	4500	Pitting on BD	Possible burn marks on neck of threads, L2 cuts on BD and PD	Y
EOL Burst w/ ISO Notch	Howard, PA	SCI	30	ALT639	69925	11/00	4500	Pitting throughout	L2 abrasion on PD, L2 abrasion on BD	Y
ISO Notch cyclic fatigue, and Burst	FDNY	SCI	45	ALT695	4304	07/98	4500	Minor pitting throughout, good threads	L2 impacts/cuts on BD, L2 cuts and abrasions throughout cylinder, L2 cuts on PD	Y
ISO Notch cyclic fatigue, and Burst	Fairfax, VA	Luxfer	45	OM	3971	08/98	4500	Good liner, threads	L2 cuts on PD, L2 impact on cylinder, L1 abrasion and impact on BD	Y
ISO Notch cyclic fatigue, and Burst	Houston, TX	Luxfer	60	OP	11129	03/99	4500	Minor pitting on cylinder wall	L2 cuts on PD, L2 chip on cylinder, L2 chip on BD	Y
ISO Notch cyclic fatigue, and Burst	South Berwick, ME	Luxfer	30	IH	1251	06/98	4500	Slight pitting on BD	L1 abrasions on BD	Y
ISO Notch cyclic fatigue, and Burst	Howard, PA	SCI	30	ALT639	17827	12/98	4500	Pitting throughout	L2 cut on cylinder wall	Y
Sulfuric Acid Hold and Burst	FDNY	SCI	45	ALT695	4333	07/98	4500	Black debris and water marks, good threads	L2 impacts/cuts on BD, L2 impacts/cuts on cylinder, L1 abrasions on cylinder, L1/2 cuts on PD	N
Sulfuric Acid Hold and Burst	Fairfax, VA	Luxfer	45	OM	3918	08/98	4500	Good liner, threads	RW on PD, L2 cut on PD, L1 abrasions throughout	N
Sulfuric Acid Hold and Burst	Kennebunkport, ME	SCI	30	ALT639	18800	01/99	4500	Good liner, threads	L2 cut on PD, L2 cut on BD	N
Sulfuric Acid Hold and Burst	South Berwick, ME	Luxfer	30	IH	1750	06/98	4500	Pitting on BD	L2 scribe on cylinder (red scribe marks), L2 on BD	N
Sulfuric Acid Hold and Burst	Howard, PA	SCI	30	ALT639	18713	01/99	4500	Good liner, threads	Good	N
Corroded liner, 10k and Burst	Fairfax, VA	Luxfer	45	OM	3985	08/98	4500	Pitting throughout, good threads	L2 impacts/chips throughout	N
Corroded liner, 10k and Burst	Fairfax, VA	Luxfer	45	OM	3960	08/98	4500	Pitting throughout, good threads	RW on BD and PD, L2 impact/chip on BD, L1 abrasions and impacts on PD	N
Corroded liner, 10k and Burst	Fairfax, VA	Luxfer	45	OM	3956	08/98	4500	Pitting throughout, good threads	L1 abrasions throughout, L2 cut w/delam on PD, L2 impact on BD, L1 abrasions throughout	N
Corroded liner, 10k and Burst	Fairfax, VA	Luxfer	45	OM	3994	08/98	4500	Minor pitting near BD, good threads	L1 abrasions on PD, RW on cylinder and BD, Short L2 cuts on BD	N
Corroded liner, 10k and Burst	Fairfax, VA	Luxfer	45	OM	4045	09/98	4500	Pitting on BD, good threads	L2 abrasions on cylinder, L2 cut on cylinder, L2 impact/cut on BD	N
Corroded liner, 10k and Burst	Fairfax, VA	Luxfer	45	OM	3969	08/98	4500	Pitting 1/2 way down cylinder and on BD, good threads	L1 abrasions on BD and PD, L2 cut on cylinder, L2 impact on PD, L1 abrasions throughout	N
Corroded liner, 10k and Burst	Fairfax, VA	Luxfer	45	OM	3973	08/98	4500	Minor pitting ~1/2 way down cylinder, good threads	RW on PD, L1 abrasions throughout, L2 impact on BD	N
Corroded liner, AF, 10k and Burst	Fairfax, VA	Luxfer	45	OM	3903	08/98	4500	Pitting 1/2 way down cylinder, good threads	L1 abrasions, L2 cut on cylinder	N
Corroded liner, AF, 10k and Burst	Fairfax, VA	Luxfer	45	OM	3982	08/98	4500	Minor pitting near BD, good threads	L1 abrasions on PD, L1 abrasions on BD, L2 impact/chips on BD	N
Corroded liner, AF, 10k and Burst	Fairfax, VA	Luxfer	45	OM	3917	08/98	4500	Pitting, good threads	RW and L2 impacts on PD, L2 impact w/delam on cylinder, L1 abrasions on BD	N
Corroded liner, AF, 10k and Burst	Fairfax, VA	Luxfer	45	OM	3957	08/98	4500	Minor pitting, good threads	L1 abrasions on both domes, L1 impact on PD	N
Corroded liner, AF, 10k and Burst	Fairfax, VA	Luxfer	45	OM	3914	08/98	4500	Pitting ~1/2 way down cylinder, good threads	L1 abrasions and RW on BD, L2 abrasions on cylinder near PD	N
Corroded liner, AF, 10k and Burst	Fairfax, VA	Luxfer	45	OM	3912	08/98	4500	Minor pitting on cylinder, good threads	L1 abrasions on BD, L2 impact on PD	N
Corroded liner, AF, 10k and Burst	Fairfax, VA	Luxfer	45	OM	3954	08/98	4500	Pitting throughout, good threads	RW and L2 impact on PD, L2 impacts on BD	N
Corroded liner, AF, 10k and Burst	Fairfax, VA	Luxfer	45	OM	3925	08/98	4500	Pitting near BD, good threads	L2 (possible L3) chips/cuts on PD, significant RW on BD, Impact on cylinder near PD	N

5.0 Physical Test Methods

5.1 End-of-life (EOL) burst test

Fifteen cylinders operated under DOT-SP 10945, and ten cylinders operated under DOT-SP 10915 were randomly sampled from five of the locales that donated civilian SCBA cylinders to the research program, and subjected to an End of Life (EOL) Burst test (Table 4.1). All pressurizations were performed at a rate of 2500 psi/min, such that a quasi-static stress state was experienced by the pressure cylinders. Prior to the ramp-up to ultimate burst, cylinders were subjected to a pressurization schedule that exposed the cylinders to two excursions to the hydrostatic test pressure of the cylinder, mimicking the test procedure in ASME Section X and the Digital Wave Corporation's DOT-SP 15720 [6, 8]. The entire EOL burst pressure schedule is shown in Figure 5.1. During the two pressurization cycles up to the hydrostatic test pressure, MAE waveforms were continually monitored and the accept/reject criteria of Sections 3.4 – 3.7 were evaluated to determine whether or not the cylinder would have been granted a five year life extension under the terms of DOT-SP 15720 [8]. MAE waveforms were also captured to gain insight into the sequence of damage processes that occur within composite overwrapped pressure cylinders during failure.

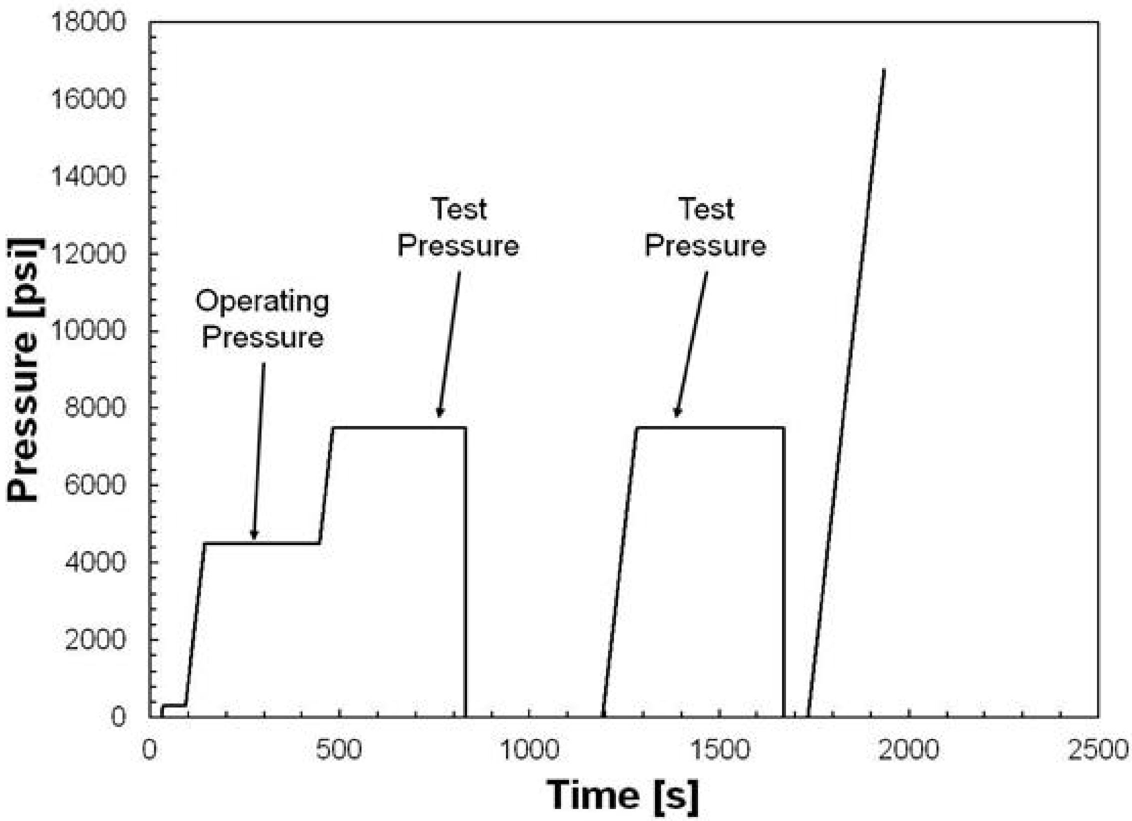

Figure 5.1 – Pressure schedule used during all EOL burst tests.

During EOL burst testing the mechanical response of the SCBA cylinders was monitored. Two strain gages were mounted onto the cylindrical portion of the SCBA cylinder, as shown in Figure 5.2, such that the strain response could be monitored throughout the entire test. The strain gages used were Micro-Measurements (CAE-06-500UW-120); each gage was wired in a quarter bridge configuration, using a three wire lead technique to compensate for lead resistance. During both test pressure holds, the axial (ε_{AXIAL}) and hoop strain (ε_{HOOP}) were measured, and used to compute the elastic expansion of a given cylinder (as would be done in a hydrostatic volumetric expansion test). The measured elastic expansion of the cylinder was subsequently compared to the rejectable elastic expansion (REE) for the given cylinder, to evaluate how effective REE is in evaluating the integrity of a cylinder.

Figure 5.2 – Strain gage attachment for EOL burst tests.

Further, the hydrostatic pressure within the cylinder was measured using an Omegadyne 33,000 psi pressure transducer (Omegadyne Model PX02S1 – 30KG10T). The principal membrane stresses at the strain gage locations were calculated using the thin wall pressure cylinder equations, i.e.

$$\sigma_{HOOP} = \frac{pr}{t} \tag{1}$$

$$\sigma_{AXIAL} = \frac{pr}{2t}. \tag{2}$$

where p is the hydrostatic pressure, r is the radius of the cylinder, and t is the pressure cylinder wall thickness. Using the calculated stresses and the measured strains the mechanical stiffness values in both the hoop and axial directions were determined before and after the hydrostatic test pressure.

5.2 Cyclic Fatigue

Fifteen cylinders operated under DOT-SP 10945, and ten cylinders operated under DOT-SP 10915, were randomly sampled from five of the locales that donated civilian SCBA cylinders to the research program, and subjected to cyclic hydrostatic pressure cycles to simulate an additional twenty years of service (per ISO 11119.2 [2]), on top of the already experienced fifteen years (Table 4.1). Cyclic fatiguing of the cylinders was performed in accordance with ISO 11119.2 section 8.5.5 [2]. The minimum pressure value for a cycle was set to 400 psi, while the maximum pressure for a cycle was set to the maximum developed pressure during fast fill (5,192 psi). This cyclic fatigue schedule resulted in a fatigue stress ratio, R, of 0.08.

Cylinders were fatigued in parallel as shown in Figure 5.3. The cyclic fatigue frequency was set to 0.008 Hz, resulting in a quasi-static stress state developed within the cylinder during each fatigue cycle. As seen in Figure 5.4 hoop strain data was acquired on the SCBA cylinders subjected to cyclic fatigue. In addition to the mechanical response of each cylinder during fatigue, three broadband MAE transducers were mounted on each of the cylinders tested (Figure 5.4). Finally, the temperature of the composite overwrap on a cylinder was monitored in order to insure consistency in test temperature, and that the composite overwrap was not developing excessive heat due to autogenous heating of the polymer matrix during cyclic fatigue.

Figure 5.3 - Ten SCBA cylinders connected in parallel to the high pressure system for cyclic fatigue testing.

Figure 5.4 – Hoop oriented strain gage, and three broadband MAE transducers were placed on each SCBA cylinder during cyclic fatigue testing.

5.3 Simulated Impact

Two cylinders from each locale were impacted following ISO 11119.2 Section 8.5.8 [2]. The impact simulation involved filling the cylinder 50% full of water, and dropping the cylinder from a height of 47" onto a ½" thick steel plate on the cylinders' domes, side, and shoulders. Figure 5.5 shows a cylinder in the apparatus used to perform the ISO impacts. One cylinder from each locale was subjected directly to an EOL burst test, while the other cylinder was subjected to the cyclic fatigue procedure described in Section 5.2.

Additionally, two cylinders from each locale were subjected to an extreme impact simulation developed by DOT and Digital Wave Corporation. The procedure of the extreme simulated impact was to fill 50% of the volume of the cylinder with water, and then drop the cylinder from a height of fifteen feet on to a concrete slab, such that the cylindrical portion of the cylinder uniformly impacted the concrete slab. Figure 5.6 shows a time lapse of a cylinder being subjected to the DOT drop procedure. Due to the geometric stress concentration that arises at the transition regions of cylindrical pressure cylinders and the need to incorporate additional windings in these areas, the greatest amount of impact damage was typically observed in the transition regions of the cylinder, as shown in Figure 5.7. One cylinder from each locale was subjected directly to an EOL burst test, while the other cylinder was subjected to the cyclic fatigue procedure described in Section 5.2.

Figure 5.5 - SCBA cylinder in the apparatus used for the impact procedure detailed in ISO 11119.2.

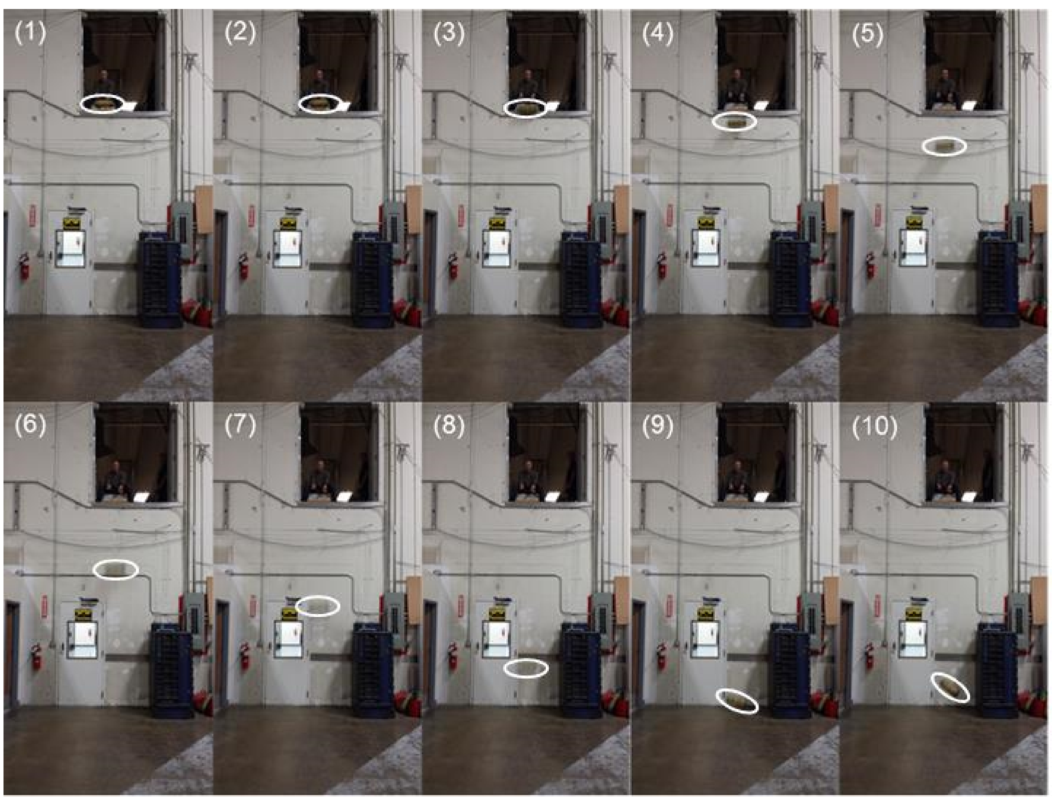

Figure 5.6 - Time lapse sequence of an SCBA cylinder subjected to the DOT drop procedure.

Figure 5.7 - Typical impact damage observed in the transition region of the SCBA cylinder as a result of the DOT/DWC extreme impact simulation.

5.4 Notch Tolerance

A total of ten SCBA cylinders were randomly sampled from the civilian SCBA cylinders that Digital Wave Corporation has received to be subjected to the notch tolerance testing described in Section 8.5.7 of ISO 11119.2 [2]. Of the ten SCBA cylinders, five were manufactured and operated under DOT-SP 10945 while the remaining five were manufactured and operated under DOT-SP 10915. One cylinder from each sample locale was subjected directly to an EOL burst test, while the other was subjected to the cyclic fatigue testing described in Section 8.5.7 of ISO 11119.2 prior to an EOL Burst test. In order to pass the notch tolerance burst test, the cylinder had to burst above 4/3 of the hydrostatic test pressure (10,000 psi). To meet the acceptance criteria of ISO 11119.2 Section 8.5.7.2, all fatigued cylinders had to withstand at least 1,000 cycles and no more than 5,000 cycles from 400 psi to 5000 psi (2/3 of the hydrostatic test pressure); a cylinder which achieves 1,000 cycles but not 5,000 cycles and fails by leakage is still deemed to pass the test.

In the notch tolerance procedure of ISO 11119.2 two notches are introduced into each cylinder. The first notch is oriented axially, while the second notch is located 120° around the circumference of the cylinder and oriented in the hoop direction. The required dimensions of the notch are a width of 0.040”, a depth of 50% of the overwrap thickness, and a length of five times the overwrap thickness. Table 5.1 summarizes all cylinder and notch dimensions. Figure 5.8 shows representative flaws that were introduced into the SCBA cylinders.

Table 5.1 - Summary of SCBA cylinders that were subjected to notch tolerance testing, including cylinder specific notch dimensions.

Location	DOT-SP	Time	Designation	SN	Mfg Date	Pressure	Vessel OD [in]	Overwrap thickness [in]	Axial Notch Depth [in]	Axial Notch Length [in]	Hoop Notch Depth [in]	Hoop Notch Length [in]
FDNY	10945	45	ALT695	3929	06/98	4500	6.30	0.250	0.130	1.25	0.130	1.25
Fairfax, VA	10915	45	OM	3984	08/98	4500	6.80	0.250	0.130	1.25	0.130	1.25
Kennebunkport, ME	10945	30	ALT639	17732	12/98	4500	5.48	0.209	0.110	1.25	0.120	1.25
South Berwick, ME	10915	30	IH	2554	07/98	4500	5.27	0.206	0.110	1.25	0.120	1.25
Howard, PA	10945	30	ALT639	69925	11/00	4500	5.48	0.209	0.110	1.25	0.120	1.25
FDNY	10945	45	ALT695	4304	07/98	4500	6.30	0.250	0.110	1.25	0.130	1.25
Fairfax, VA	10915	45	OM	3971	08/98	4500	6.80	0.250	0.130	1.25	0.130	1.25
Houston, TX	10915	60	OP	11129	01/99	4500	6.88	0.250	0.130	1.25	0.120	1.25
South Berwick, ME	10915	30	IH	1251	06/98	4500	5.27	0.206	0.110	1.25	0.110	1.25
Howard, PA	10945	30	ALT639	17827	12/98	4500	5.48	0.209	0.120	1.25	0.110	1.25

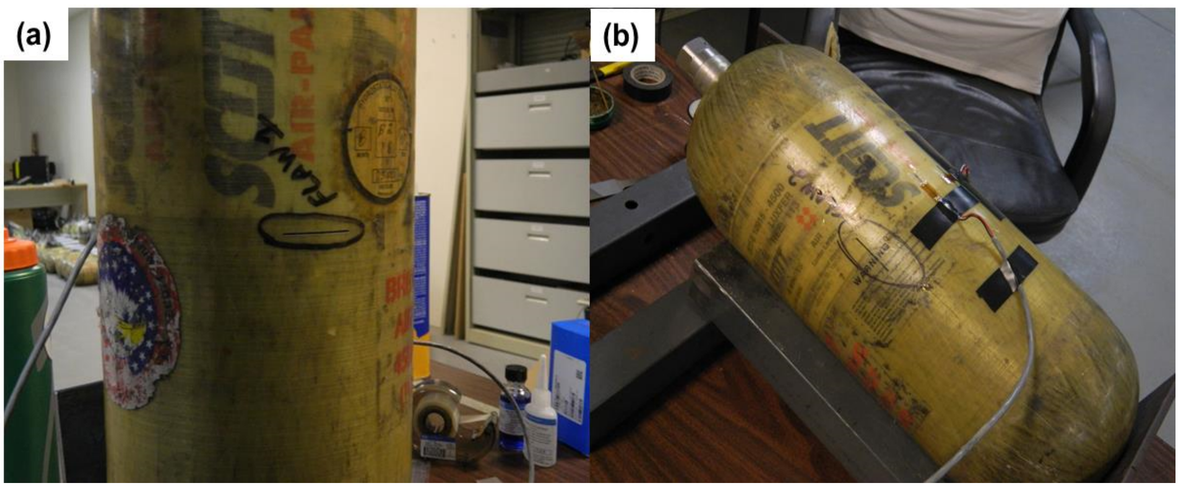

Figure 5.8 - Representative (a) hoop, and (b) axially oriented flaws which were introduced into the SCBA cylinders to evaluate the cylinders' notch tolerance.

5.5 Sulfuric Acid Resistance

One cylinder from each locale was subjected to a sulfuric acid exposure during a pressure hold at service pressure following ISO 11515 Section 8.5.17 [4]. A 40% concentrated solution of sulfuric acid was mixed, and then a 6" ring was painted on to the surface of the SCBA cylinder as shown in Figure 5.9a. After the sulfuric acid patch was painted on, the patch was covered with a polymer sheet to prevent the acid vapor from corroding the high pressure test system (Figure 5.9b). In order simulate a worst case scenario three of the five cylinders were subjected to the fifteen foot drop described in Section 5.3, and then cycled for 1000 cycles from 400 - 5192 psi prior to the sulfuric acid exposure.

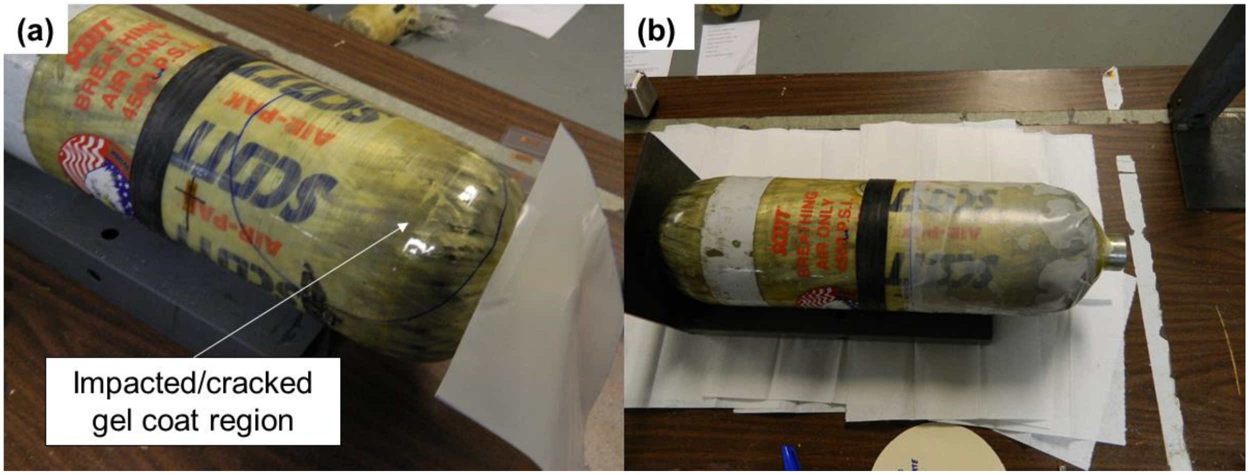

Figure 5.9 – (a) cracked region of the gel coat due to fifteen foot impact and 1,000 cycles with the 6" diameter sulfuric acid patch highlighted in blue, and (b) the protective polymer film used to cover sulfuric acid patch to prevent outgassing and corrosion of the high pressure system.

Once the cylinders had the 6" sulfuric acid patch painted on, the cylinders were pressurized to 4500 psi (service pressure) and held at that pressure for 100 hours. During the pressurization and hold, three broadband MAE transducers were attached on the surface of each cylinder. Following the 100 hour hold at service pressure, cylinders were de-pressurized, the sulfuric acid patch was neutralized, and then the cylinders were subjected to an EOL burst as described in Section 5.1.

5.6 Re-autofrettage and corroded liners

As was pointed out in Section 4.0, a large percentage (62.0%) of the civilian SCBA cylinders which were donated to the present study exhibited indications of corrosion of the aluminum liner. Most of the corrosion indications were in the form of white spotting on the internal wall of the aluminum liner (Figure 5.10a); this spotting is believed to be due to mineral deposits, resulting from prolonged exposure to hard water. However, the true significance of this type of corrosion was found from a piece of an aluminum liner after an EOL burst test, as shown in Figure 5.10b. From Figure 5.10b, a large number of minute flaws (having a preferential axial orientation) were discovered in the centers of the white spotting after the EOL burst test. The opened flaws were far more visible after the EOL burst test due to the fact that the aluminum liner was plastically deformed to such an extent as to open up the crack mouths. While these corrosion induced flaws do not reduce the ultimate burst pressure of the CFFC pressure cylinders, it will be shown in the following results sections and theoretically confirmed in Section 9.0 that cylinder leakage due to crack growth through the Aluminum liner during cyclic hydrostatic fatigue did occur due to these types of flaws acting as crack initiation sites.

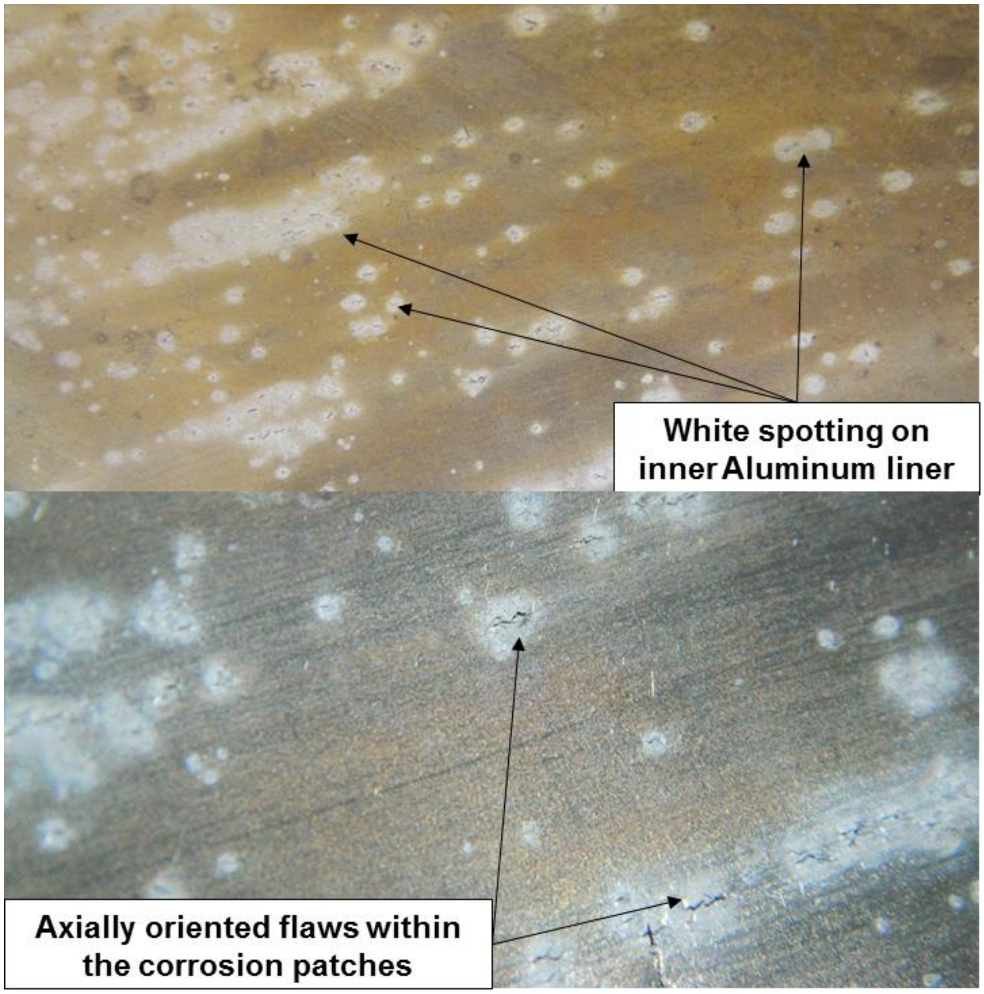

Figure 5.10 – (a) common white spotting corrosion on the internal aluminum observed during the internal visual inspection, and (b) opened crack mouths (by means of an EOL burst test) found inside of the corrosion spots.

While a crack that grows through the aluminum liner has been shown to only result in leakage of the cylinder (not catastrophic burst), such leakage is problematic from a life extension perspective. To address this issue Digital Wave Corporation investigated the use of a re-autofrettage procedure (tensile overload) to put the aluminum liner back into residual compression. From a fracture mechanics perspective, the tensile overload will develop a plastic zone at the crack tip, effectively blunting the crack tips and retarding the growth rate of the corrosion assisted flaws. For this portion of the study, fifteen DOT-SP 10915 cylinders (all donated from Fairfax, VA) were used in order to eliminate variability due to the varying service conditions from the different locales. All fifteen of the cylinders were found to have signs of corrosion during the internal visual inspection (Table 4.1). To study the efficacy of crack tip blunting, eight of the fifteen cylinders were subjected to the re-autofrettage pressure while the remaining seven cylinders were not; all fifteen cylinders were then subjected to a maximum of 10,000 cycles following the procedure given in Section 5.2.

The eight cylinders which were subjected to the re-autofrettage pressure were first subjected to the pressure schedule of Figure 5.1, with the test pressure modified to 8500 psi (1000 psi greater than any previously experienced pressure by the cylinder). By taking the cylinder 1000 psi above any pressure that it had previously seen, the aluminum liner would again plastically deform, and upon unloading of the cylinder the aluminum liner (and all corrosion initiated flaw sites that had been introduced into the liner) were put into residual compression. Section 9.0 provides fracture mechanics calculations of the created plastic zone size at the crack tip which retards crack growth, as well as Paris Law and Wheeler model computations which compare the remaining fatigue life of the re-autofrettaged and non-re-autofrettaged corroded aluminum liners. The included computations are in good agreement with the experimental data.

6.0 Physical and Modal Acoustic Emission (MAE) Testing Results

6.1 End of Life Burst Tests

6.1.1. Mechanical Response

It was observed that both cylinder designs (DOT-SP 10915 and DOT-SP 10945) responded in a bi-modulus fashion; this was due to the fact that once the original autofrettage pressure of the cylinder had been reached, the 6061-T6 Al liner began to deform plastically and no longer significantly contributed to the stiffness of the cylinder, effectively reducing the stiffness response of the structure to simply the stiffness of the composite overwrap. Figure 6.1 presents a representative stress-strain response for a DOT-SP 10915 SCBA cylinder in both the axial and hoop directions, while Figure 6.2 presents a representative stress-strain curve for a DOT-SP 10945 SCBA cylinder in both the axial and hoop directions. Plots of the initial and secondary modulus determination are presented in Figure 6.3 and Figure 6.4 for the DOT-SP 10915 and DOT-SP 10945 cylinders, respectively.

In addition to the stiffness response of the cylinders, the ultimate burst strength was also recorded for all cylinders. All stiffness and ultimate burst strength data are summarized in Table 6.1, images of all failed cylinders are presented in Section 10.0, and the stress-strain response of all cylinders is shown in Appendix A. From Table 6.1 it is observed that twenty-four of the twenty-five cylinders met the minimum required burst pressure of the DOT CFFC 5th Revision (15,300 psi), and that the initial and secondary modulus in both the hoop and axial directions for each variant was consistent across equivalent size cylinders.

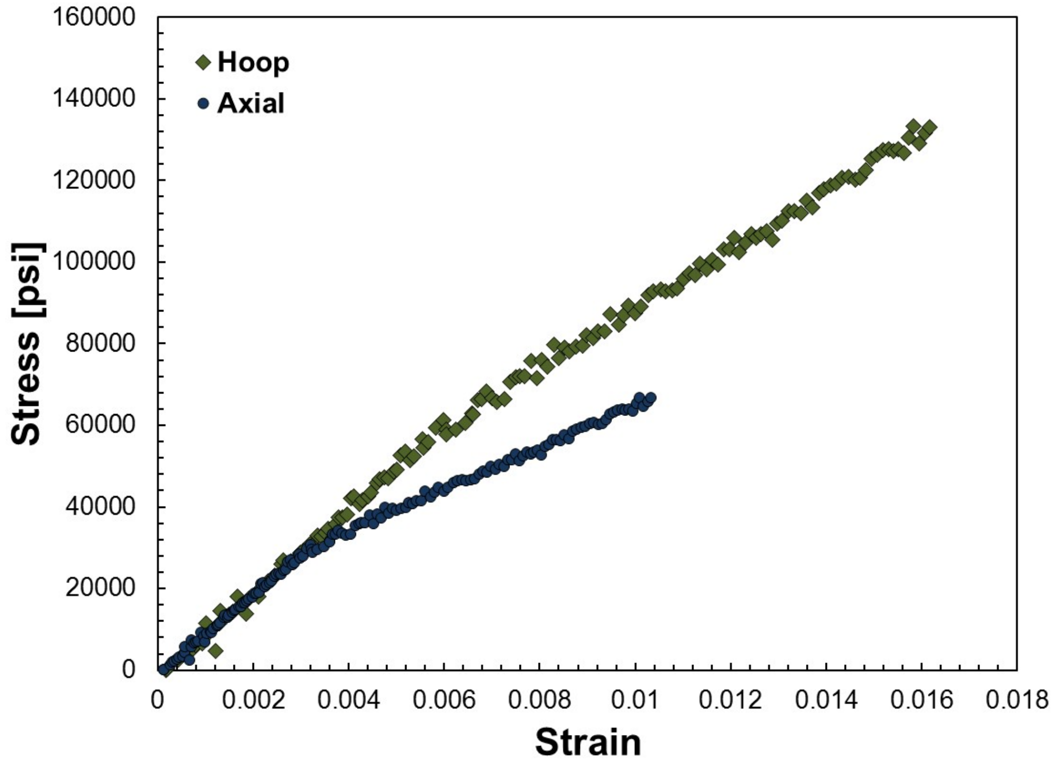

Figure 6.1 – Stress-strain response in the axial and hoop directions of DOT-SP 10915 (OM3962).

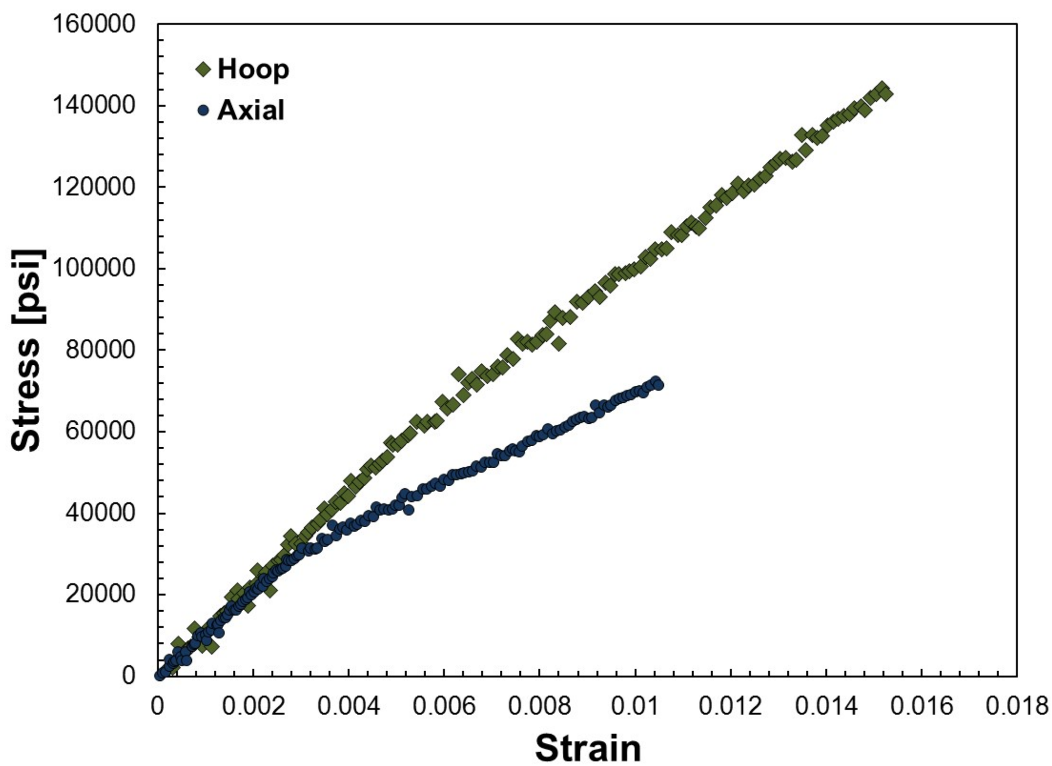

Figure 6.2 – Stress-strain response in the axial and hoop directions of DOT-SP 10945 (ALT695-3650).

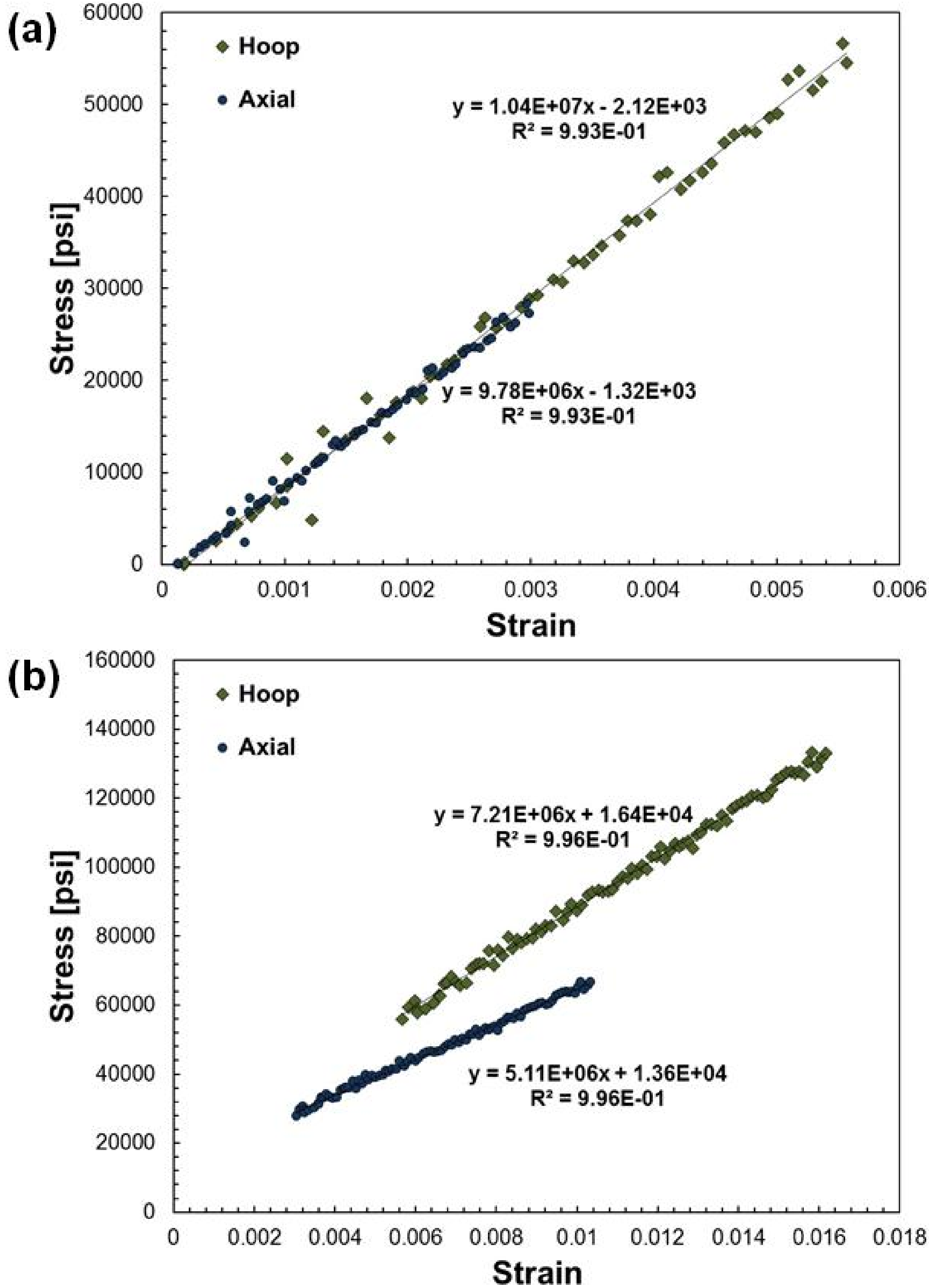

Figure 6.3 – (a) Initial, and (b) secondary modulus determination for E10915 OM3962..

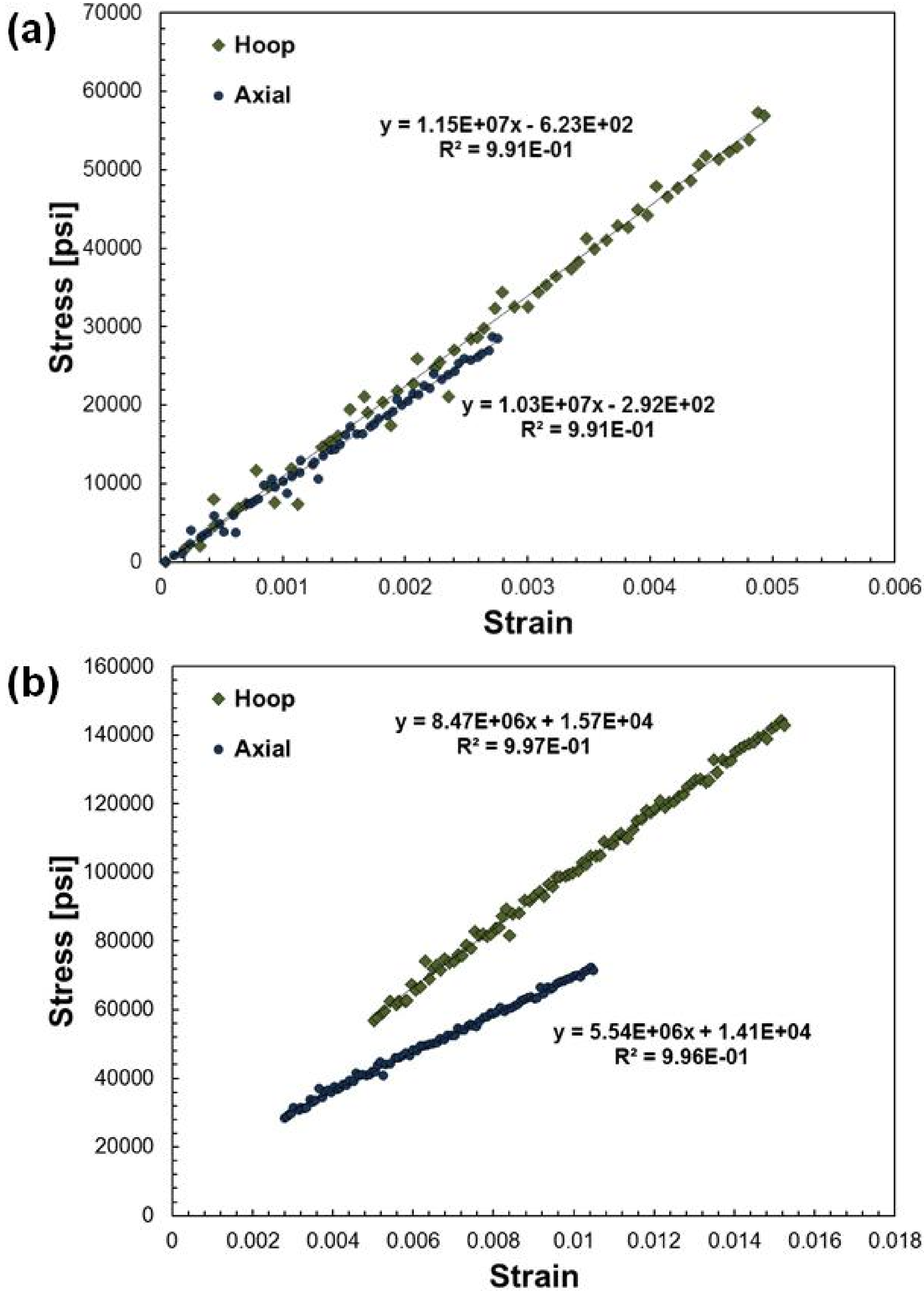

Figure 6.4 – (a) Initial, and (b) secondary modulus determination for E10945 ALT695-3650.

Table 6.1 – Summary of Burst pressure, BEOP, Visual Inspection Results, MAE life extension results, Elastic Expansion, testing results, initial and secondary modulus data.

Manufacturer	Time	Designation	SN	Mfg Date	Pressure	Visually Condemned [Y/N]	Burst Pressure [psi]	BEOP [psi]	BEOP % Burst	MAE Life Extension Met [Y/N]	Initial Hoop Modulus [Msi]	Initial Axial Modulus [Msi]	Secondary Hoop Modulus [Msi]	Secondary Axial Modulus [Msi]	Elastic Expansion [cc]	REE [cc]	Pass Hydro [Y/N]
SCI	60	ALT 604	3742	05/98	4500	N	14734	7671	52.1%	N (BEO)	10.2	10.7	8.8	6.9	136.0	140.0	Y
SCI	45	ALT 695	4436	07/98	4500	Y	17837	11088	62.2%	Y	11.7	10.6	9.1	6.6	91.1	105.0	Y
SCI	60	ALT 604	4962	08/98	4500	N	20285	13003	64.1%	Y	10.9	10.1	9.0	6.8	130.9	140.0	Y
SCI	45	ALT 695	3650	06/98	4500	Y	19317	14091	72.9%	Y	11.5	10.3	8.5	5.5	88.9	105.0	Y
SCI	45	ALT 695	4494	07/98	4500	N	19451	11909	61.2%	Y	12.4	10.1	10.0	6.5	85.9	105.0	Y
Luxfer	45	OM	3915	08/98	4500	N	17300	12447	71.9%	Y	12.4	8.3	9.9	4.3	90.9	113.0	Y
Luxfer	45	OM	3990	08/98	4500	N	16725	10850	64.9%	Y	9.8	10.0	6.7	5.1	103.7	113.0	Y
Luxfer	45	OM	3934	08/98	4500	N	16050	10528	65.6%	Y	9.9	9.5	7.1	5.0	104.4	113.0	Y
Luxfer	45	OM	3941	08/98	4500	N	17200	10283	59.8%	Y	-	8.2	-	4.1	-	113.0	-
Luxfer	45	OM	3962	08/98	4500	N	17675	9829	55.6%	Y	10.4	9.8	7.2	5.1	99.6	113.0	Y
SCI	30	ALT 639	14969	12/98	4500	N	18980	12508	65.9%	Y	13.6	13.0	10.3	7.2	67.6	71.1	Y
SCI	30	ALT 639	17663	12/98	4500	N	20674	12654	61.2%	Y	13.8	13.0	10.5	7.4	67.2	71.1	Y
SCI	30	ALT 639	18023	12/98	4500	N	19554	12713	65.0%	Y	13.4	13.7	9.8	8.4	67.3	71.1	Y
SCI	30	ALT 639	69216	10/00	4500	N	20599	13108	63.6%	Y	12.2	13.1	7.3	7.3	73.7	71.1	N
SCI	30	ALT 639	18629	01/99	4500	N	20181	11698	58.0%	Y	14.0	-	11.3	-	-	-	-
Luxfer	30	IH	1740	06/98	4500	N	19275	12817	66.5%	Y	13.9	11.7	10.0	5.9	62.0	76.0	Y
Luxfer	30	IH	1855	06/98	4500	N	18089	11352	62.8%	Y	12.3	12.0	9.1	5.7	68.6	76.0	Y
Luxfer	30	IH	1763	06/98	4500	N	20402	12260	60.1%	Y	13.3	11.3	9.9	6.0	65.0	76.0	Y
Luxfer	30	IH	1135	06/98	4500	N	19378	10003	51.6%	Y	12.6	12.0	9.5	6.1	66.8	76.0	Y
Luxfer	30	IH	1929	06/98	4500	N	19378	11760	60.7%	Y	10.6	11.1	8.7	6.0	78.9	76.0	N
SCI	60	ALT 604	6739	12/98	4500	N	21780	12302	56.5%	Y	9.8	10.5	7.8	7.5	134.9	143.0	Y
SCI	30	ALT 639	17688	12/98	4500	N	20878	13987	67.0%	Y	14.2	13.6	10.4	8.1	64.6	71.1	Y
SCI	30	ALT 639	18862	01/99	4500	N	20244	12288	60.7%	Y	17.4	12.9	15.5	7.5	56.1	71.1	Y
SCI	30	ALT 639	18507	01/99	4500	N	21548	10649	49.4%	Y	13.6	13.4	10.0	7.8	66.3	71.1	Y
SCI	30	ALT 639	18793	01/99	4500	N	19480	11938	61.3%	Y	14.5	13.3	9.8	7.3	63.8	71.1	Y

Further, statistical analysis of the baseline EOL burst strength data was performed, and will be subsequently compared to the statistical distributions form other testing procedures to evaluate the impact of the given testing protocols. As shown in Figure 6.5, the burst strength of all twenty-five EOL burst tests was modeled as both a normal (or Gaussian) distribution, and a two-parameter Weibull distribution. The mean value and standard deviation from the normal distribution fit of the EOL burst test data was found to be 19,080 psi and 1742.3 psi, respectively. The two parameters of a Weibull distribution are the scale parameter (κ), and the shape parameter (β). The scale parameter is analogous to the mean of a normal distribution and is equal to the (1 – 1/e) percentile of the distribution, while the shape parameter describes the breadth of the distribution. A large shape parameter (>10) is indicative of a low variability distribution, while a small shape parameter (<10) is indicative of a highly variable distribution. The scale and shape parameters of the Weibull distribution fit of the EOL burst test data were 19,840 psi, and 13.3, respectively. From Figure 6.5 (and a Kolmogorov-Smirnov test of the goodness of fit), the two-parameter Weibull distribution more adequately modeled the distribution of burst strengths, and will used for comparison in the remaining sections.

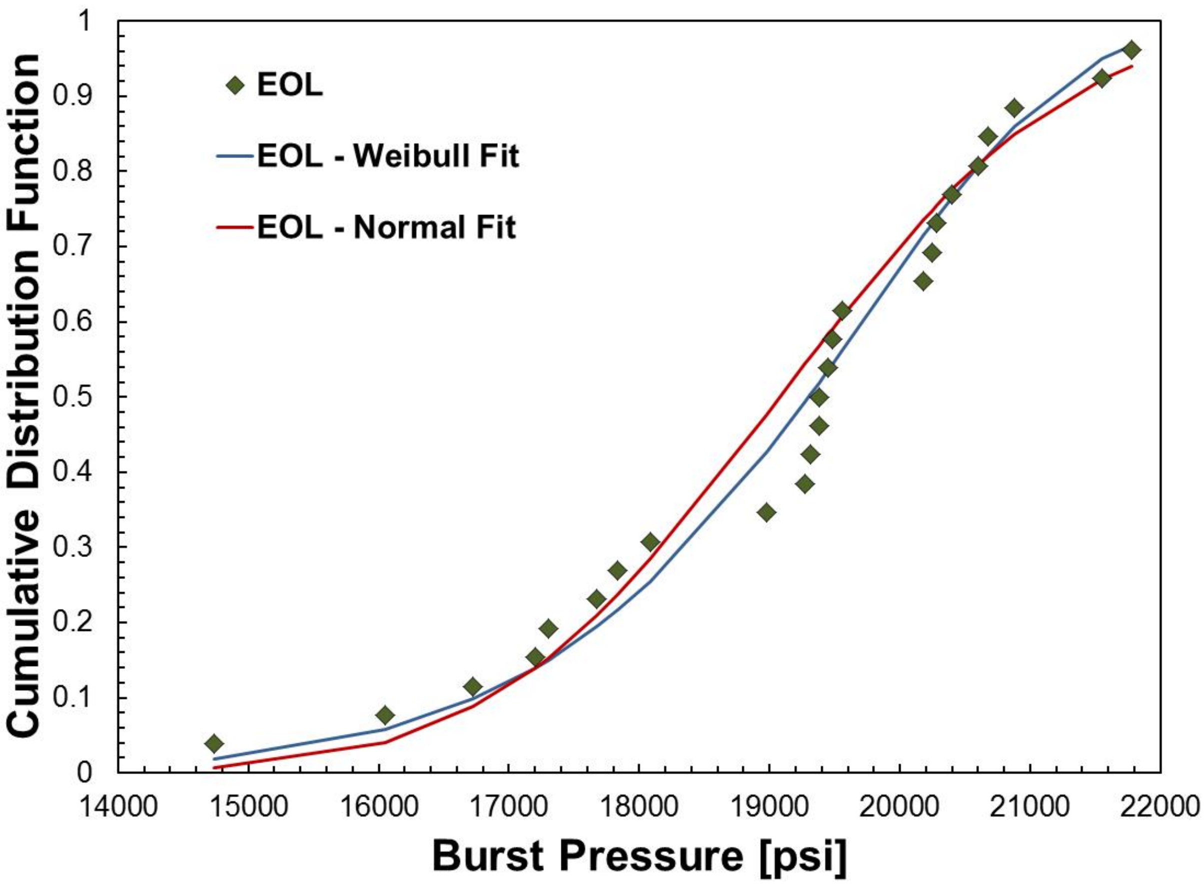

Figure 6.5 – Distribution of the EOL Burst strengths of the twenty-five tested CFFC cylinders with the corresponding normal distribution fit (μ = 19,080 psi, σ = 1742.3 psi), and two parameter Weibull distribution fit (κ = 19,840 psi, β = 13.3).

6.1.2. MAE analysis

For the MAE life extension requirements of [8], all cylinders passed the stability requirements, and were found to have no significant fiber bundle breaks (i.e., energy greater than $2.7\text{x}10^{-16}$ J) or large energy single events (i.e., energy greater than $2.7\text{x}10^{-14}$ J) on the second cycle to test pressure. Of the twenty-five pressure cylinders tested, twenty-four of the cylinders passed the BEO requirements for life extension at test pressure, while one failed. The cylinder that failed the MAE BEO life extension requirement (ALT 604 – 3742) failed due to background energy oscillations on the second cycle to test pressure as shown in Figure 6.6. Importantly, this was also the cylinder that was found to burst below the minimum required burst pressure (Table 6.1); the significance of this result will be elaborated upon in Section 6.7. A representative plot of the background energy oscillations during the burst pressurization cycle for a cylinder that burst above the minimum design requirement is shown in Figure 6.7. The background energy oscillation pressure (BEOP) was determined as the pressure within the cylinder at which the BEO's become greater than a factor (M_O) of two; all BEOP determinations are presented in Appendix B.

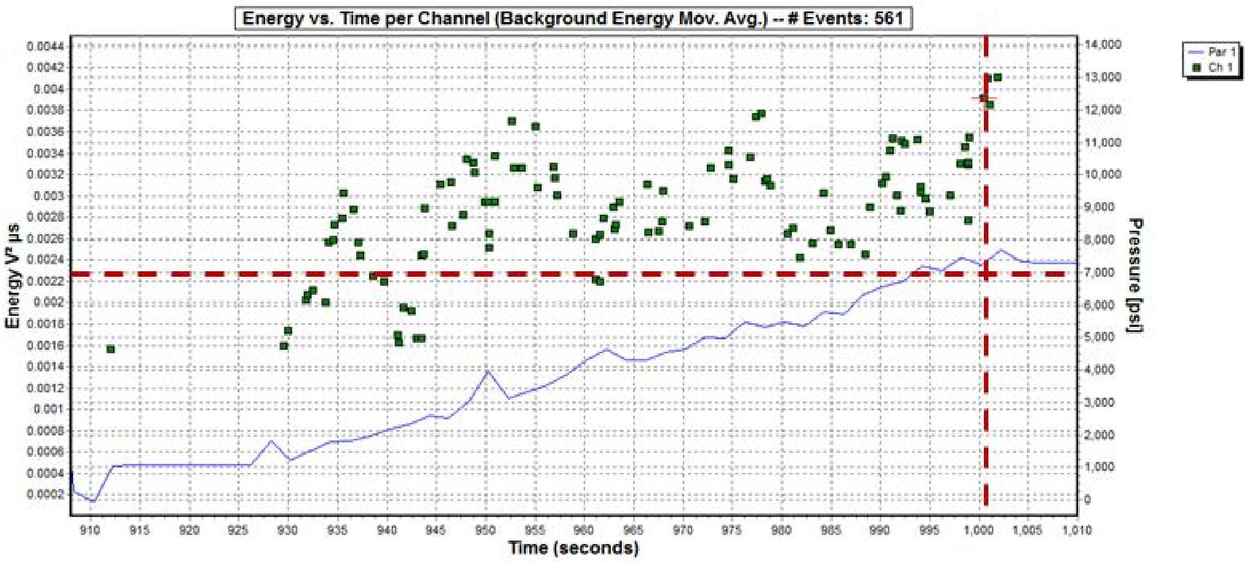

Figure 6.6 - BEO on the second test pressure cycle for ALT604 – 3742. Such an oscillation in the background energy caused the cylinder to fail the MAE life extension requirement.

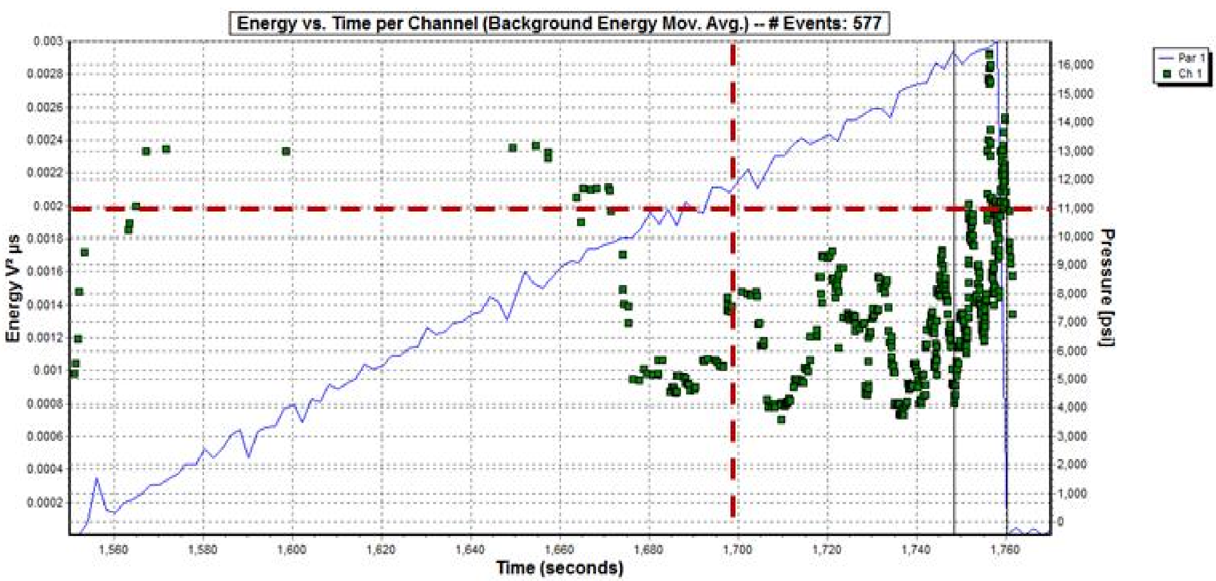

Figure 6.7 - Determination of Background Energy Oscillation Pressure (indicated by the dashed red crosshairs) for DOT-SP 10915 OM3915.

6.2 Cyclic Fatigue

6.2.1. Mechanical Response

From the design requirements in the DOT CFFC 5th Revision [1], the stress in the fiber at the operating pressure of a cylinder must be below 30%. Hence, the fibers (the primary load bearing member of the design) are not stressed to a great enough level such that the composite overwrap could begin to deteriorate and compromise the cylinders strength. Evidence to support the fact that the composite overwrap's stiffness is not degrading during cyclic fatigue to the maximum developed pressure (in addition to the lack of real MAE data) is shown in Figure 6.8, where the maximum and minimum strain for each cycle during a fatigue test can be seen. From Figure 6.8 it is clear that the maximum and minimum hoop strain values were not changing (accounting for peak pressure variability and temperature stability) from cycle to cycle, indicating that the stiffness of the composite overwrap was not being degraded due to cyclic fatigue. Finally, the temperature of the cylinders was monitored during the cyclic fatigue process to insure that autogenous heating was not taking place in the cylinder (Figure 6.9). Figure 6.9 shows that the temperature of an SCBA cylinder as a function of time, where it is clear that the temperature of the outer layer of the cylinders is reasonably consistent at 68 °F, and doesn't exceed 72 °F at any point during the cyclic fatigue test.

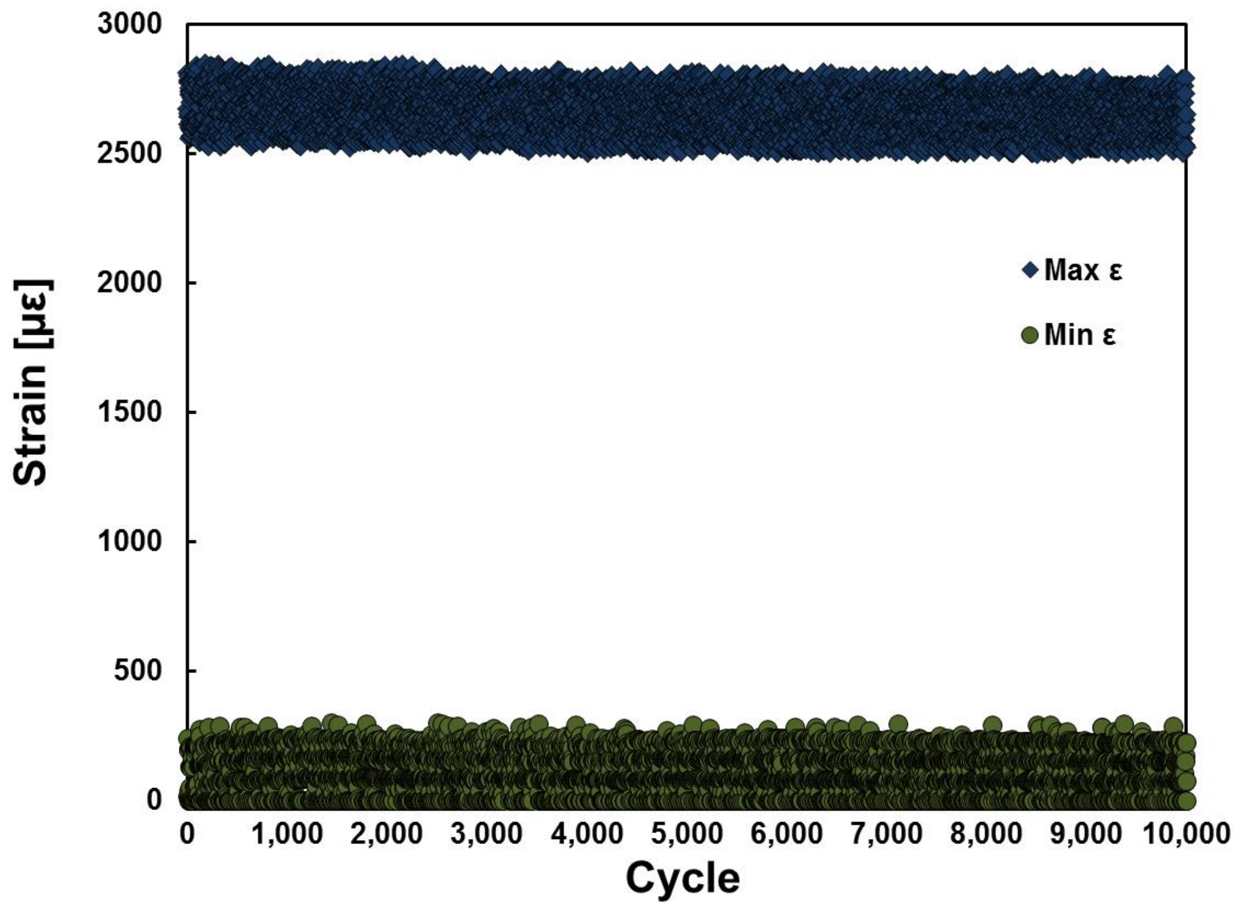

Figure 6.8 – Maximum and minimum strain values on each cycle of a cyclic fatigue test.

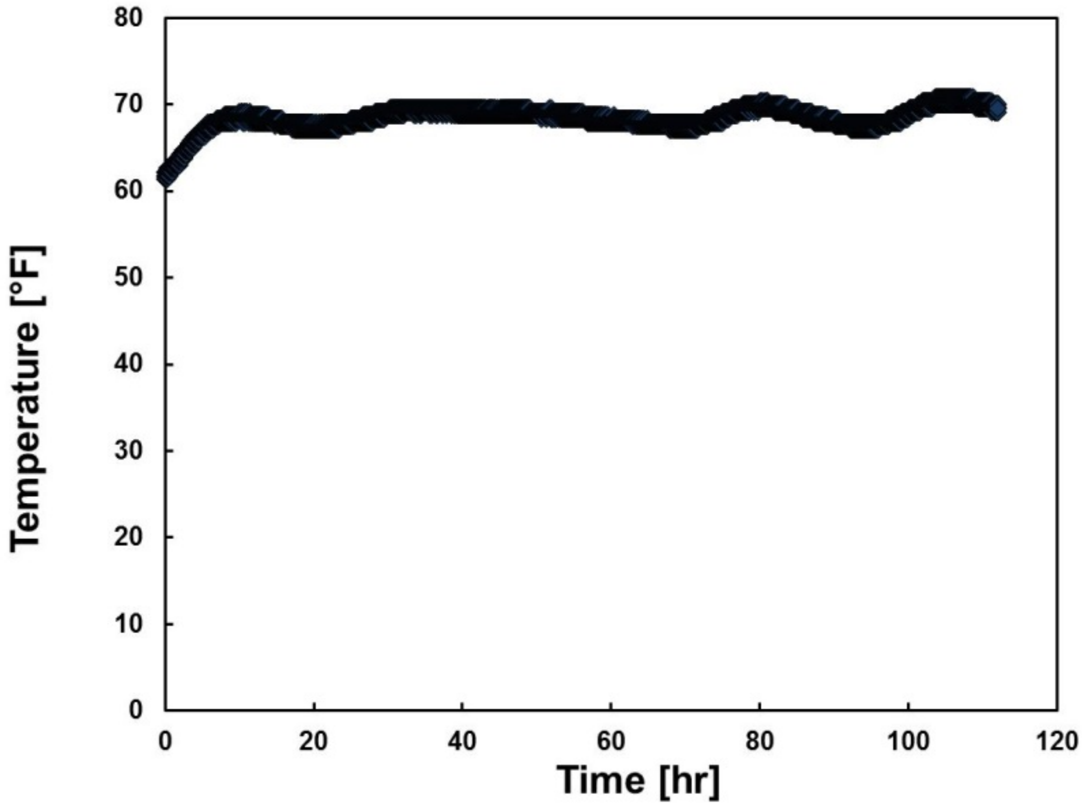

Figure 6.9 – Temperature as a function of time of the outer layer of a SCBA pressure during a cyclic fatigue test.

In agreement with the observations in Section 6.1.1, all cylinders were found to respond in a bi-modulus fashion. The typical response of a cylinder after 10,000 cycles is shown in Figure 6.10, while stress-strain curves for all cylinders are provided in Appendix A. Results for stiffness, burst pressure, MAE life extension results, and visual inspection results are presented in Table 6.2. From Table 6.2, it is highlighted that of the twenty-one burst tests summarized in this report, all twenty-one cylinders met or exceeded the required minimum burst pressure of the DOT CFFC 5th Revision. Also, in comparing the stiffness values from Section 6.1.1 to the stiffness values reported in Table 6.2 (comparing like designs and capacities), no statistical difference was found. Such findings indicate that no deleterious effects were experienced by the composite overwrap of the SCBA cylinder when subjected to a simulated additional twenty years of service life.

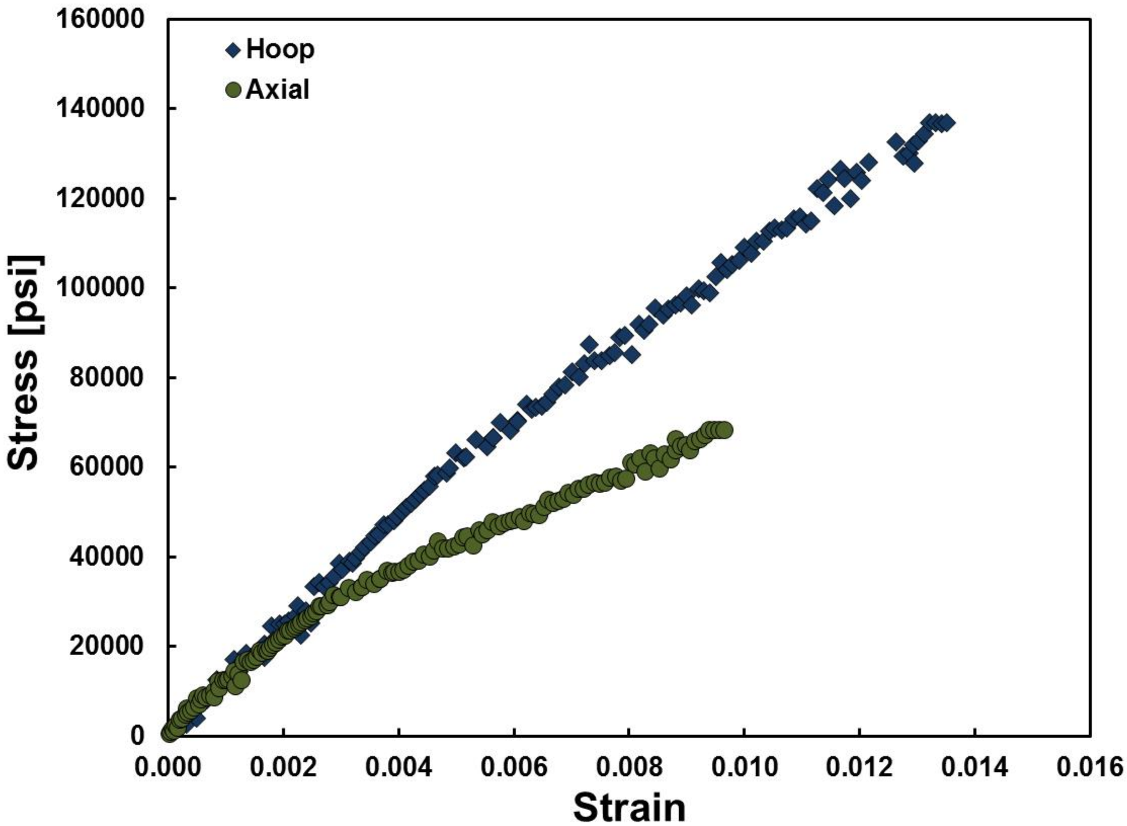

Figure 6.10 – Stress-strain response of OM3794 operated under DOT-SP 10915.

Table 6.2 – Stiffness, burst pressure, MAE life extension results, elastic expansion, and visual inspection results for all cylinders that were subjected to an additional simulated twenty years of service life.

Test	Location	DOT-SP	Time	Designation	SN	Mfg Date	Pressure	Visually Condemned [Y/N]	Burst Pressure [psi]	BEOP [psi]	BEOP % Burst	MAE Life Extension Met [Y/N]	Initial Hoop Modulus [Msi]	Initial Axial Modulus [Msi]	Secondary Hoop Modulus [Msi]	Secondary Axial Modulus [Msi]	Elastic Expansion [cc]	REE [cc]	Pass Hydro [Y/N]
10k and Burst	FDNY	SCI	45	ALT 695	1700	03/98	4500	Y	19350	12597	65.1%	Y	12.1	10.9	8.8	5.9	93.8	105.0	Y
10k and Burst	FDNY	SCI	45	ALT695	6058	09/98	4500	N	19181	9022	47.0%	Y	12.4	12.4	10.1	6.6	80.2	105.0	Y
10k and Burst	FDNY	SCI	45	ALT695	5353	09/98	4500	Y	18700	13190	70.5%	Y	11.1	9.5	8.7	5.7	94.0	105.0	Y
10k and Burst	FDNY	SCI	45	ALT695	4745	07/98	4500	N	19600	11323	57.8%	Y	10.7	9.8	8.2	5.3	95.4	105.0	Y
10k and Burst	FDNY	SCI	45	ALT695	1668	03/98	4500	Y	>17550	11411	-	Y	12.1	11.2	9.2	6.1	97.3	105.0	Y
10k and Burst	Fairfax, VA	Luxfer	45	OM	3947	08/98	4500	N	Leaked at 9388 cycles	-	-	-	-	-	-	-	-	-	-
10k and Burst	Fairfax, VA	Luxfer	45	OM	3950	08/98	4500	N	16855	9565	56.7%	Y	11.4	11.8	9.3	6.3	107.8	113.0	Y
10k and Burst	Fairfax, VA	Luxfer	45	OM	3921	08/98	4500	N	Leaked at 9048 cycles	-	-	-	-	-	-	-	-	-	-
10k and Burst	Fairfax, VA	Luxfer	45	OM	3928	08/98	4500	N	15716	8701	55.4%	Y	10.5	10.2	8.1	5.0	104.1	113.0	Y
10k and Burst	Fairfax, VA	Luxfer	45	OM	3913	08/98	4500	N	17212	8920	51.8%	Y	11.4	10.9	8.2	6.0	94.7	113.0	Y
10k and Burst	Fairfax, VA	Luxfer	45	OM	3985	08/98	4500	N	Leaked at 5369 cycles	-	-	-	-	-	-	-	-	-	-
10k and Burst	Fairfax, VA	Luxfer	45	OM	3960	08/98	4500	N	Leaked at 5364 cycles	-	-	-	-	-	-	-	-	-	-
10k and Burst	Fairfax, VA	Luxfer	45	OM	3956	08/98	4500	N	Leaked at 8680 cycles	-	-	-	-	-	-	-	-	-	-
10k and Burst	Fairfax, VA	Luxfer	45	OM	3994	08/98	4500	N	Leaked at 5369 cycles	-	-	-	-	-	-	-	-	-	-
10k and Burst	Fairfax, VA	Luxfer	45	OM	4045	09/98	4500	N	19042	10532	55.3%	Y	11.1	9.3	7.8	4.7	102.7	113.0	Y
10k and Burst	South Berwick, ME	Luxfer	30	IH	1271	06/98	4500	N	18818	13271	70.5%	Y	14.1	12.3	9.7	6.1	63.0	76.0	Y
10k and Burst	South Berwick, ME	Luxfer	30	IH	2483	07/98	4500	N	19710	11894	60.3%	Y	13.0	11.5	9.8	6.0	70.0	76.0	Y
10k and Burst	South Berwick, ME	Luxfer	30	IH	1748	06/98	4500	N	19890	12978	65.2%	Y	13.9	11.7	9.8	6.0	65.8	76.0	Y
10k and Burst	South Berwick, ME	Luxfer	30	IH	1820	06/98	4500	N	18598	11909	64.0%	Y	12.6	11.4	9.7	6.0	68.0	76.0	Y
10k and Burst	South Berwick, ME	Luxfer	30	IH	1027	06/98	4500	N	Leaked at 6295 cycles	-	-	-	-	-	-	-	-	-	-
10k and Burst	Kennebunkport, ME	SCI	30	ALT639	18974	01/99	4500	N	21132	12758	60.4%	Y	14.7	13.3	10.7	8.6	66.3	69.9	Y
10k and Burst	Kennebunkport, ME	SCI	30	ALT639	18799	01/99	4500	N	20649	10297	49.9%	Y	13.6	14.7	10.2	8.9	69.2	71.1	Y
10k and Burst	Kennebunkport, ME	SCI	30	ALT639	18790	01/99	4500	N	19741	11206	56.8%	Y	13.4	14.4	9.6	8.0	70.2	71.1	Y
10k and Burst	Houston, TX	SCI	60	ALT695	1653	03/98	4500	N	17734	10063	56.7%	Y	12.5	11.2	9.1	6.0	94.7	105.0	Y
10k and Burst	Houston, TX	SCI	60	ALT604	4342	07/98	4500	N	18233	9887	54.2%	Y	13.7	13.2	12.2	9.6	137.2	143.0	Y
10k and Burst	Howard, PA	SCI	30	ALT639	39764	11/99	4500	N	20414	13412	65.7%	Y	13.0	15.0	9.3	8.4	70.8	69.9	N
10k and Burst	Howard, PA	SCI	30	ALT639	18435	01/99	4500	N	20400	13681	67.1%	Y	13.9	13.3	11.2	8.1	69.5	69.9	Y
10k and Burst	Howard, PA	SCI	30	ALT639	39694	11/99	4500	N	20195	11250	55.7%	Y	12.4	14.3	8.6	7.7	73.9	71.1	N
10k and Burst	Howard, PA	SCI	30	ALT639	18683	01/99	4500	N	17822	11074	62.1%	Y	13.9	13.5	10.9	7.9	69.3	71.1	Y
10k and Burst	Howard, PA	SCI	30	ALT639	18020	01/99	4500	N	Leaked at 6297 cycles	-	-	-	-	-	-	-	-	-	-

To further confirm that a simulated twenty years of additional service life had no deleterious effects on the SCBA burst pressure strength, Figure 6.11 compares the two parameter Weibull distributions for cylinders which only experienced fifteen years of service life (presented in Section 6.1.1) to the distribution of cylinders which experienced fifteen years of service life and an additional simulated twenty years of service. From Figure 6.11 it was observed that the scale and shape parameters of the Weibull distribution for cylinders which experienced fifteen years of service life was 19,840 psi and 13.3, respectively, while the scale and shape parameters of the Weibull distribution for cylinders which experienced fifteen years of service life and a simulated additional twenty years of service was 19,597 psi and 17.1, respectively. Such findings indicate that a negligible change in burst strength was observed between the fifteen year old cylinders and the simulated thirty-five year old cylinders, while a marked tightening of the burst strength distribution was observed for the cylinders subjected to the additional twenty years of service life.

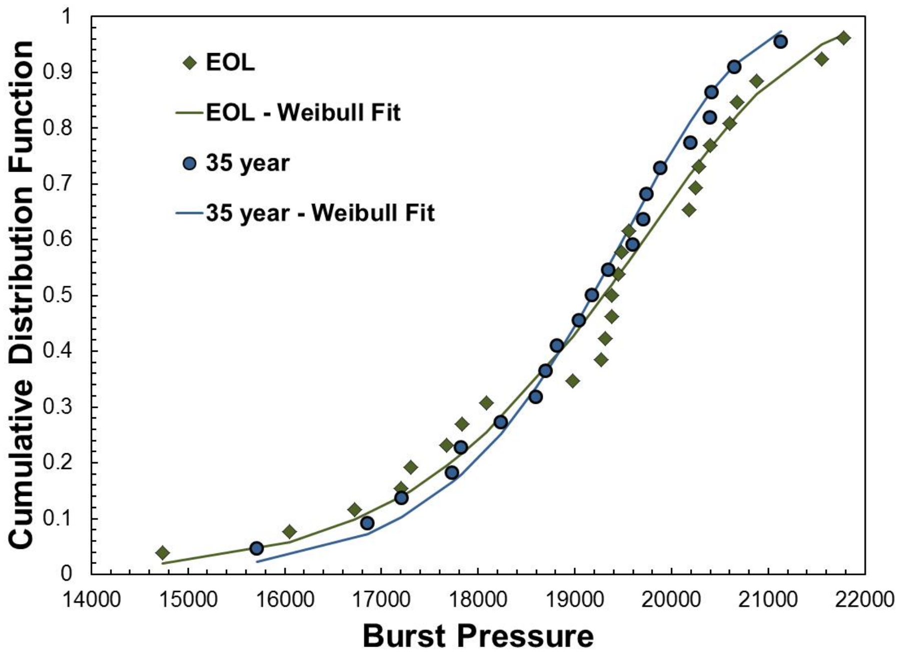

Figure 6.11 – A comparison of the two parameter Weibull distributions for cylinders which experienced fifteen years of service life (κ = 19,840 psi, β = 13.3) to cylinders which experienced fifteen years of service life and a simulated additional twenty years of service (κ = 19,597 psi, β = 17.1).

As shown in Table 6.2, twenty-one of the twenty-five SCBA cylinders that were subjected to a simulated twenty years of life extension managed to withstand the additional 10,000 cycles. The four cylinders, OM3921, OM3947, IH 6295, and ALT639-18020, that did not manage to sustain the additional 10,000 cycles leaked at 9,048 cycles (18.1 years additional service life), 9,388 cycles (18.8 years additional service life), 6,295 cycles (12.6 years additional service life), and 6,297 cycles (12.6 years additional service life), respectively. All cylinders failed in a "leak before burst" fashion, validating the fail safe nature of the DOT CFFC 5th Revision design requirements.

6.2.2. MAE Analysis

During cyclic fatigue a copious amount of MAE data was acquired. For undamaged cylinders that were cycled up to the maximum developed pressure during fast filling (i.e., no notches, impact damage, etc.), none of the waveforms were from sources that were compromising the structural integrity of the cylinder; a majority of the waveforms were due to mechanical rubbing from the containment fixture and flow noise during the de-pressurization stage. The reason for no real MAE data is due to the fact that the cylinders have been subjected to several cycles up to the maximum developed pressure, and theoretically three pressurizations up to test pressure. Thus, no new damage was accumulated in the composite during the cyclic fatiguing. As mentioned previously, from the design requirements in the DOT CFFC 5th Revision [1], the stress in the fiber at the operating pressure of a cylinder must be below 30%. Hence, the fibers (the primary load bearing member of the design) are not stressed to a great enough level such that the composite overwrap could begin to deteriorate and compromise the cylinders strength.

During the EOL burst test, the MAE analysis of the two test pressure cycles before the burst pressurization ramp for the cylinders that were subjected to an additional twenty years of service life (summarized in Table 6.2), all twenty-one tested cylinders were found to meet the MAE life extension requirements of [8], and all twenty-one cylinders burst above the minimum required burst pressure (15,300 psi).

A representative plot of the background energy oscillations during the burst pressurization cycle for a cylinder that was subjected to a simulated additional twenty years of service life and burst above the minimum design requirement is shown in Figure 6.12. The background energy oscillation pressure (BEOP) was determined as the pressure within the cylinder at which the background energy oscillation multiplicative factor (M_O) of two was exceeded; all BEOP determinations are presented in Appendix B.

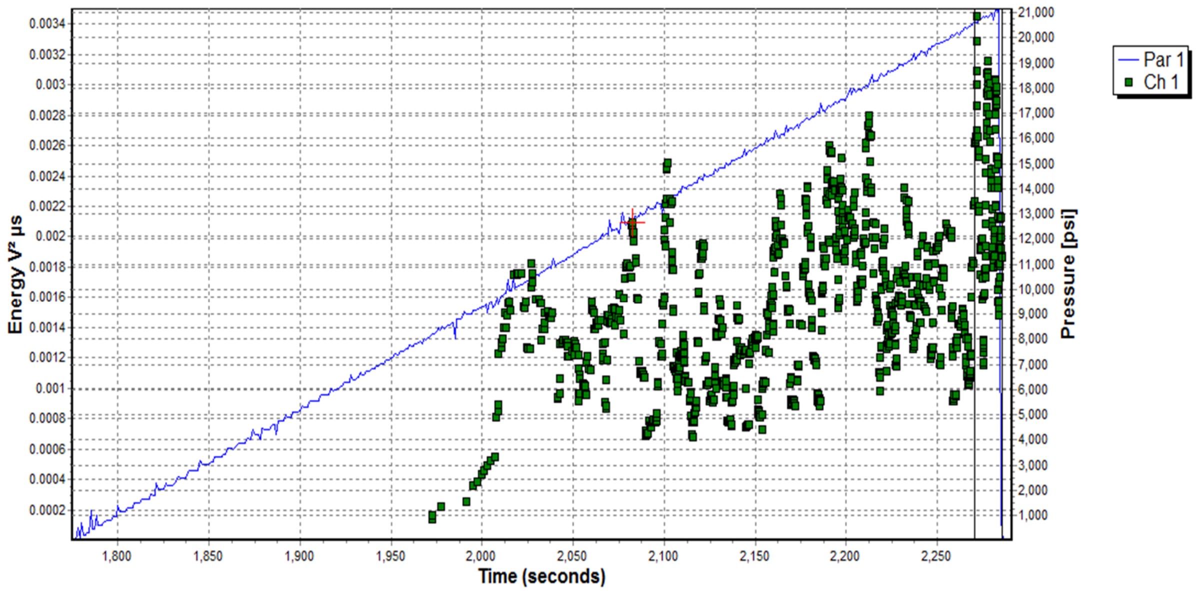

Figure 6.12 – Background Energy Oscillation for ALT639 – 18974.

6.3 Simulated Impact

6.3.1. Mechanical Response

Table 6.3 presents the results from all cylinders that were subjected to a simulated impact and then an EOL Burst test or cycled and then subsequently an EOL Burst test (Section 5.3). All cylinders which were subjected to an EOL Burst test, burst above the minimum design requirements of the DOT-CFFC 5th Revision [1]. It was observed that of the five SCBA cylinders that were subjected to the ISO simulated impact, three of the five cylinders managed to achieve an additional twenty years of simulated service life while the remaining two cylinders, ALT604 – 5582 and ALT639 – 40157, leaked at 5474 (10.9 years additional service life) and 6651 cycles (13.3 years additional service life), respectively. Further it is pointed out that none of the five cylinders that were subjected to the DOT/DWC extreme impact simulation were able to achieve an additional twenty years of simulated service life. It is believed that the extreme nature of the impact causes a delamination between the composite overwrap and the aluminum liner which allows a localized bending moment within the aluminum liner which causes the liner to fatigue at a greater rate due to the superimposed membrane and bending stresses. The greater state of stress provides a greater crack driving force, resulting in greater crack growth rates and cylinder leakage. Due to the extreme nature of the impact simulation, the number of cycles to achieve may need some revision, potentially 2500 cycles such that it could be shown that a severely impacted cylinder could withstand an additional five years of service, and then be identified by MAE (Section 6.3.2) at the five year re-qualification.

Table 6.3 – Cyclic pressurization result, stiffness, burst pressure, MAE life extension results, , elastic expansion, and visual inspection results for all cylinders that were subjected to a simulated impact and/or a simulated impact with subsequent cyclic pressurizations to the maximum developed pressure during fast fill.

Test	Location	DOT-SP	Time	Designation	SN	Mfg Date	Pressure	Visually Condemned [Y/N]	Burst Pressure [psi]	BEOP [psi]	BEOP % Burst	MAE Life Extension Met [Y/N]	Initial Hoop Modulus [Msi]	Initial Axial Modulus [Msi]	Secondary Hoop Modulus [Msi]	Secondary Axial Modulus [Msi]	Elastic Expansion [cc]	REE [cc]	Pass Hydro [Y/N]
ISO Drop and Burst	FDNY	SCI	60	ALT 604	3567	05/98	4500	Y	19719	12084	61.3%	Y	9.9	10.1	9.2	7.0	141.1	143.0	Y
ISO Drop and Burst	Fairfax, VA	Luxfer	45	OM	3983	08/98	4500	N	18207	12831	70.5%	Y	10.5	9.9	8.0	5.6	104.1	113.0	Y
ISO Drop and Burst	South Berwick, ME	Luxfer	30	IH	2482	07/98	4500	N	19579	11806	60.3%	Y	13.0	11.2	9.7	6.0	69.5	76.0	Y
ISO Drop and Burst	Houston, TX	SCI	60	ALT604	4371	07/98	4500	N	20975	10561	50.4%	Y	12.1	13.8	11.7	9.4	139.3	143.0	Y
ISO Drop and Burst	Howard, PA	SCI	30	ALT639	18722	01/99	4500	N	21275	13896	65.3%	Y	14.3	13.8	11.1	8.3	67.1	69.0	Y
ISO Drop, 10k cycle and burst	FDNY	SCI	60	ALT 604	6021	10/98	4500	Y	20362	12773	62.7%	Y	11.0	12.0	9.6	8.2	122.4	143.0	Y
ISO Drop, 10k cycle and burst	Fairfax, VA	Luxfer	45	OM	3938	08/98	4500	N	16349	10561	64.6%	Y	11.7	10.9	8.1	5.7	94.9	113.0	Y
ISO Drop, 10k cycle and burst	South Berwick, ME	Luxfer	30	IH	2036	06/98	4500	N	20283	10942	53.9%	Y	12.8	11.5	10.4	6.0	71.8	76.0	Y
ISO Drop, 10k cycle and burst	Houston, TX	SCI	60	ALT604	5582	11/98	4500	N	Leaked at 5474 cycles	-	-	-	-	-	-	-	-	-	-
ISO Drop, 10k cycle and burst	Howard, PA	SCI	30	ALT639	40157	12/99	4500	N	Leaked at 6651 cycles	-	-	-	-	-	-	-	-	-	-
DOT Drop and Burst	FDNY	SCI	45	ALT 695	3794	06/98	4500	N	17168	11264	65.6%	Y	12.4	10.4	9.0	5.6	83.8	105.0	Y
DOT Drop and Burst	Fairfax, VA	Luxfer	45	OM	3948	08/98	4500	N	16552	9975	60.3%	Y	11.0	10.5	7.6	5.6	100.4	113.0	Y
DOT Drop and Burst	Houston, TX	Luxfer	60	OP	11769	03/99	4500	N	18686	10927	58.5%	Y	12.7	11.5	9.7	5.9	133.1	150.0	Y
DOT Drop and Burst	South Berwick, ME	Luxfer	30	IH	2533	07/98	4500	N	17338	11068	63.8%	Y	13.1	12.0	9.7	6.1	67.9	76.0	Y
DOT Drop and Burst	Howard, PA	SCI	30	ALT639	18699	01/99	4500	N	19319	13192	68.3%	Y	14.8	13.2	10.1	7.7	63.3	71.1	Y
DOT Drop, 10k cycle and burst	FDNY	SCI	45	ALT 695	4638	07/98	4500	N	Leaked at 4640 cycles	-	-	-	-	-	-	-	-	-	-
DOT Drop, 10k cycle and burst	Fairfax, VA	Luxfer	45	OM	3975	08/98	4500	N	Leaked at 8255 cycles	-	-	-	-	-	-	-	-	-	-
DOT Drop, 10k cycle and burst	Kennebunkport, ME	SCI	30	ALT639	17697	12/98	4500	N	Leaked at 3819 cycles	-	-	-	-	-	-	-	-	-	-
DOT Drop, 10k cycle and burst	South Berwick, ME	Luxfer	30	IH	1854	06/98	4500	N	Leaked at 5473 cycles	-	-	-	-	-	-	-	-	-	-
DOT Drop, 10k cycle and burst	Howard, PA	Luxfer	30	ALT639	18601	01/99	4500	N	Leaked at 4188 cycles	-	-	-	-	-	-	-	-	-	-

In agreement with the Sections 6.1.1 and 6.2.1, all cylinders were found to respond in a bi-modulus fashion. The typical response of an impacted cylinder is shown in Figure 6.13, while stress-strain curves for all cylinders are provided in Appendix A. Results for stiffness, burst pressure, MAE life extension results, and visual inspection results are also summarized in Table 6.3. From Table 6.3, it is highlighted that of the thirteen burst tests summarized in this section, all thirteen cylinders met or exceeded the required minimum burst pressure of the DOT CFFC 5th Revision [1]. Such findings indicate that no deleterious effects on the strength of the SCBA cylinder were experienced when subjected to a simulated impact or a simulated impact and an additional twenty years of service life.

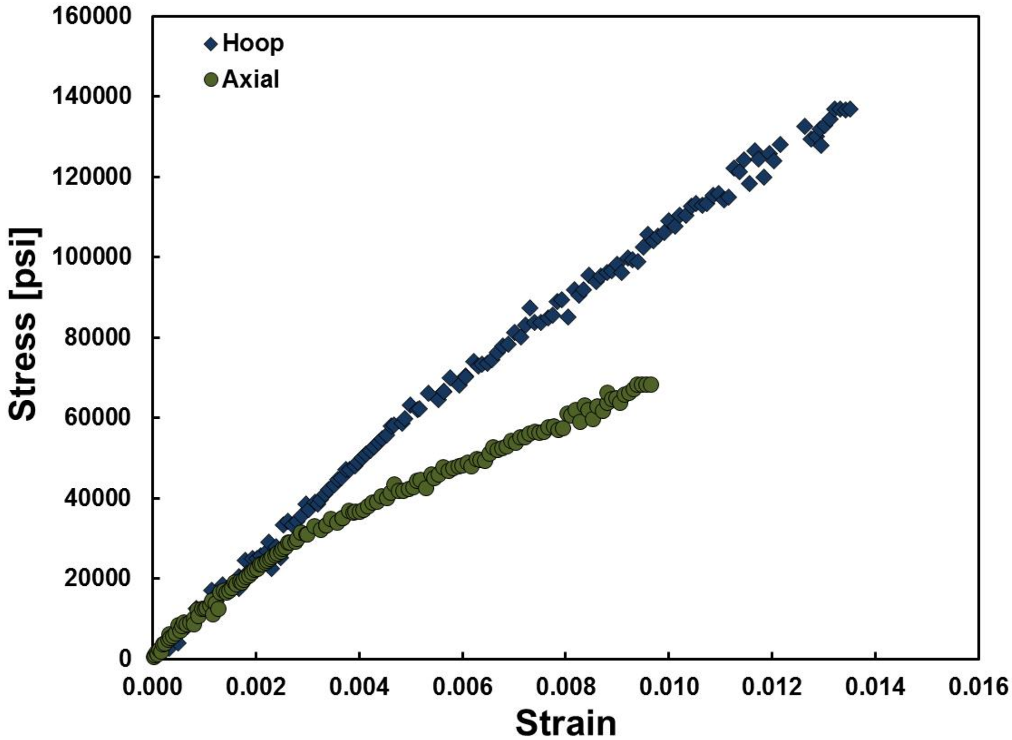

Figure 6.13 – Stress-strain response of ALT695-3794 operated under DOT-SP 10945.

To further confirm that a simulated impact and/or a simulated impact and twenty years of simulated additional service life had no deleterious effects on the SCBA burst pressure strength, Figure 6.14 compares the two parameter Weibull distributions for cylinders which only experienced fifteen years of service life (Section 1) to the distribution of cylinders which experienced a simulated impact and/or a simulated impact with an additional simulated twenty years of service. From Figure 6.14 it was observed that the scale and shape parameters of the Weibull distribution for cylinders which experienced fifteen years of service life was 19,840 psi and 13.3, respectively, while the scale and shape parameters of the Weibull distribution for cylinders which experienced fifteen years of service life and a simulated impact or a simulated impact and an additional twenty years of service was 19,635 psi and 13.8, respectively. Such findings indicate that a negligible change in burst strength was observed between the fifteen year old cylinders and the cylinders which experienced a simulated or a simulated impact with an additional simulated twenty years of service life.

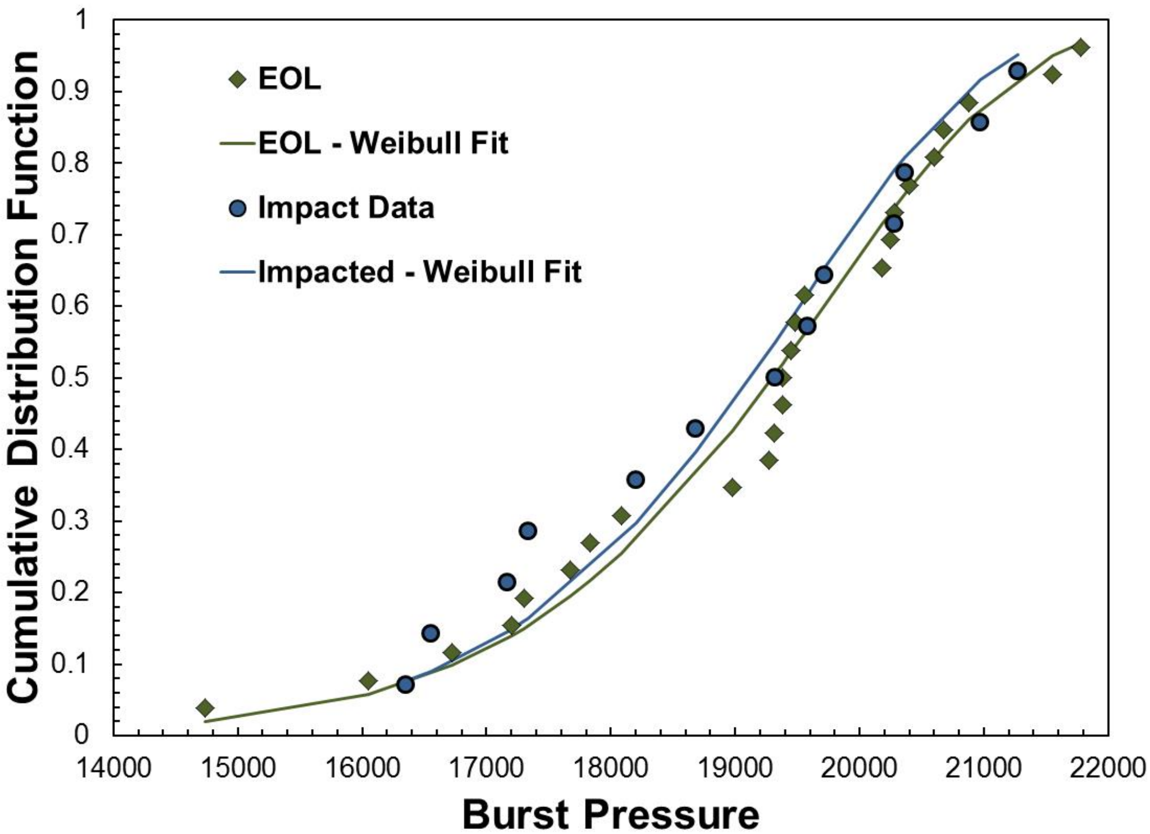

Figure 6.14 – A comparison of the two parameter Weibull distributions for cylinders which experienced fifteen years of service life (κ = 19,840 psi, β = 13.3) to cylinders which experienced fifteen years of service life and a simulated impact and/or a simulated impact and an additional twenty years of service (κ = 19,635 psi, β = 13.8).

6.3.2. MAE Analysis

Unlike the MAE data from undamaged SCBA cylinders that were cycled (Section 6.2.2) which did not exhibit any damage MAE events, cylinders which experienced a form of simulated impact exhibited a very specific and consistent type of damage mechanism during fatigue loading. To identify source mechanisms from the MAE waveforms, the weighted peak frequency (WPF), and concept of partial power (PP) was used to identify natural clustering of the various damage mechanisms which occur within composite materials as they are subjected to a stress state.

To highlight the utility of source mechanism classification, we first present a plot of partial power vs. weighted peak frequency for an impacted cylinder during a burst test. The data from the burst cycle of OM3938 (ISO drop, 10k cycle, and EOL Burst) is first analyzed because at the higher stress levels all of the damage mechanisms occur, while during fatigue it was found that one particular damage mechanism was prevalent. Figure 6.15 shows the partial power versus weighted peak frequency for OM3938 during the burst test of the cylinder. In Figure 6.15 the blue diamonds identify matrix cracking events, the green diamonds correspond to interfacial failure events, and the red diamonds signify fiber fracture events. From Figure 6.15, the natural clustering in the frequency domain of the damage mechanisms occurring within the composite material is readily observed; from this analysis, the power of source mechanism classification in the evaluation of the health of a composite material is evident as the approach undeniably identifies a clear segregation of the various failure mechanisms which occur in a composite material during its progression to failure.

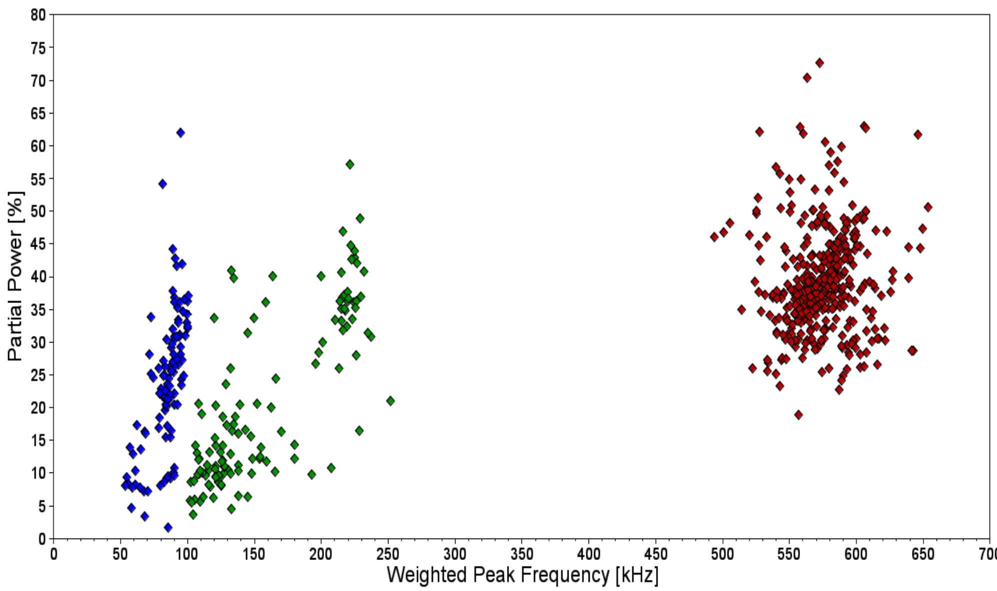

Figure 6.15 – Partial power versus weight peak frequency during a burst test pressurization for OM3938. The blue diamonds identify matrix cracking events, the green diamonds correspond to interfacial failure events, and the red diamonds signify fiber fracture events.

With the power of source mechanism classification recognized, the MAE data from fatigue testing of impacted cylinders may now be properly interpreted. Prior to performing source mechanism classification all events which corresponded to mechanical rubbing and flow noise were removed from the data set. Figure 6.16 presents the partial power versus weighted peak frequency plot for OM3938 during the 10,000 fatigue cycles. From Figure 6.16 it is observed that very few matrix cracking and fiber fracture events were observed, but a large number of interfacial failure events were observed. Due to the impact damage that was imparted on the cylinder, delamination between the various layers of the composite overwrapped pressure cylinder was present, and as the cylinder was cycled the delaminations were able to grow, as well as having the separated crack faces rub against one another generating frictional acoustic emission. Thus, the MAE signature during fatigue loading of a cylinder with simulated impact damage was found to be distinct and classifiable.

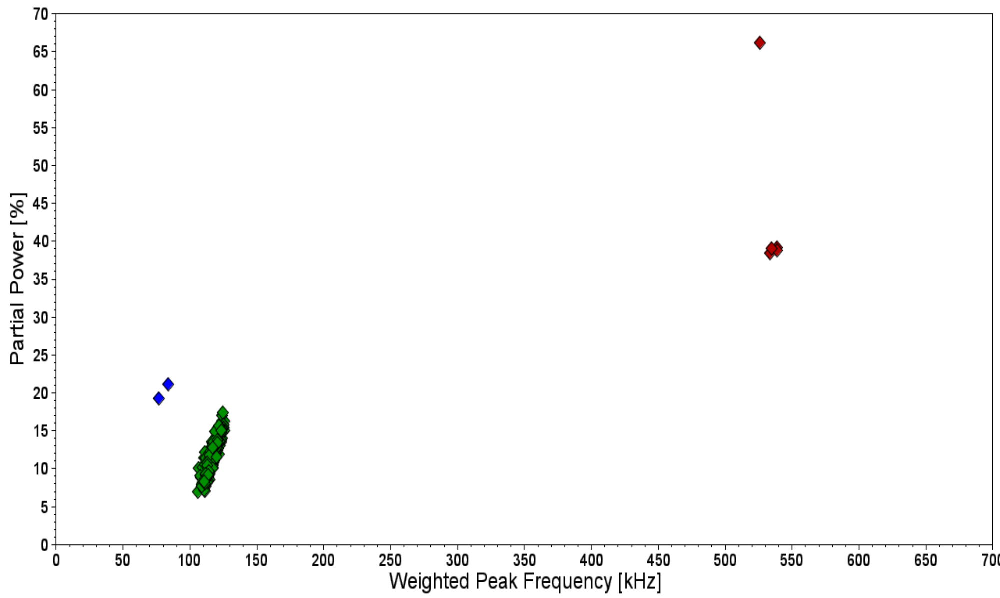

Figure 6.16 – Partial power versus weight peak frequency during 10,000 cycles to maximum developed pressure for OM3938.

For the thirteen cylinders with simulated impact damage that were subjected to the EOL burst testing, seven of the thirteen cylinders were found to exhibit at least one large delamination event (a representative waveform is shown in Figure 6.17) on the first test pressurization cycle, while emitting nothing on the second test pressure cycle. From the waveform shown in Figure 6.17, both the extensional and flexural wave modes are clearly evident with the flexure mode dominating the relative amount of energy in the waveform. The dominant amount of flexural mode is characteristic of out-of-plane sources commonly associated with delamination. Delamination type sources are not surprising in light of the fact that a new damage state was introduced to the composite microstructure during the simulated impact. On the first test pressure cycle after the simulated impact event, several acoustic emissions were released as the damage state within the composite evolved and reestablished equilibrium. The absence of the delamination type sources on the second test pressure cycle indicates that the damage state did not significantly compromise the stability of the composite overwrap, which is confirmed in the mechanical stiffness and burst pressure data presented in Table 6.3.

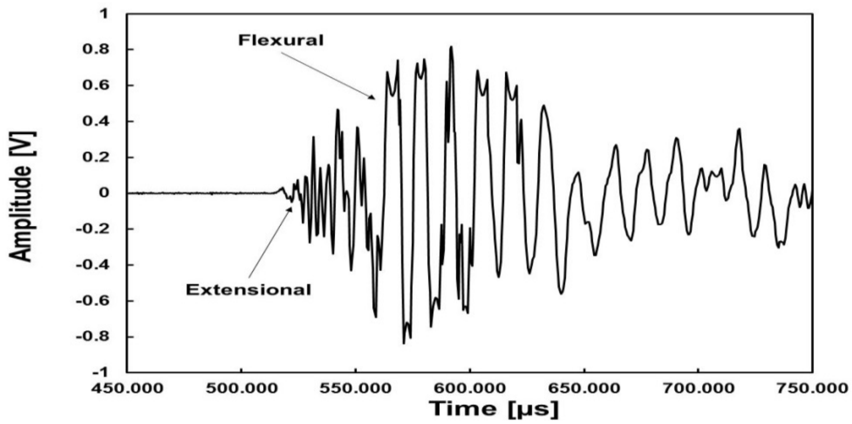

Figure 6.17 – Representative delamination waveform emitted from OM3948 during the first test pressurization cycle.

During the EOL burst test, the MAE analysis of the two test pressure cycles before the burst pressurization ramp for the cylinders that were subjected to a simulated impact, or a simulated impact and an additional twenty years of service life (summarized in Table 6.3), all thirteen tested cylinders were found to meet the MAE life extension requirements of [8], and all thirteen cylinders burst above the minimum required burst pressure (15,300 psi).

A representative plot of the background energy oscillations for a two channel test during the burst pressurization cycle for a cylinder that was subjected to the DOT extreme impact simulation and burst above the minimum design requirement is shown in Figure 6.18. The background energy oscillation pressure (BEOP) was determined as the pressure within the cylinder at which the background energy oscillation multiplicative factor (M_O) was exceeded; all BEOP determinations are presented in Appendix B. From Figure 6.18, it was found that the BEOP for channels 1 and 2 were 58.5% and 59.4% of the burst pressure of OP11769, respectively. Such findings demonstrate that the BEOP is relatively insensitive to sensor placement for a 60 minute SCBA sized cylinder.

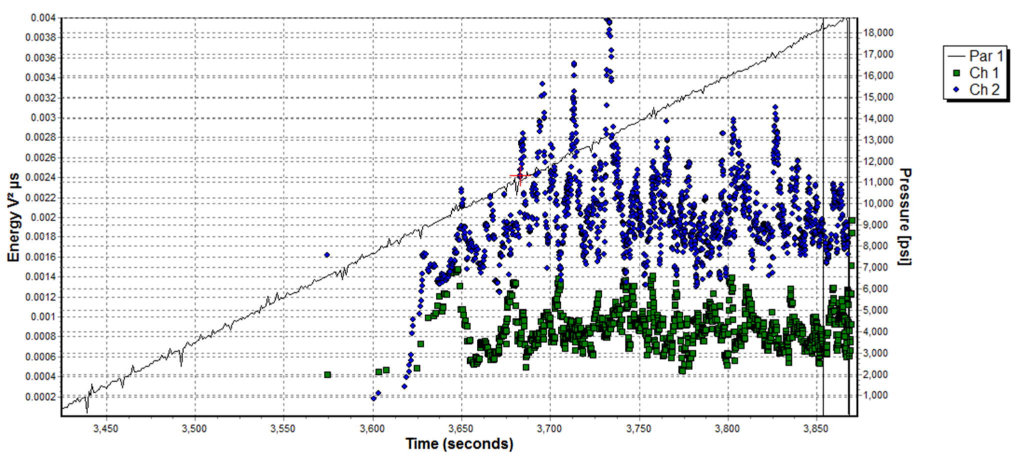

Figure 6.18 - Background Energy Oscillation for OP11769.

6.4 Notch Tolerance

6.4.1. Mechanical Response

For the nine cylinders with notches that were subjected to the EOL burst testing, all cylinders were found to meet the minimum required burst strength of 10,000 psi [2], and seven of the nine cylinders were found to meet the minimum burst pressure (15,300 psi) requirements of DOT CFFC 5th revision [1]. From a stiffness response perspective, all cylinders were found to respond in a bi-modulus fashion. The typical response of a cylinder is shown in Figure 6.19, while stress-strain curves for all notched cylinders are provided in Appendix A. Due to extreme delamination of the sacrificial layer, certain stress-strain curves did not perfectly follow the clean bi-modulus response that was observed in all other cylinders subjected to an EOL burst. Table 6.4 summarizes the physical testing of all notched SCBA cylinders covered in this report.

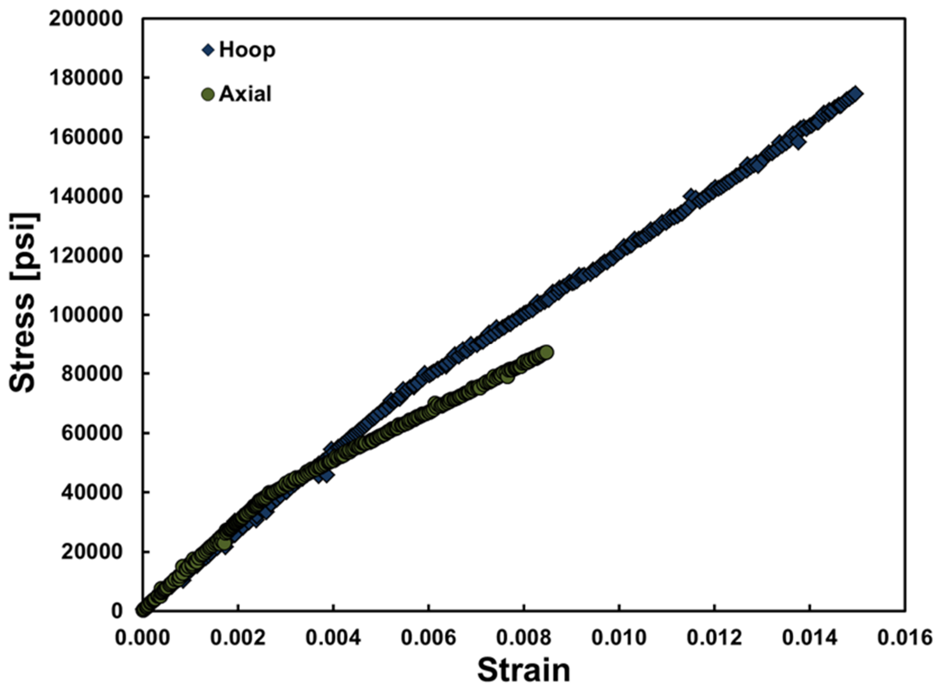

Figure 6.19 - Stress-strain response of ALT639-17732 operated under DOT-SP 10945.

Table 6.4 - Summary of burst strength, stiffness data, visual inspection results, elastic expansion results, and MAE life extension requirements results for all notched SCBA cylinders.

Test	Location	DOT-SP	Time	Designation	SN	Mfg Date	Pressure	Visually Condemned [Y/N]	Burst Pressure [psi]	BEOP [psi]	BEOP % Burst	MAE Life Extension Met [Y/N]	Initial Hoop Modulus [Msi]	Initial Axial Modulus [Msi]	Secondary Hoop Modulus [Msi]	Secondary Axial Modulus [Msi]	Elastic Expansion [cc]	REE [cc]	Pass Hydro [Y/N]
EOL Burst w/ ISO Notch	FDNY	SCI	45	ALT695	3929	06/98	4500	Y	17461	12020	68.8%	Y	12.5	12.9	8.8	3.8	81.1	105.0	Y
EOL Burst w/ ISO Notch	Fairfax, VA	Luxfer	45	OM	3984	08/98	4500	Y	14090	6054	43.0%	N (BEO)	16.5	7.0	N/A	N/A	81.3	113.0	Y
EOL Burst w/ ISO Notch	Kennebunkport, ME	SCI	30	ALT639	17732	12/98	4500	Y	18232	9345	51.3%	Y	13.3	14.8	10.5	8.2	70.2	71.1	Y
EOL Burst w/ ISO Notch	South Berwick, ME	Luxfer	30	IH	2554	07/98	4500	Y	16020	7119	44.4%	N (BEO)	14.5	11.1	11.2	6.0	63.8	76.0	Y
EOL Burst w/ ISO Notch	Howard, PA	SCI	30	ALT639	69925	11/00	4500	Y	19697	11704	59.4%	Y	13.3	6.8	10.0	7.7	76.8	71.1	N
ISO Notch cyclic fatigue, and Burst	FDNY	SCI	45	ALT695	4304	07/98	4500	Y	16948	9301	54.9%	Y	-	-	-	-	-	-	-
ISO Notch cyclic fatigue, and Burst	Fairfax, VA	Luxfer	45	OM	3971	08/98	4500	Y	Leaked at 4448 cylces	-	-	-	-	-	-	-	-	-	-
ISO Notch cyclic fatigue, and Burst	Houston, TX	Luxfer	60	OP	11129	03/99	4500	Y	13881	9169	66.1%	N (FRAE)	12.4	11.4	9.2	6.2	124.9	150.0	Y
ISO Notch cyclic fatigue, and Burst	South Berwick, ME	Luxfer	30	IH	1251	06/98	4500	Y	16298	10034	61.6%	Y	13.8	11.8	9.7	6.2	65.2	76.0	Y
ISO Notch cyclic fatigue, and Burst	Howard, PA	SCI	30	ALT639	17827	12/98	4500	Y	17280	9345	54.1%	Y	14.3	13.6	10.7	8.4	67.4	71.1	Y

Figure 6.20 compares the two parameter Weibull distributions for cylinders which only experienced fifteen years of service life (Section 6.1.1) to the distribution of notched SCBA cylinders. From Figure 6.20 it was observed that the scale and shape parameters of the Weibull distribution for cylinders which experienced fifteen years of service life was 19,840 psi and 13.3, respectively, while the scale and shape parameters of the Weibull distribution for cylinders which experienced fifteen years of service life and were notched or notched and subjected to 5,000 cycles was 17,461 psi and 10.7, respectively. Such findings indicate that introducing two notches, which were over 50% of the depth of the composite overwrap, had a measurable effect on the burst strength of the SCBA cylinders. A 12% reduction in the scale parameter of the Weibull distribution for notched cylinders as compared to un-notched cylinders was found. The surprising finding comes from the perspective that using the notched SCBA cylinder Weibull distribution, only 21.7% of SCBA cylinders with such a significant notch would burst below the minimum required burst pressure of DOT-CFFC 5th Revision [1].

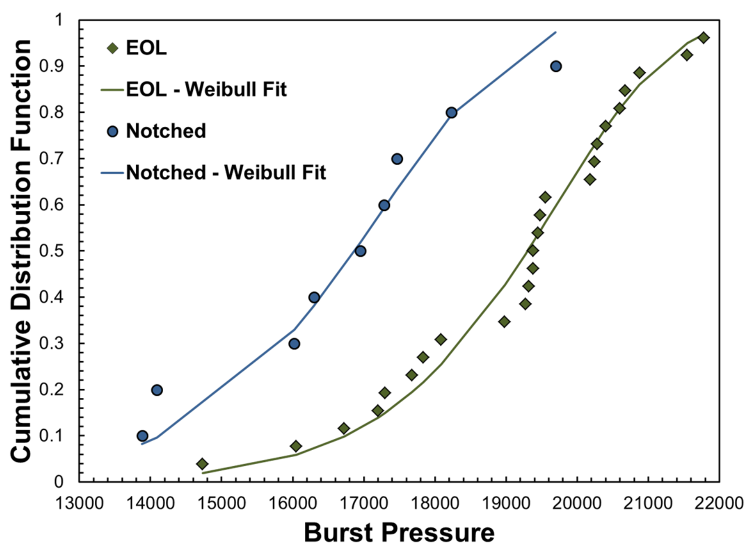

Figure 6.20 - A comparison of the two parameter Weibull distributions for cylinders which experienced fifteen years of service life (κ = 19,840 psi, β = 13.3) to cylinders which experienced fifteen years of service life and subjected to the notch tolerance testing (κ = 17,461 psi, β = 10.7).

All five cylinders that were subjected to cyclic fatigue testing met the requirements of ISO 11119.2 Section 8.5.7.2 [2], with only one of the five cylinders (OM3971) leaking during cyclic fatigue; OM 3971 leaked at 4,448 cycles. During cycling fatigue delamination originating from the tips of the axially oriented notch were noted (Figure 6.21), and confirmed through MAE source classification analysis.

Figure 6.21 – Delamination of the sacrificial glass fiber layers from the structural carbon fiber layers as a result of cyclic fatigue.

6.4.2. MAE Analysis

Using the power of source mechanism classification (highlighted in Section 6.3.2), the MAE data from notched cylinders could be properly interpreted. Prior to performing source mechanism classification all events which corresponded to mechanical rubbing and flow noise were removed from the data set. As a representative example, MAE data from the EOL burst test of ALT695-3929 was analyzed. Figure 6.22 presents the partial power versus weighted peak frequency for the EOL burst test of ALT695-3929, from which it was observed that a large number of interfacial failure events (particularly delaminations) were observed. Due to notching the cylinders, a free surface was created at which the hoop and helical wraps will tend to delaminate due to the extreme Poisson Ratio mismatch of the plies. As an example of this type of behavior, Figure 6.23 shows a notched SCBA cylinder that was taken to approximately 95% of its' burst strength and then de-pressurized in order to photograph the damage state. From Figure 6.23, the large amount of delamination originating from the free surfaces created at the axial notch was quite obvious, providing strong evidence that the MAE signature during pressurization of a notched cylinder was found to be distinct and classifiable.

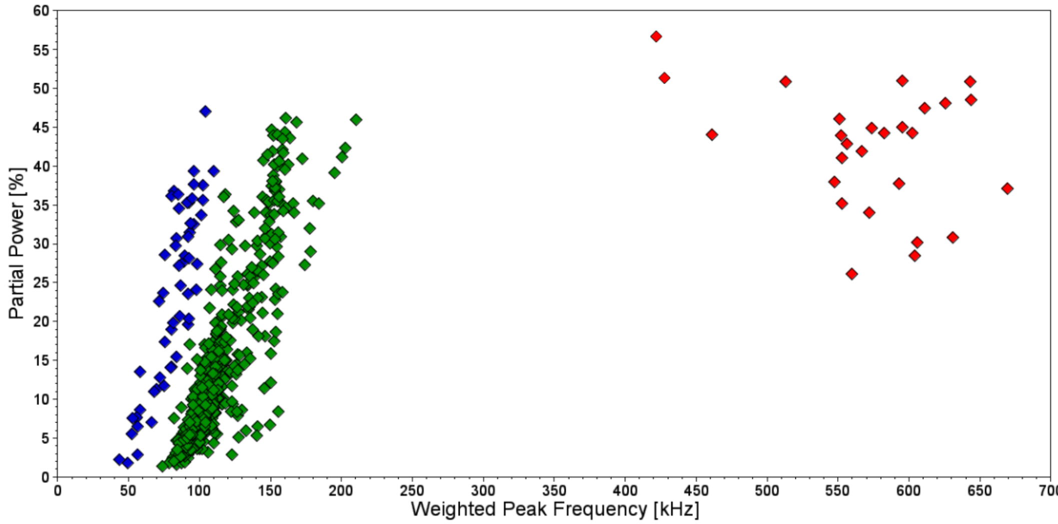

Figure 6.22 – Partial power versus weight peak frequency during a burst test pressurization for ALT695-3929. The blue diamonds identify matrix cracking events, the green diamonds correspond to interfacial failure events, and the red diamonds signify fiber fracture events.

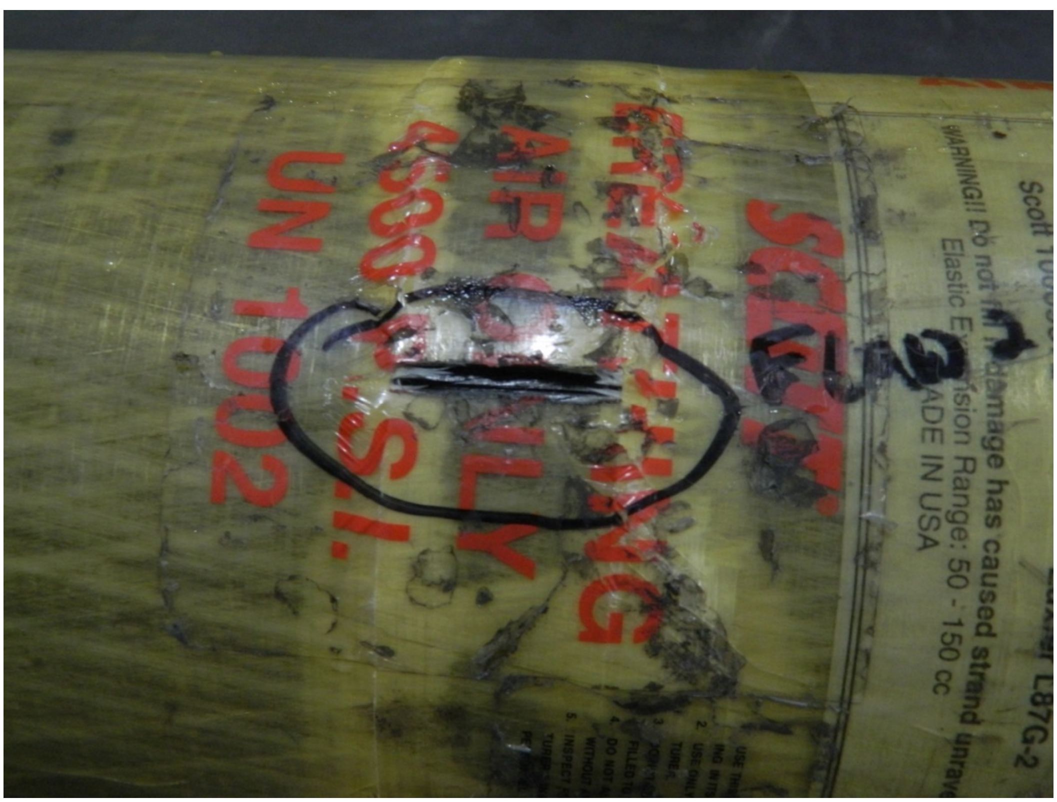

Figure 6.23 – Extreme amount of delamination originating from the axially oriented notch on a cylinder that was pressurized to 95% of its' burst pressure.

The two cylinders which burst below the minimum required burst pressure of DOT CFFC 5th revision [1] failed Digital Wave's MAE life extension requirements [8]. OM3984 failed the

MAE life extension requirements due to background energy oscillations on both test pressure cycles, while OP11129 failed the single event energy criterion on the second test pressure cycle. Additionally, one other cylinder (IH2554) failed Digital Wave's MAE life extension due to background energy oscillation on the first test pressure cycle; however, the cylinder did burst at 16,020 psi. For IH2554 (as with all notched cylinders), the ratio of background energy oscillation pressure to burst pressure was lower as compared to un-notched cylinders, due to the extreme stress concentrator that was put into the notched SCBA cylinders. An example of the determination of the background energy oscillations for a notched cylinder is shown in Figure 6.24, while all BEO plots are presented in Appendix B.

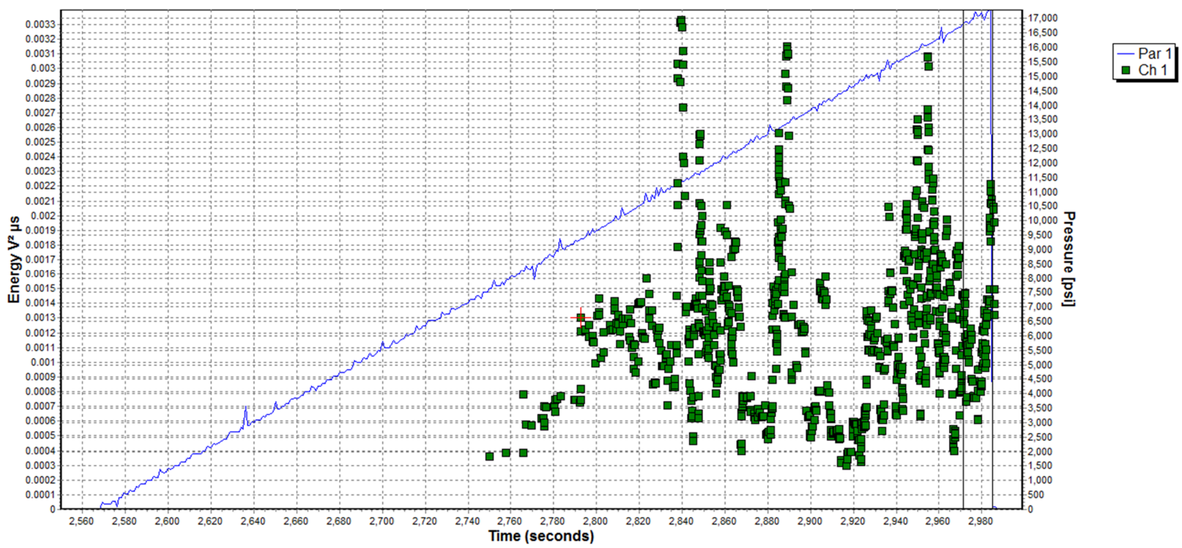

Figure 6.24 – Background Energy Oscillation for ALT639 - 17827.

6.5 Sulfuric Acid Resistance

6.5.1. Mechanical Response

Results for stiffness, burst pressure, MAE life extension, and visual inspection are summarized in Table 6.5 for the five cylinders which were held at operating pressure for 100 hours with a 6" sulfuric acid patch painted on the cylinder wall and then subsequently burst or subjected to the DOT drop, cycled from 200 – 5192 psi for 1,000 cycles, exposed to sulfuric acid for 100 hours while being held at service pressure, and then burst (Section 5.5). It was observed that all five SCBA cylinders that were subjected to the sulfuric acid exposure burst well above the minimum burst pressure requirements of [1]. Such findings indicate that no deleterious effects on the strength of the SCBA cylinders were experienced when subjected to sulfuric acid. In agreement with the Sections 6.1-6.4 all cylinders were found to respond in a bi-modulus fashion. The typical stress-strain response of a sulfuric acid exposed cylinder is shown in Figure 6.25, while all stress-strain curves are provided in Appendix A.

Table 6.5 - Summary of burst strength, stiffness data, visual inspection results, elastic expansion results, and MAE life extension requirements results for all SCBA cylinders subjected to sulfuric acid exposure.

Test	Location	DOT-SP	Time	Designation	SN	Mfg Date	Pressure	Visually Condemned [Y/N]	Burst Pressure [psi]	BEOP [psi]	BEOP % Burst	MAE Life Extension Met [Y/N]	Initial Hoop Modulus [Msi]	Initial Axial Modulus [Msi]	Secondary Hoop Modulus [Msi]	Secondary Axial Modulus [Msi]	Elastic Expansion [cc]	REE [cc]	Pass Hydro [Y/N]
Sulfuric Acid Hold and Burst	FDNY	SCI	45	ALT695	4333	07/98	4500	N	20268	11528	56.9%	Y	13.2	10.9	10.0	6.2	93.51	105	Y
Sulfuric Acid Hold and Burst	Fairfax, VA	Luxfer	45	OM	3918	08/98	4500	N	16284	9164	56.3%	Y	13.1	12.6	9.4	6.3	96.26	113	Y
Sulfuric Acid Hold and Burst	Kennebunkport, ME	SCI	30	ALT639	18800	01/99	4500	N	19008	10019	52.7%	Y	11.7	12.9	10.0	6.5	80.14	71.1	N
Sulfuric Acid Hold and Burst	South Berwick, ME	Luxfer	30	IH	1750	06/98	4500	N	16416	10576	64.4%	Y	13.1	12.4	9.7	6.2	68.04	76	Y
Sulfuric Acid Hold and Burst	Howard, PA	SCI	30	ALT639	18713	01/99	4500	N	17148	11440	66.7%	Y	13.2	12.6	9.3	7.5	73.28	71.1	N

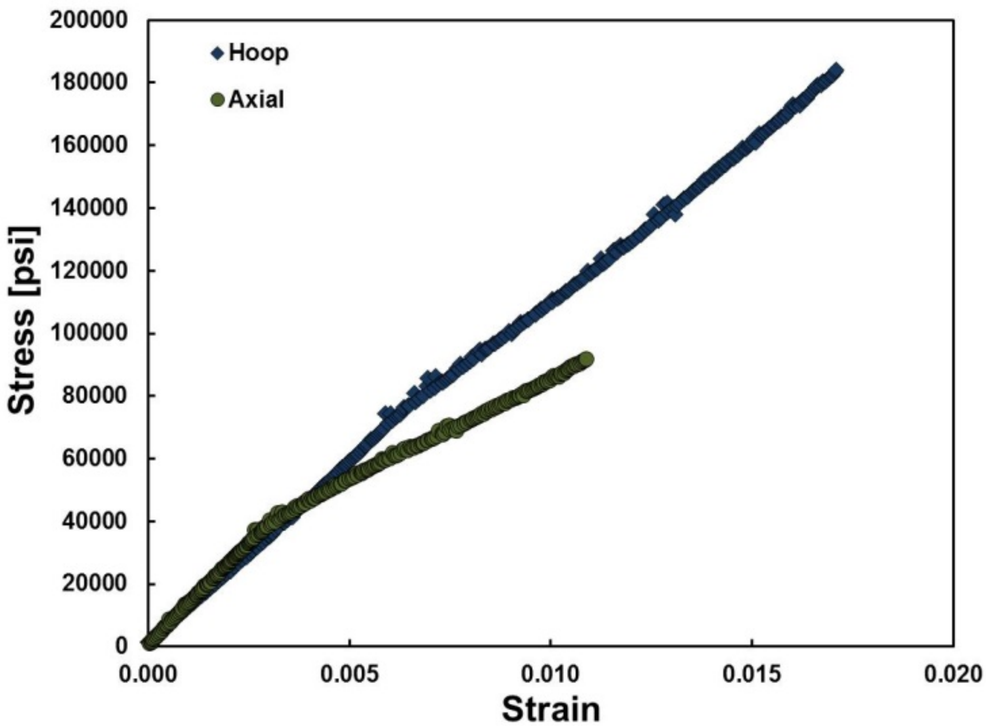

Figure 6.25 – Stress-strain response of ALT639-18800 during EOL burst. ALT639-18800 was subjected to a 100 hour hold at operating pressure while being exposed to sulfuric acid, and subsequently burst.

After the 100 hour hold at operating pressure with the sulfuric acid patch painted on the cylinder, the only physical sign of acid exposure were patches of discoloration of the gel coat of all DOT-SP 10945 cylinders (as shown in Figure 6.26). The DOT-SP 10915 cylinders did not show any physical signs of acid exposure.

Figure 6.26 – Typical discoloration of the gel coat of DOT-SP 10945 cylinders after 100 hours of sulfuric acid exposure while being held at operating pressure.

6.5.2. MAE Analysis

No MAE waveforms were detected during the 100 hour hold at service pressure on any of the sulfuric acid exposed DOT-CFFC cylinders which indicate that sulfuric acid attack of the reinforcing carbon fibers was not occurring. Because the sulfuric acid could not penetrate the gel coat and sacrificial layers, no sulfuric acid attack could occur to the strength member (carbon fibers). During the EOL burst test, the MAE data from the test pressure cycles before the burst pressurization ramp for the cylinders that were subjected to sulfuric acid exposure while being held at service pressure, or a simulated DOT impact, followed by 1000 cycles to maximum developed pressure (Section 5.2), and then held at operating pressure while exposed to sulfuric acid was analyzed; all five tested cylinders were found to meet the MAE life extension requirements of [8], and all five cylinders burst above the minimum required burst pressure (15,300 psi, Table 6.5).

A representative plot of the background energy oscillations for a cylinder that was subjected to the sulfuric acid exposure and burst above the minimum design requirement is shown in Figure 6.27. The background energy oscillation pressure (BEOP) was determined as the pressure within the cylinder at which the background energy oscillation multiplicative factor (M_O) was exceeded; all BEOP determinations are presented in Appendix B. From Figure 6.27, it was found that the BEOP for ALT639-18713 occurred at 66.7% of the burst pressure of the cylinder.

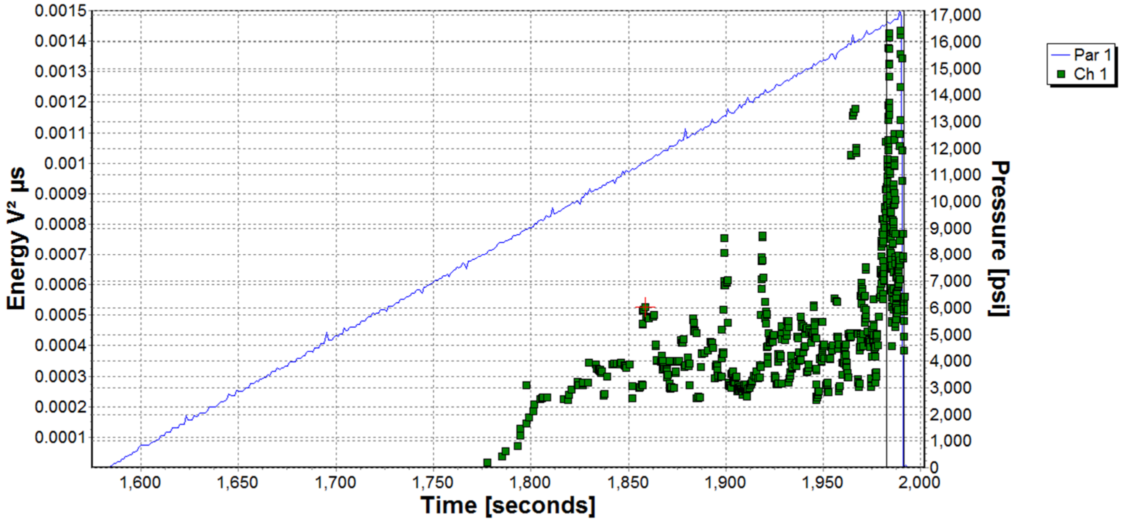

Figure 6.27 – Background energy oscillation pressure determination for ALT639-18713.

6.6 Re-autofrettage and corroded liners

6.6.1. Mechanical Response

A representative stress-strain response in the hoop direction during the two re-autofrettage cycles is shown in Figure 6.28. In Figure 6.28, it is seen that the SCBA pressure cylinder exhibits a bi-modulus response up to an internal pressure of 7500 psi on the first re-autofrettage cycle, past which point the aluminum liner is plastically deforming. Upon removal of the internal pressure, a permanent amount of deformation (plastic strain, ε_p) had been imparted on the SCBA pressure cylinder. The average amount of permanent deformation from the first re-autofrettage pressure cycle for all eight cylinders was found to be 358 $\mu\varepsilon$. On the second test pressure cycle, the SCBA pressure cylinder responded in a linear elastic fashion up to the “new test pressure” of 8500 psi (Figure 6.28).

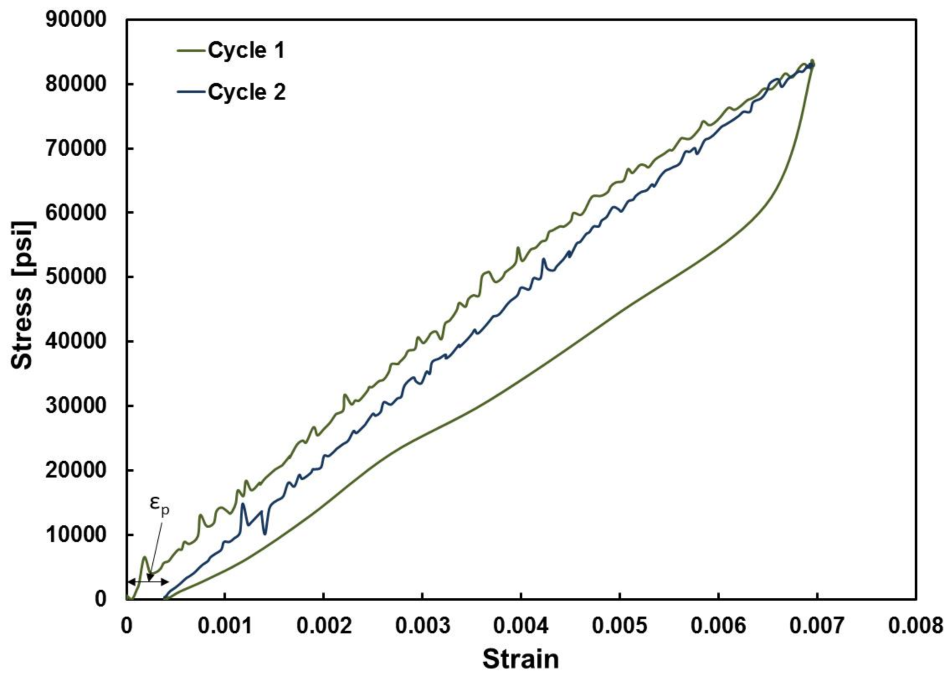

Figure 6.28 – Typical stress-strain response in the hoop direction of an SCBA cylinder during the re-autofrettage procedure.

In agreement with Section 6.2, it was again found that during cyclic fatigue testing the composite overwrap's properties were not degrading during cyclic fatigue to the maximum developed pressure (Figure 6.29). Figure 6.29 presents the maximum and minimum strain for each cycle during cyclic fatigue testing for a cylinder that was re-autofrettaged, from which it is clear that the maximum and minimum hoop strain values were not changing from cycle to cycle (when accounting for the variability in temperature and true peak pressure). Such a mechanical response confirms that the stiffness of the composite overwrap was not being degraded due to cyclic fatigue.

Results for number of cycles obtained, stiffness, burst pressure, MAE life extension, and visual inspection are summarized in Table 6.6 for the eight cylinders that were re-autofrettaged, and the seven cylinders which were not re-autofrettaged. Seven of the eight (87.5%) cylinders which were re-autofrettaged achieved 10,000 fatigue cycles up to the maximum developed pressure. Conversely, six of the seven (85.7%) cylinders which were not re-autofrettaged leaked before obtaining 10,000 cycles to the maximum developed pressure. Such findings strongly support the approach of re-autofrettaging the aluminum liners in order to blunt any existing cracks which were caused by improper hydrostatic testing. Section 9.0 provides an analysis of the estimation of the fatigue life for the cylinders that were and were not re-autofrettaged. The fatigue life estimations of Section 9.0 were in good agreement with the cyclic fatigue results presented in this section.

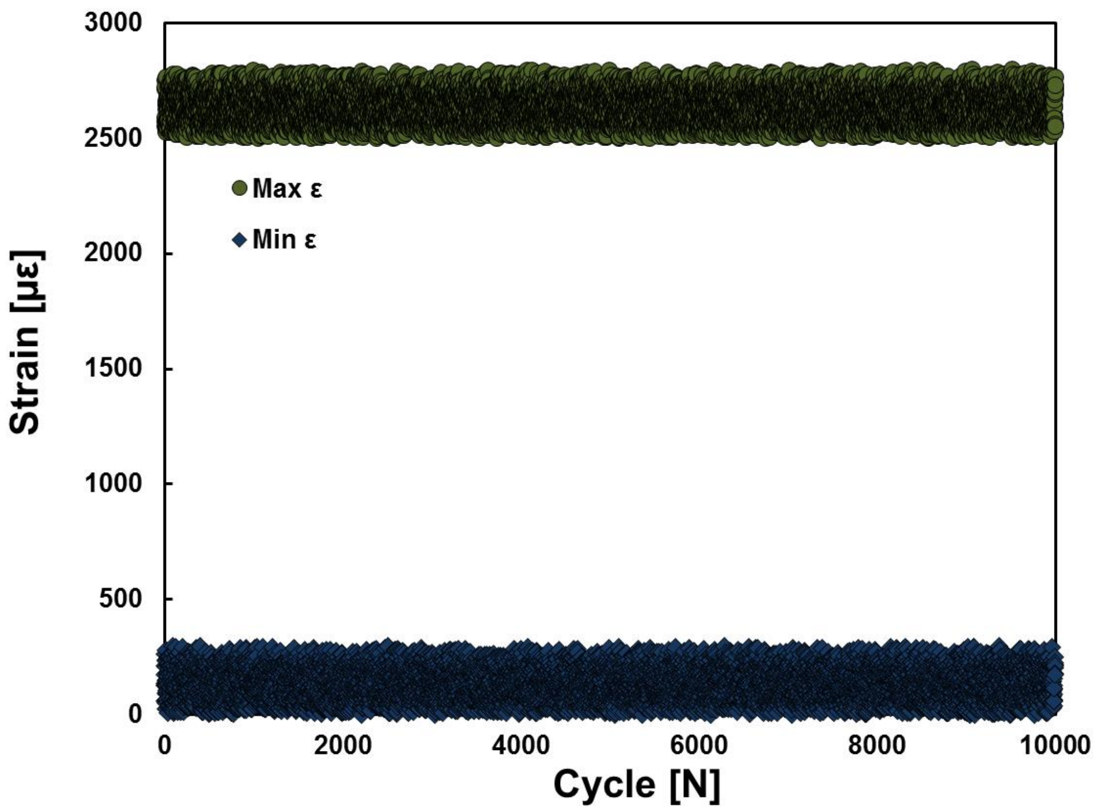

Figure 6.29 - Maximum and minimum strain values on each cycle of a cyclic fatigue test for a cylinder that was re-autofrettaged.

Table 6.6 – Summary of number of cycles achieved, stiffness, burst strength, MAE life extension analysis, visual inspection, and elastic expansion results for the SCBA's with heavily corroded liners that were and were not re-autofrettaged.

Test	Location	DOT-SP	Time	Designation	SN	Mfg Date	Pressure	Visually Condemned [Y/N]	Burst Pressure [psi]	BEOP [psi]	BEOP % Burst	MAE Life Extension Met [Y/N]	Initial Hoop Modulus [Msi]	Initial Axial Modulus [Msi]	Secondary Hoop Modulus [Msi]	Secondary Axial Modulus [Msi]	Elastic Expansion [cc]	REE [cc]	Pass Hydro [Y/N]
Corroded liner, 10k and Burst	Fairfax, VA	Luxfer	45	OM	3985	08/98	4500	N	Leaked at 5369 cycles	-	-	-	-	-	-	-	-	-	-
Corroded liner, 10k and Burst	Fairfax, VA	Luxfer	45	OM	3960	08/98	4500	N	Leaked at 5364 cycles	-	-	-	-	-	-	-	-	-	-
Corroded liner, 10k and Burst	Fairfax, VA	Luxfer	45	OM	3956	08/98	4500	N	Leaked at 8680 cycles	-	-	-	-	-	-	-	-	-	-
Corroded liner, 10k and Burst	Fairfax, VA	Luxfer	45	OM	3994	08/98	4500	N	Leaked at 5369 cycles	-	-	-	-	-	-	-	-	-	-
Corroded liner, 10k and Burst	Fairfax, VA	Luxfer	45	OM	4045	09/98	4500	N	19042	10532	55.3%	Y	11.1	9.34	7.77	4.66	102.74	113	Y
Corroded liner, 10k and Burst	Fairfax, VA	Luxfer	45	OM	3969	08/98	4500	N	Leaked at 6986 cycles	-	-	-	-	-	-	-	-	-	-
Corroded liner, 10k and Burst	Fairfax, VA	Luxfer	45	OM	3973	08/98	4500	N	Leaked at 6568 cycles	-	-	-	-	-	-	-	-	-	-
Corroded liner, AF, 10k and Burst	Fairfax, VA	Luxfer	45	OM	3903	08/98	4500	N	Leaked at 6984 cycles	-	-	-	-	-	-	-	-	-	-
Corroded liner, AF, 10k and Burst	Fairfax, VA	Luxfer	45	OM	3982	08/98	4500	N	16723	9375	56.1%	Y	12.4	12.1	9.2	6.7	102.1	113	Y
Corroded liner, AF, 10k and Burst	Fairfax, VA	Luxfer	45	OM	3917	08/98	4500	N	16298	9433	57.9%	Y	12.6	12.0	9.3	6.3	100.29	113	Y
Corroded liner, AF, 10k and Burst	Fairfax, VA	Luxfer	45	OM	3957	08/98	4500	N	17256	11684	67.7%	Y	12.9	13.3	9.37	7.18	96.09	113	Y
Corroded liner, AF, 10k and Burst	Fairfax, VA	Luxfer	45	OM	3914	08/98	4500	N	15581	9589	61.5%	Y	12.6	12.6	9.25	6.28	97.84	113	Y
Corroded liner, AF, 10k and Burst	Fairfax, VA	Luxfer	45	OM	3912	08/98	4500	N	16166	9434	58.4%	Y	12.9	11.6	9.4	5.69	98.25	113	Y
Corroded liner, AF, 10k and Burst	Fairfax, VA	Luxfer	45	OM	3954	08/98	4500	N	15815	9501	60.1%	Y	12.6	11.8	9.76	5.83	100.99	113	Y
Corroded liner, AF, 10k and Burst	Fairfax, VA	Luxfer	45	OM	3925	08/98	4500	N	17456	10458	59.9%	Y	13	12.4	9.49	6.12	97.85	113	Y

In agreement with all previous sections, all cylinders were found to respond in a bi-modulus fashion. The one caveat to the similarity of the stress-strain response for the re-autofrettaged cylinders was that the secondary modulus did not occur until 8500 psi (as opposed to 7500 psi for all other cylinders) due to the work hardening that occurred within the aluminum liner during the re-autofrettage process. A typical stress-strain response of a re-autofrettaged cylinder is shown in Figure 6.30, while all other stress-strain curves are provided in Appendix A. All cylinders with heavily corroded liners (re-autofrettaged and not) were found to burst above the minimum required burst pressure of [1], thus, the re-autofrettage pressure (8500 psi) did not adversely affect the burst strength of the SCBA CFFC cylinders.

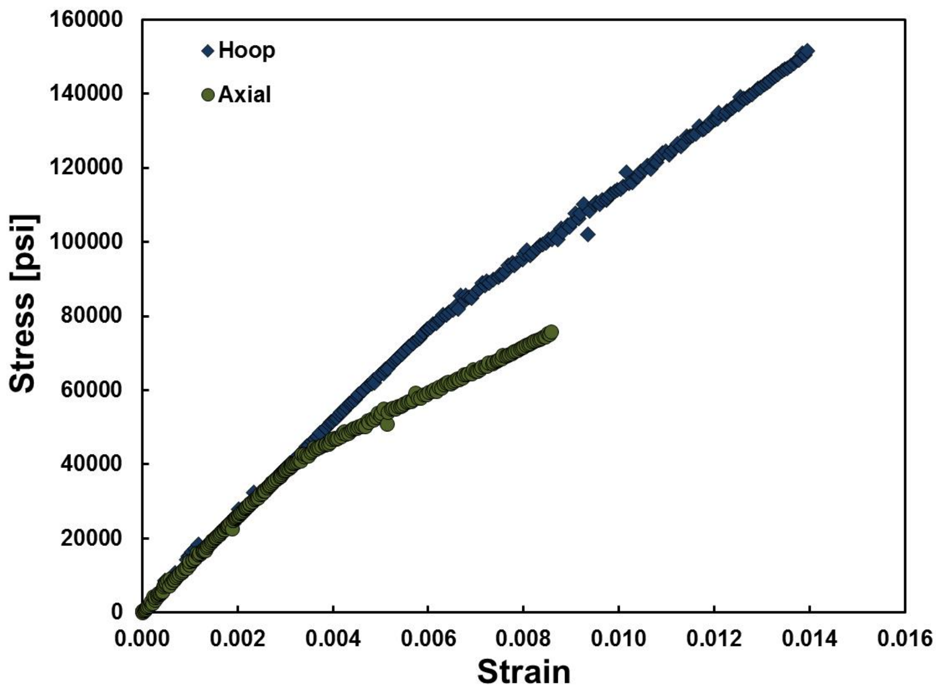

Figure 6.30 – Stress-strain response for a re-autofrettaged SCBA CFFC cylinder.

Moreover, it could be argued that a test pressure of 8500 psi for DOT-CFFC cylinders provides a more appropriate comparison of cylinder performance when comparing the test pressure of the cylinder to the minimum design burst pressure of the cylinder. DOT-FRP1 SCBA cylinders that have an operating pressure of 4500 psi, have a test pressure of 7500 psi, and a minimum design burst pressure of 13,500 psi (test pressure/minimum design burst pressure equal to 55.5%). Analogously, DOT-CFFC SCBA cylinders that have an operating pressure of 4500 psi, have a test pressure of 7500 psi, and a minimum design burst pressure of 15,300 psi (test pressure/minimum design burst pressure equal to only 49.0%). If a test pressure of 8500 psi were used on DOT-CFFC cylinders, then the ratio of test pressure to minimum design burst pressure would mimic that of the DOT-FRP1 SCBA pressure cylinders.

6.6.2. MAE Analysis

During cyclic fatigue a copious amount of MAE data was acquired. For the SCBA DOT-CFFC cylinders with heavily corroded liners (both re-autofrettaged and not) that were cycled up to the maximum developed pressure during fast filling, none of the detected MAE waveforms were from sources that were compromising the structural integrity of the cylinder; a majority of the waveforms were due to mechanical rubbing from the containment fixture and flow noise during the de-pressurization stage. The reason for no real MAE data is due to the fact that the cylinders have been subjected to several cycles up to the maximum developed pressure, and theoretically three pressurizations up to test pressure (with an additional two pressurizations up to 8500 psi for the re-autofrettaged cylinders). Thus, no new damage was accumulated in the composite during the cyclic fatiguing up to the maximum developed pressure during fast filling. As mentioned previously, from the design requirements in the DOT CFFC 5th Revision [1], the stress in the fiber at the service pressure of a cylinder must be below 30%. Hence, the fibers (the primary load bearing member of the design) are not stressed to a great enough level such that the composite overwrap could begin to deteriorate and compromise the cylinder's strength.

During the EOL burst test, MAE analysis of the two test pressure cycles before the burst pressurization ramp for the cylinders that were subjected to an additional twenty years of service life was performed (summarized in Table 6.6). All eight burst tested cylinders were found to meet the MAE life extension requirements of [8], and all eight cylinders burst above the minimum required burst pressure (15,300 psi).

A representative plot of the background energy oscillations during the burst pressurization cycle for a cylinder that was subjected to a simulated additional twenty years of service life after the re-autofrettage procedure and burst above the minimum design requirement is shown in Figure 6.31. The background energy oscillation pressure (BEOP) was determined as the pressure within the cylinder at which the background energy oscillation multiplicative factor (M_O) was exceeded; all BEOP determinations are presented in Appendix B.

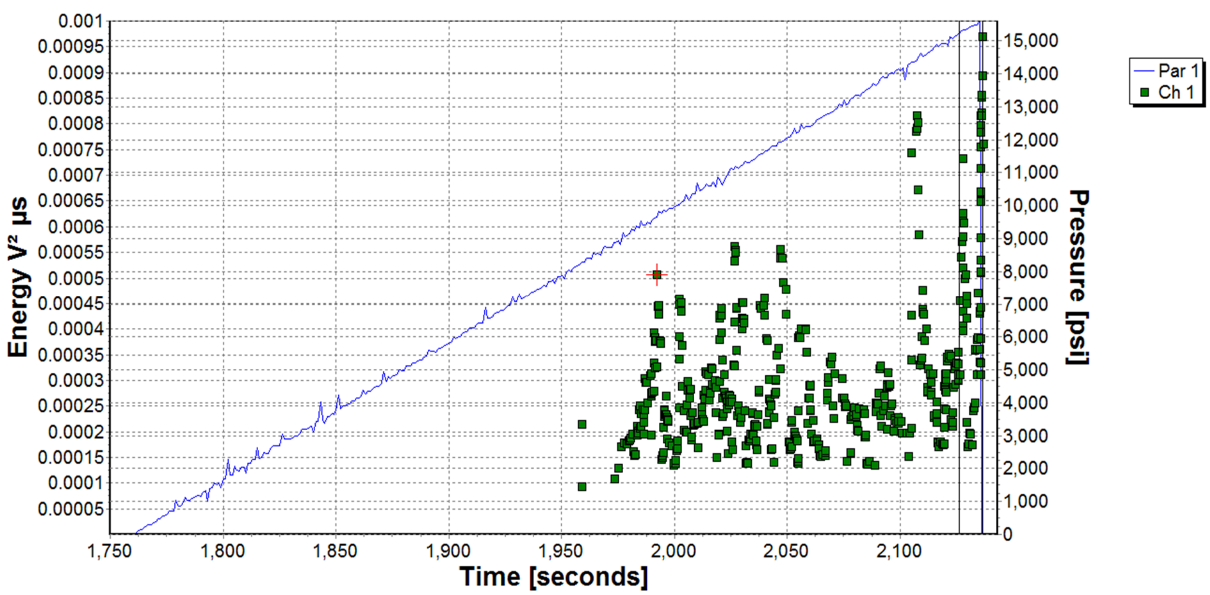

Figure 6.31 – Background Energy Oscillation Pressure for an SCBA CFFC cylinder (OM 3914) which was re-autofrettaged, achieved 10,000 cycles up to the maximum developed pressure during fast fill, and then burst above the minimum required burst pressure.

6.7 Predictive capability of MAE

It was shown in [3] that the Background Energy began oscillating at a consistent pressure relative to the ultimate burst strength of a given cylinder. The data from [3] is represented here for completeness in Figure 6.32. From Figure 6.32, it is seen that on average a cylinder began oscillating at a pressure of 61.6% of its' respective burst pressure. Further, it was found that the distribution of normalized Background Energy Oscillation Pressures (BEOP/P_B) was tightly grouped about the mean (a standard deviation of 4.6%). Hence, due to the consistent onset of BEOP, and the tight clustering of the distribution of the BEOP, it was found that the BEOP can be used as a reliable predictive metric for the burst strength of a given SCBA pressure cylinder [3].

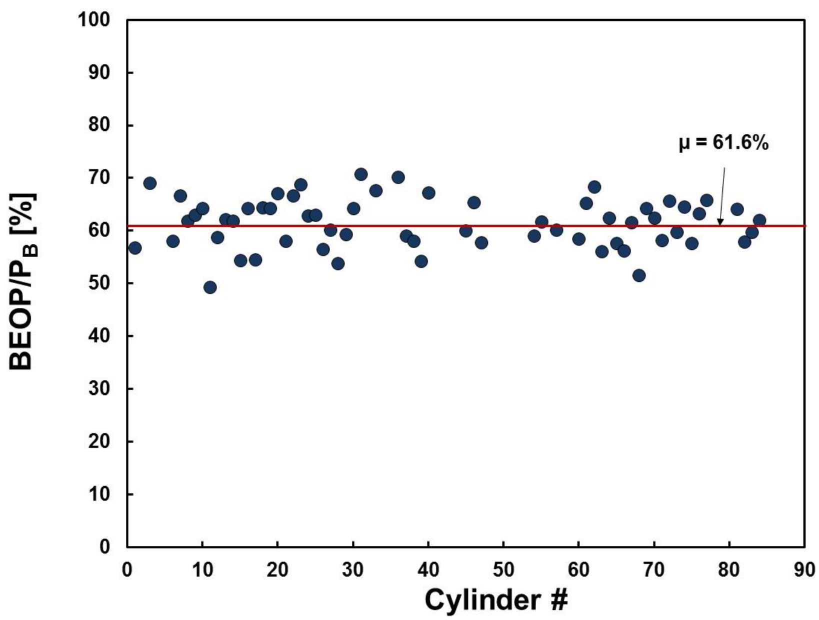

Figure 6.32 – Background Energy Oscillation Pressure (BEOP) as a function of burst pressure (P_B) for all cylinders tested in the Navy SCBA test program [1].

Similarly, in this study the normalized Background Energy Oscillation Pressure (BEOP/P_B) was found to occur at a consistent value (Figure 6.33). From Figure 6.33, it is seen that on average for the civilian SCBA pressure cylinders tested, a cylinder began oscillating at a pressure of 60.7% of its' respective burst pressure. Further, it was found that the distribution of normalized Background Energy Oscillation Pressures (BEOP/P_B) was tightly grouped about the mean (a standard deviation of 5.7%). Thus, the predictive capability of the Background Energy Oscillations and Modal Acoustic Emission has again been shown in this study.

To further demonstrate the relationship between the Background Energy Oscillation Pressure and the burst pressure of an SCBA pressure cylinder, Figure 6.34 shows the burst pressure of a cylinder as a function of the Background Energy Oscillation Pressure. From Figure 6.34, it is observed that a strong correlation (goodness of fit coefficient equal to 0.51) existed between the BEOP and the burst pressure of a cylinder. Such a strong correlation further validates the predictive capability of the BEOP.

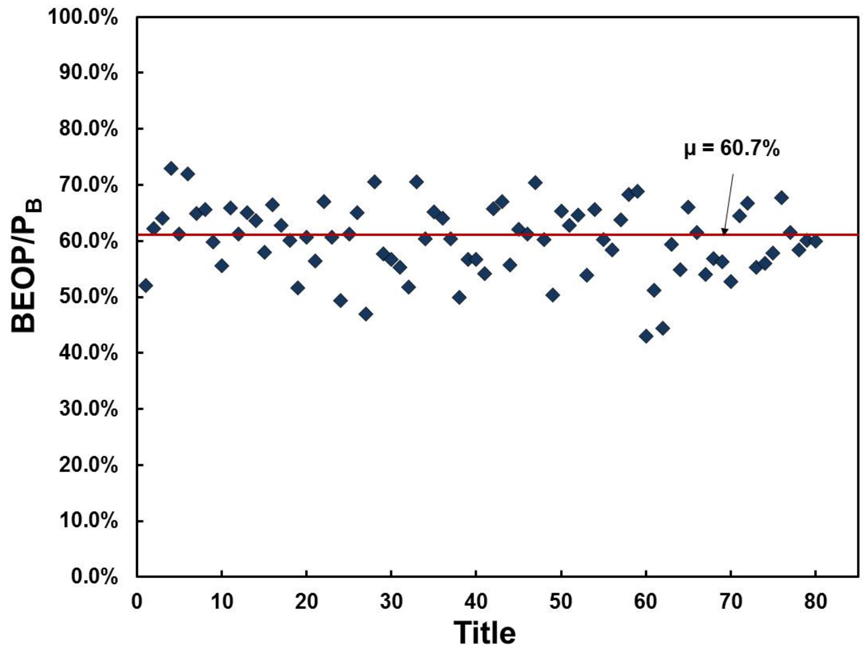

Figure 6.33 - Background Energy Oscillation Pressure (BEOP) as a function of burst pressure (P_B) for all cylinders tested in the current study.

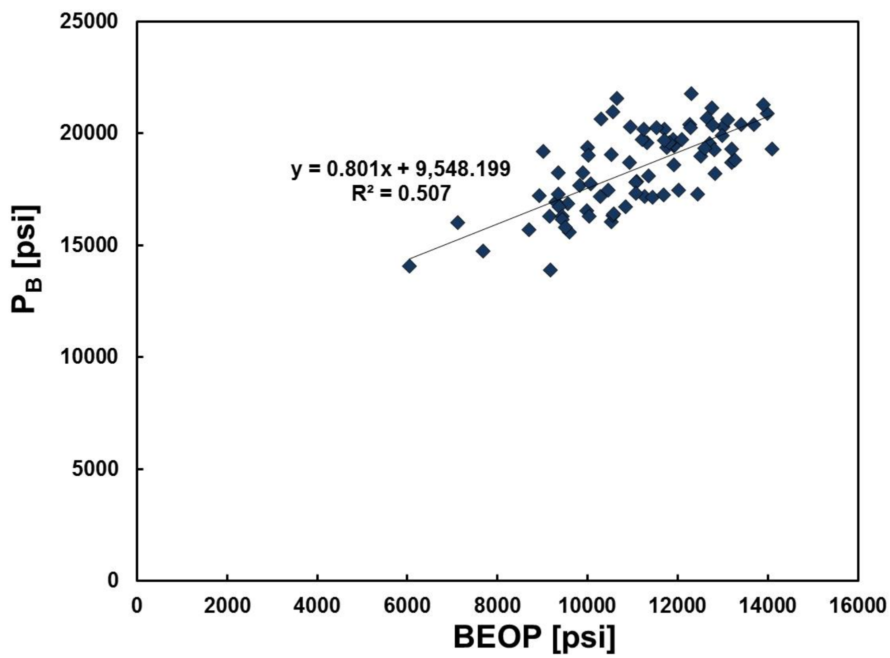

Figure 6.34 – Burst pressure of a cylinder as a function of BEOP for all civilian SCBA cylinders.

The efficacy of Modal Acoustic Emission, visual inspection, and elastic expansion for all cylinders which were burst tested in Sections 6.1 through 6.6 was compared. The percentage of the time that the respective NDE technique agreed with whether or not an SCBA pressure cylinder burst above the minimum required burst strength was compared (Figure 6.35). It was found that MAE properly identified 98.2% of the cylinders tested, while visual inspection and elastic expansion both only properly identified 86.4% of the cylinders. Of concern, the elastic expansion measurement at test pressure passed all three cylinders which burst below the minimum required burst strength. The majority of the misses for the visual inspection and elastic expansion technique were of the false-positive variety; however, false-negatives (which are far more concerning) for both visual inspection and elastic expansion occurred. ALT 604 – 3742 passed the visual inspection (and hydrostatic test), but burst below the minimum required pressure of DOT CFFC 5th Revision [1]. Such an occurrence points out the lack of sensitivity of the visual inspection and elastic expansion measurement to microstructural damage, which is the controlling factor in cylinder burst strength. It is pointed out that MAE properly identified and rejected ALT604-3742 which had compromised burst strength. The one miss that MAE had was a false-positive in which Background Energy Oscillations on the second test pressure cycle caused IH2554 to fail the MAE life extension requirements, with the cylinder bursting at 16,000 psi.

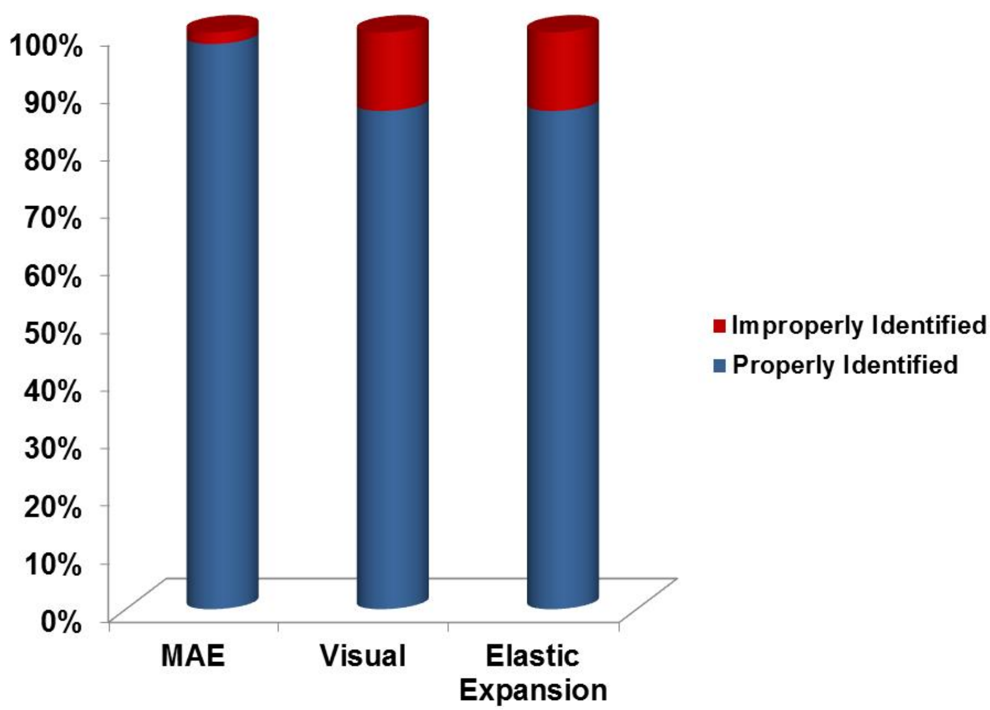

Figure 6.35 – Evaluation of how often the result of the various NDE inspection technique agreed with the minimum required burst pressure of the CFFC 5th Revision [2].

7.0 Conclusions

From the entirety of the physical testing contained herein, several observations about the structural integrity of DOT-CFFC SCBA pressure cylinders past their allotted fifteen year service life were made. No reduction in burst strength for cylinders at the end of their fifteen year service life or at the end of their fifteen year service life with an additional twenty years of simulated service was observed. Moreover, through the monitoring of pressure and strain during cyclic fatigue and EOL burst testing, it was found that the stiffness of the carbon fiber composite overwrap was not compromised by fatigue cycling the cylinders to the maximum developed pressure during fast fill. Laminated plate theory computations in Section 9.1 confirm that the state of stress in the fiber at the operating pressure of 4500 psi DOT-CFFC pressure cylinders is less than 30% of common unidirectional carbon fiber composite laminate strength values.

The impact resistance of the DOT-CFFC design was evaluated, in which it was found that the ISO 11119.2 impact simulation caused no reduction in fatigue performance or burst strength. A more aggressive impact simulation developed by DOT and Digital Wave Corporation found no degradation in burst strength for DOT-CFFC cylinders, but an issue in fatigue in which due to the severe impact simulation the aluminum liner delaminates from the carbon fiber composite overwrap.

While the performance testing summarized in the preceding paragraphs was extremely important relative to proving that the composite material's properties are not being degraded from in service use or additional simulated life, the application of Modal Acoustic Emission (MAE) is critical for detecting a cylinder that has been subjected to unusual condition (e.g. excessive impact or acid exposure). One of the key components to this work was the application of MAE during physical testing and MAE's ability in predicting a composite cylinder with a compromised strength, caused due to various damage mechanisms that were occurring within the composite microstructure. During this research, MAE identified all of the DOT-CFFC SCBA cylinders that did not meet the minimum required burst pressure, a claim no other current inspection technique can make.

Further, through the use of modal acoustic emission it was again found that background energy oscillations began at an average value of 60.7% with a standard deviation of 5.7%. Due to the consistent and repeatable nature of the onset of the background energy oscillations a confidence interval can be set on the burst pressure of a cylinder, and cylinders which are identified as having a high probability of having inadequate burst strength may be rejected. The ability of Modal Acoustic Emission to quantify the "effect of a defect," in the composite cylinders, is a giant leap forward in the nondestructive evaluation of composite materials. A few key observations of the benefits of the research program are

- A total of eighty-one DOT-CFFC cylinders were burst test, 96.3% (78 of 81) of the cylinders met the CFFC 5th Revision burst requirements.
- MAE identified and rejected all three cylinders (two of which were intentionally damaged) that did not meet the required minimum burst strength, including one cylinder which was not intentionally damaged and had no obvious signs of being structurally compromised and passed visual and hydrostatic inspection.
- MAE out-performed the currently used visual inspection and elastic expansion criteria, in properly evaluating the health of DOT-CFFC SCBA pressure cylinders.
- Twenty-five CFFC cylinders were subjected to an additional 10,000 cycles after their 15 year service life; 84% (21 of 25) of the CFFC cylinders sustained an additional 10,000 cycles (20 years of service life). All twenty-one cylinders then burst above minimum design burst from DOT-CFFC 5th Revision. The four cylinders that did not withstand the additional 10,000 cycles all failed via leakage, not catastrophic burst.
- Fifteen cylinders (all with heavily corroded liners) were subjected to the 10,000 cycle fatigue testing. Eight of the fifteen cylinders were "re-autofrettaged" at 8500 psi prior to cycling (in order to blunt the crack tips and retard crack growth rate), while seven of the cylinders were not (used as a control group). 87.5% of the heavily corroded liners that were re-autofrettaged sustained an additional 10k cycles, and then burst above DOT-CFFC 5th Revision minimum design burst pressure. Conversely, 85.7% of the DOT-CFFC cylinders that had heavily corroded liners that were not re-autofrettaged failed via leakage. During the re-autofrettage process the cylinders were monitored with MAE to insure no damage was occurring within the composite cylinder. The results from the re-autofrettage process appear promising to DWC as a means of mitigating the effects of corrosion due to previous water exposure from improper hydro-testing.
- All notched DOT-CFFC cylinders met the requirements of ISO 11119.2 Section 8.5.7, and seven of the nine burst tested cylinders met the minimum design burst pressure requirement of DOT-CFFC 5th Revision. As previously mentioned, MAE easily identified and failed the two cylinders with compromised burst strengths.
- MAE identified all notched cylinders during cyclic fatigue and the hydrostatic test pressure pressurizations, by waveforms with dominant flexure mode content caused by the delamination growth at the notches. While the notches used in this study could be observed visually, MAE possesses the advantage that it can identify notch type damage even if it has occurred to inner wraps of the composite pressure cylinder (perhaps during manufacture), which visual inspection simply cannot do.
- For the ISO impact simulation, all five CFFC cylinders which were EOL burst test met minimum design burst pressure requirements. Three of the five impacted cylinders achieved 10,000 cycles and then burst above the minimum design burst pressure requirement; the two cylinders that did not achieve 10,000 cycles failed via leakage not catastrophic burst.
- For the DOT impact simulation, all five impacted cylinders that were EOL burst tested met the minimum design burst pressure requirement. All five impacted cylinders which were cycled leaked. After looking at the Navy [3] and civilian data on the fifteen foot drop and subsequent cycling, attempting to obtain 10,000 cycles after this type of

extreme impact appears unreasonable. While 10,000 cycles would be ideal, the impact simulation is extreme, and a reduction in the number of fatigue cycles to obtain to 2500 cycles is recommended. With 2500 cycles a DOT-CFFC cylinder would theoretically sustain the cylinders operation for an additional five years which would get the cylinder to its' next requalification test, at which point a proper non-destructive technique (MAE) can identify the significant impact damage and disqualify the cylinder from further service life. All five cylinders in this study would have met the 2500 cycle requirement.

- MAE identified cylinders with impact damage during the hydrostatic test pressure pressurizations, by waveforms with dominant flexure mode content caused by the delamination growth at the damage sites of impacted cylinders. Several of the impacted cylinders showed no signs of impact damage, or were classified as having barely visible damage (BVD).
- Corrosion and/or flaw initiation sites within the aluminum liner caused by not properly drying the inside of the SCBA pressure cylinder were a large issue relative to cyclic fatigue performance of the DOT-CFFC cylinders. Clear signs of corrosion were apparent in 62% of the cylinders which were internally visually inspected. These corrosion areas were found to be the location of several flaw initiation sites. While problematic, the re-autofrettage process (Sections 5.6 and 6.6) which blunts all of the crack tips, putting them in compression and retarding crack growth provided a promising result for mitigating this issue without compromising the burst strength of the pressure cylinder.

8.0 Bibliography

[1] Department of Transportation, "Basic requirements for fully wrapped carbon-fiber reinforced aluminum lined cylinders (DOT-CFFC)," DOT, 2007.

[2] (ISO), International Standards Organization, "11119-2 Gas cylinders of composite construction - specification and test methods Part 2: Fully wrapped fibre reinforced composite gas cylinders with load-sharing metal liners," ISO, Geneva, Switzerland, 2002.

[3] Digital Wave Corporation, "SCBA Materials and Modal Acoustic Emission Testing Life Extension Report," Digital Wave Corporation, Centennial, CO, 2012.

[4] Digital Wave Corporation, "DOT-SP 15720," Centennial, CO, 2013.

[5] (ISO), International Standards Organization, "11515 Gas cylinders - Refillable composite reinforced tubes of water capacity between 150 L and 3 000 L - Design, construction, and testing," International Standards Organization (ISO), 2010.

[6] C. G. A. (CGA), "CGA C-6.2 - 2013 Standard for Visual Inspection and Requalification of Fiber Reinforced High Pressure Cylinders," CGA, Chantilly, VA, 2013.

[7] American Society of Mechanical Engineers (ASME), "Boiler and Pressure Cylinder Code," in *Section X: Fiber Reinforced Plastic Pressure Cylinders*, 2010, pp. 136-140.

[8] National Board of Inspectors Code (NBIC), "National Board Inspection Code," Columbus, OH, 2013.

[9] J. Wagner, "Optical Detection of Ultrasound," in *Ultrasonic Measurement Methods*, San Diego, Academic Press, 1990, pp. 201-240.

[10] S. Mettu, I. Raju and R. Forman, "Stress intensity factors for part-through surface cracks in hollow cylinders," Johnson Space Center/Lockheed Engineering Services, JSC Report 25685/LESC Report 30124, 1192.

[11] J. Newman Jr., "Fracture analysis of surface and through cracks in cylindrical pressure cylinders," NASA TN D-8325, 1976.

[12] I. Raju and J. Newman Jr., "Stress-intensity factors for internal and external surface cracks in cylindrical cylinders," *Journal of Pressure Cylinder Technology, Transactions of ASME,* vol. 104, pp. 293-298, 1982.

[13] A. Liu, "Summary of stress-intensity factors," in *ASM Handbook Volume 19, Fatigue and Fracture*, Materials Park, OH, ASM International, 1996, pp. 980-1000.

[14] A. Riberio, A. Jesus and A. Fernandes, "Fatigue crack propagation rates of the aluminum alloy 6061-T651," in *18th International Congress of Mechanical Engineering*, Ouro Preto, 2005.

[15] R. I. Stephens, A. Fatemi, R. R. Stephens and H. O. Fuchs, Metal Fatigue in Engineering 2nd Edition, New York: Wiley Inter-Science, 2001.

[16] B. Sheu and P. Song, "Shaping exponent in Wheeler model under a single overload," *Engineering Fracture Mechanics,* vol. 51, no. 1, pp. 135-143, 1995.

[17] M. Gorman, "Modal AE Analysis of Fracture and Failure in Composite Materials, and the Quality and Life of High Pressure Composite Pressure Cylinders," Journal of Acoustic Emission, vol. 29, pp. 1-28, 2011.

9.0 Appendix - Fatigue life prediction and the effect of the "re-autofrettage"

During hydrostatic cyclic fatigue testing of the SCBA pressure cylinders, it was shown in Section 6.2 that 16% of the randomly selected cylinders failed due to leakage before obtaining the objective of 10,000 cycles (an additional 20 years of service life). The internal visual inspection of all tested cylinders revealed that a significant number of cylinders (62%) exhibited signs of corrosion (Figure 5.10a) of the 6061-T6 Aluminum liner, which were found to result in flaw initiation sites (Figure 5.10b). Thus, during the cyclic fatigue testing the initial flaws grew until the critical flaw grew through the aluminum liner, resulting in leakage of the SCBA pressure cylinder. While "leak before burst" is a desirable failure mode for SCBA pressure cylinders, too large of the population exhibiting this type of failure is problematic from a life extension perspective.

Hence, in Section 6.6 the effect of re-autofrettaging the aluminum liner of SCBA pressure cylinders which exhibited signs of corrosion of the 6061-T6 Aluminum liner was investigated. These cylinders were selected as they were deemed worst case scenarios from a crack growth through the aluminum liner perspective. It was found that 87.5% of "re-autofrettaged" corroded liner SCBA pressure cylinders were able to achieve 10,000 cycles to maximum developed pressure, while not adversely affecting the burst strength of the pressure cylinder. Conversely, 85.7% of SCBA pressure cylinders with corroded liners which were not "re-autofrettaged" failed by leakage before obtaining 10,000 cycles to maximum developed pressure. Such findings provide promise that a procedure (commonly used in metallic part manufacture) exists to reduce the number of cylinders which fail due to leakage. The analysis contained herein is intended to provide a quantitative validation of the benefits of re-autofrettaging the 6061-T6 Aluminum liner of SCBA pressure cylinders, and blunting any existing crack tips.

To perform a proper fatigue life estimation analysis, an adequate stress intensity factor for an internally pressurized thin-walled cylinder is required. To this end, the K solutions of [11 - 14] were utilized. The stress intensity factor (*K*) for a thin walled cylinder with an axially oriented notch subjected to internal pressure is

$$K = \sigma\alpha\sqrt{\frac{\pi a}{Q}} \tag{8.1}$$

where σ is the hoop stress within the aluminum liner, a is the current crack length, Q is the flaw shape parameter, and α is defined as

$$\alpha = \left(\frac{t}{R}\right)\left(\frac{r^2}{(r^2 - R^2)}\right)\left[2H_0 - 2H_1\left(\frac{a}{R}\right) + 3H_2\left(\frac{a}{R}\right)^2 - 4H_3\left(\frac{a}{R}\right)^3\right]. \tag{8.2}$$

In equation 8.2 r and R are the inner and outer radius of the aluminum liner, respectively, t is the thickness of the aluminum liner, and H_i is a function of R/t, a/c, a/t, and the angle within the crack face. As Liu proposed [13], letting $\frac{\alpha}{\sqrt{Q}}$ be equated to a parameter, F, equation (8.1) may be written as

$$K = \sigma F \sqrt{\pi a}. \tag{8.3}$$

Figure 8.1 provides the relationship between F and the ratio of crack depth to liner thickness for a flaw with a ratio a/c equal to 0.2, and a ratio of R/t = 30 for both 0° and 90° on the crack face, taken from Table 17 of [6].

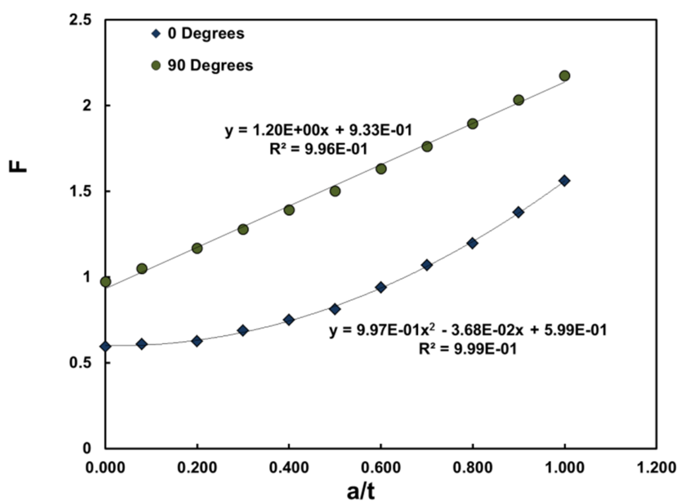

Figure 8.1 – Relationship between F and a/t for R/t = 30, and a/c = 0.6, as reported in Liu [6].

9.1 Laminated Plate Theory analysis

To properly determine σ within the aluminum liner in equations (8.1) and (8.3), the distribution of stresses through the thickness of the composite overwrapped pressure cylinder laminate must be considered. To this end, we utilize an anisotropic classical laminated plate theory (CLPT) analysis to calculate the distribution of stresses through the thickness of the laminated plate, and extract the state of stress within the aluminum liner. Table 8.1 summarizes the ply material, ply orientation, and ply thickness for a 45 minute, 4500 psi DOT-CFFC pressure cylinder. Table 8.2 provides the elastic constants used in the CLPT analysis. Figure 8.2a provides a schematic of the SCBA COPV laminate lay-up (excluding the non-structural sacrificial glass fiber layers). To obtain the maximum hoop stress in the aluminum liner, a representative stress element of the entire laminate was subjected to biaxial tensile traction loads (Figure 8.2b) that were equivalent to what the cylindrical portion of the SCBA pressure cylinder experiences at maximum developed pressure (5192 psi).

Table 8.1 – Summary of the laminate definition used in the CLPT analysis.

Ply material	Ply orientation [degrees]	Ply thickness [inch]
S2/913	90	0.016
S2/913	16	0.008
S2/913	-16	0.008
T700/913	90	0.063
T700/913	16	0.040
T700/913	-16	0.040
T700/913	90	0.047
6061-T6 Aluminum	-	0.100

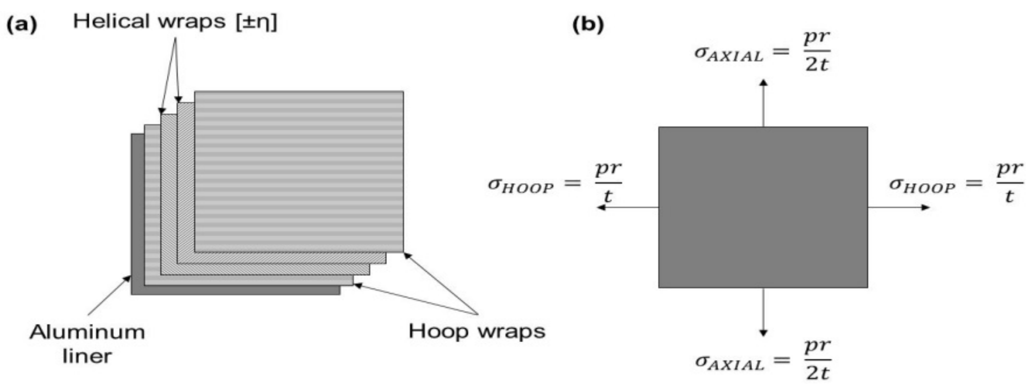

Figure 8.2 – (a) Schematic of the SCBA pressure cylinder laminate, and (b) biaxial loads applied to a representative stress element to simulate the state of stress within the cylindrical portion of the pressure cylinder due to internal pressure.

Table 8.2 – Lamina constants used in CLPT analysis

Ply material	T800/913	S2/913	6061-T6 Aluminum
E_{11} [Msi]	22.06	7.83	10.00
E_{22} [Msi]	0.96	2.32	10.00
G_{12} [Msi]	0.61	1.02	3.85
G_{23} [Msi]	0.31	0.87	3.85
ν_{12}	0.25	0.25	0.30

Figure 8.3 shows the first (axial) principal stress, while Figure 8.4 shows the second (hoop) principal stress. From Figure 8.4 it can be seen that the maximum hoop stress within the aluminum liner at the maximum developed pressure was found to be 391.7 MPa (56,800 ksi), which is the value for the hoop stress within the aluminum liner that will be used in all subsequent fatigue life estimation analyses. Note the yield strength of the 6061-T6 Aluminum was taken as the maximum stress within the aluminum liner when subjected to the initial autofrettage pressure of (7500 ksi), resulting in S_y = 82.1 ksi.

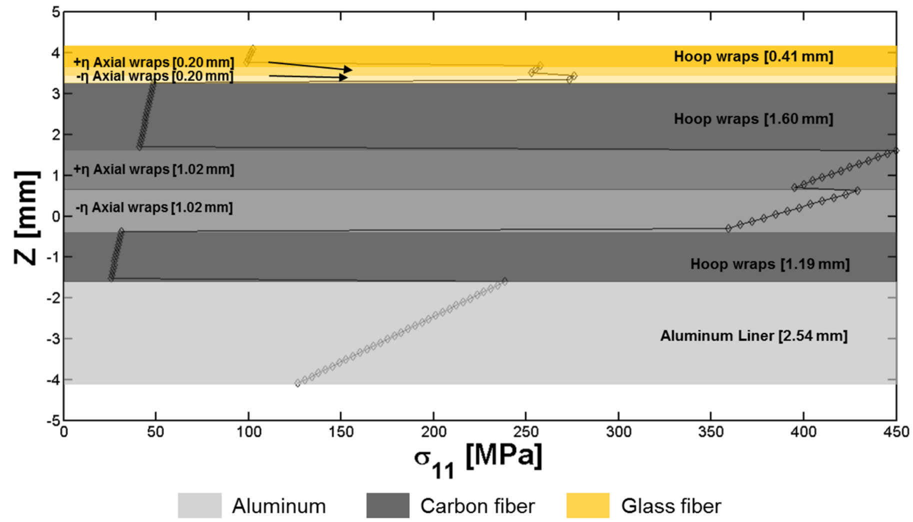

Figure 8.3 – Distribution of axial stress through the laminate thickness for a representative SCBA CFFC pressure cylinder at maximum developed pressure during fast fill (5,192 psi).

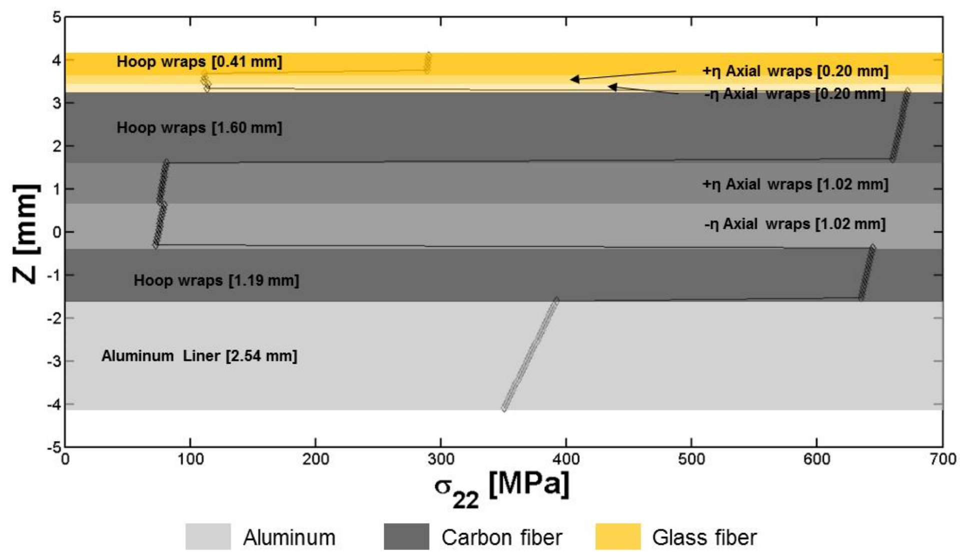

Figure 8.4 – Distribution of hoop stress through the laminate thickness for a representative SCBA CFFC pressure cylinder at maximum developed pressure during fast fill (5,192 psi).

9.2 Fatigue life estimation

First, consider the case of an SCBA pressure cylinder which was not re-autofrettaged, but had a semi-elliptical flaw axially oriented in the cylindrical portion of the pressure cylinder with an initial depth (a_0) of 0.005", and initial width ($2c_0$) of 0.050". The remaining life of the aluminum liner may then be determined using the standard Paris law equation

$$\frac{da}{dN} = A\Delta K^M \tag{8.4}$$

where $\frac{da}{dN}$ is the crack growth rate, A and M are the Paris law constants for 6061-T6 Aluminum, and ΔK is the stress intensity factor range during a given fatigue cycle. Values of A (3.7086E-12) and M (4.2) were taken from [14]. With the proper material constants equation (8.4) may be integrated numerically for a given number of cycles (N) to determine the final crack length as

$$a_N = a_0 + \sum_{i=1}^{N} A\Delta K^M. \tag{8.5}$$

To consider the effects of the re-autofrettage process and crack tip blunting, the crack tip plasticity model of Wheeler was used [15]. In Wheeler's model the plastic zone size at the crack tip under plane stress conditions is calculated as

$$2r = \frac{1}{4\pi}\left(\frac{\Delta K}{S_y}\right)^2 \tag{8.6}$$

in which r is the radius of the plastic zone size, and S_y is the yield strength of the aluminum liner. In Wheeler's model, the plastic zone size is calculated for the tensile overload (r_{OL}), as well as on the i^{th} fatigue cycle (r_i), and then used to determine the retardation parameter C_i

$$C_i = \left[\frac{r_i}{(a_{OL} + r_{OL}) - a_i}\right]^q. \tag{8.7}$$

In equation (8.7) a_{OL} is the crack length at the overload cycle, a_i is the crack length on the i^{th} cycle, and q is a material constant. The value of q was taken from [16], and was 1.67. Using the retardation parameter for the i^{th} cycle (C_i), the crack length for N cycles of fatigue loading is then computed as

$$\frac{da}{dN} = C_i A\Delta K^M \tag{8.8}$$

which is evaluated numerically by separating variables, and integrating through N cycles to determine the resulting crack length (a_N)

$$a_N = a_0 + \sum_{i=1}^{N} C_i A\Delta K^M. \tag{8.9}$$

Figure 8.5 provides the crack length as a function of the number of cycles to maximum developed for the representative DOT-CFFC cylinders that were and were not re-autofrettaged. The Paris law model predicts that the considered initial flaw (a_0 = 0.005”, $2c_0$ = 0.050”) would grow to a depth of 0.076” in 10,000 cycles. A slightly larger flaw (only one to two thousandths of an inch) would grow through the remaining 0.024” before 10,000 cycles, resulting in leakage of the aluminum liner. Also, in good agreement with the observations of Section 6.6, specifically the re-autofrettaged SCBA cylinders, the Wheeler model predicts reduced crack growth behavior (as compared to cylinders which did not experience the tensile overload). This reduced crack growth rate behavior is due to all existing cracks being blunted and put into residual compression upon the removal of the tensile overload; such behavior is what enabled 87.5% of the heavily corroded liners to achieve an additional 10,000 fatigue cycles to maximum developed pressure during fast fill (Table 6.6).

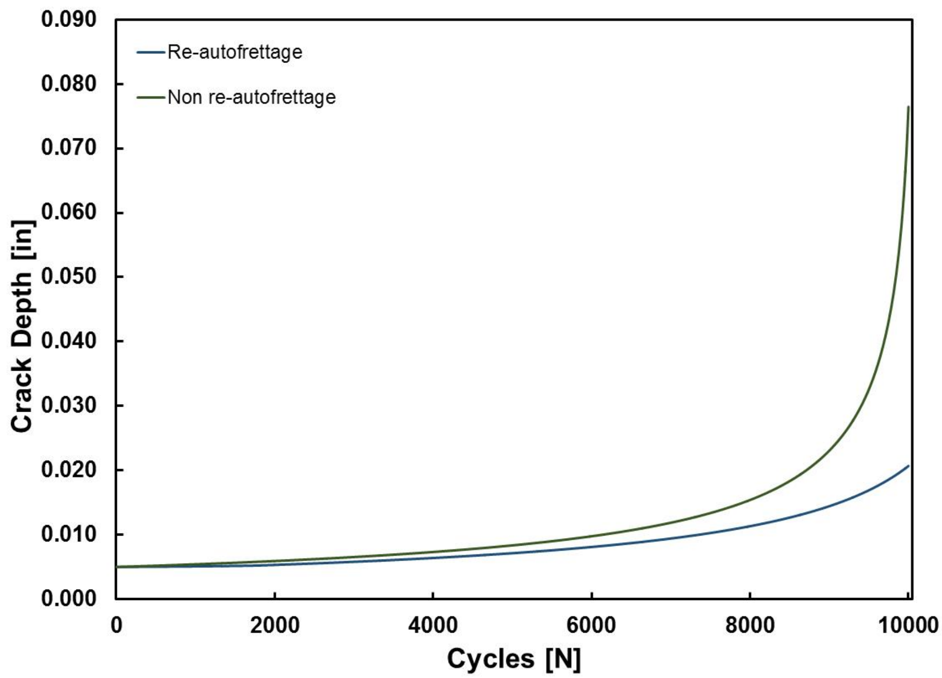

Figure 8.5 – Crack depth as a function of the number of cycles to maximum developed pressure for Aluminum liners that were and were not re-autofrettaged.

While the two proposed models reflect the experimental observations of Sections 6.2 and 6.6 quite well, several influencing factors should be considered. First, the initial flaw size (a_0 = 0.005", $2c_0$ = 0.050") was estimated from visual inspection of aluminum liners using 10x magnification. The effect of the initial flaw size will greatly influence the number of cycles which can be obtained by a given Aluminum liner. Figure 8.6 shows the effect of the initial flaw depth (a_0) on the number of cycles to maximum developed pressure before the crack grows through the aluminum liner. Clearly, for equivalent sized flaws, by re-autofrettaging the DOT-CFFC SCBA pressure cylinder the number of obtainable cycles prior to leakage is increased.

Second, the position of the flaw could have a significant effect on whether or not an aluminum liner leaks. The work presented herein only considers the case when a flaw is located on the cylindrical portion of the pressure cylinder. If a flaw were oriented at one of the transitions in the pressure cylinder, the stress state will be magnified (due to the local bending moment caused by the requirement of continuity of deformations), which will increase the crack driving force (ΔK), resulting in diminished fatigue life. To properly analyze such a scenario a more sophisticated analysis (non-linear finite element analysis) would be required to quantify ΔK. Finally, the Paris law parameters taken from [14] were developed for 6061-T651 Aluminum while the crack was growing in air. These material constants were selected as they provide for realistic crack growth rates during service; not accelerated crack growth rates due to the crack being submerged in water [15], as was the case in this experimental test program. Thus, in-service fatigue life may be longer than what was measured experimentally in Sections 6.2 and 6.6.

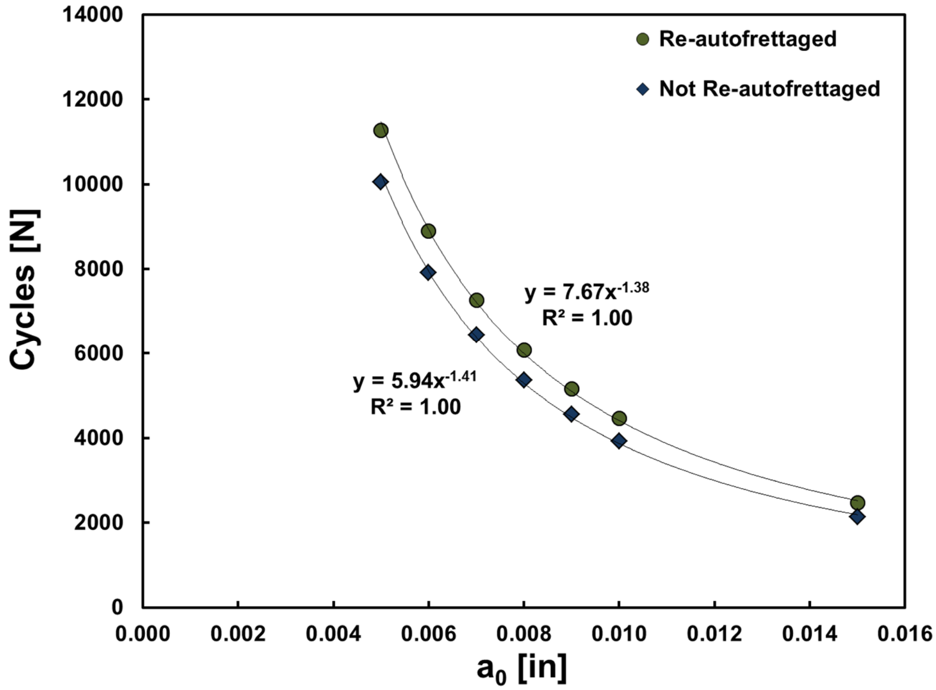

Figure 8.6 – Effect of the initial flaw depth (a_0) on the total number of obtainable fatigue cycles to maximum developed pressure prior to the flaw growing through the aluminum liner.

10.0 Appendix – Failed Cylinders

Figure 10.1 – Image of ALT604-3742 after EOL Burst testing.

Figure 10.2 – Image of ALT604-4436 after EOL Burst testing.

Figure 10.3 – Image of ALT604-4962 after EOL Burst testing.

Figure 10.4 – Image of ALT604-3650 after EOL Burst testing.

Figure 10.5 – Image of ALT604-4494 after EOL Burst testing.

Figure 10.6 – Image of OM3915 after EOL Burst testing.

Figure 10.7 – Image of OM3990 after EOL Burst testing.

Figure 10.8 – Image of OM3934 after EOL Burst testing.

Figure 10.9 – Image of OM3941 after EOL Burst testing.

Figure 10.10 – Image of OM3962 after EOL Burst testing.

Figure 10.11 - – Image of ALT639-14969 after EOL Burst testing.

Figure 10.12 – Image of ALT639-17663 after EOL Burst testing.

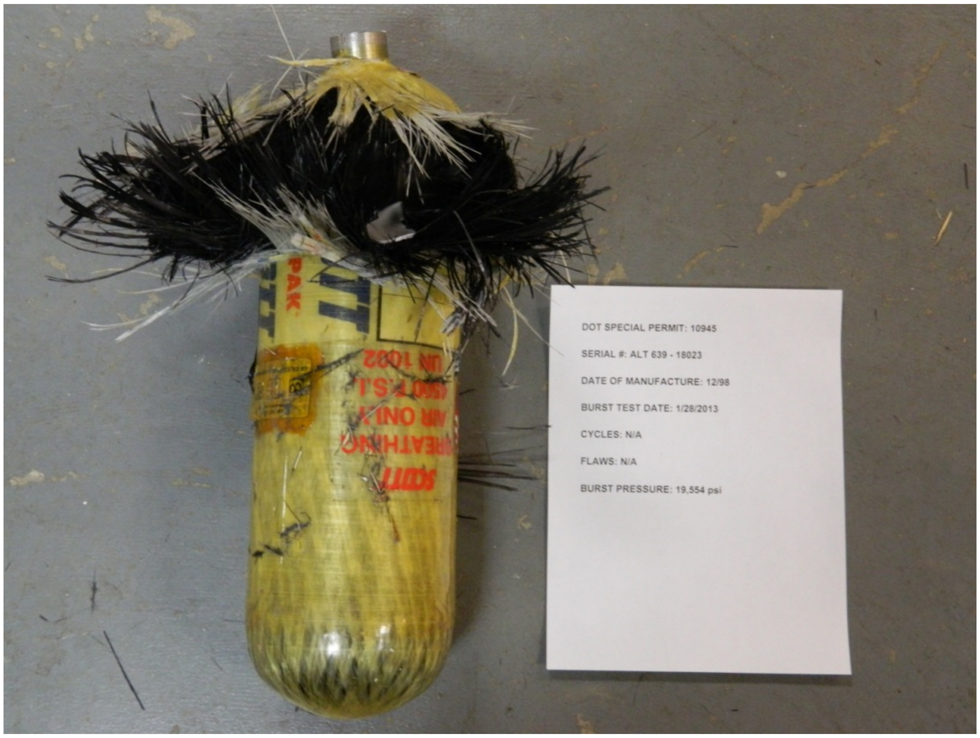

Figure 10.13 – Image of ALT639-18023 after EOL Burst testing.

Figure 10.14 – Image of ALT639-69216 after EOL Burst testing.

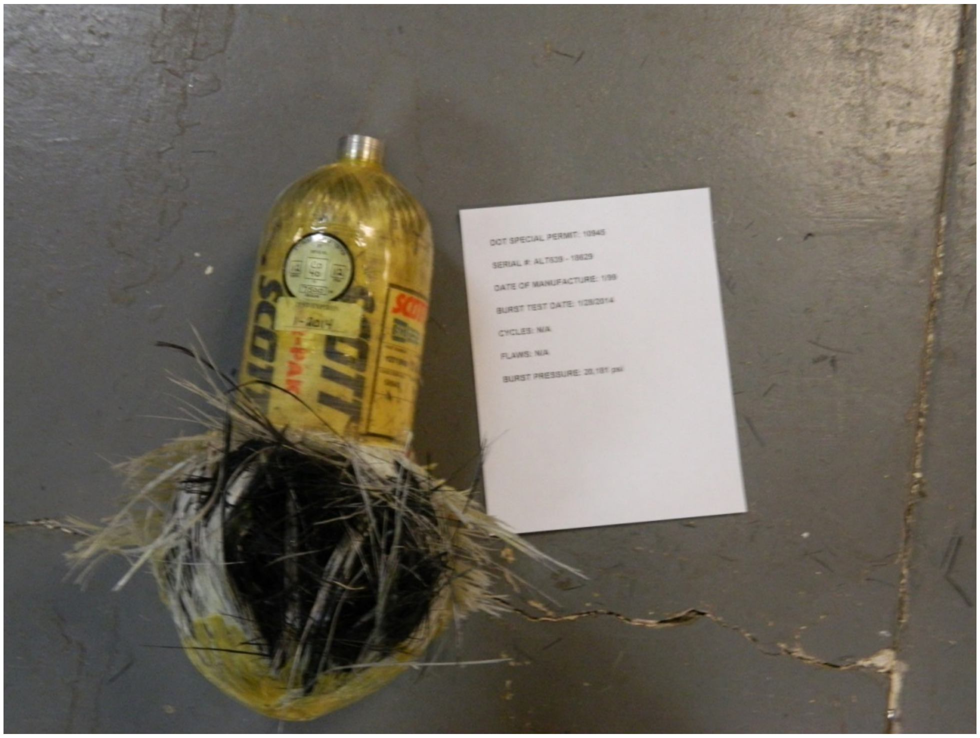

Figure 10.15 – Image of ALT639-18629 after EOL Burst testing.

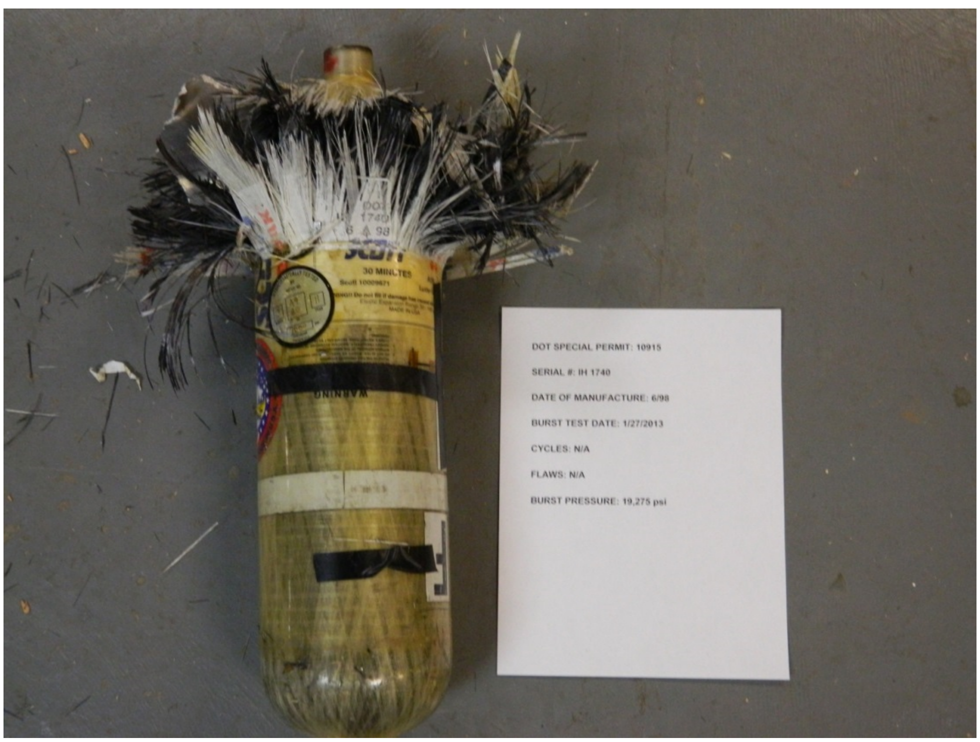

Figure 10.16 – Image of IH1740 after EOL Burst testing.

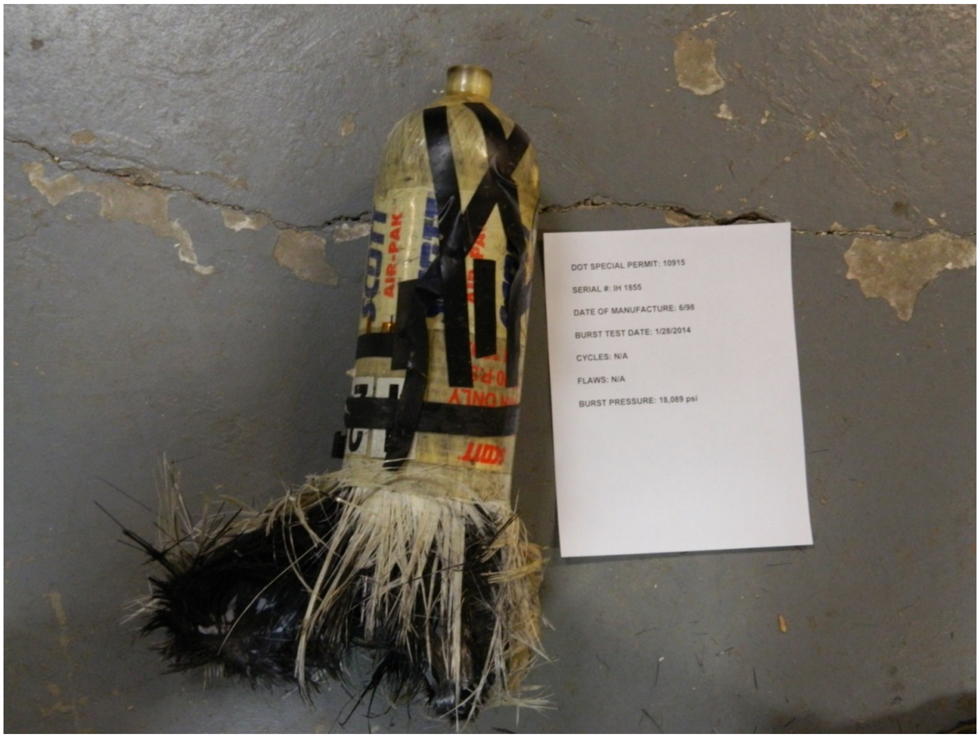

Figure 10.17 – Image of IH1855 after EOL Burst testing.

Figure 10.18 – Image of IH1763 after EOL Burst testing.

Figure 10.19 – Image of IH1135 after EOL Burst testing.

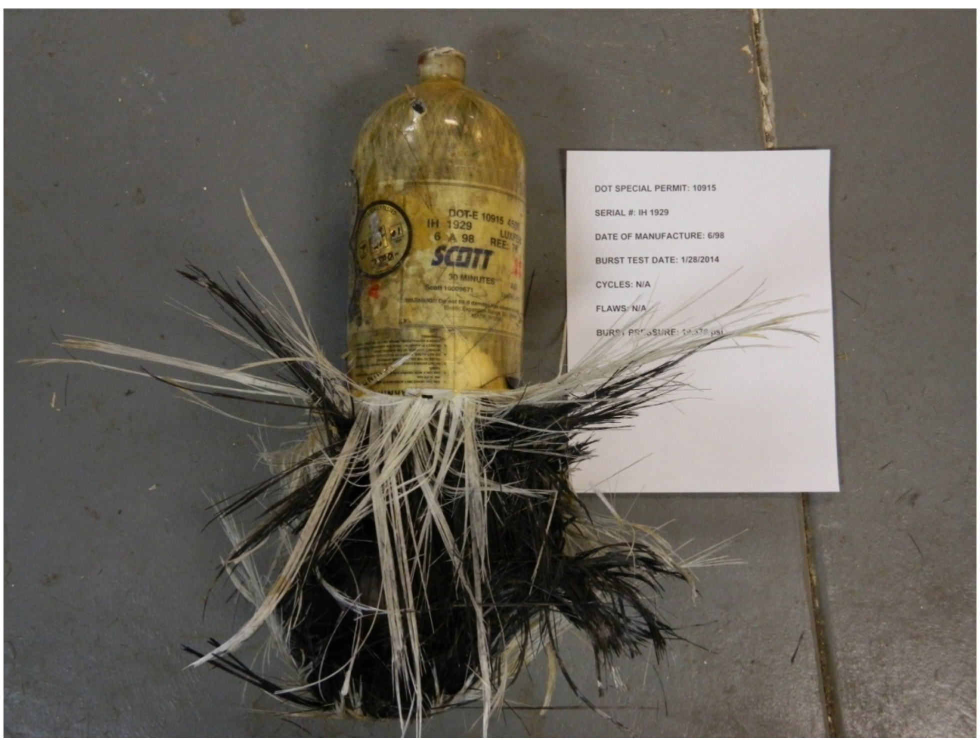

Figure 10.20 – Image of IH1929 after EOL Burst testing.

Figure 10.21 – Image of ALT604-6739 after EOL Burst testing.

Figure 10.22 – Image of ALT639-17688 after EOL Burst testing.

Figure 10.23 – Image of ALT639-18862 after EOL Burst testing.

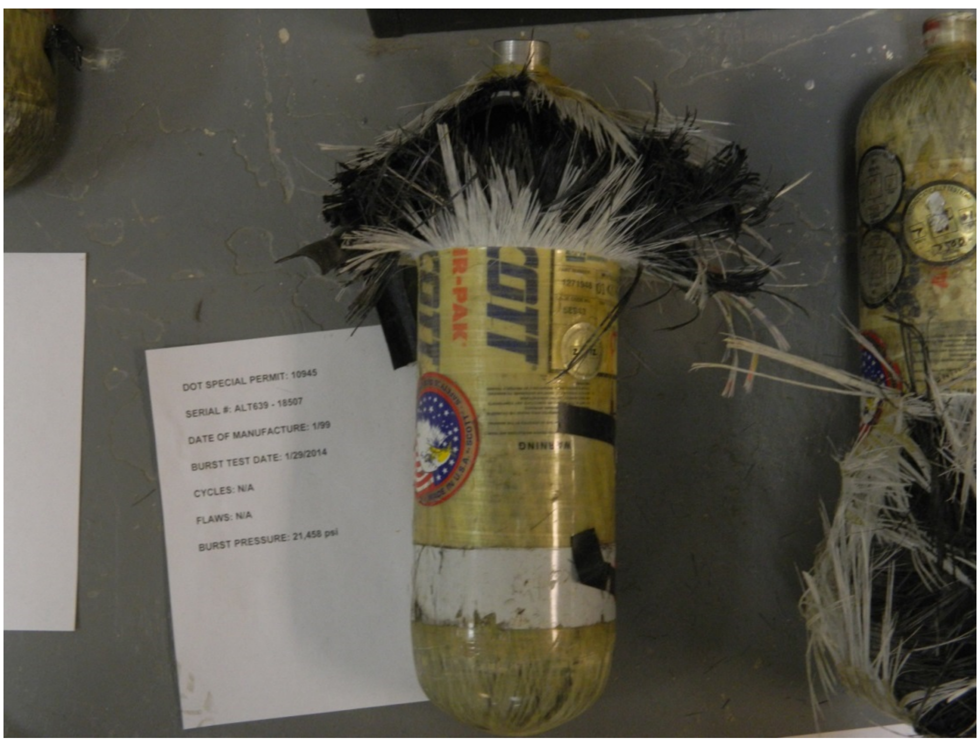

Figure 10.24 – Image of ALT639-18507 after EOL Burst testing.

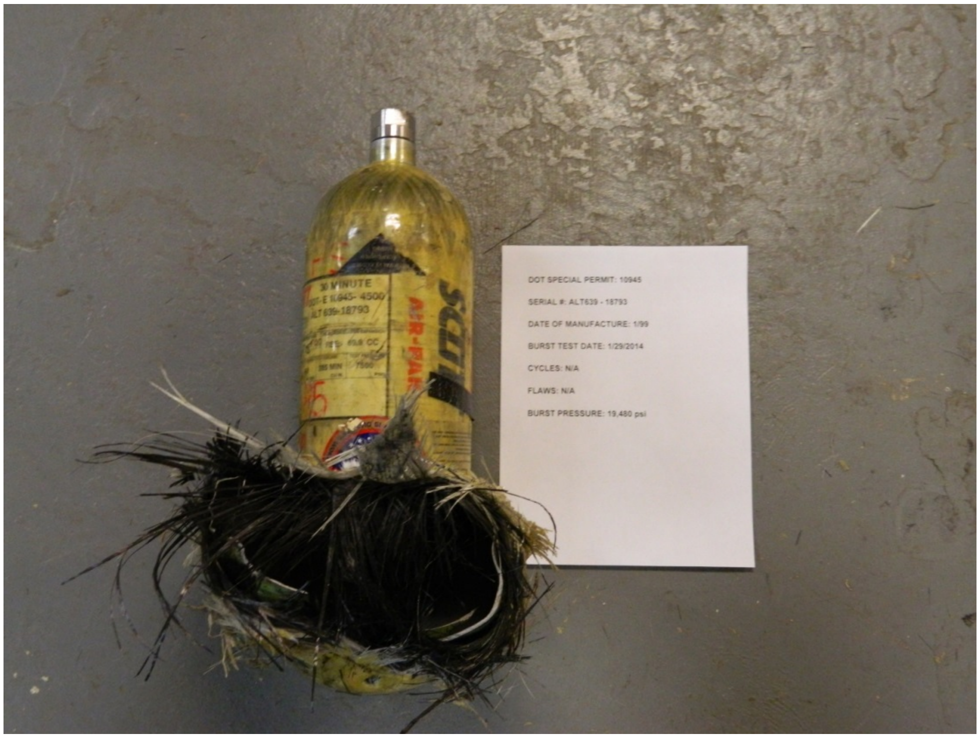

Figure 10.25 – Image of ALT639-18793 after EOL Burst testing.

Figure 10.26 – Image of ALT695-1700 after EOL Burst testing.

Figure 10.27 – Image of ALT695-6058 after EOL Burst testing.

Figure 10.28 – Image of ALT695-5353 after EOL Burst testing.

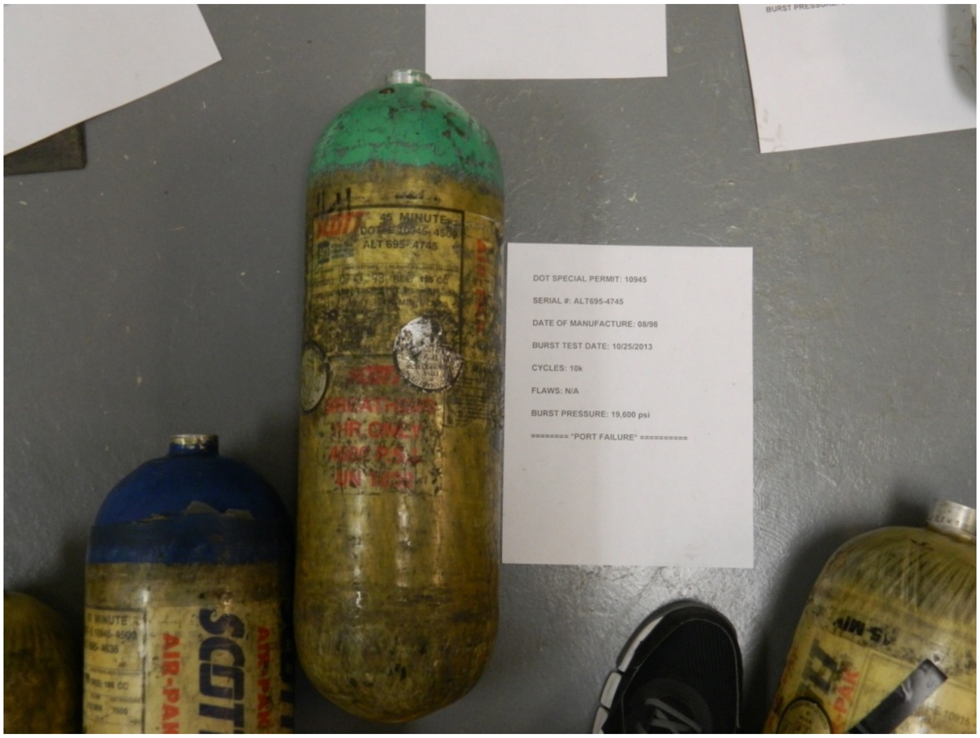

Figure 10.29 – Image of ALT695-4745 after EOL Burst testing.

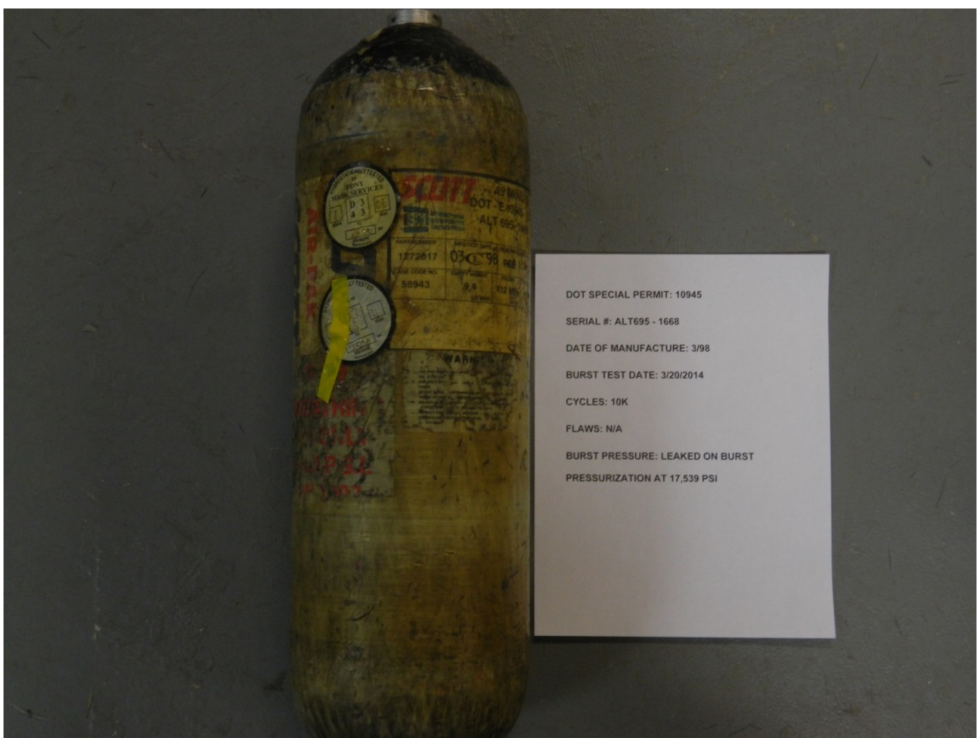

Figure 10.30 – Image of ALT695-1668 after EOL Burst testing.

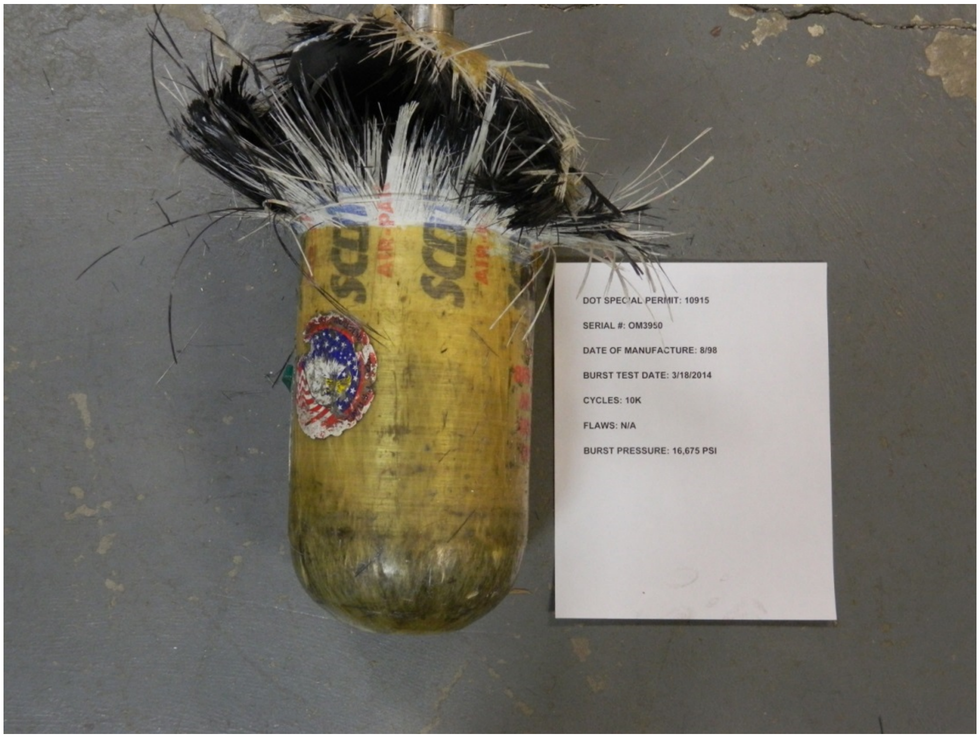

Figure 10.31 – Image of OM3950 after EOL Burst testing.

Figure 10.32 – Image of OM3928 after EOL Burst testing.

Figure 10.33 – Image of OM3913 after EOL Burst testing.

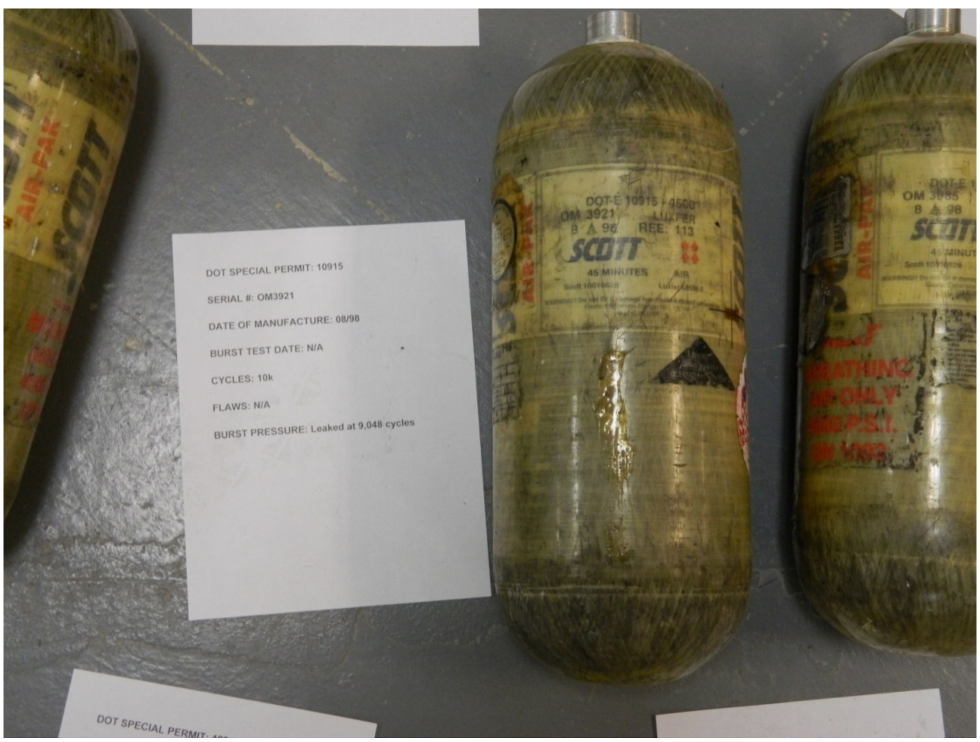

Figure 10.34 – Image of OM3921 after EOL Burst testing.

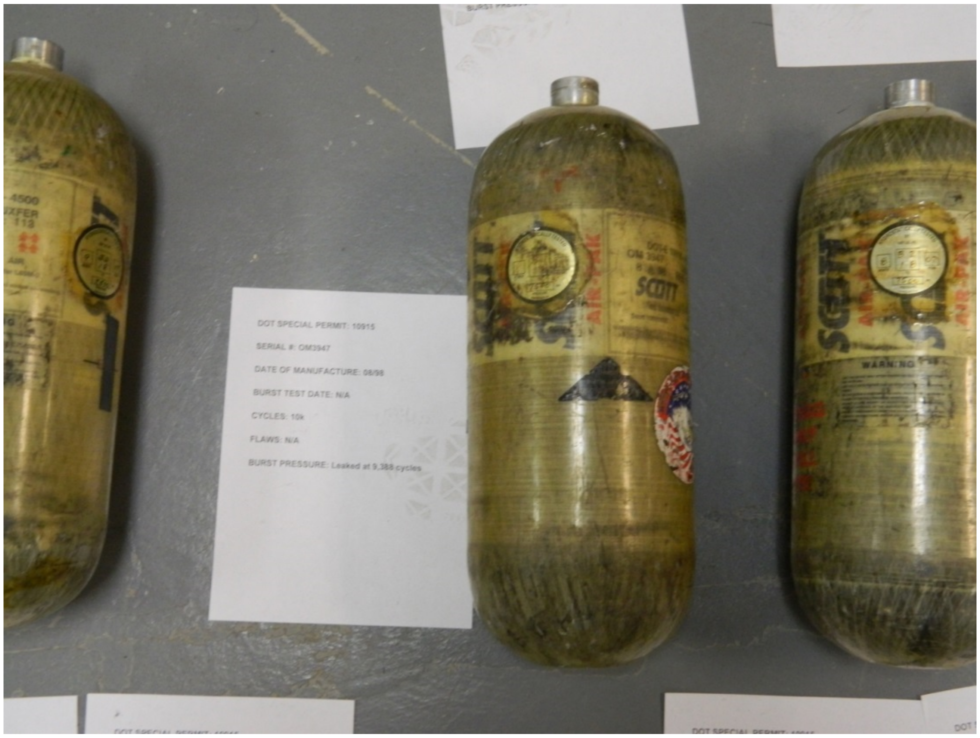

Figure 10.35 – Image of OM3947 after EOL Burst testing.

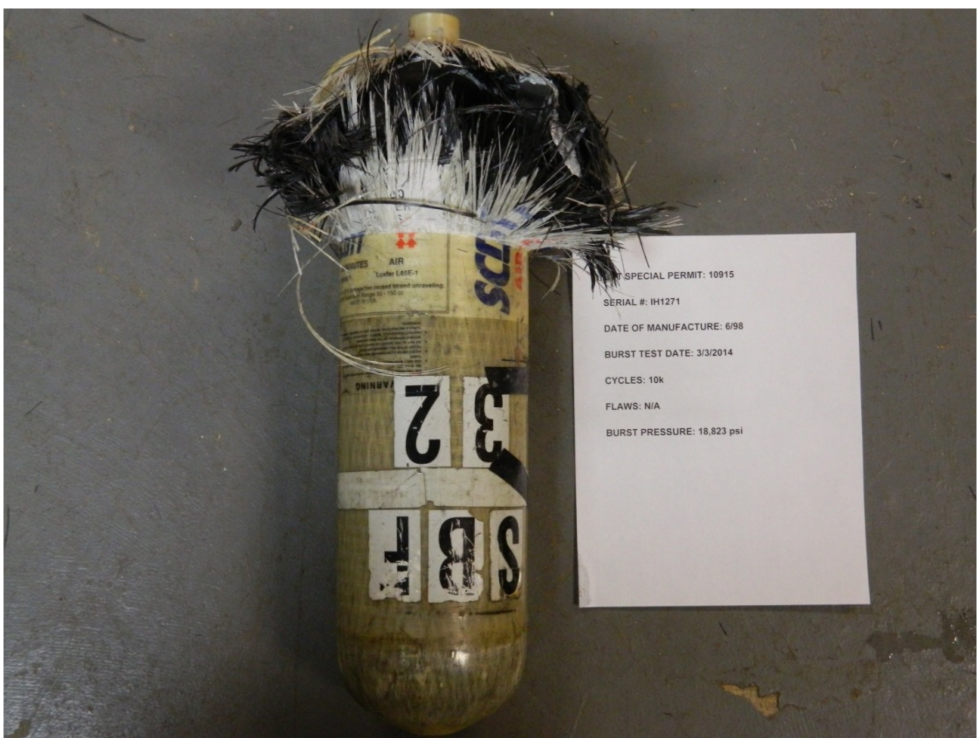

Figure 10.36 – Image of IH1271 after EOL Burst testing.

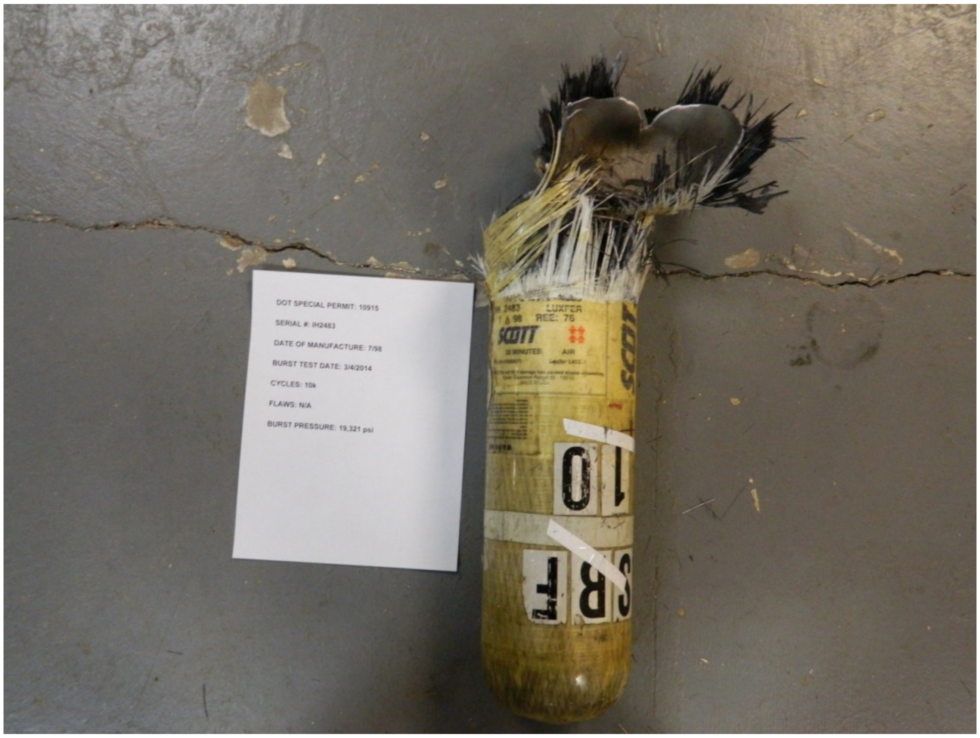

Figure 10.37 – Image of IH2483 after EOL Burst testing.

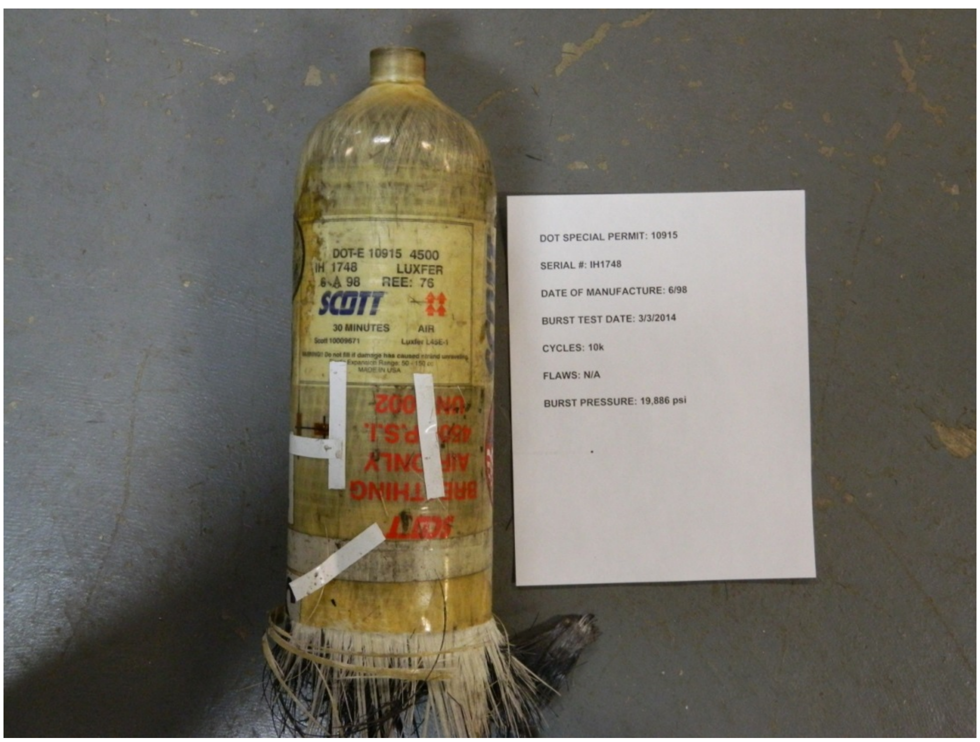

Figure 10.38 – Image of IH1748 after EOL Burst testing.

Figure 10.39 – Image of IH1820 after EOL Burst testing.

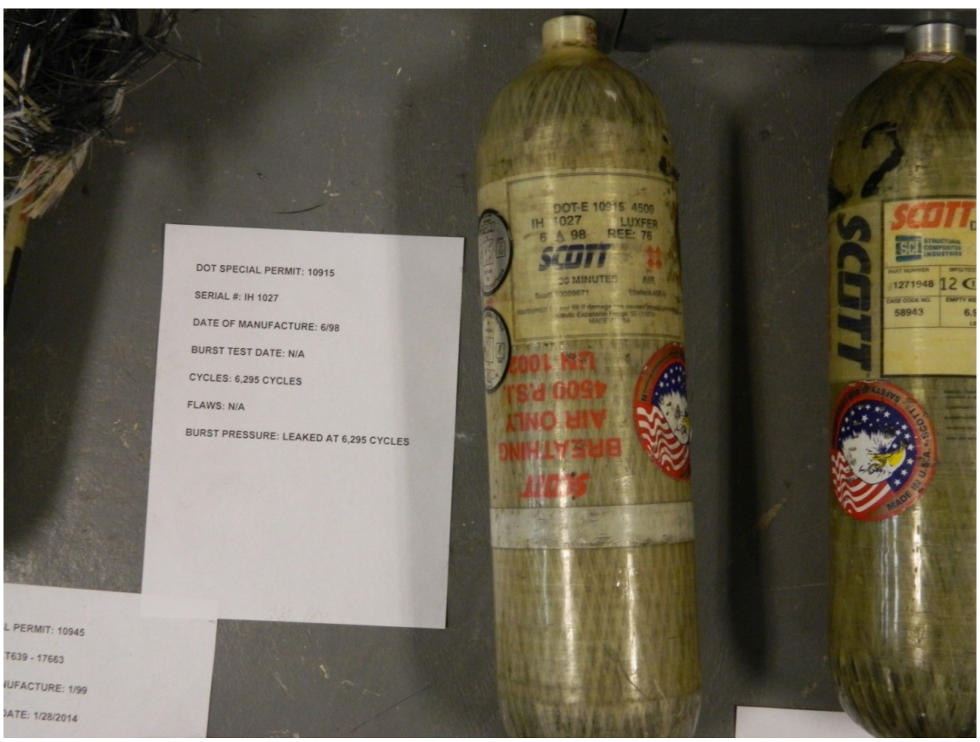

Figure 10.40 – Image of IH1027 after EOL Burst testing.

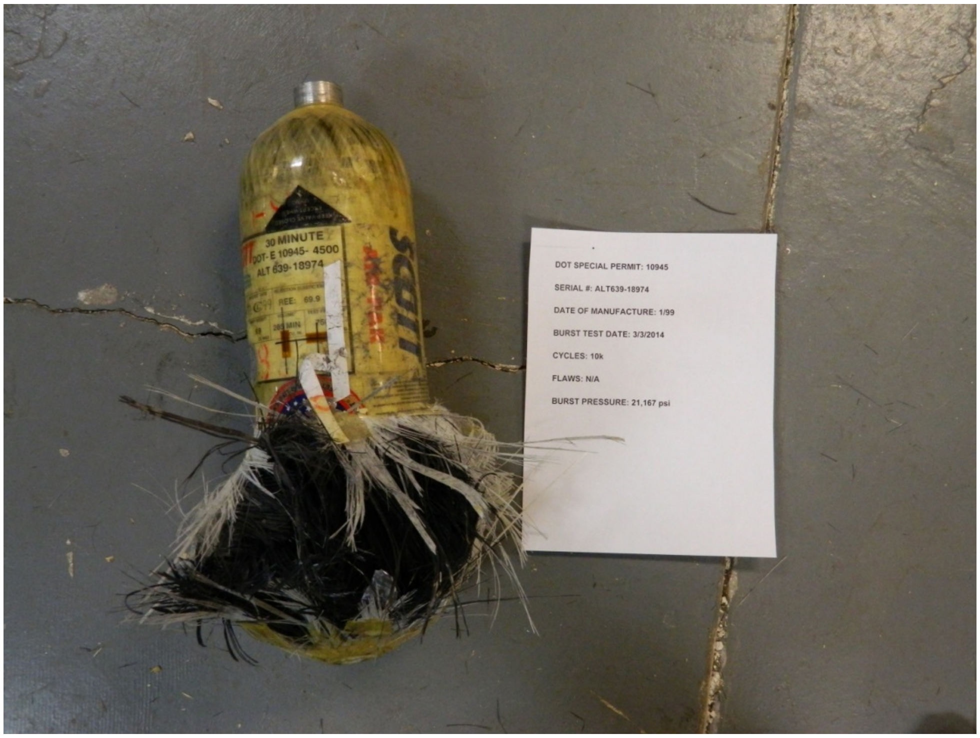

Figure 10.41 – Image of ALT639-18974 after EOL Burst testing.

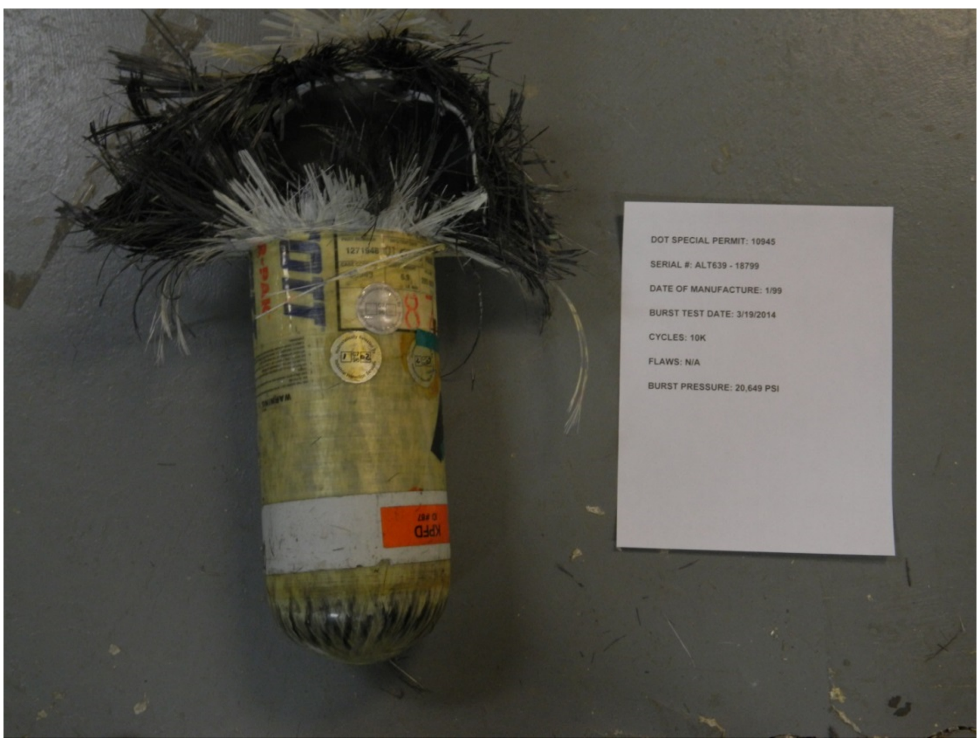

Figure 10.42 – Image of ALT639-18799 after EOL Burst testing.

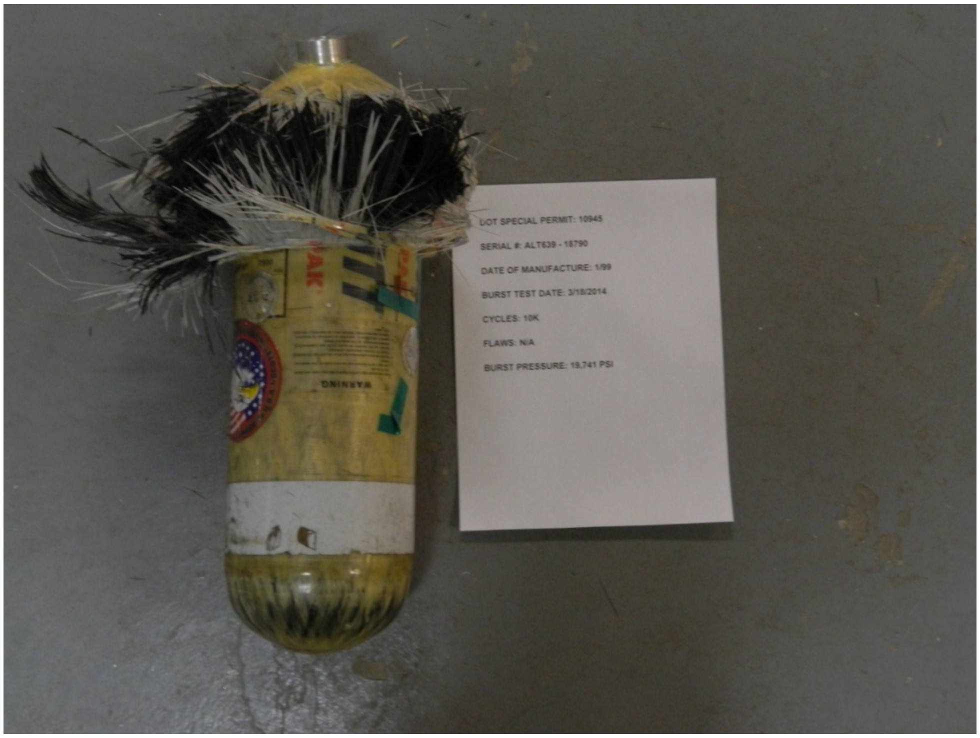

Figure 10.43 – Image of ALT639-18790 after EOL Burst testing.

Figure 10.44 – Image of ALT695-1653 after EOL Burst testing.

Figure 10.45 – Image of ALT604-4342 after EOL Burst testing.

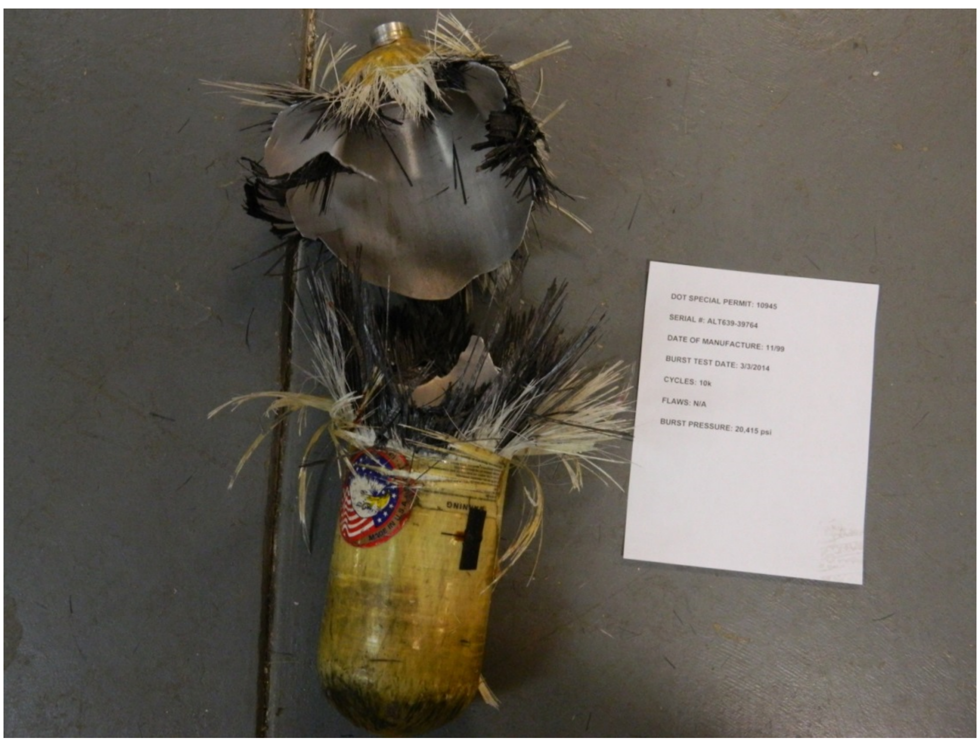

Figure 10.46 – Image of ALT639-39764 after EOL Burst testing.

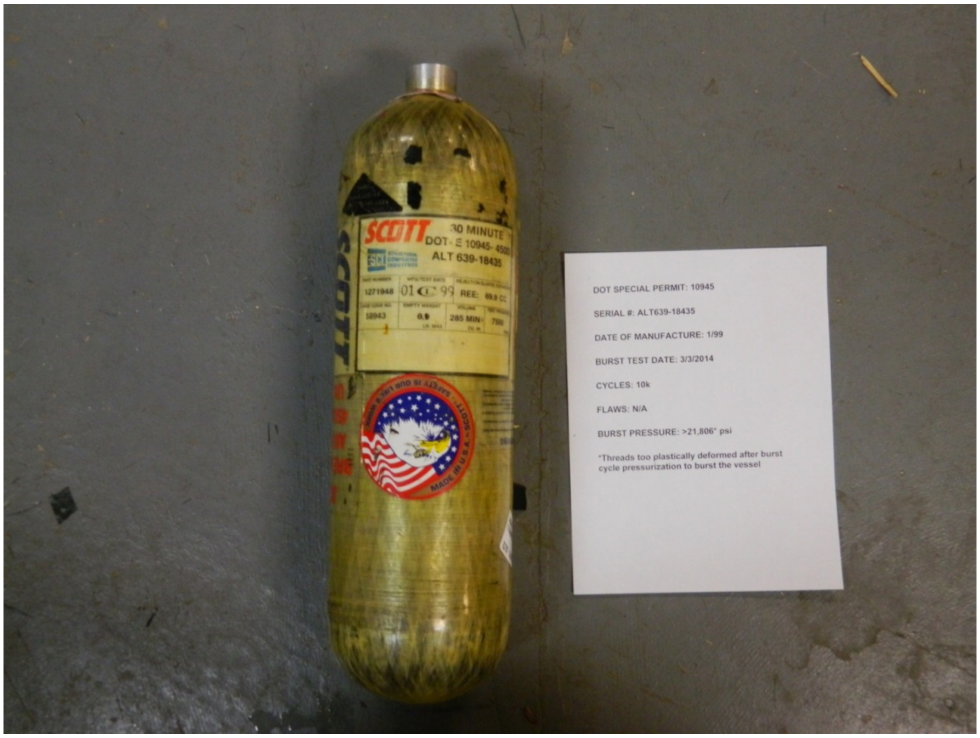

Figure 10.47 – Image of ALT639-18435 after EOL Burst testing.

Figure 10.48 – Image of ALT639-39694 after EOL Burst testing.

Figure 10.49 – Image of ALT639-18683 after EOL Burst testing.

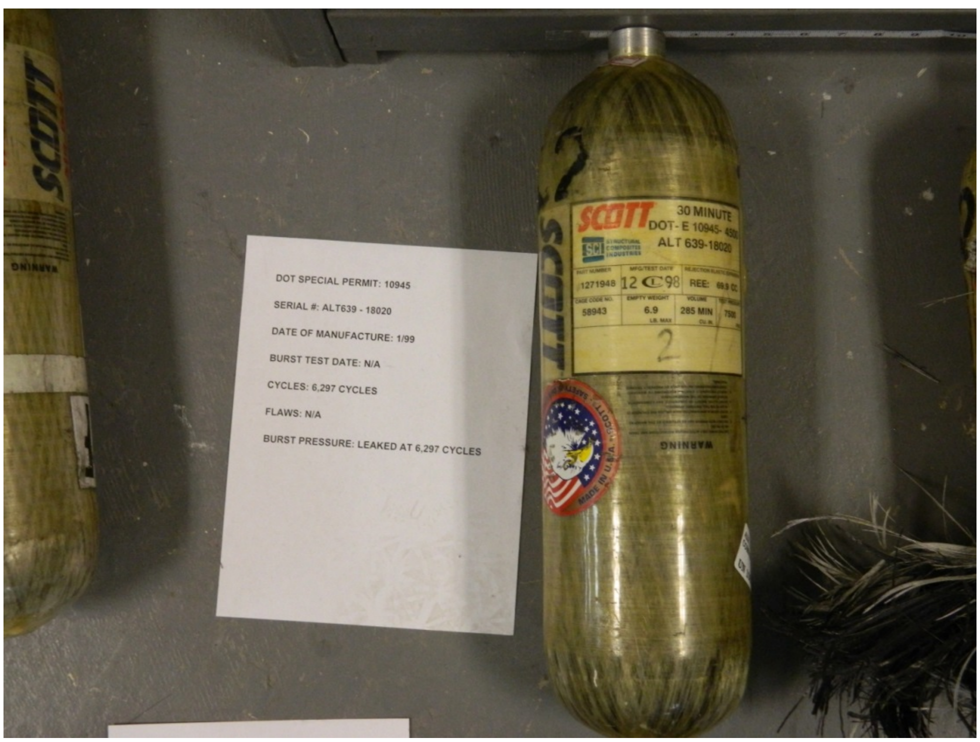

Figure 10.50 – Image of ALT639-18020 after EOL Burst testing.

Figure 10.51 – Image of ALT639-3567 after EOL Burst testing.

Figure 10.52 – Image of OM3983 after EOL Burst testing.

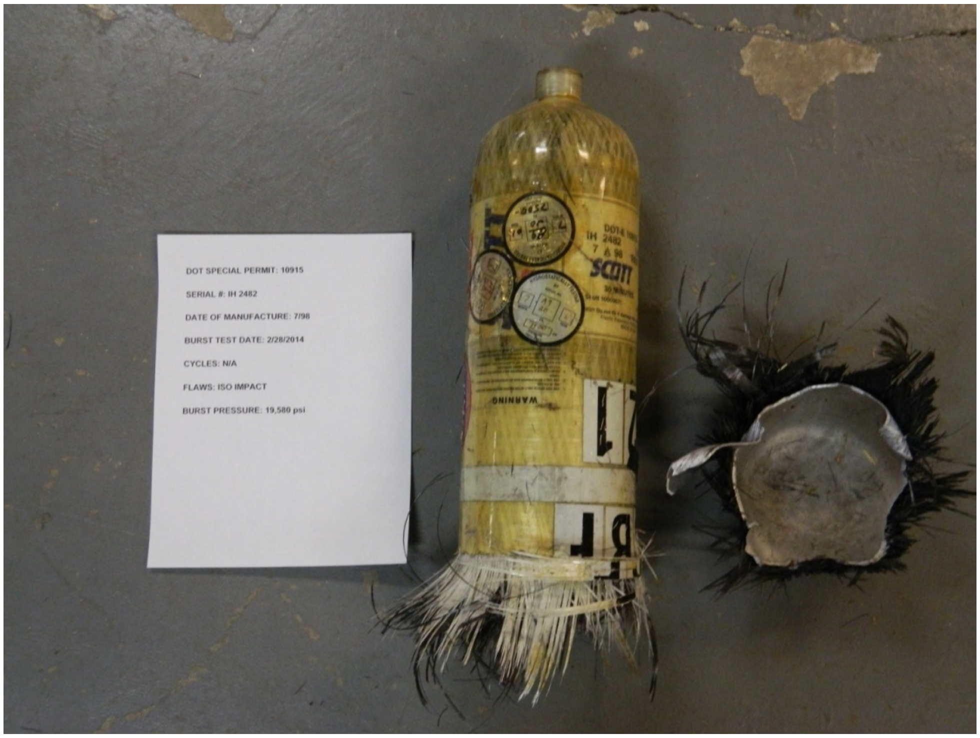

Figure 10.53 – Image of IH2482 after EOL Burst testing.

Figure 10.54 – Image of ALT604-4371 after EOL Burst testing.

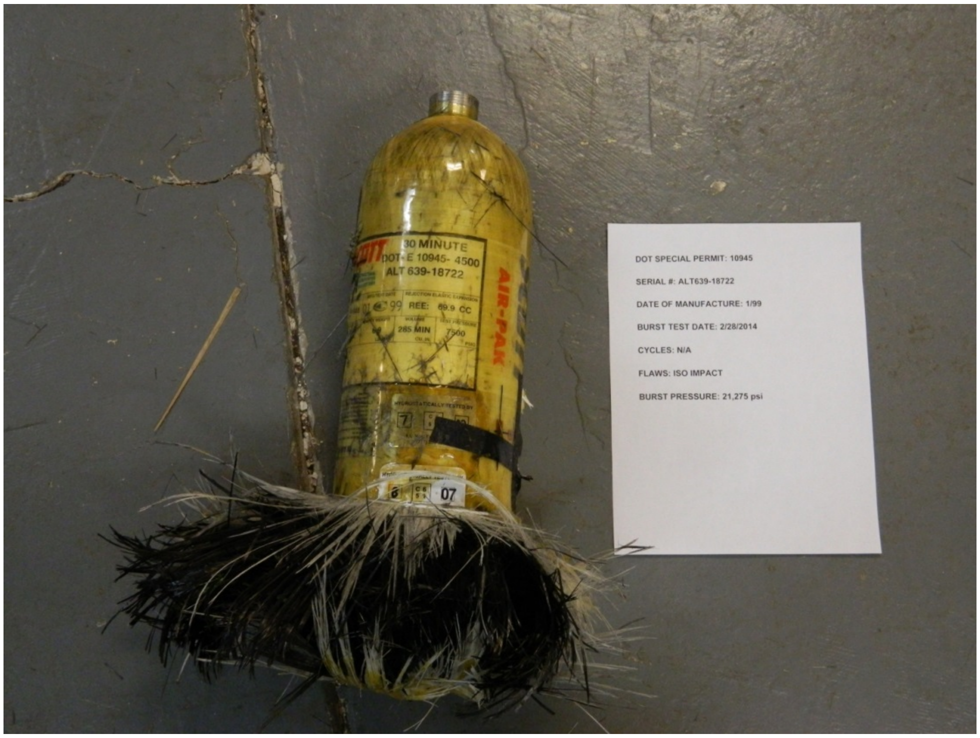

Figure 10.55 – Image of ALT639-18722 after EOL Burst testing.

Figure 10.56 – Image of ALT604-6021 after EOL Burst testing.

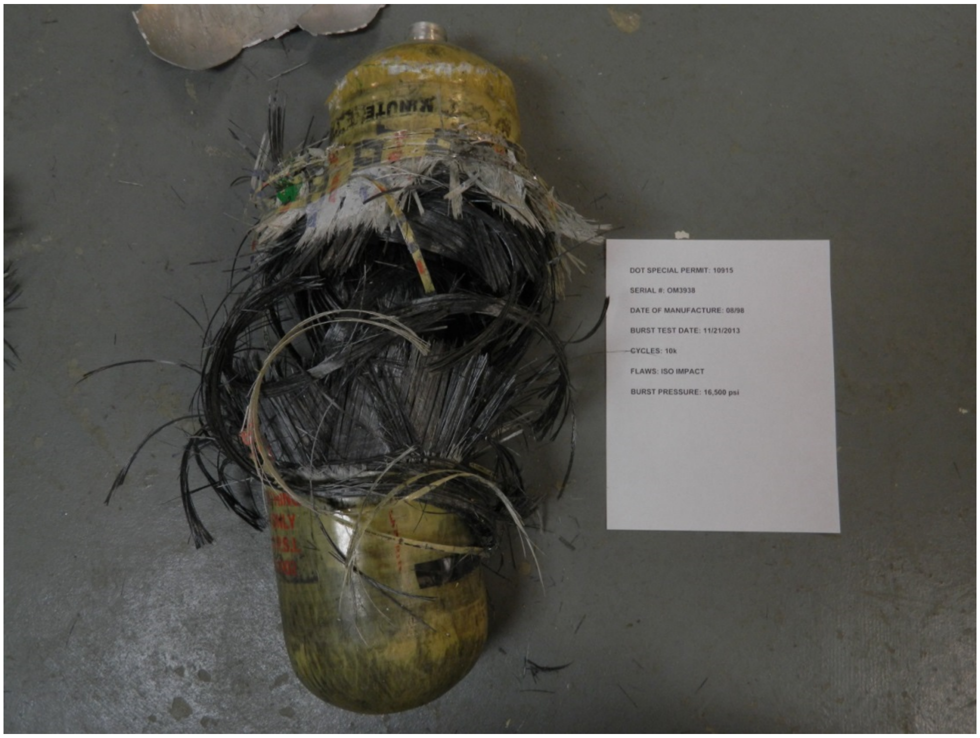

Figure 10.57 – Image of OM3938 after EOL Burst testing.

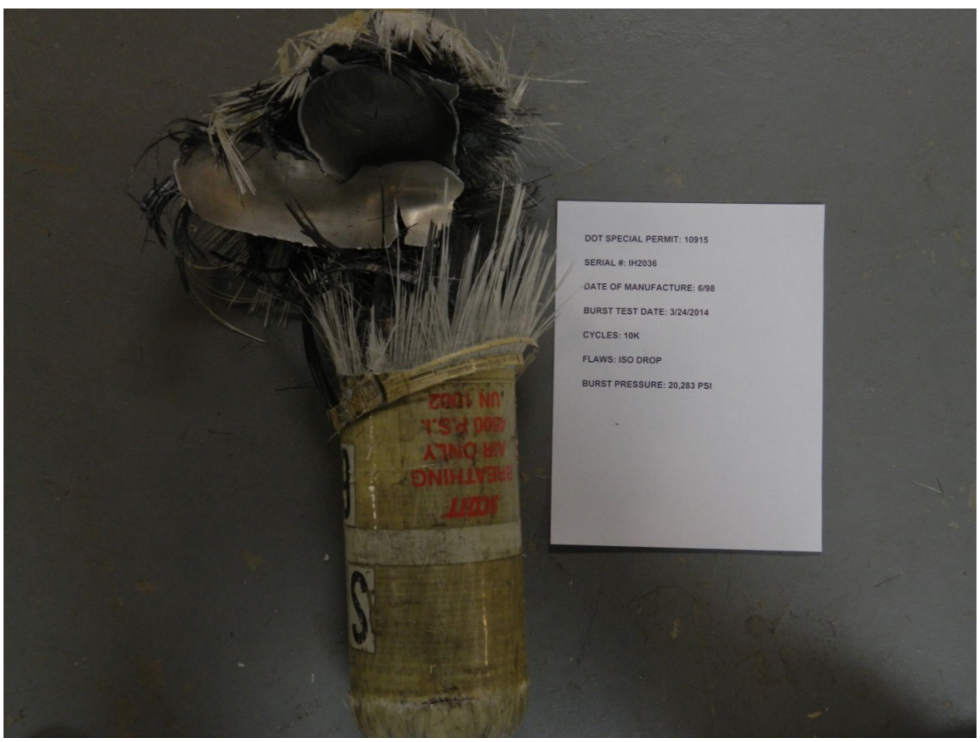

Figure 10.58 – Image of IH2036 after EOL Burst testing.

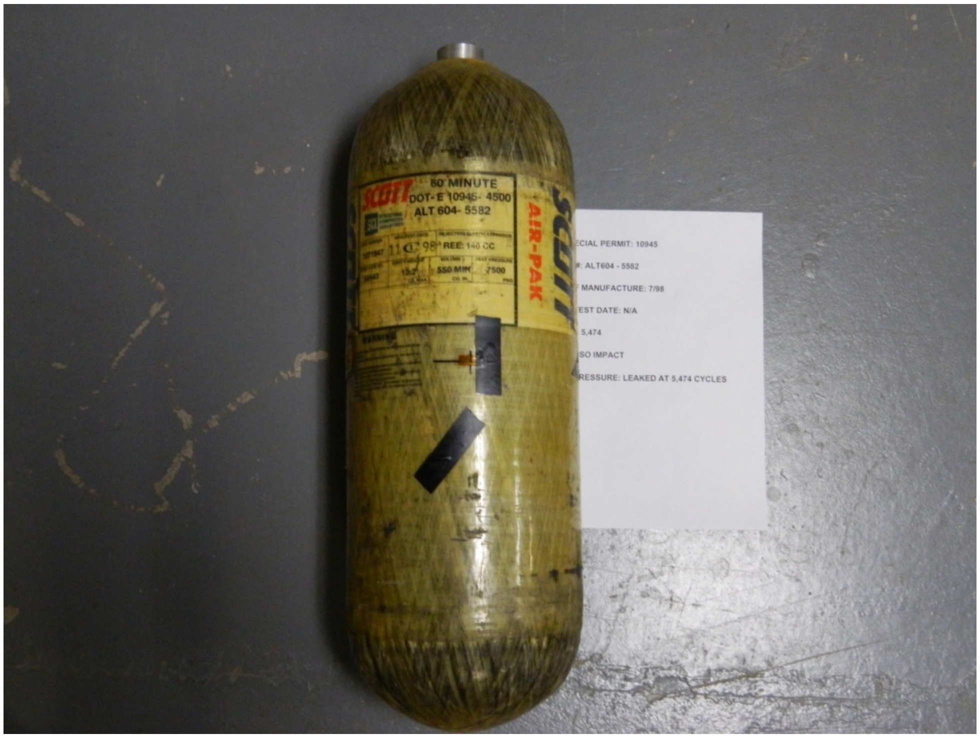

Figure 10.59 – Image of ALT604-5582 after EOL Burst testing.

Figure 10.60 – Image of ALT639-40157 after EOL Burst testing.

Figure 10.61 – Image of ALT695-3794 after EOL Burst testing.

Figure 10.62 – Image of OM3948 after EOL Burst testing.

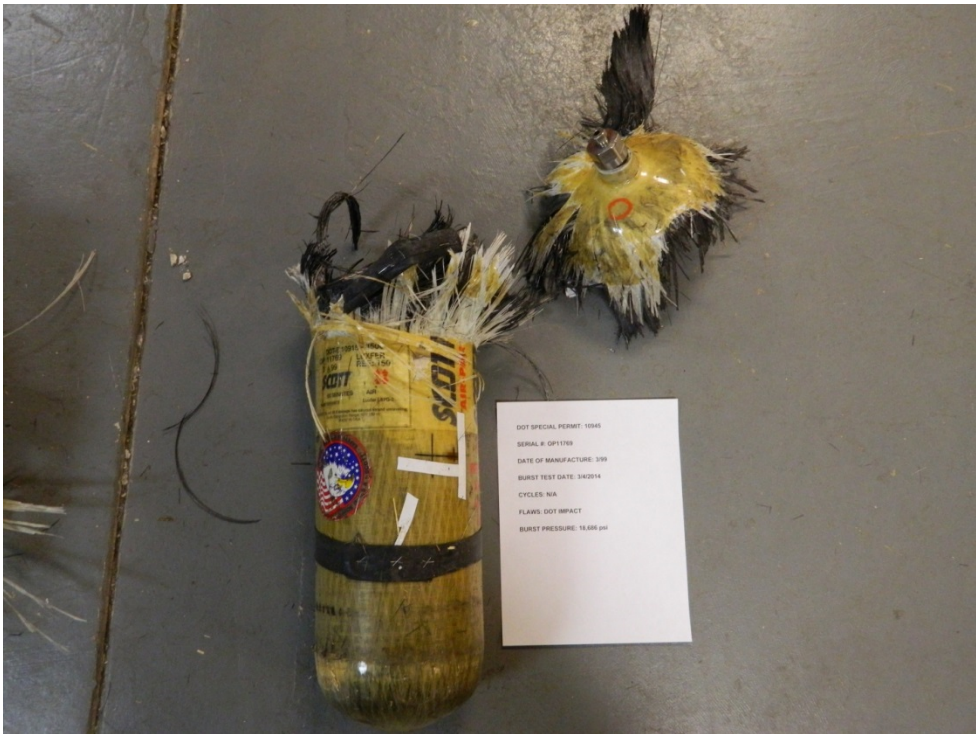

Figure 10.63 – Image of OP11769 after EOL Burst testinzg.

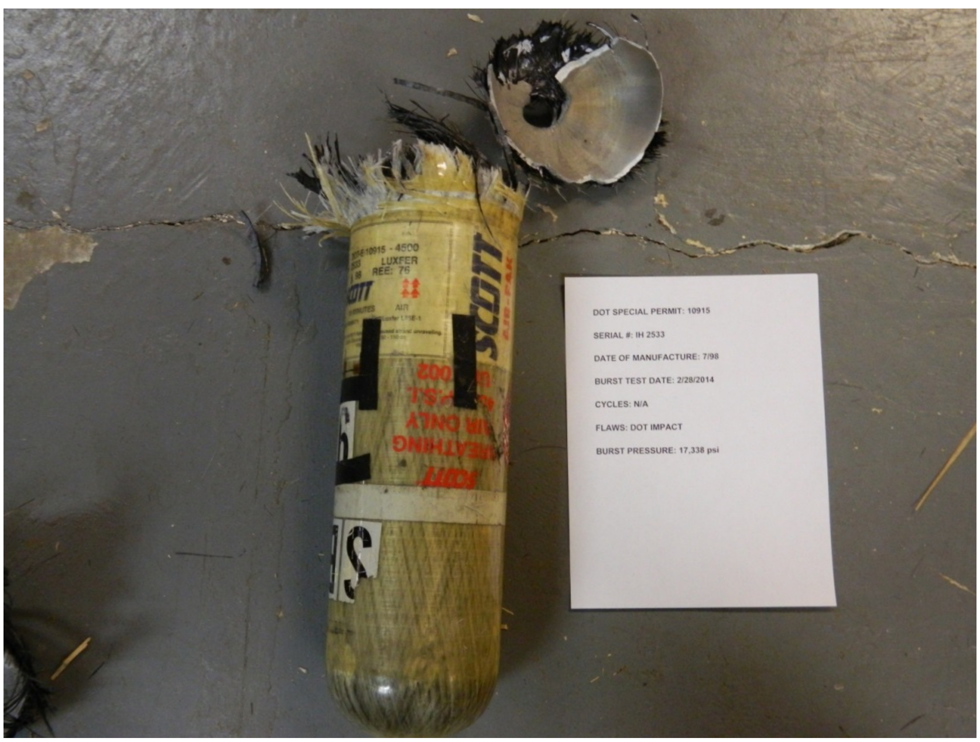

Figure 10.64 – Image of IH2533 after EOL Burst testing.

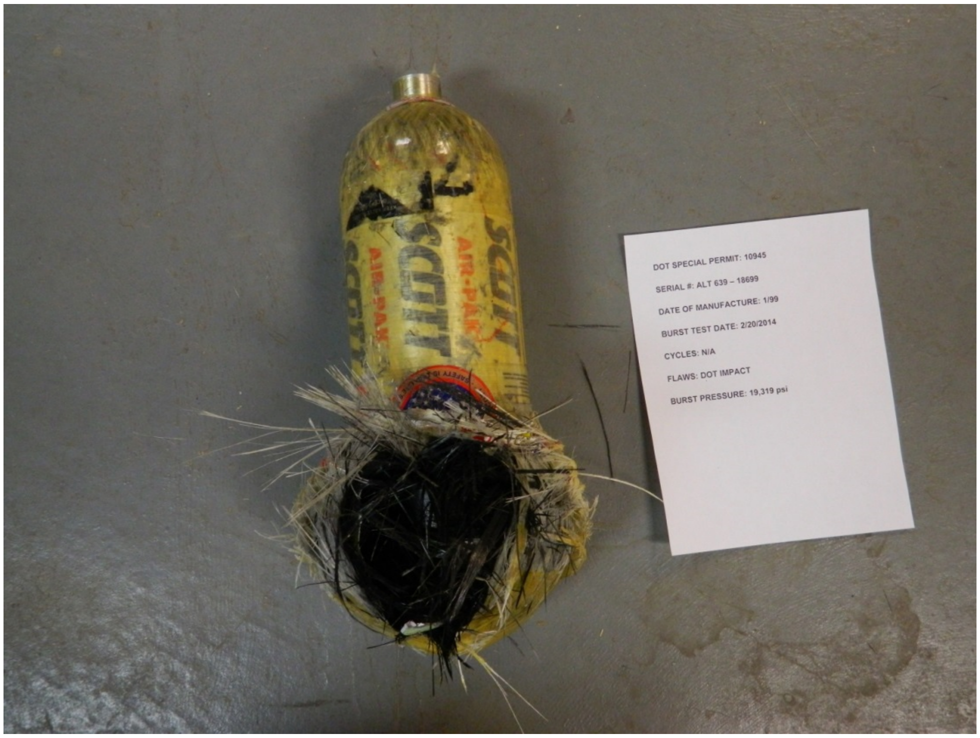

Figure 10.65 – Image of ALT639-18699 after EOL Burst testing.

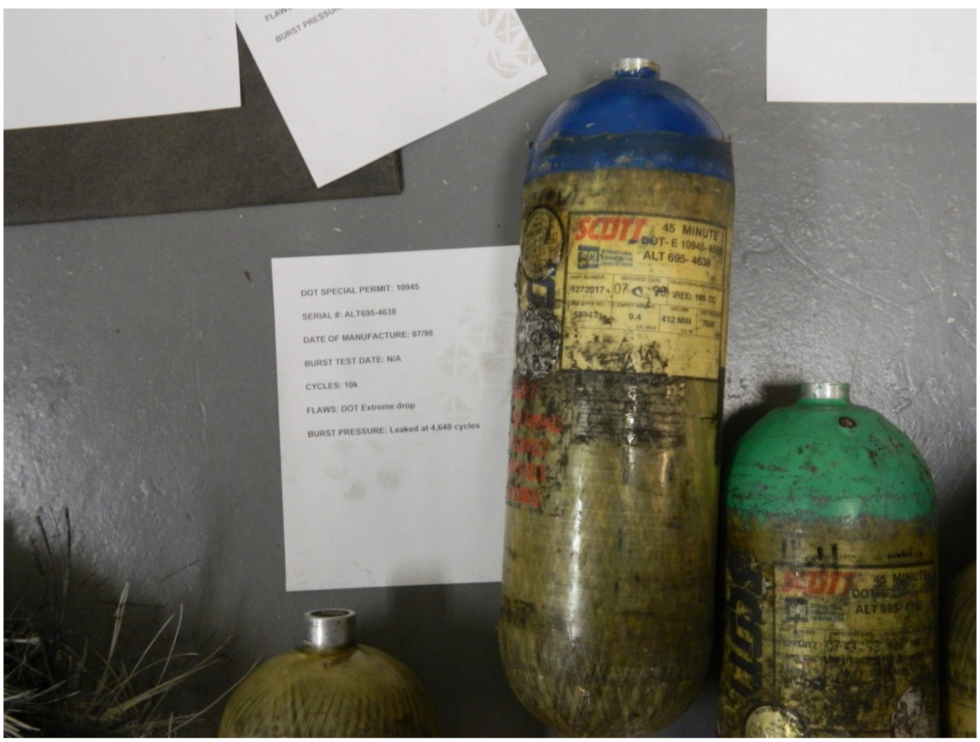

Figure 10.66 – Image of ALT695-4638, leaked after 4640 cycles.

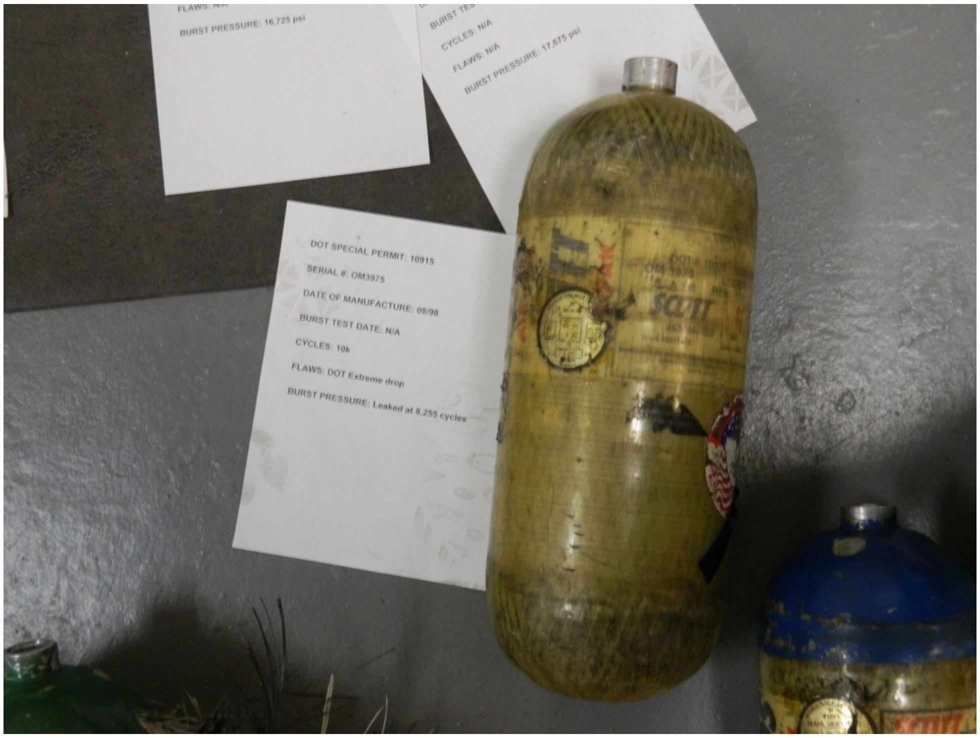

Figure 10.67 – Image of OM3957, leaked after 8,255 cycles.

Figure 10.68 – Image of ALT639-17697 after EOL Burst testing.

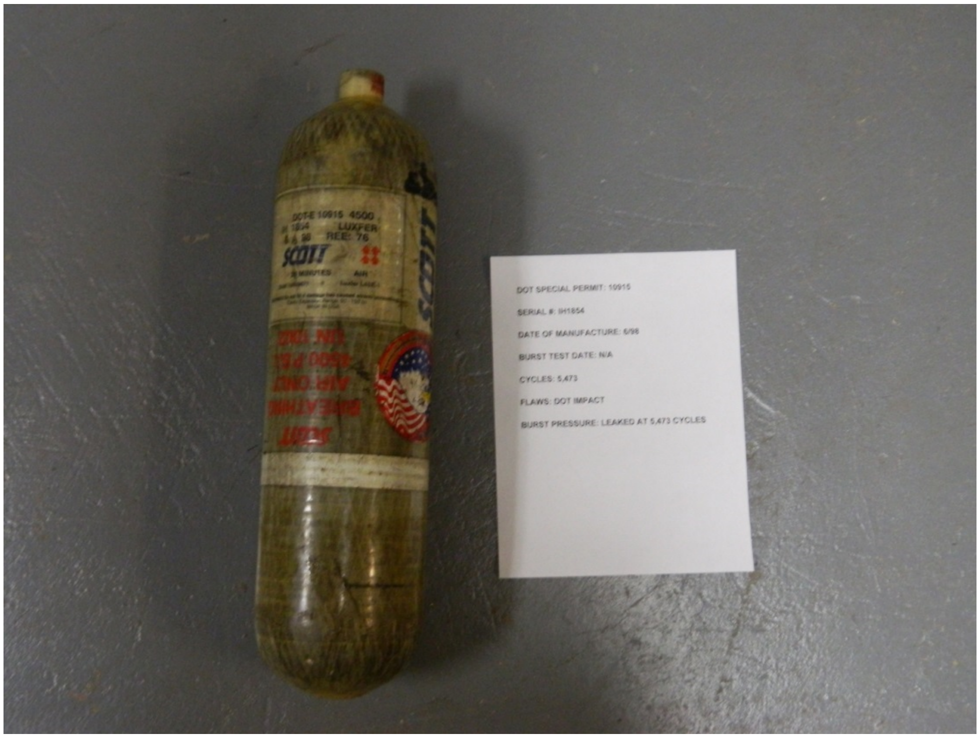

Figure 10.69 – Image of IH1854 after EOL Burst testing.

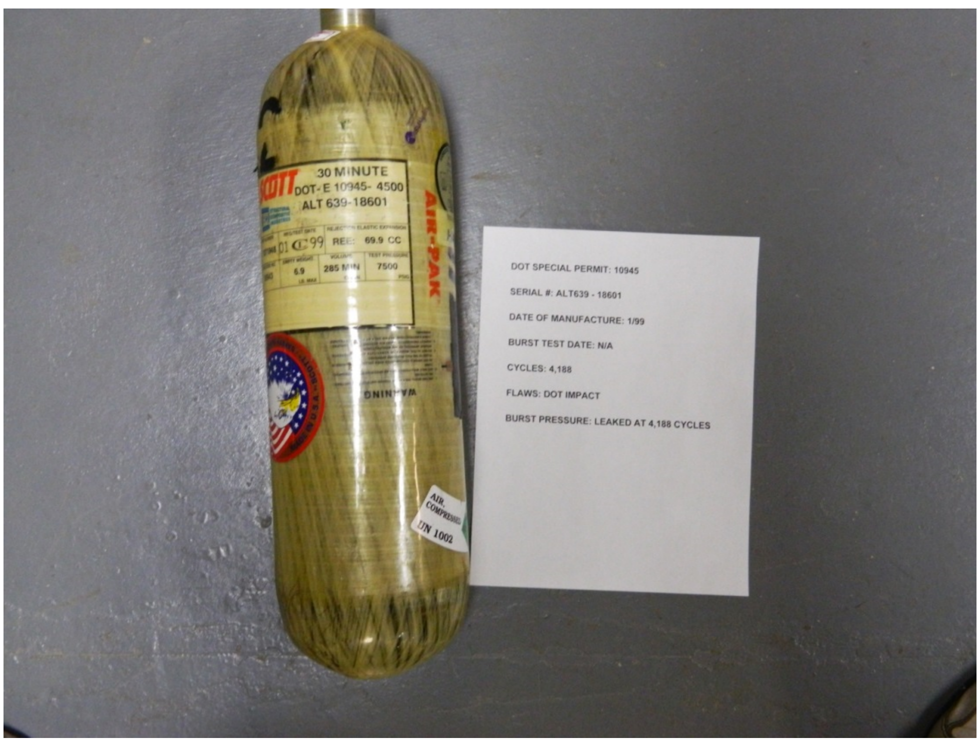

Figure 10.70 – Image of ALT639-18601 after EOL Burst testing.

Figure 10. 71 – Image of ALT695-3929 after EOL Burst testing.

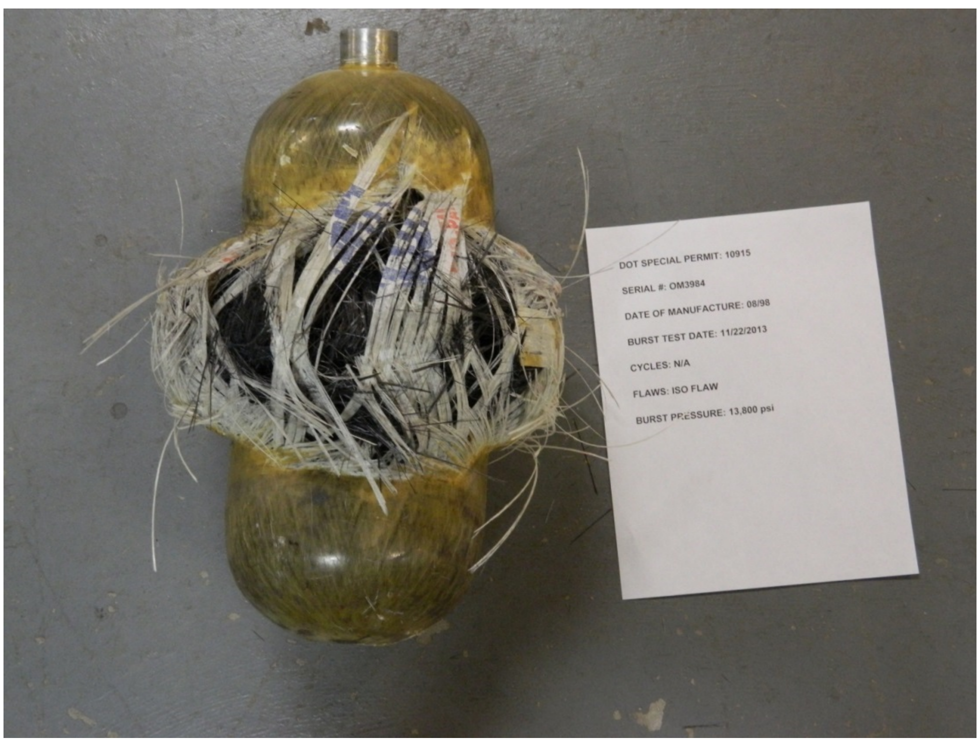

Figure 10.72 – Image of OM3984 after EOL Burst testing.

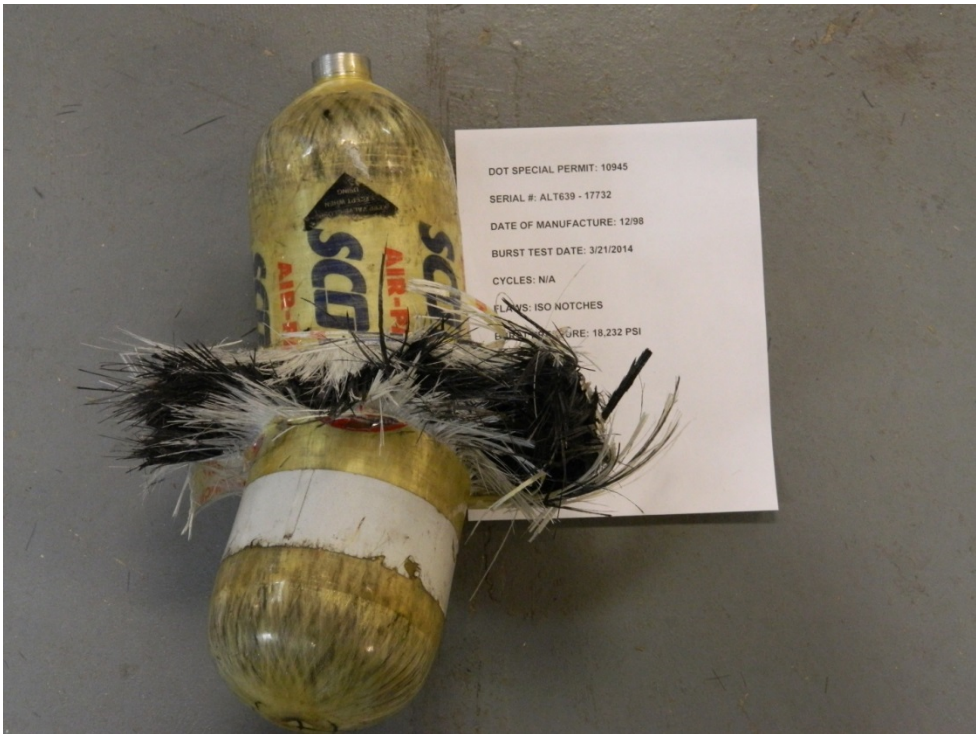

Figure 10.73 – Image of ALT639-17732 after EOL Burst testing.

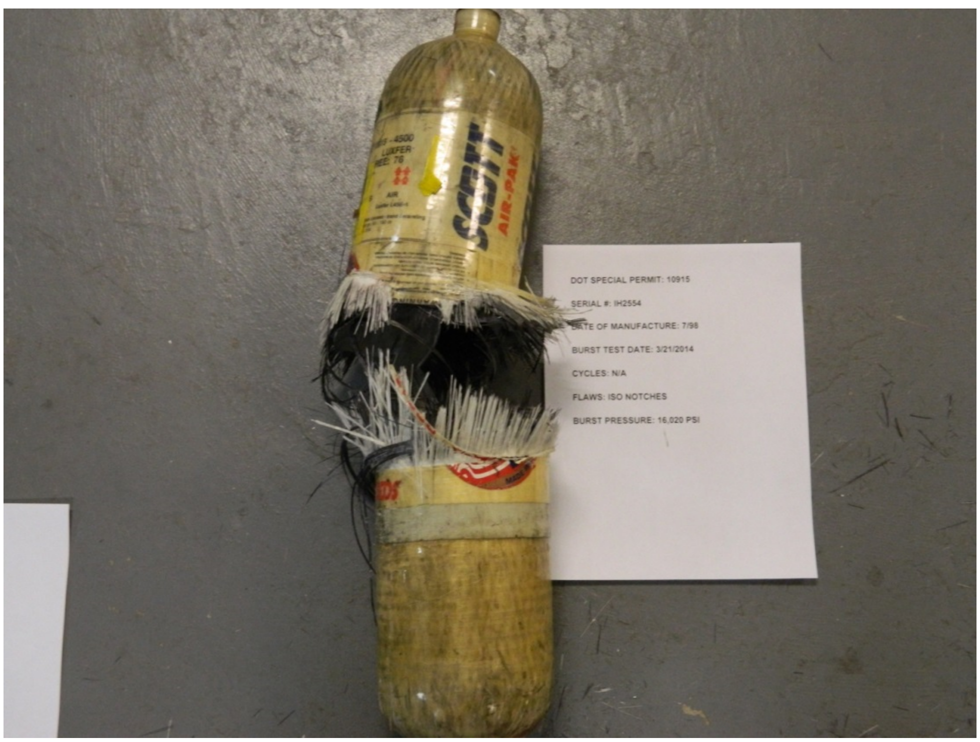

Figure 10.74 – Image of IH2554 after EOL Burst testing.

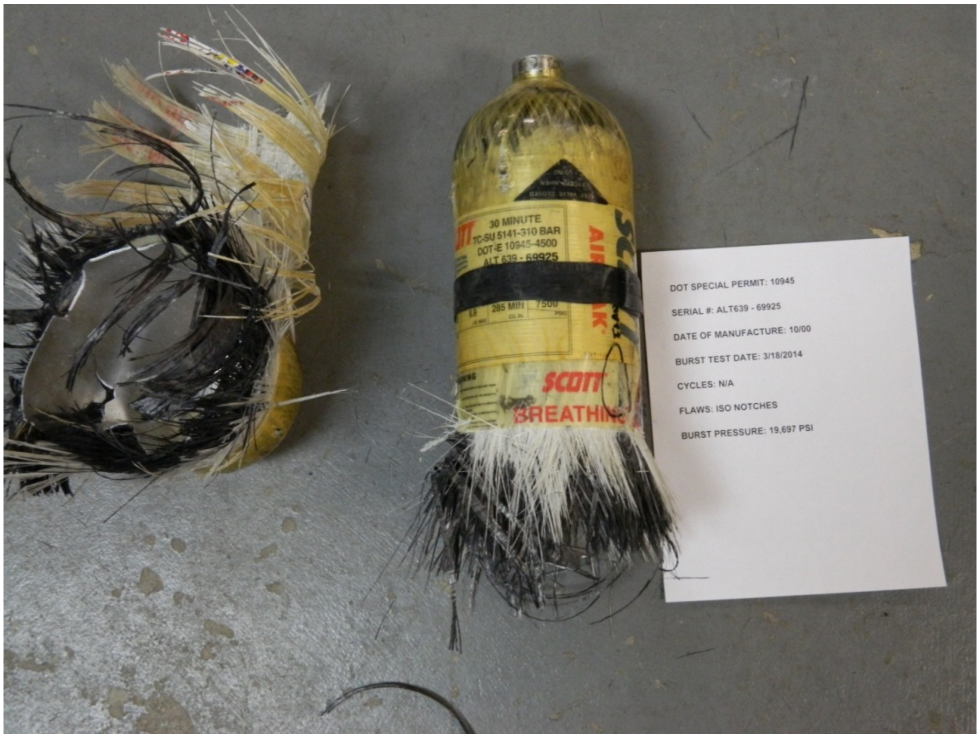

Figure 10.75 – Image of ALT639-69925 after EOL Burst testing.

Figure 10.76 – Image of ALT695-4304 after EOL Burst testing.

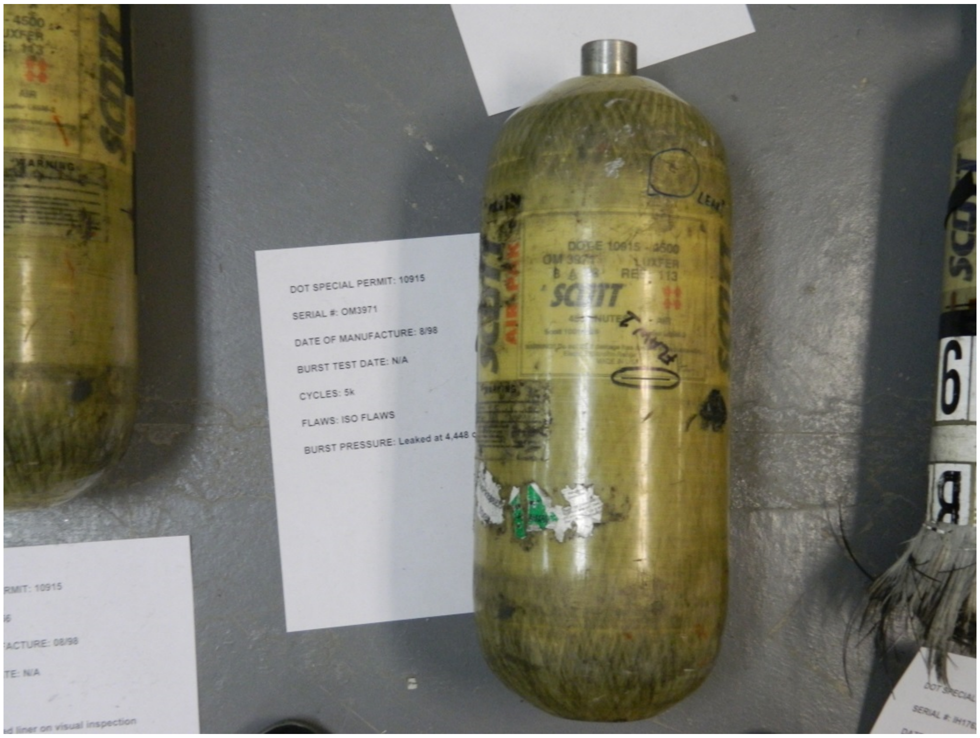

Figure 10.77 – Image of OM3957, leaked after 4,448 cycles.

Figure 10.78 – Image of OP11129 after EOL Burst testing.

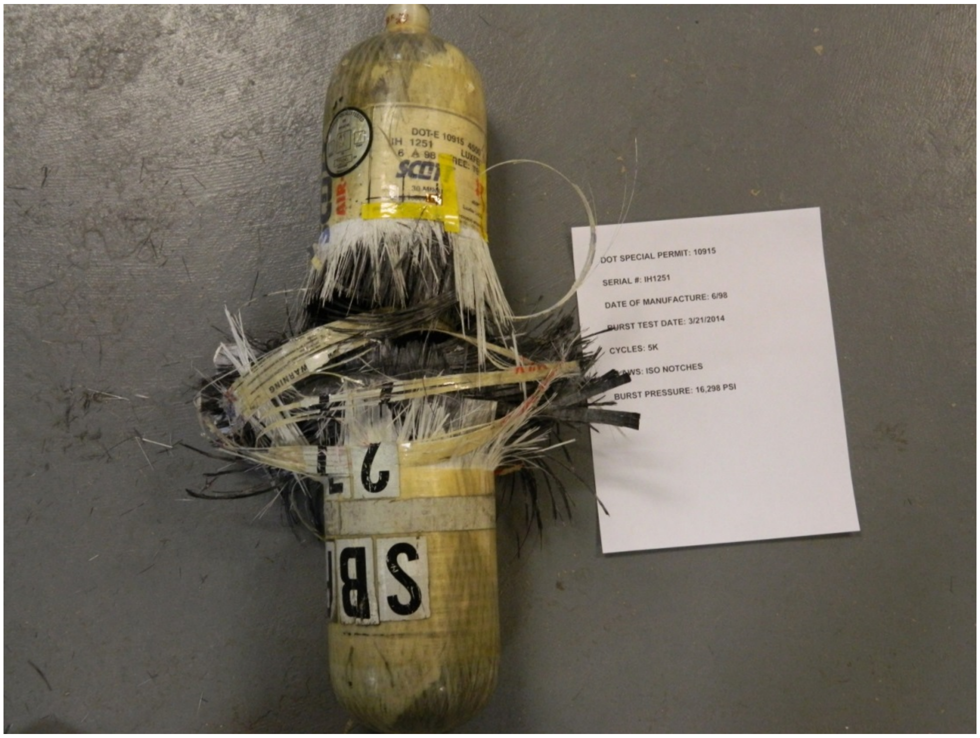

Figure 10.79 – Image of IH1251 after EOL Burst testing.

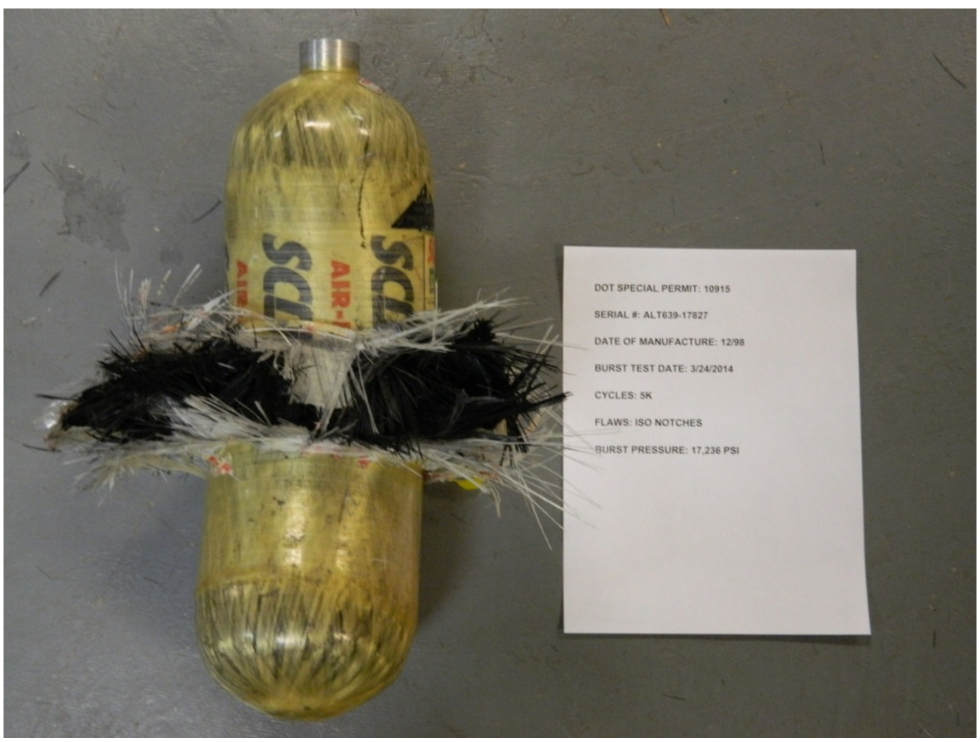

Figure 10.80 – Image of ALT639-17827 after EOL Burst testing.

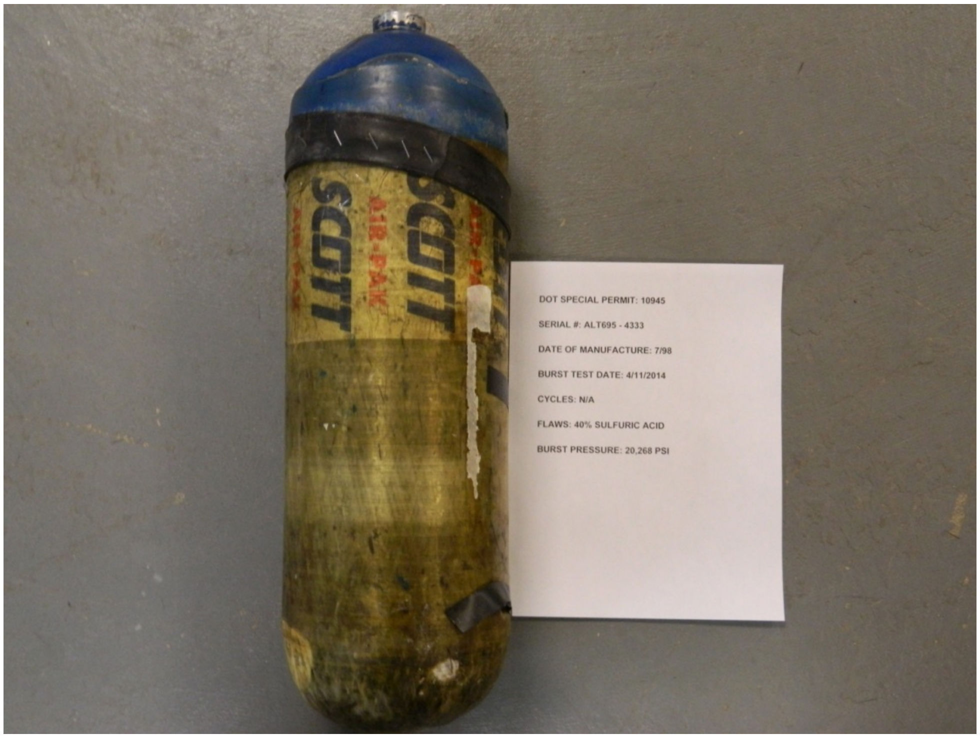

Figure 10.81 – Image of ALT695-4333 after EOL Burst testing.

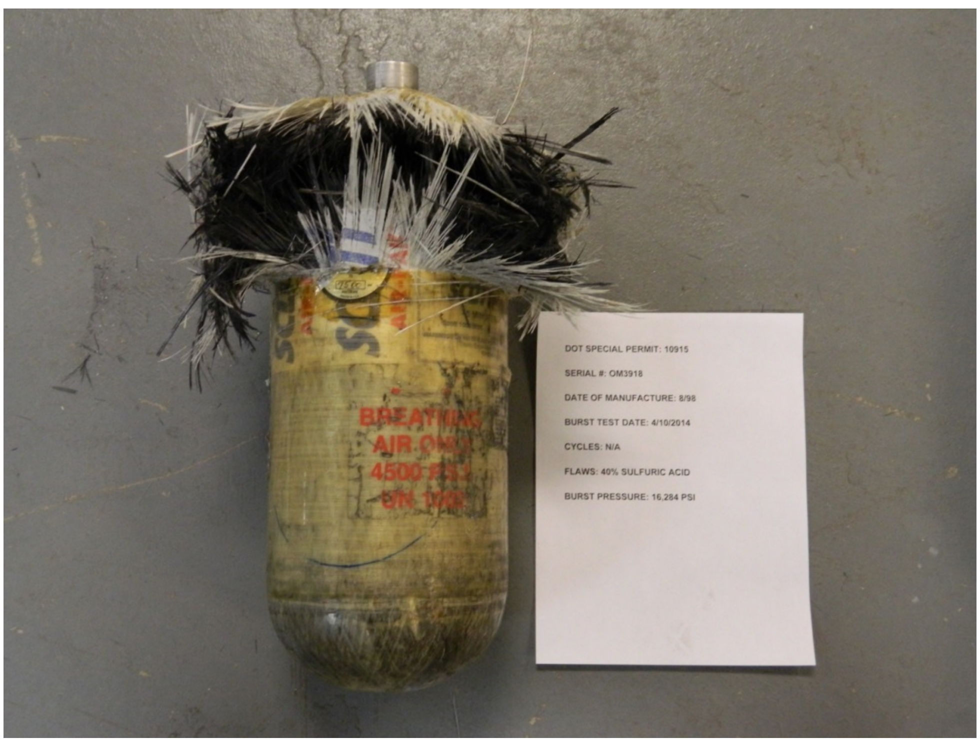

Figure 10.82 – Image of OM3918 after EOL Burst testing.

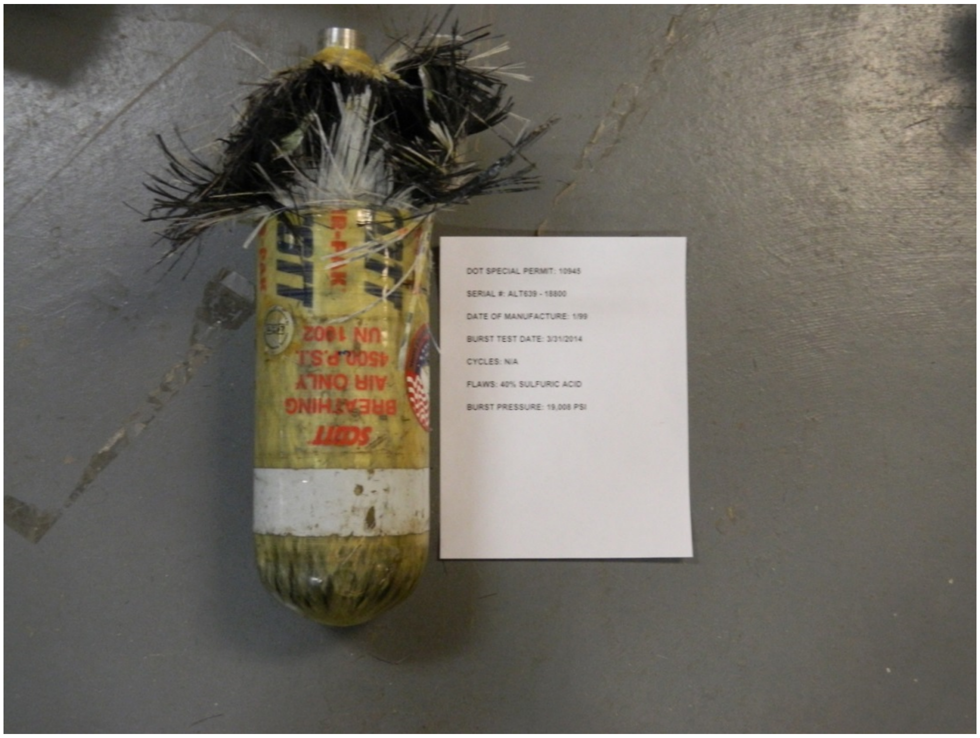

Figure 10.83 – Image of ALT639-18800 after EOL Burst testing.

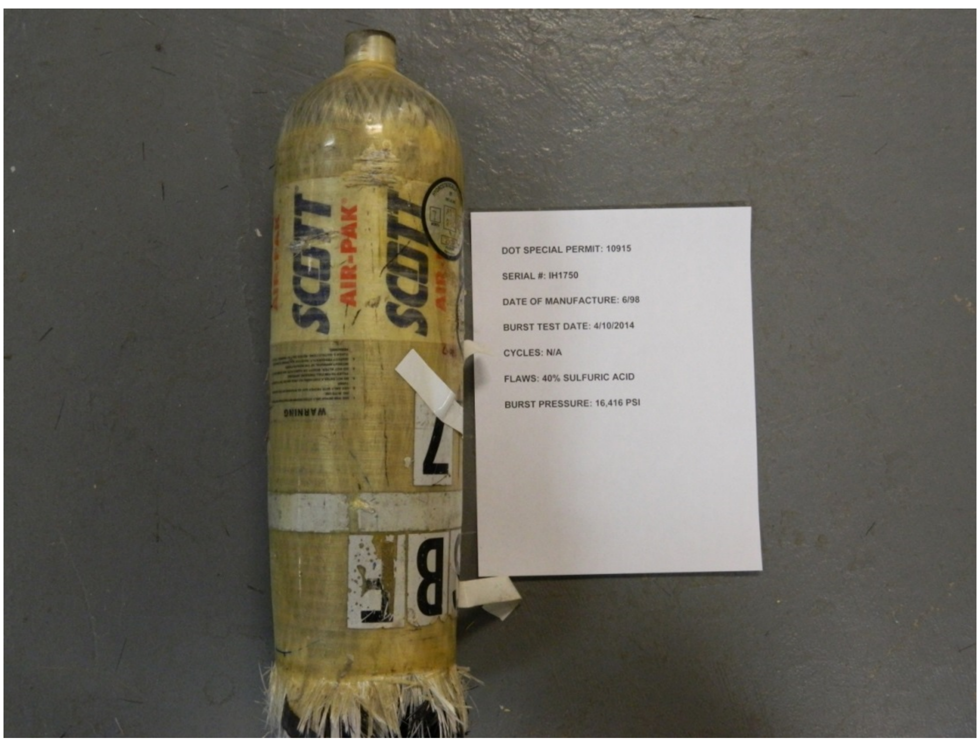

Figure 10.84 – Image of IH1750 after EOL Burst testing.

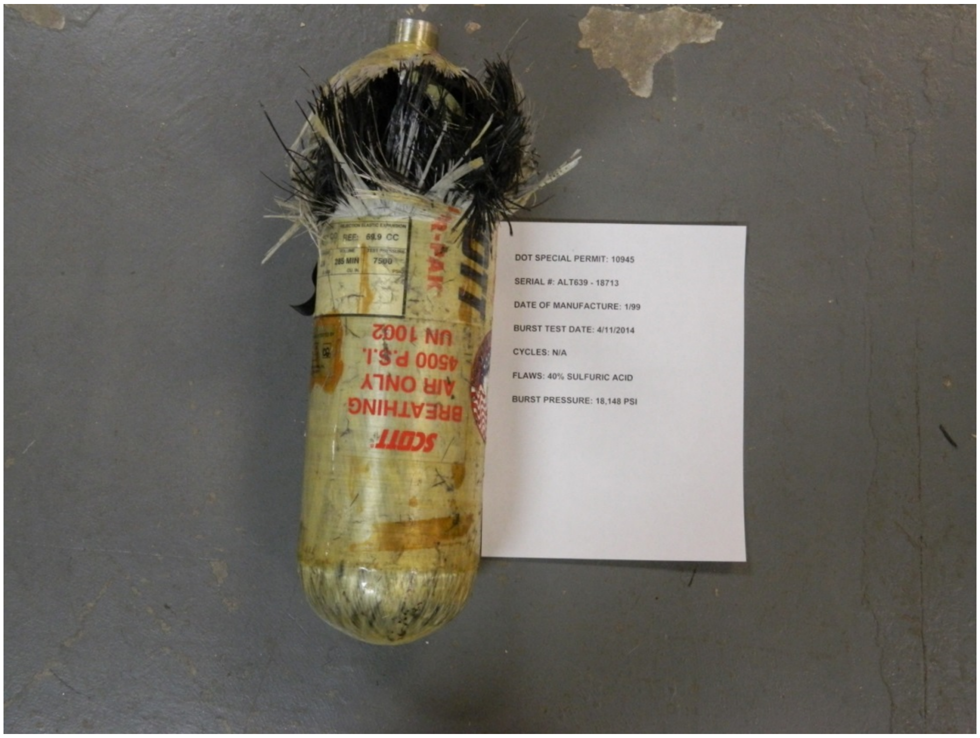

Figure 10.85 – Image of ALT639-18713 after EOL Burst testing.

Figure 10.86 – Image of OM3985, leaked after 5,369 cycles.

Figure 10.87 – Image of OM3960, leaked after 5,364 cycles.

Figure 10.88 – Image of OM3956, leaked after 8,680 cycles.

Figure 10.89 – Image of OM3994, leaked after 5,369 cycles.

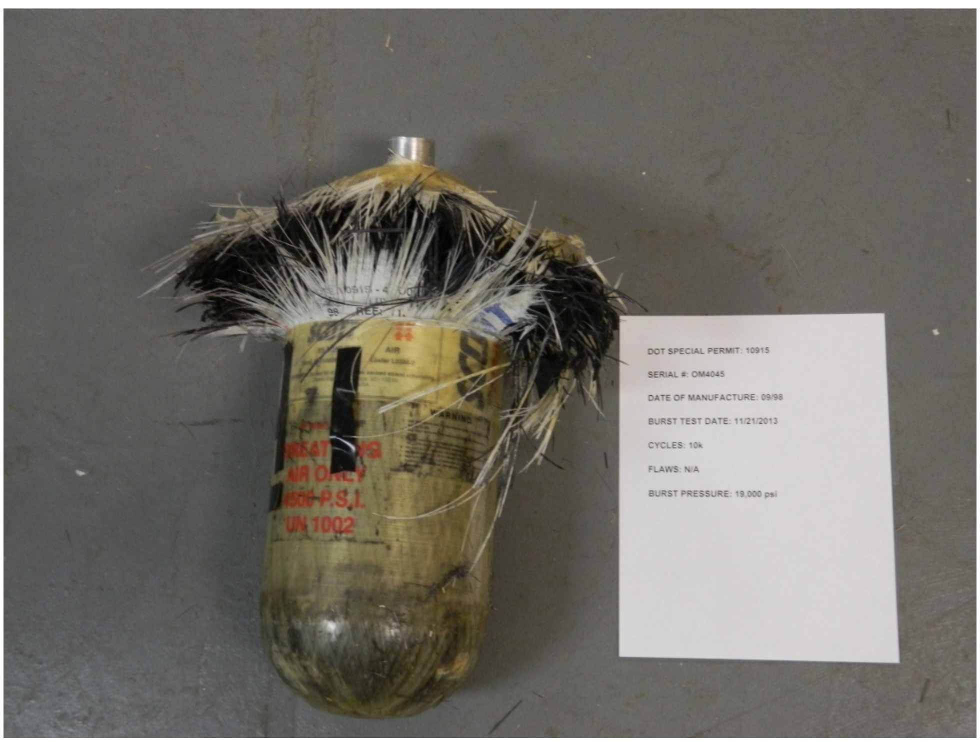

Figure 10.90 – Image of OM4045, after EOL Burst test.

Figure 10.91 – Image of OM3969, leaked after 6,986 cycles.

Figure 10.92 – Image of OM3973, leaked after 6,568 cycles.

Figure 10.93 – Image of OM3985, leaked after 6,984 cycles.

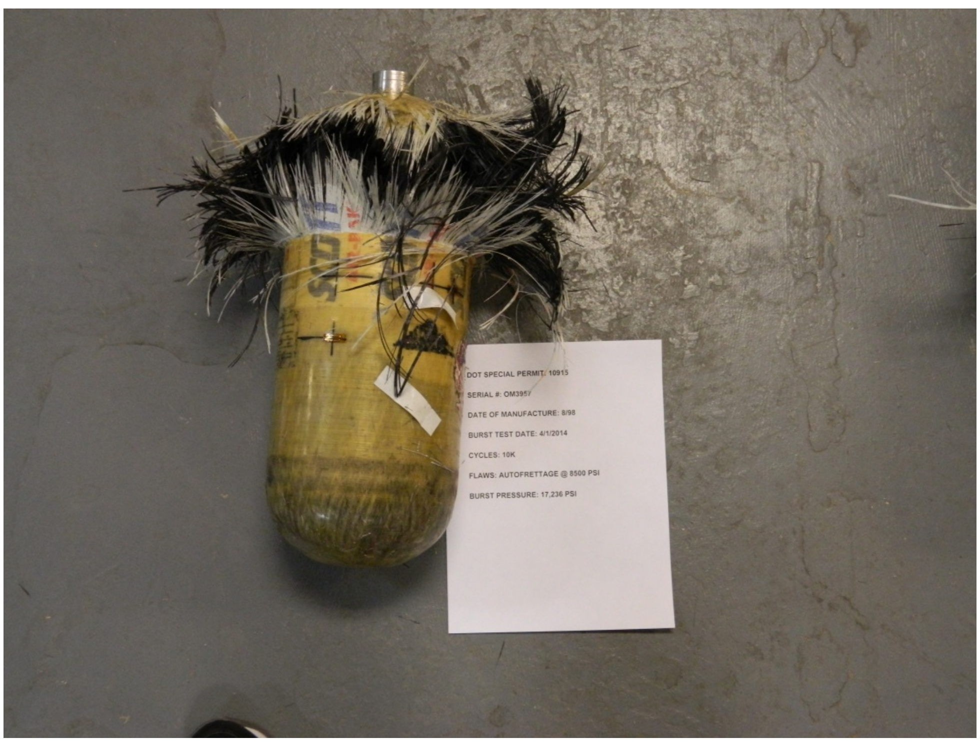

Figure 10.94 – Image of OM3957, after EOL Burst.

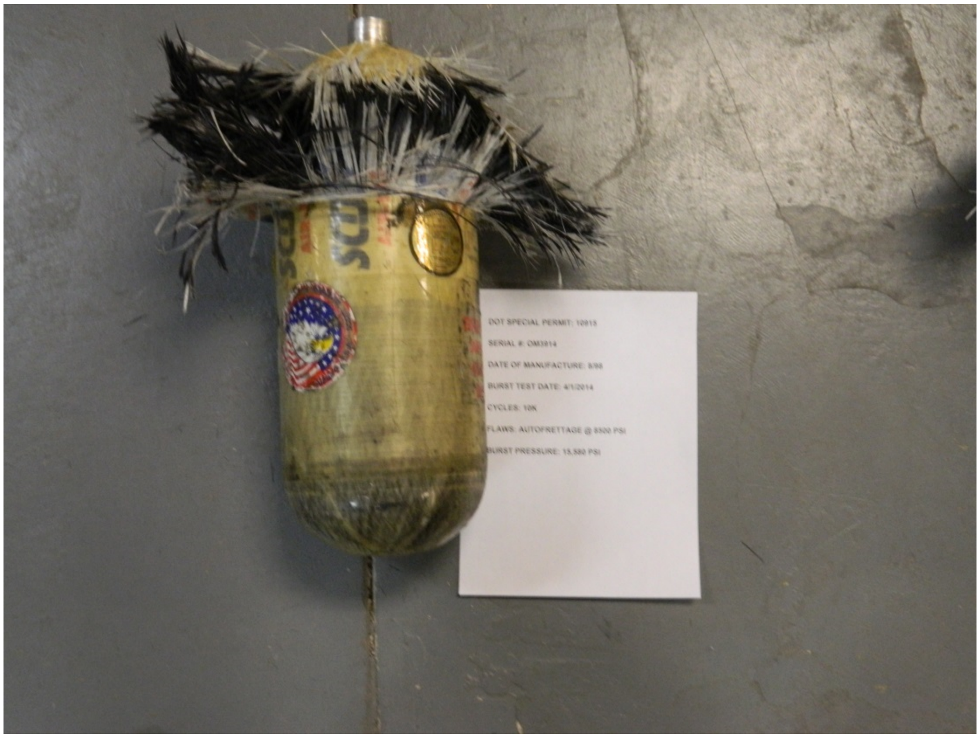

Figure 10.95 – Image of OM3914, after EOL Burst.

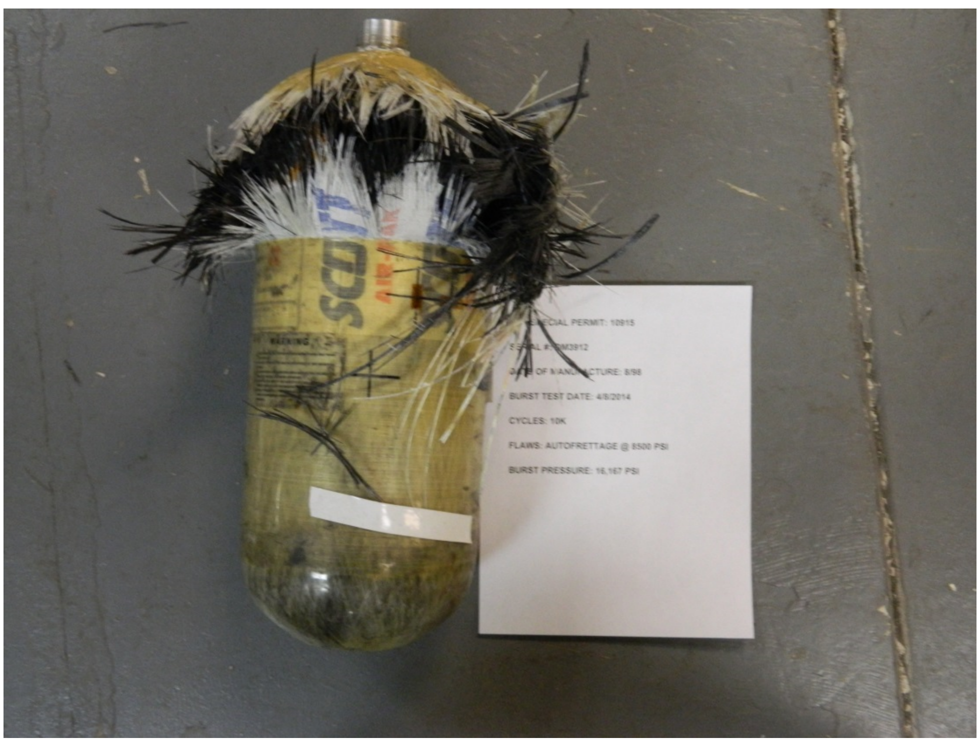

Figure 10.96 – Image of OM3912, after EOL Burst.

Figure 10.97 – Image of OM3954, after EOL Burst.

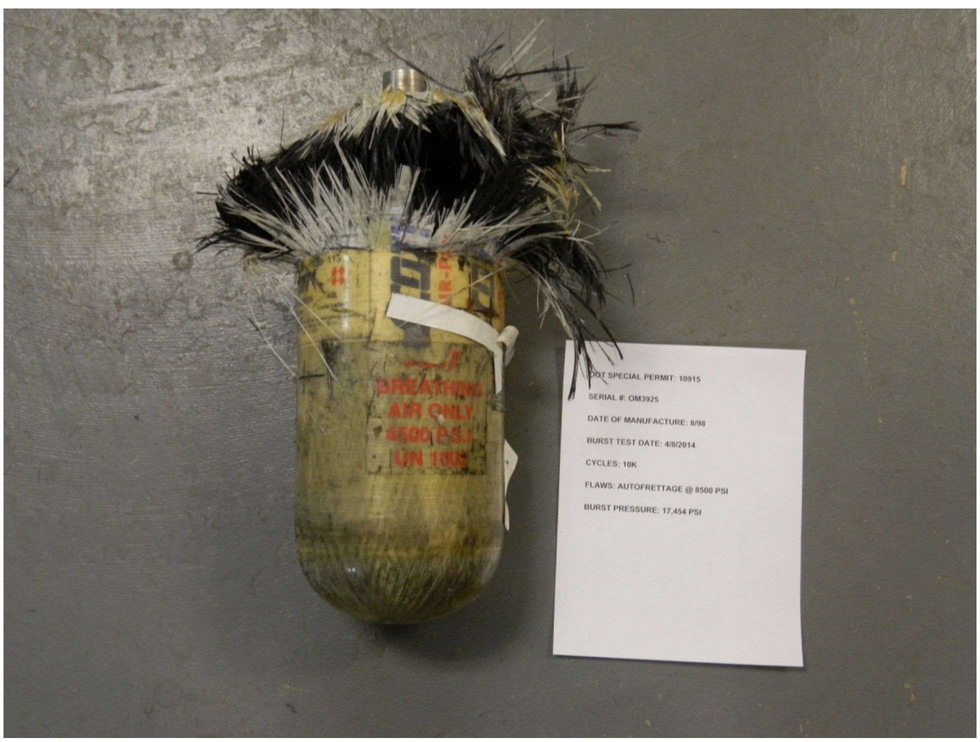

Figure 10.98 – Image of OM3925, after EOL Burst.

Figure 10.99 – Image of OM3917, after EOL Burst.

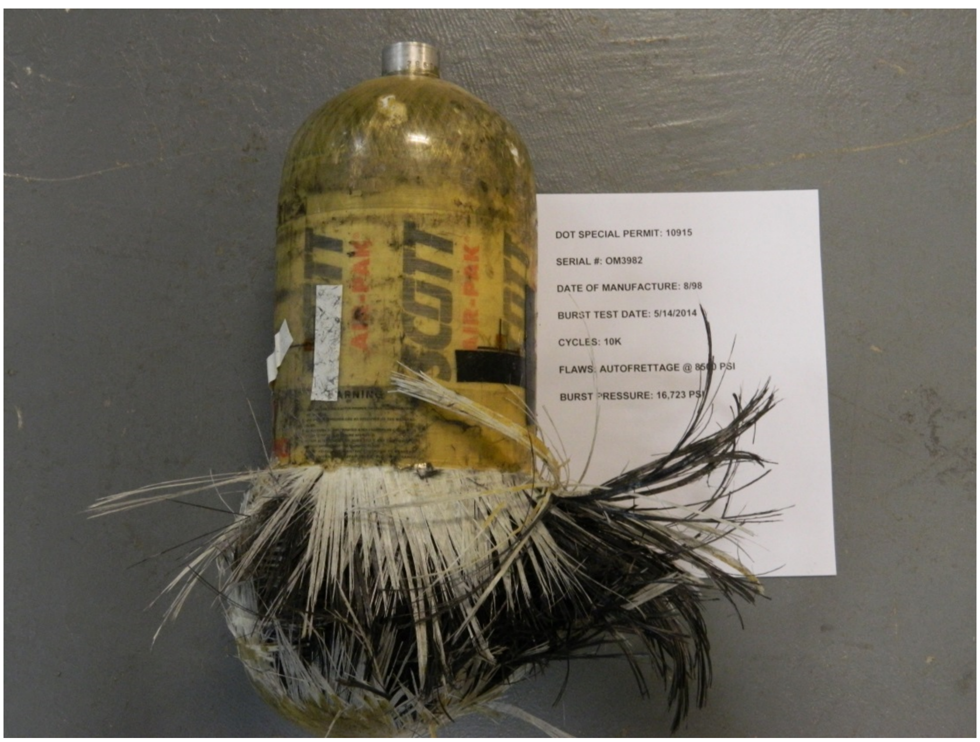

Figure 10.100 - – Image of OM3982, after EOL Burst.

11.0Appendix A – Stress Strain Curves

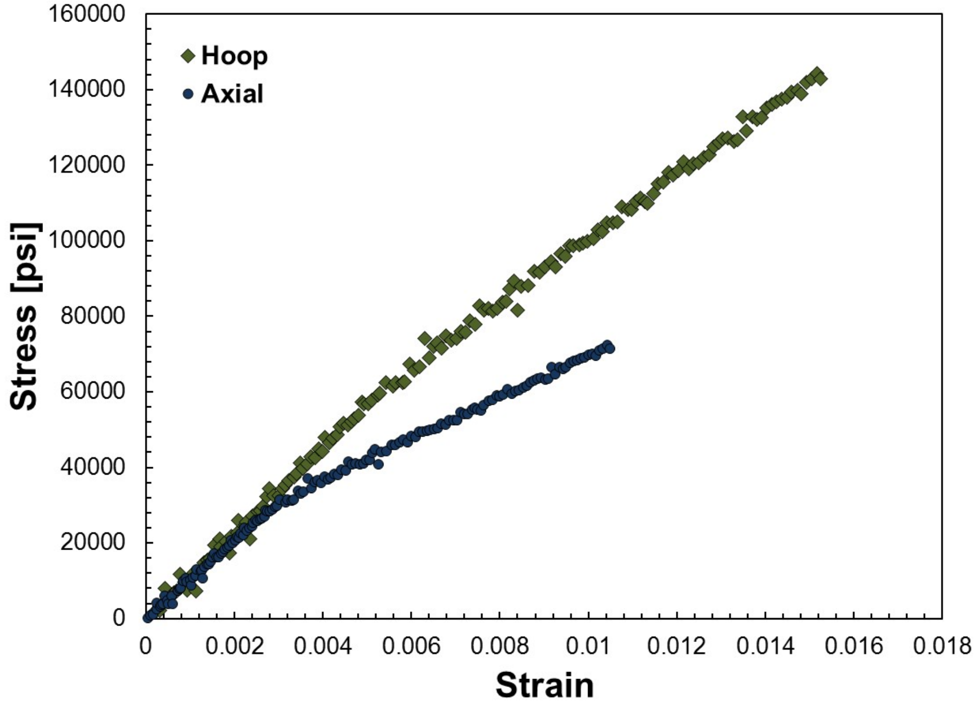

Figure A. 1 – Stress-strain response of ALT695 – 3650.

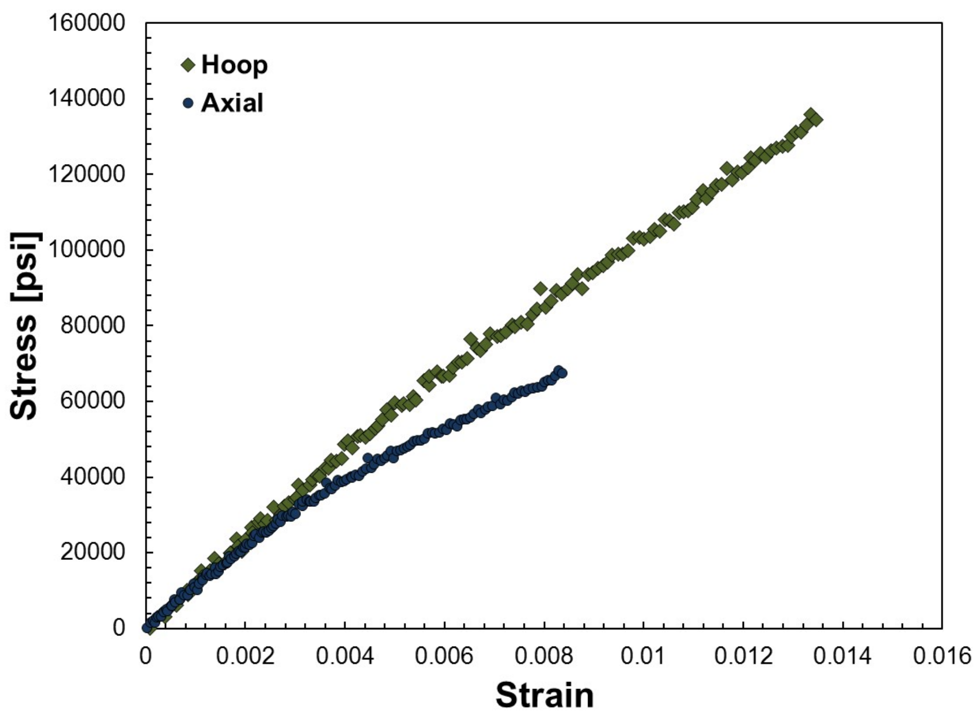

Figure A. 2 - Stress-strain response of ALT695 – 4436.

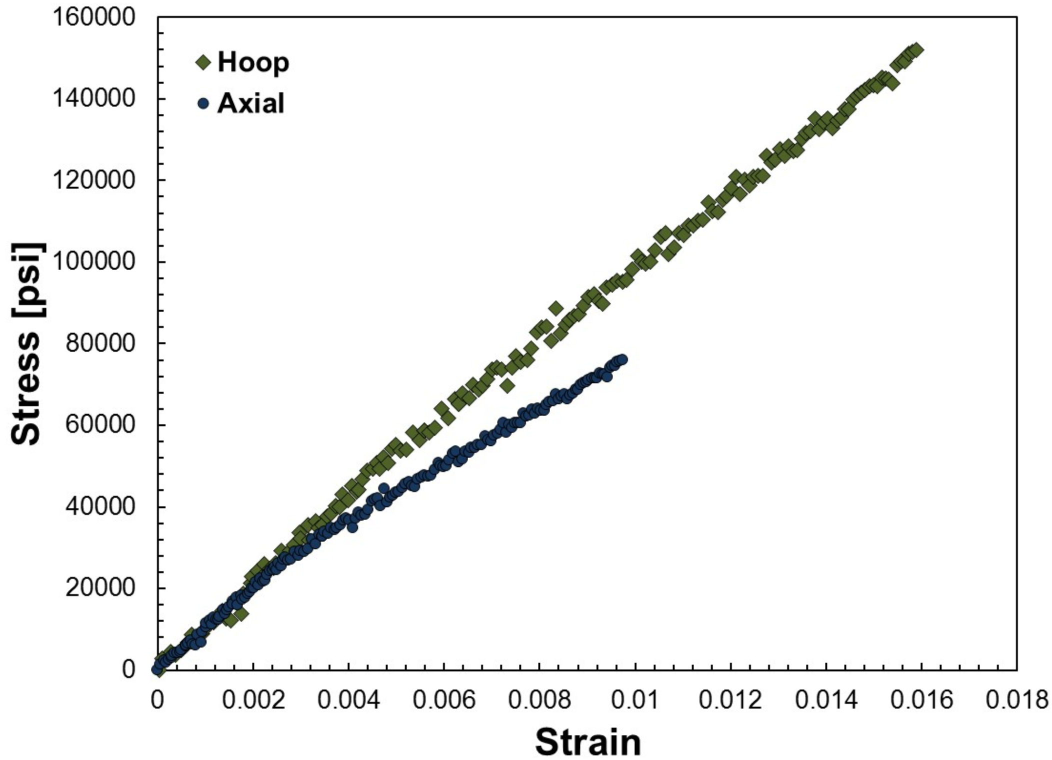

Figure A. 3 - Stress-strain response of ALT604 – 4962.

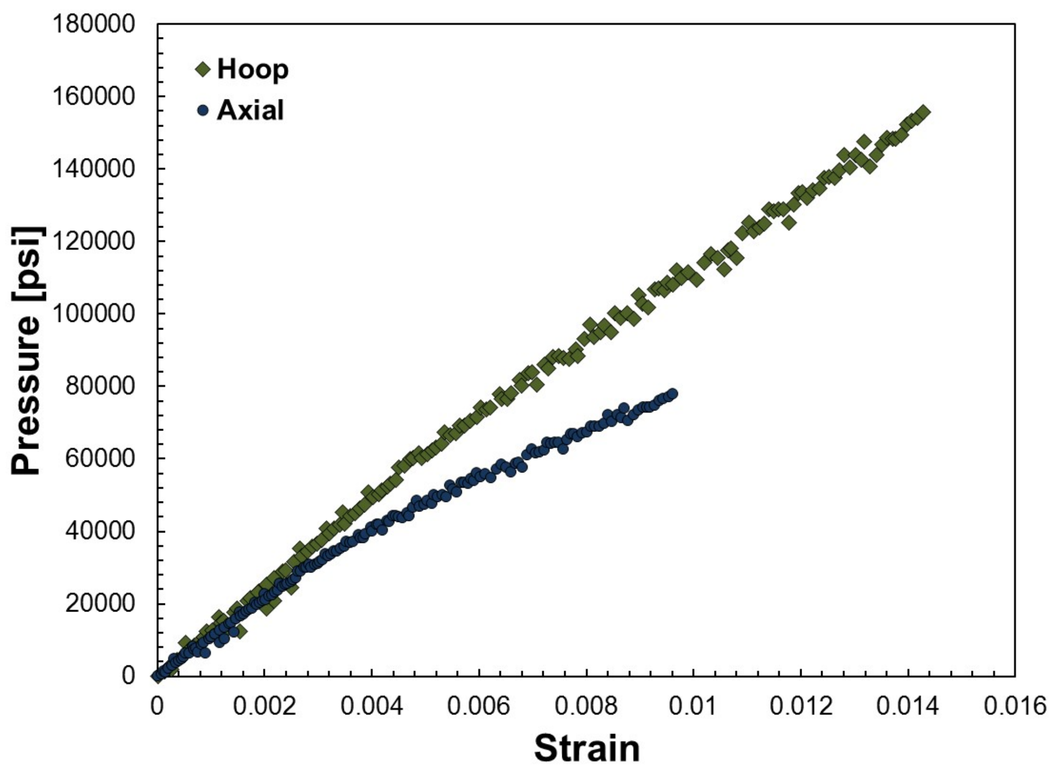

Figure A. 4 – Stress-strain response of ALT695 – 4494.

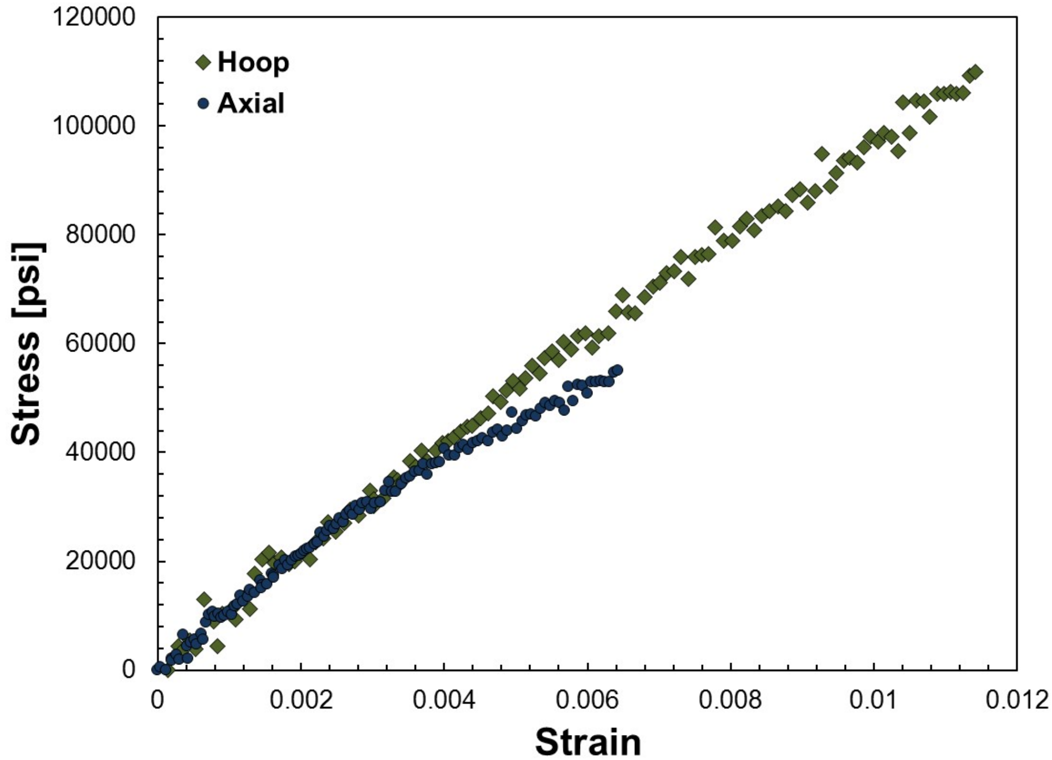

Figure A. 5 - Stress-strain response of ALT604 – 3742.

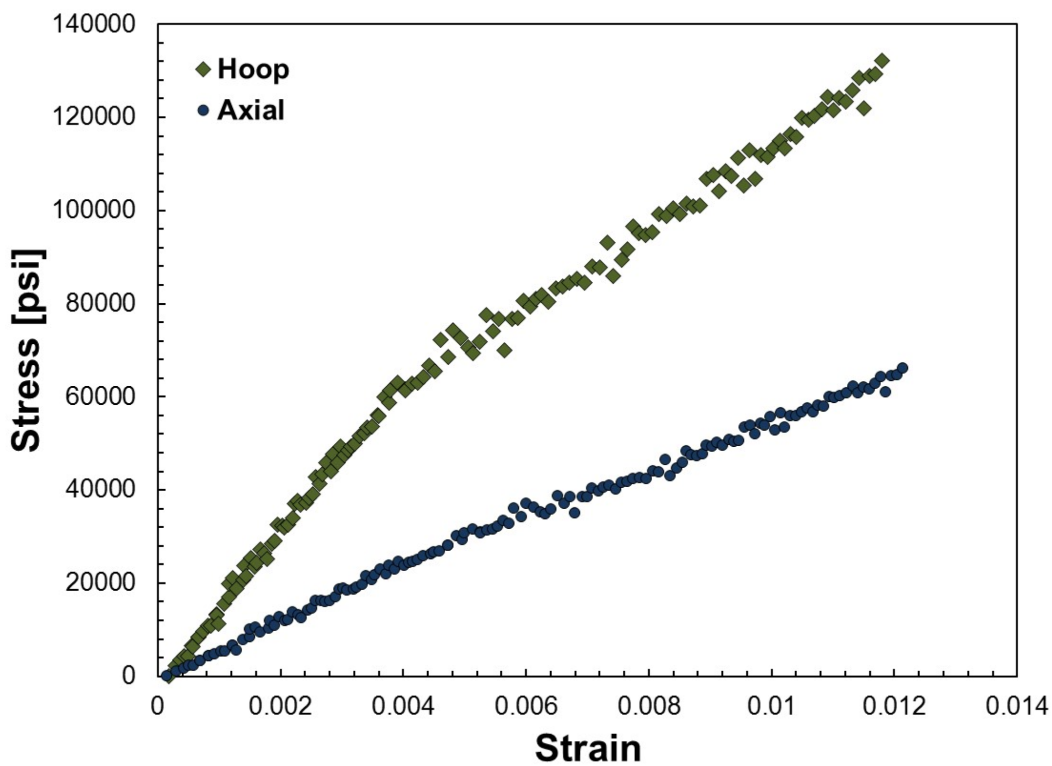

Figure A. 6 – Stress-strain response of OM3915.

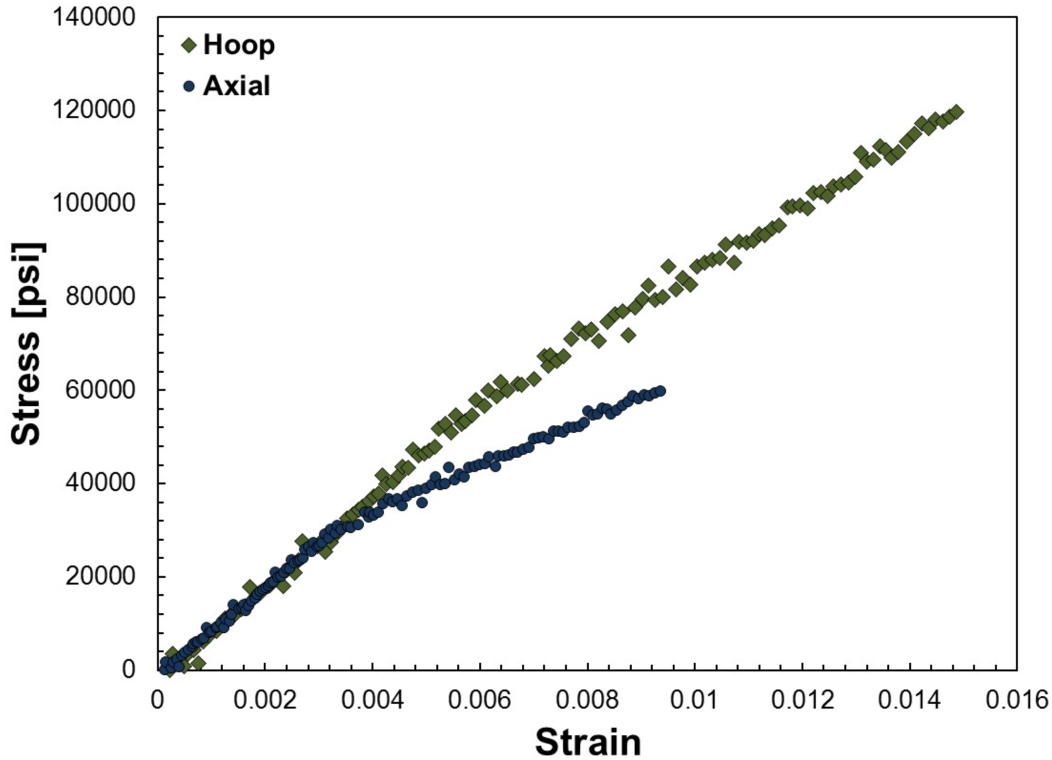

Figure A. 7 – Stress-strain response of OM3934.

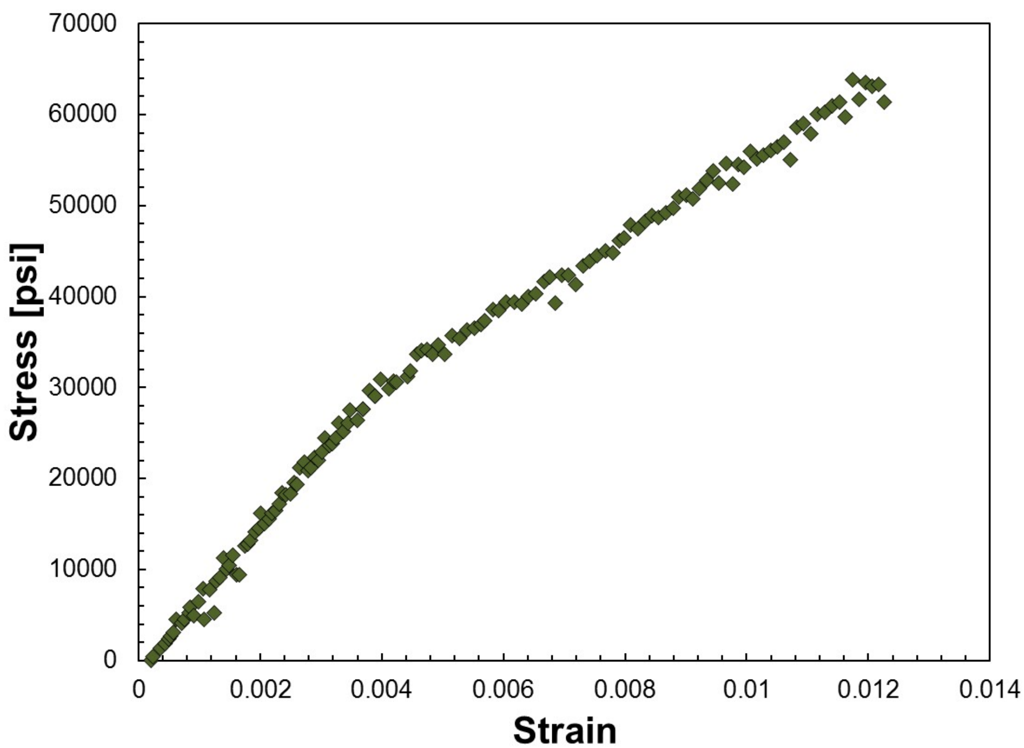

Figure A. 8 – Axial stress-strain response of OM3941. The hoop strain gage data became corrupted during the test.

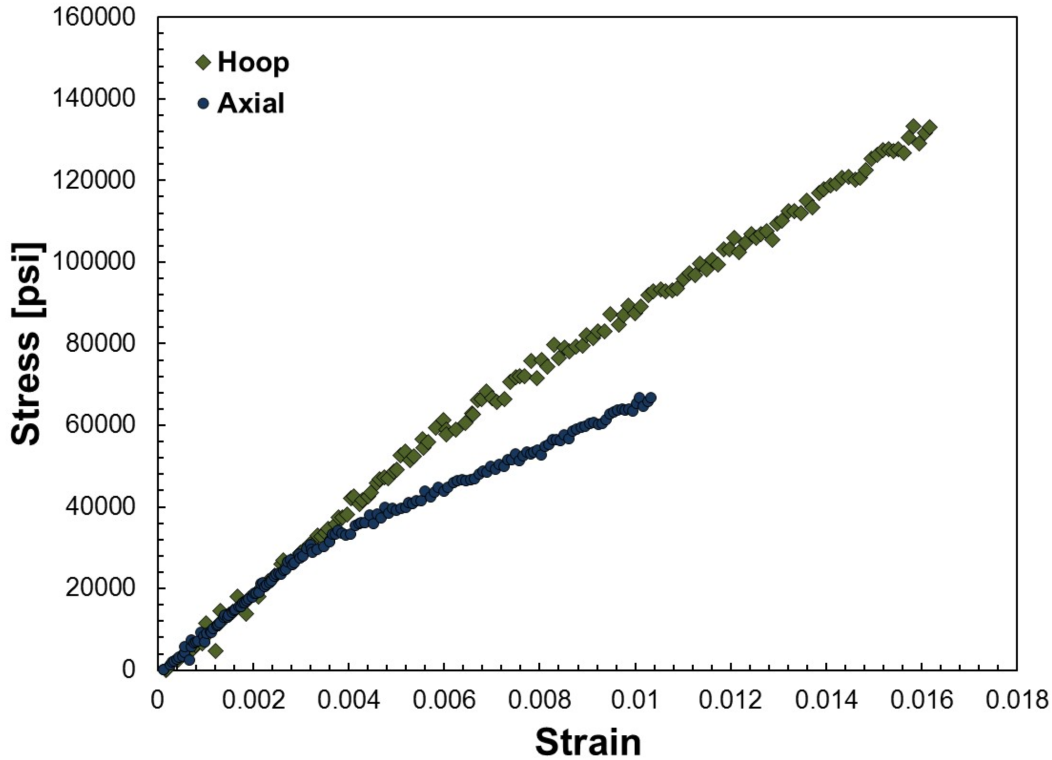

Figure A. 9 – Stress-strain response of OM3962.

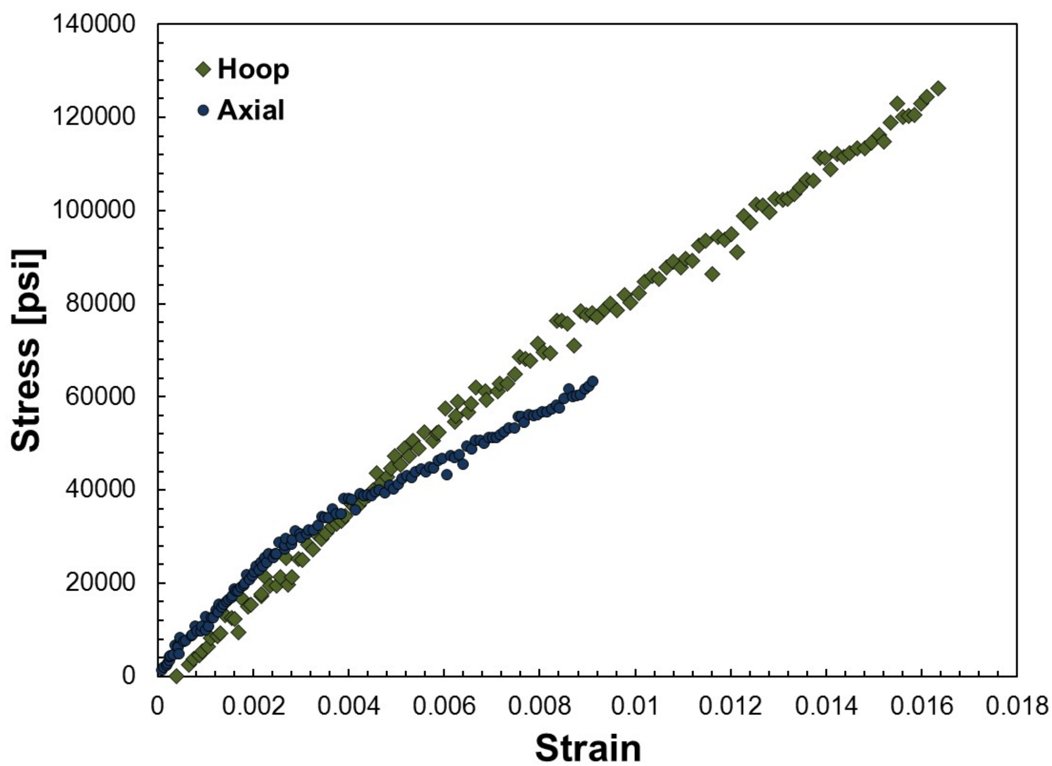

Figure A. 10 – Stress-strain response of OM3990.

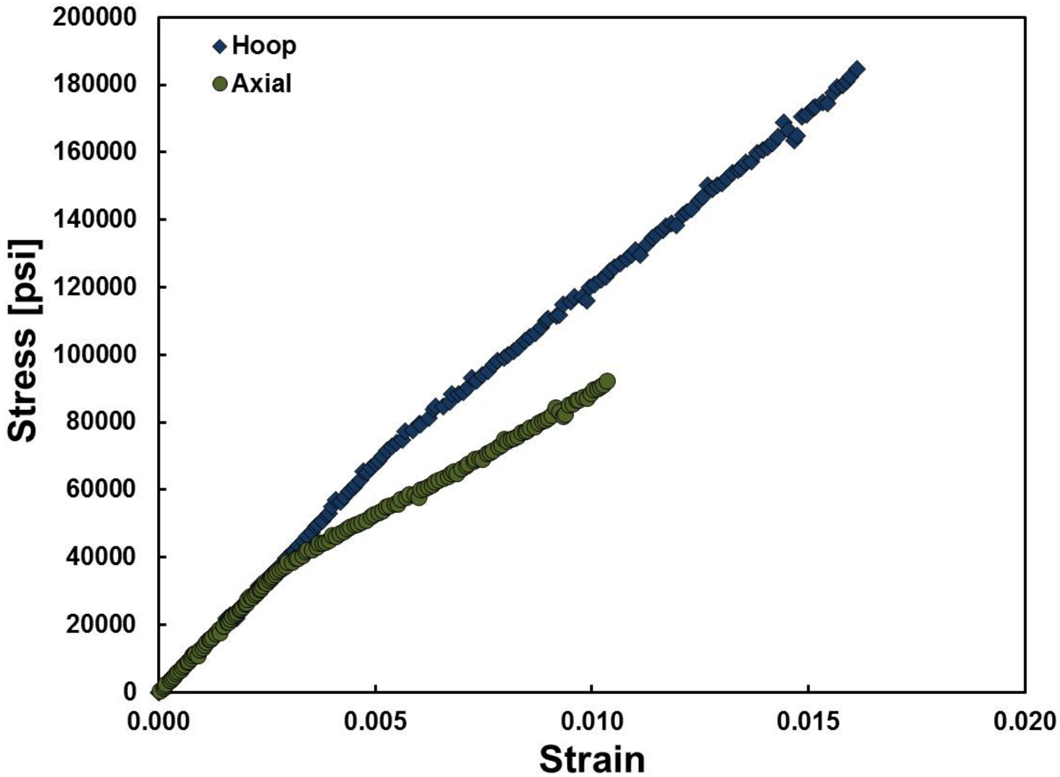

Figure A. 11 - Stress-strain response of ALT639 - 14969.

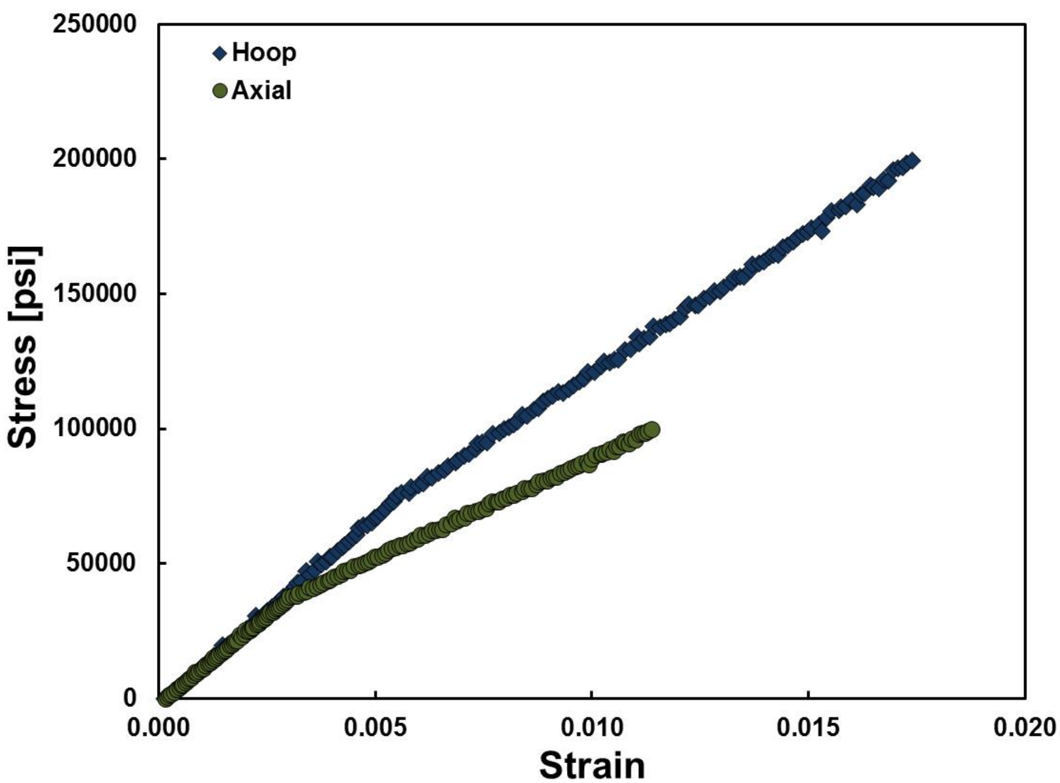

Figure A. 12 - Stress-strain response of ALT639 - 17663.

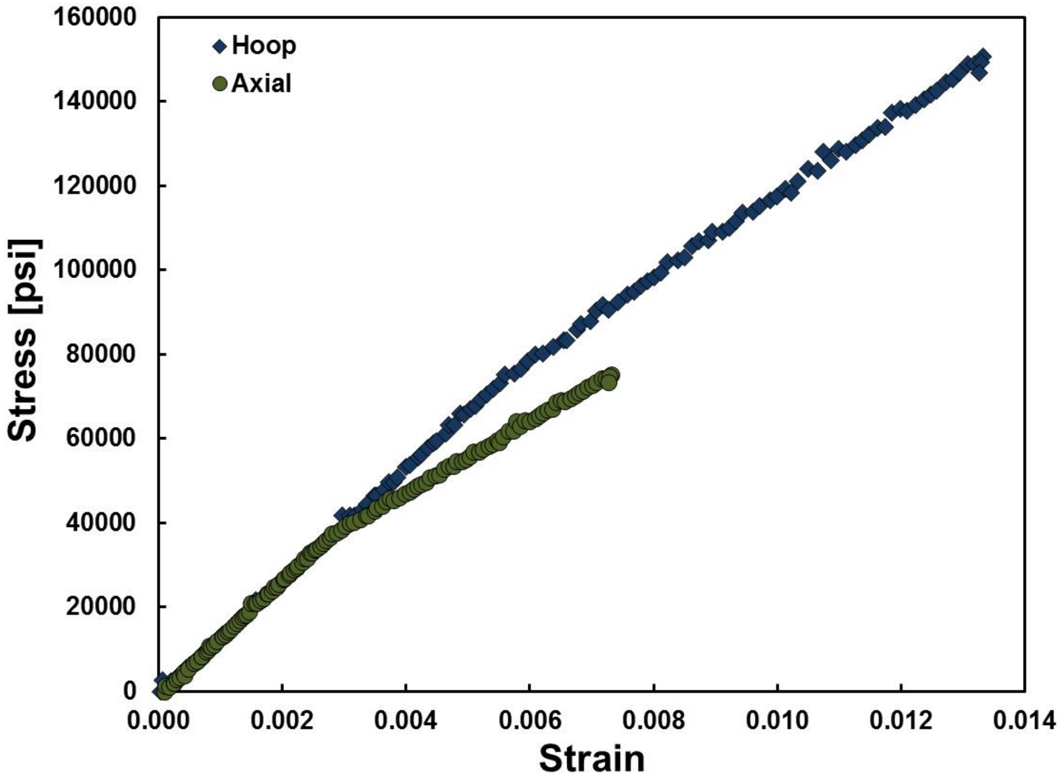

Figure A. 13 - Stress-strain response of ALT639 - 18023.

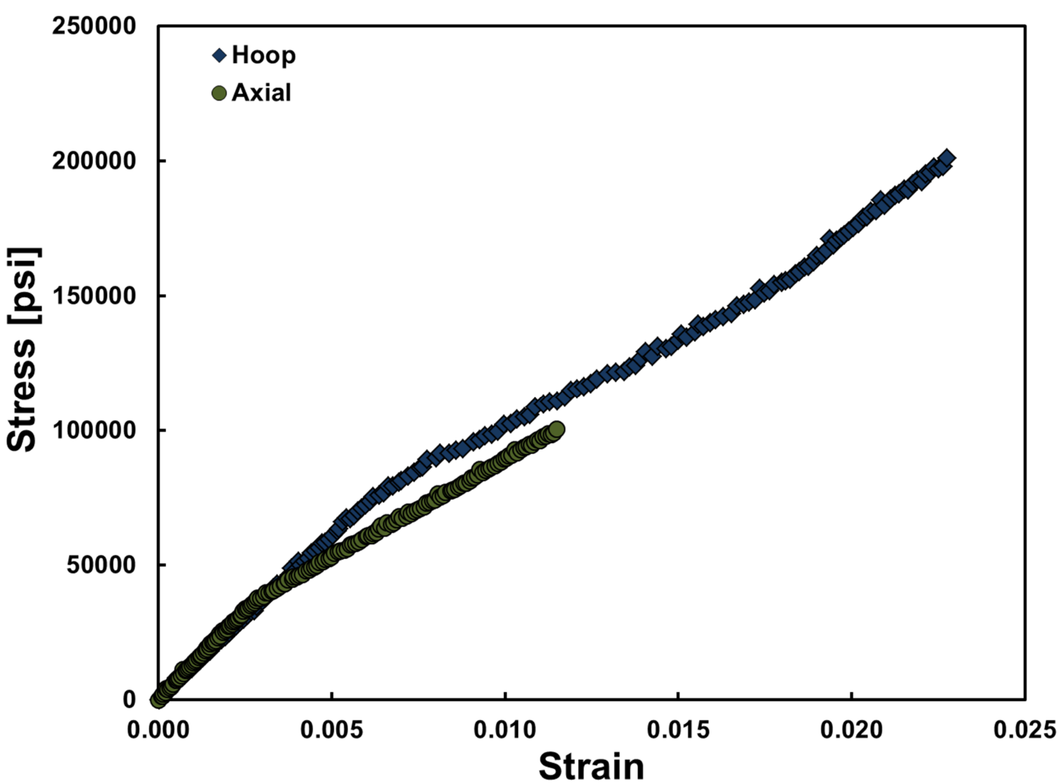

Figure A. 14 - Stress-strain response of ALT639 - 69216.

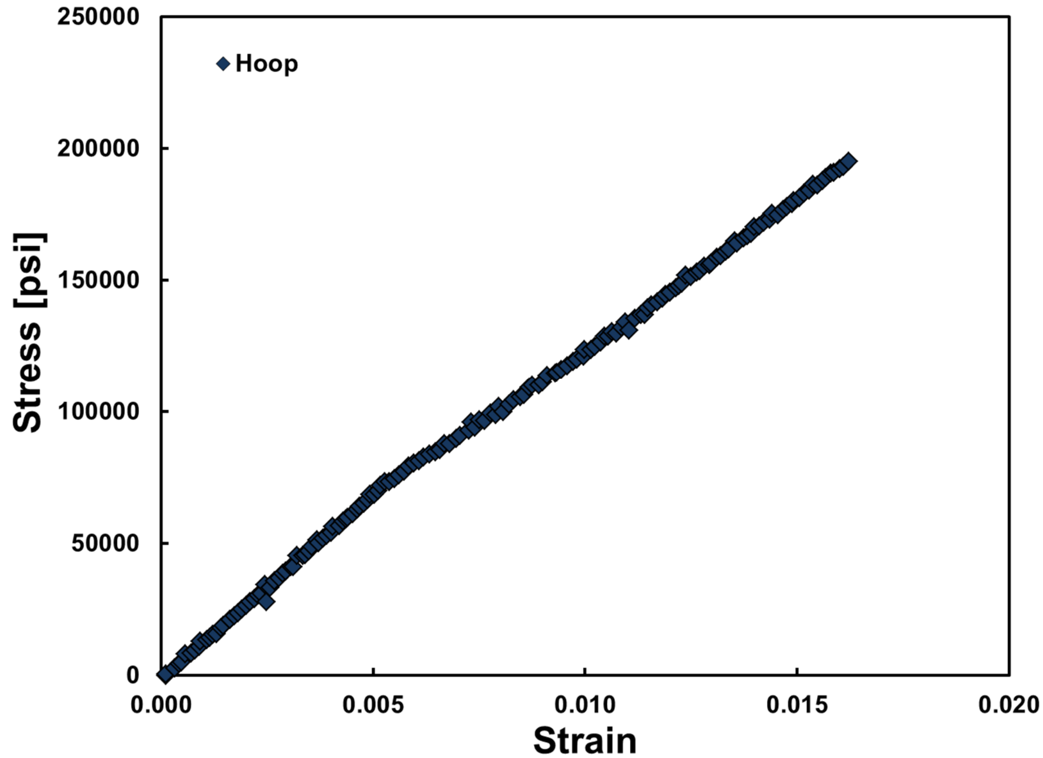

Figure A. 15 - Hoop stress-strain response of ALT639 - 18629. The axial strain gage data became corrupted during the test.

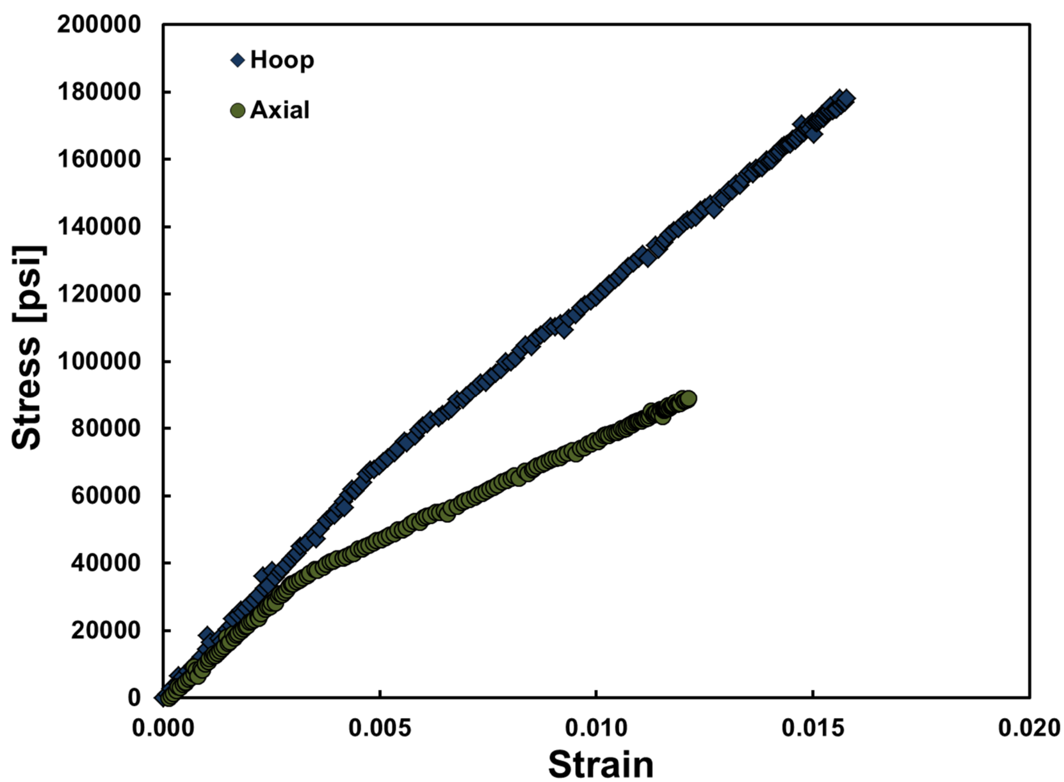

Figure A. 16 - Stress-strain response of IH1740.

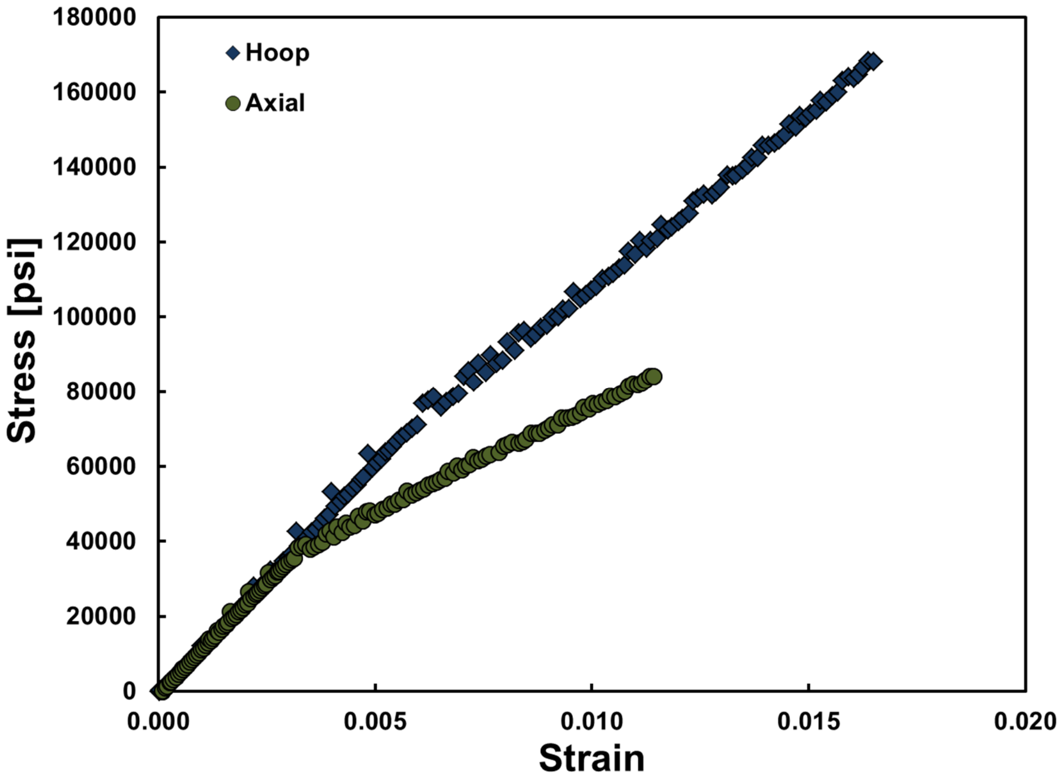

Figure A. 17 - Stress-strain response of IH1855.

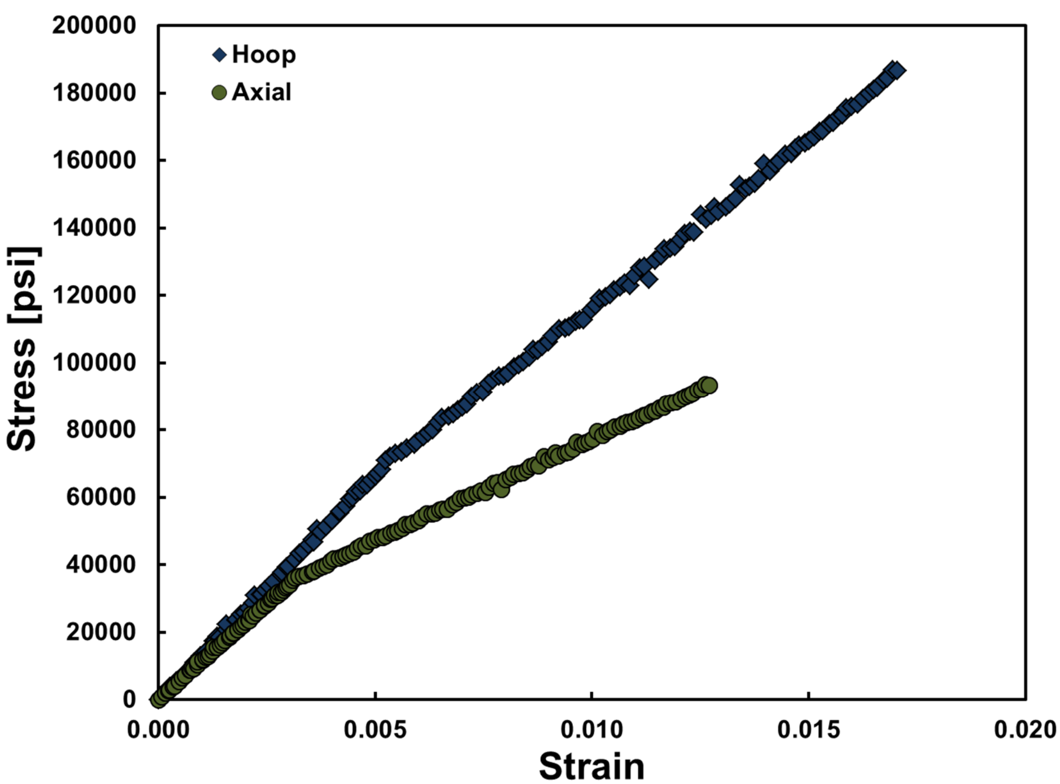

Figure A. 18 - Stress-strain response of IH1763.

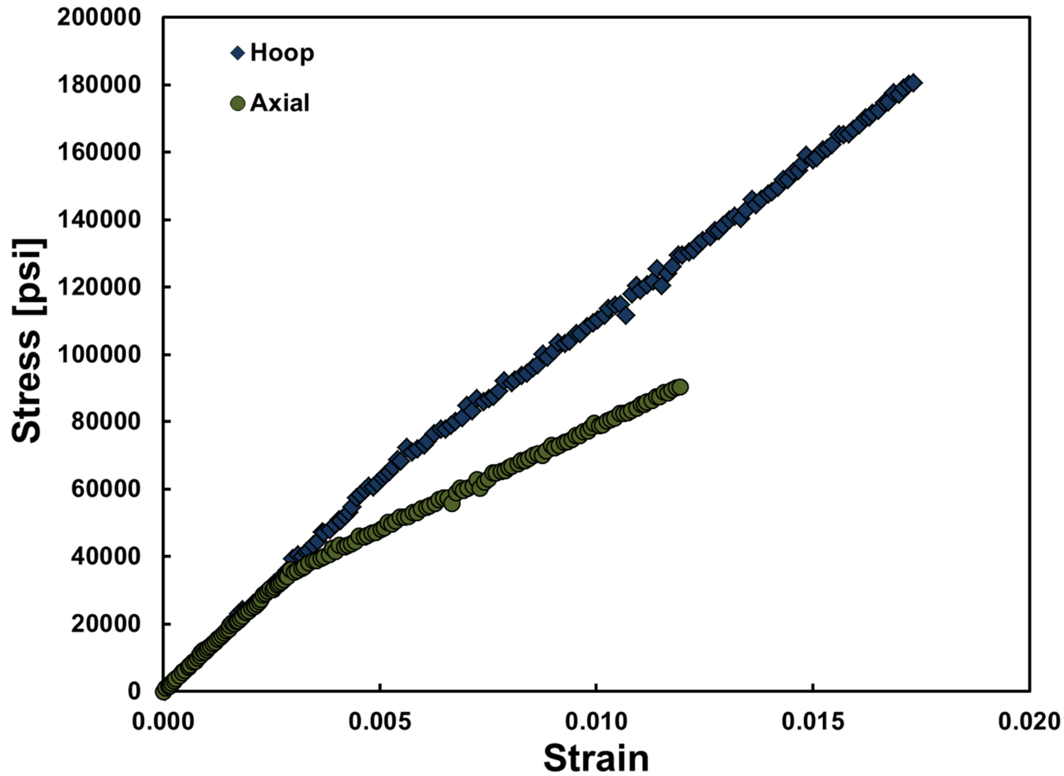

Figure A. 19 - Stress-strain response of IH1135.

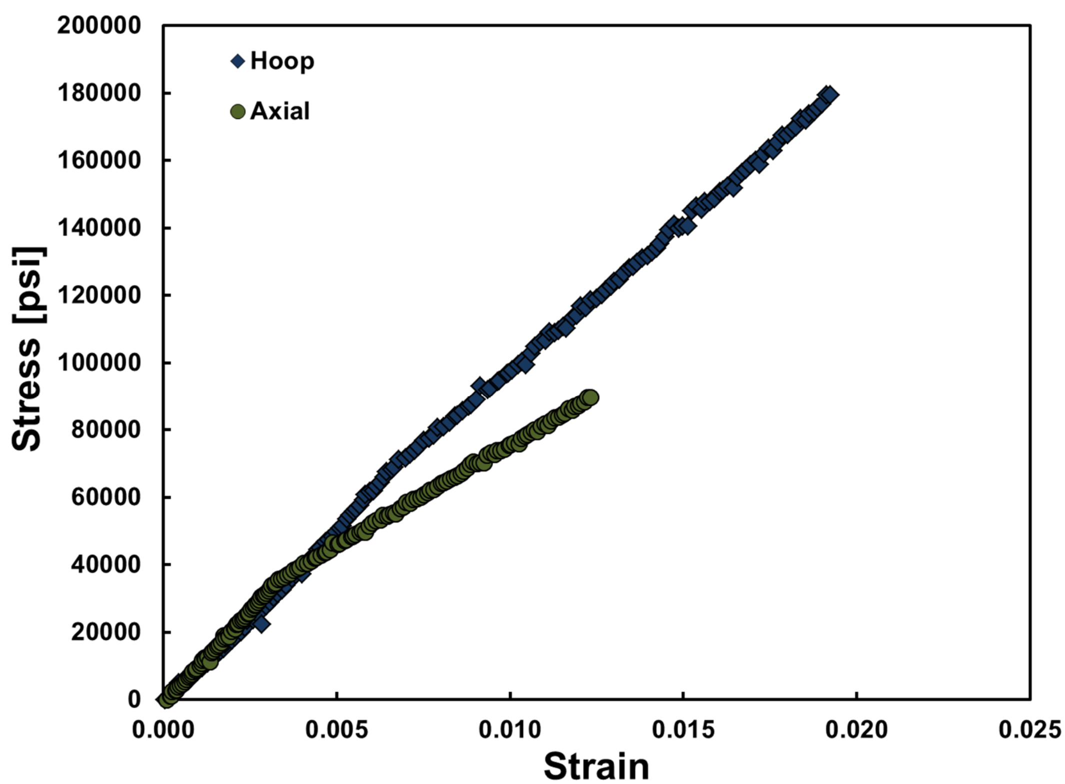

Figure A. 20 - Stress-strain response of IH1929.

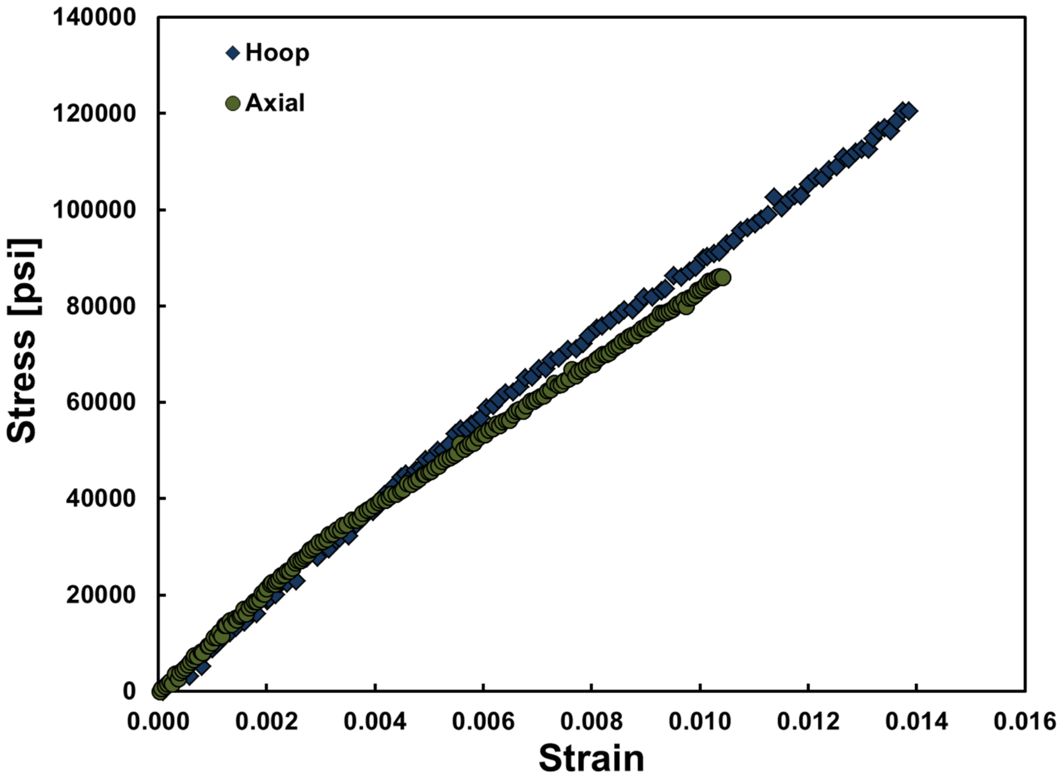

Figure A. 21 - Stress-strain response of ALT604 - 6739.

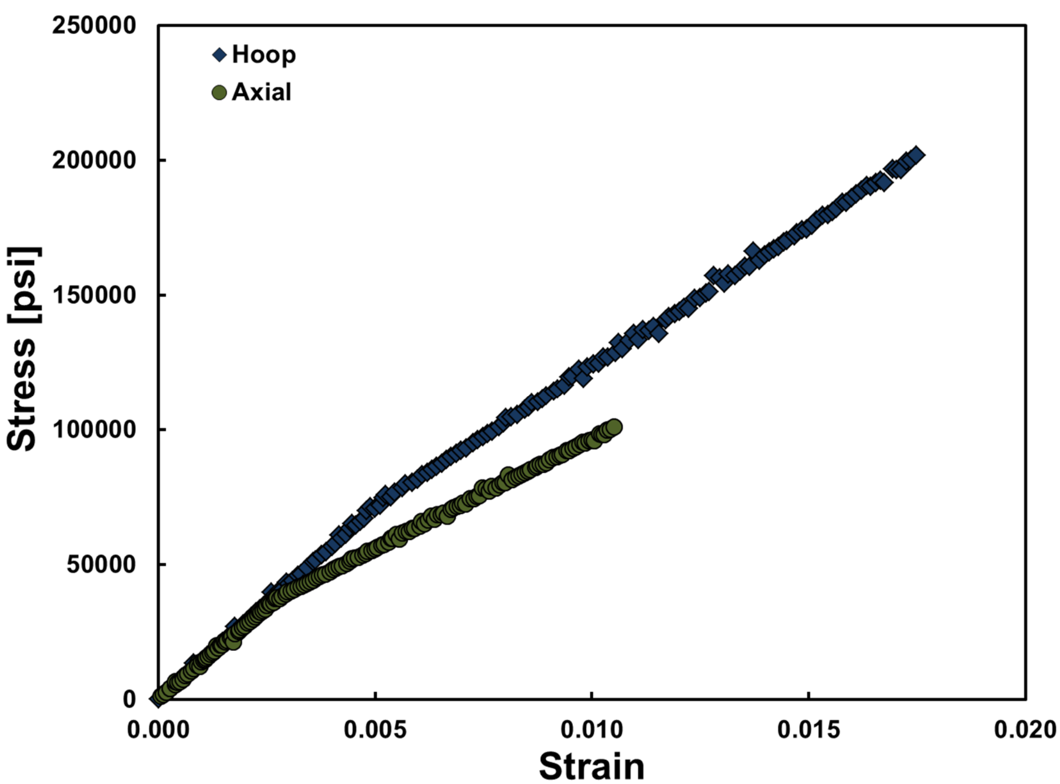

Figure A. 22 - Stress-strain response of ALT639 - 17688.

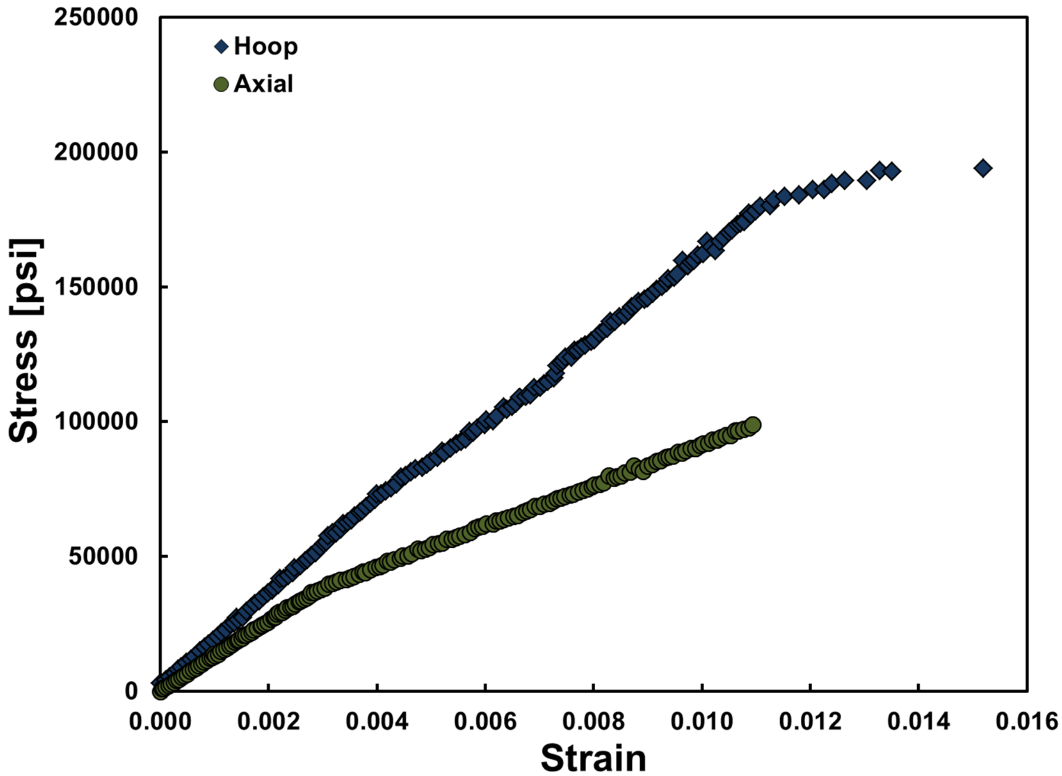

Figure A. 23 - Stress-strain response of ALT639 - 18862.

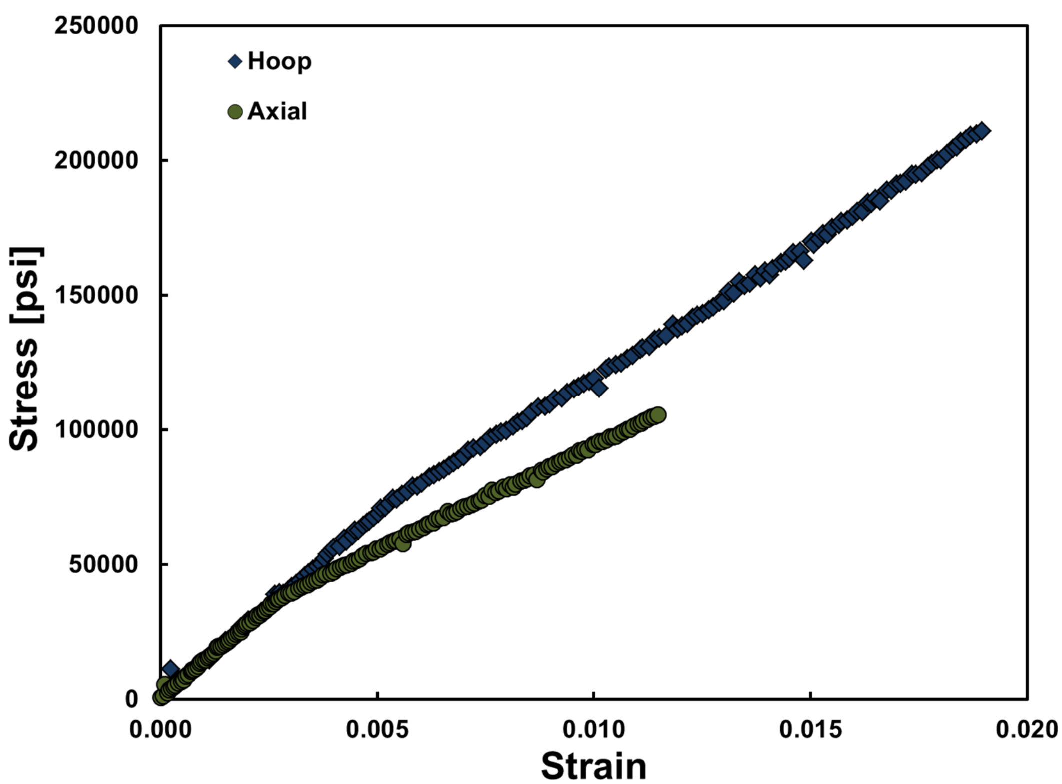

Figure A. 24 - Stress-strain response of ALT639 - 18507.

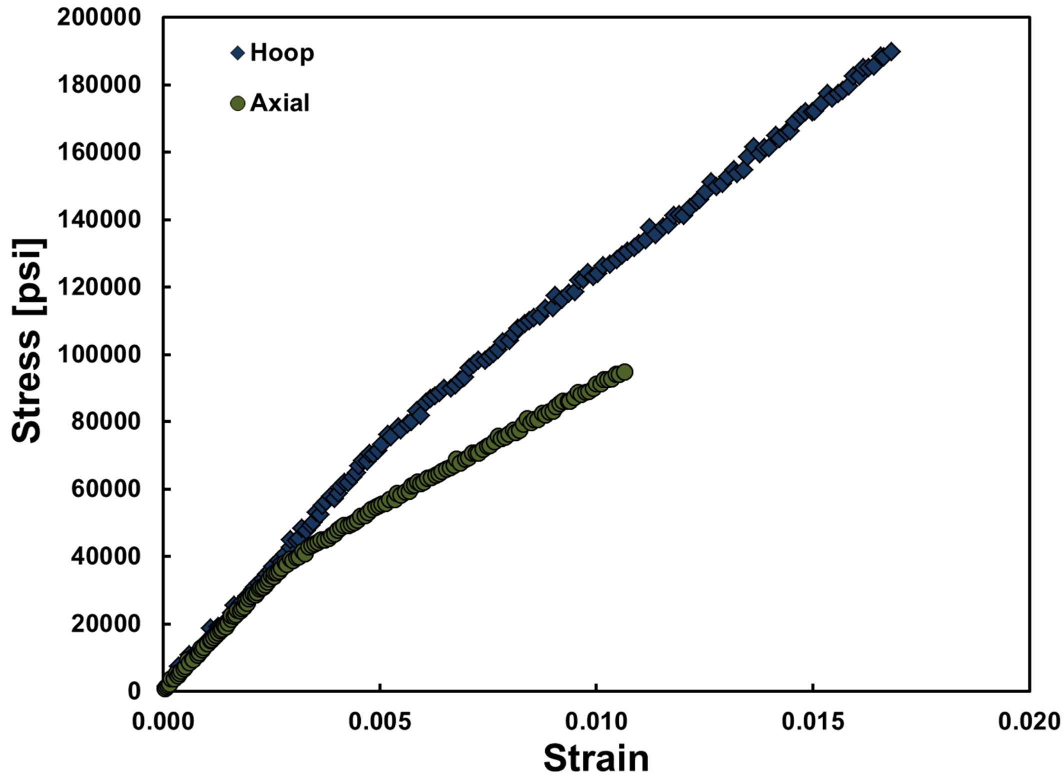

Figure A. 25 - Stress-strain response of ALT639 - 18793.

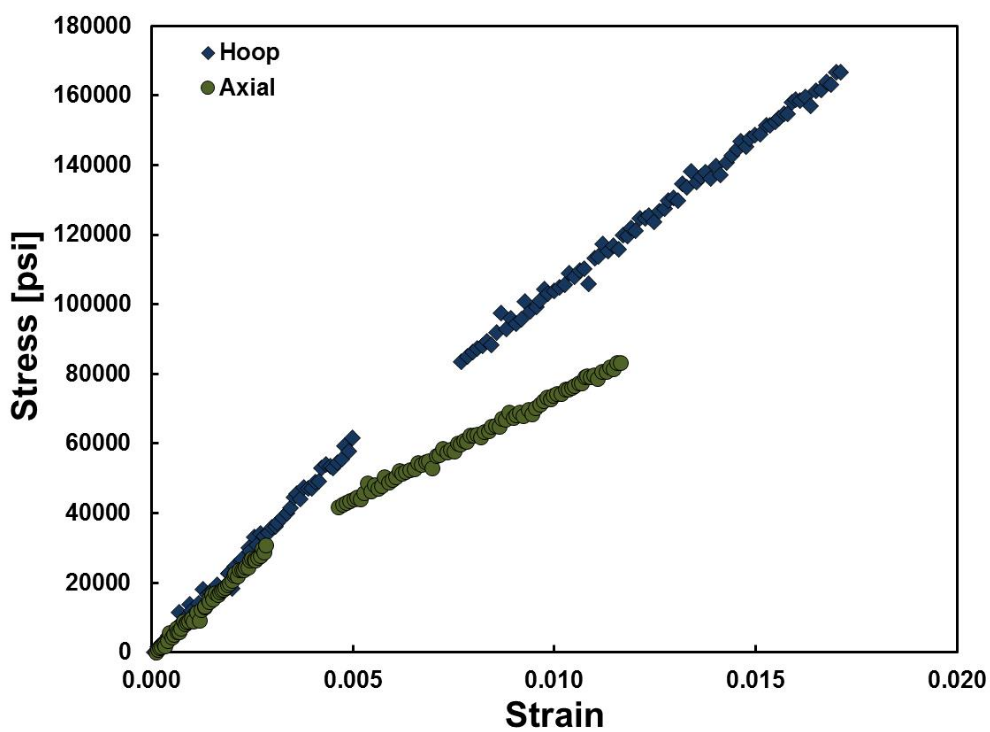

Figure A. 26 – Stress-strain response of ALT695 – 1700.

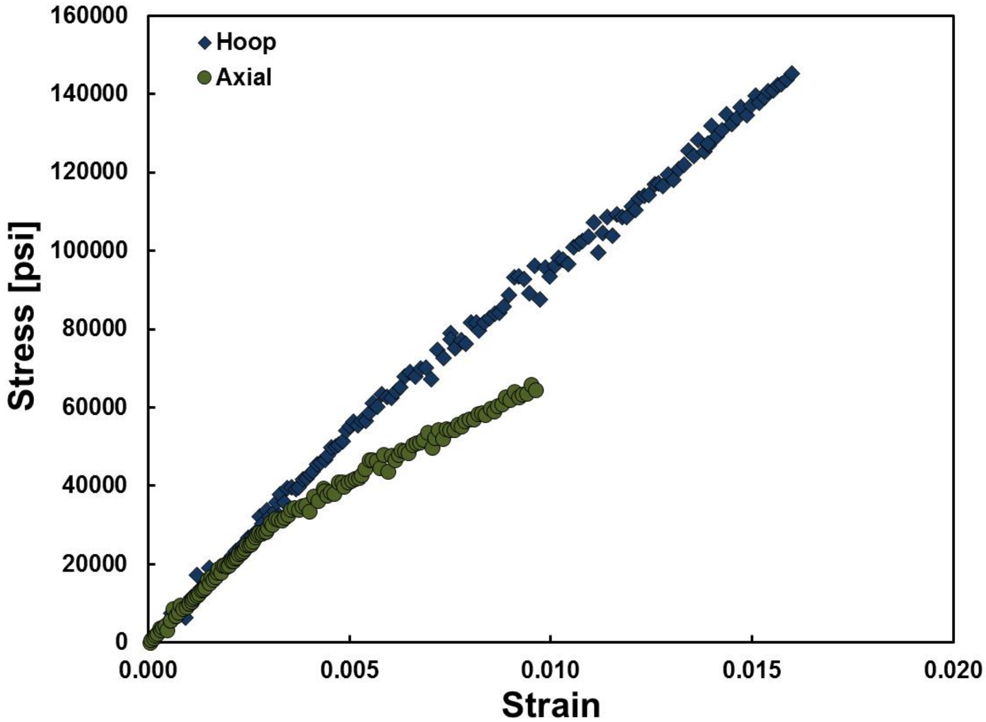

Figure A. 27 – Stress-strain response of ALT695 – 4745.

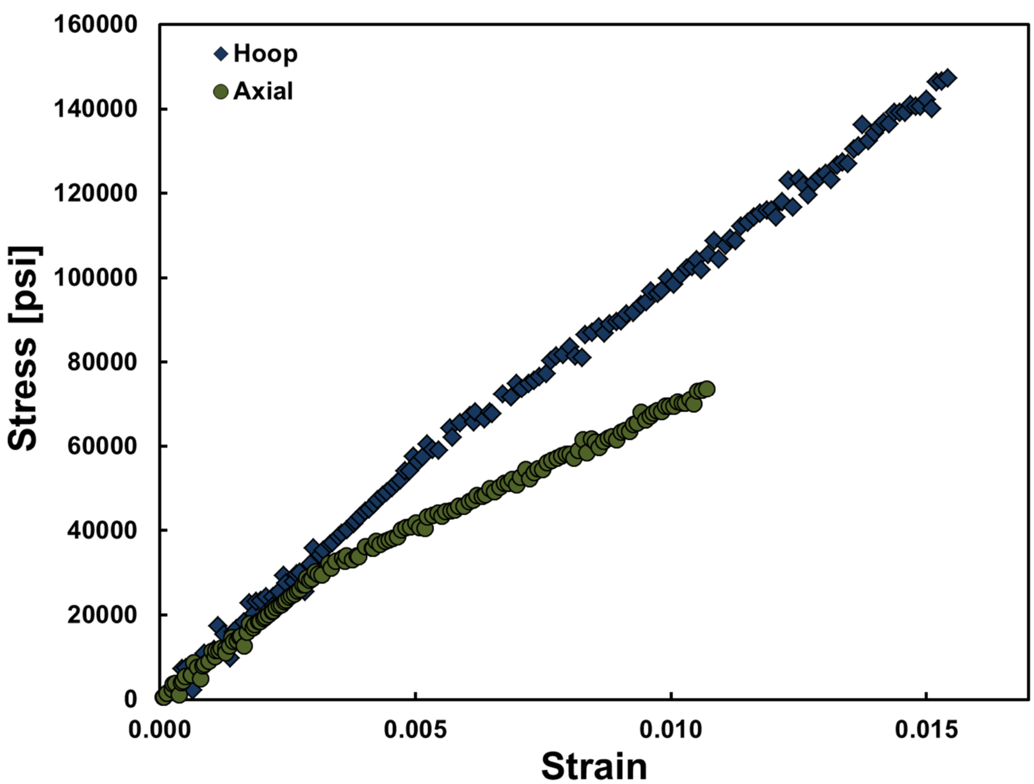

Figure A. 28 - Stress-strain response of ALT695 – 5353.

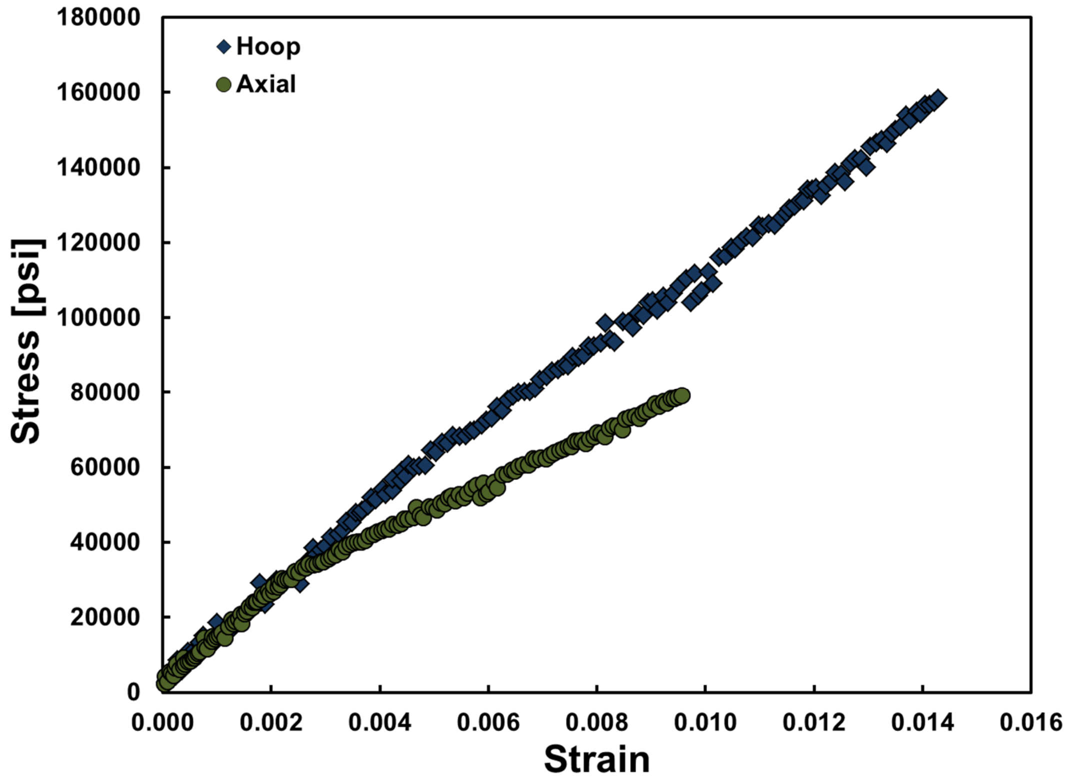

Figure A. 29 – Stress-strain response of ALT695 - 6058.

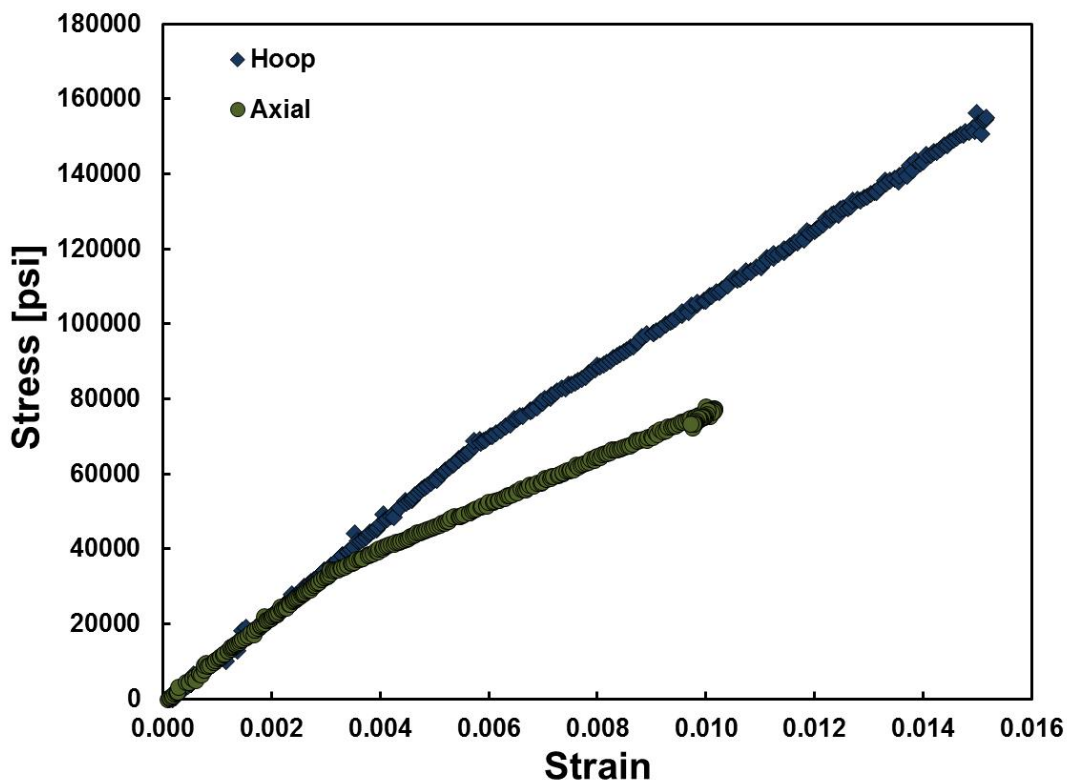

Figure A. 30 - Stress-strain response of ALT695 – 1668.

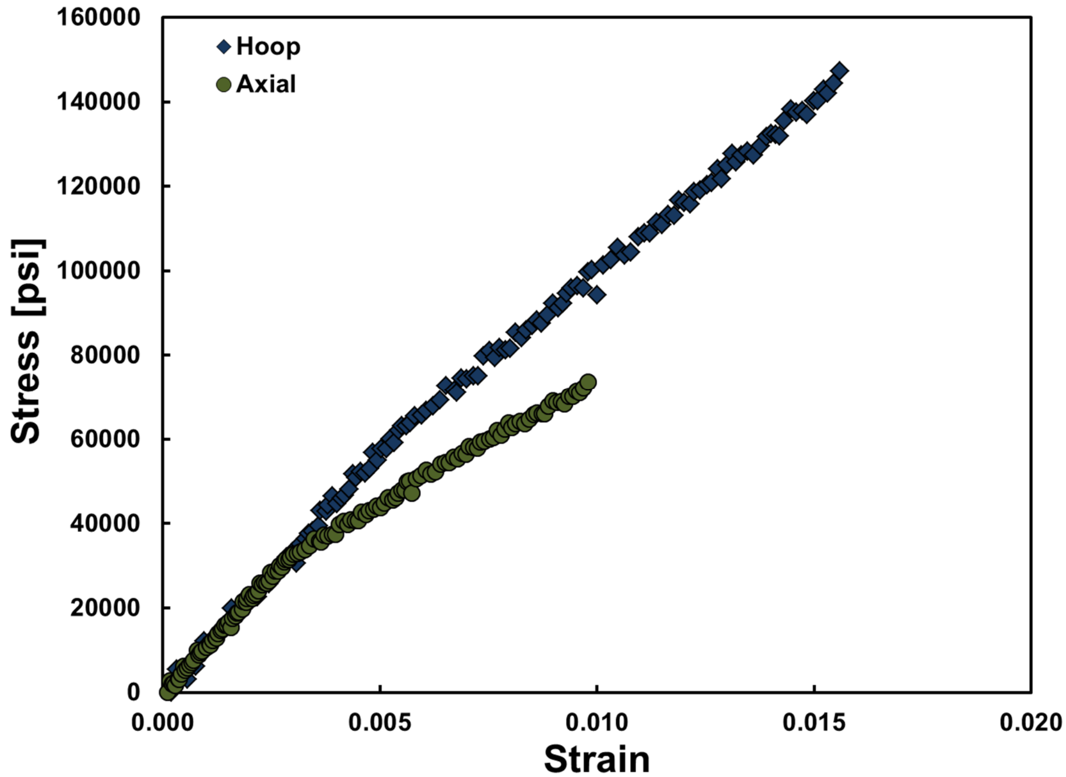

Figure A. 31 – Stress-strain response of OM3913.

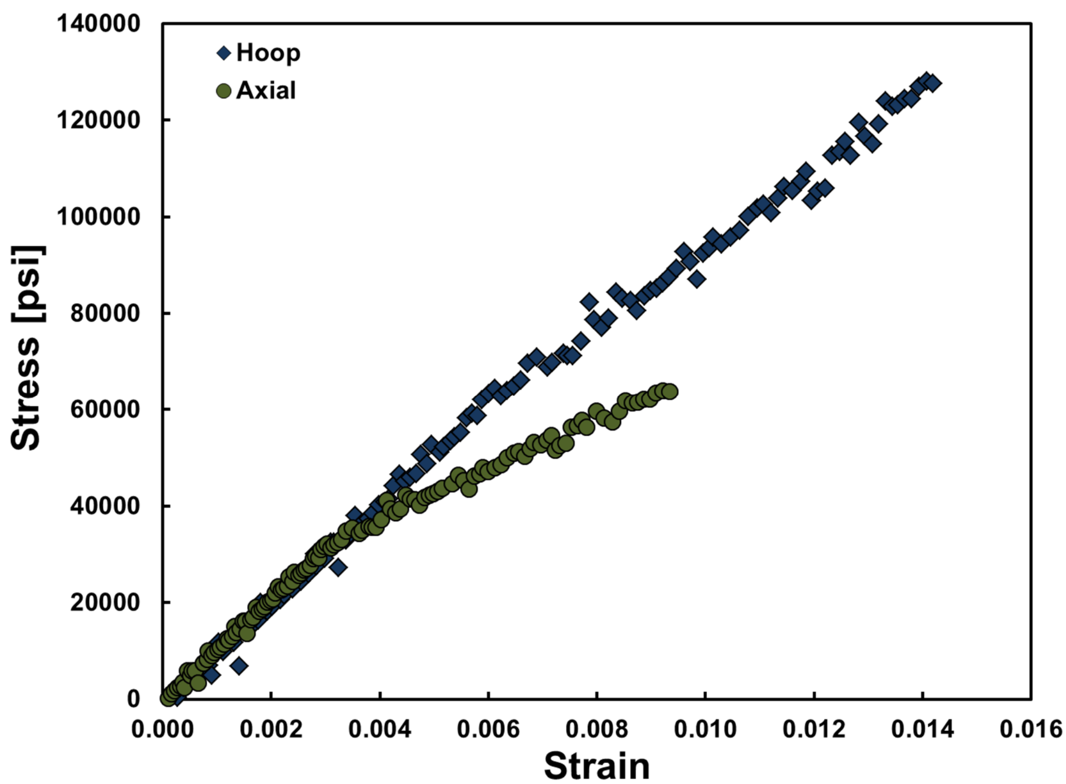

Figure A. 32 – Stress-strain response of OM3928.

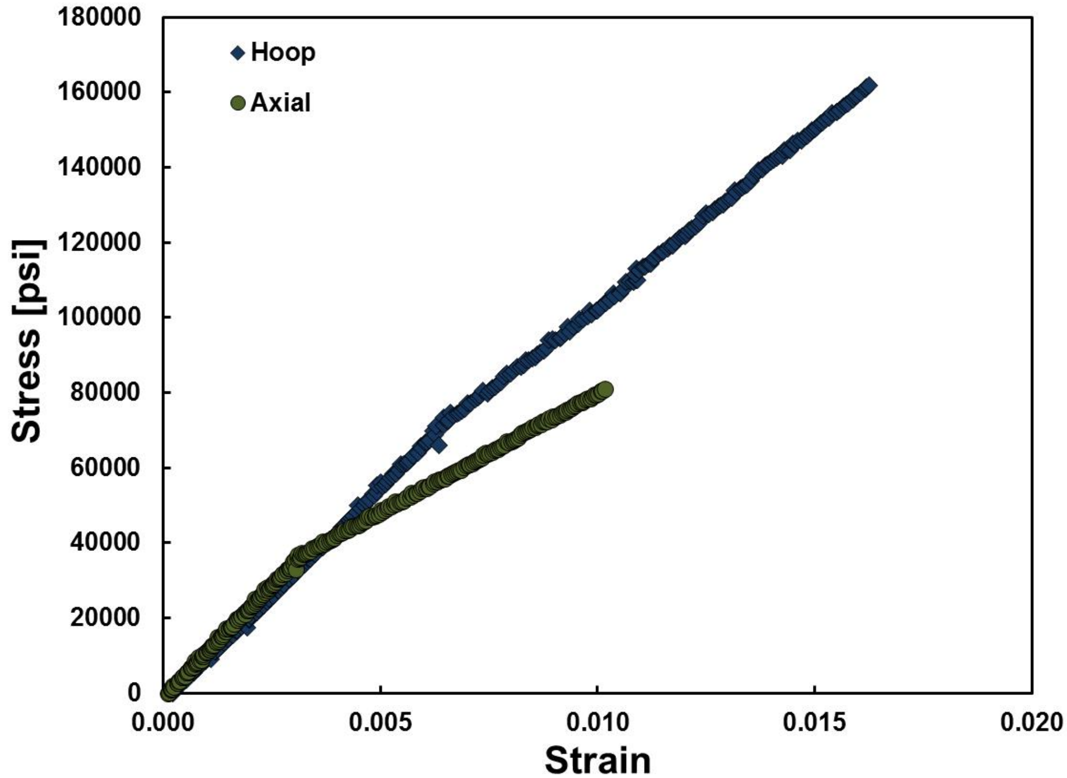

Figure A. 33 - Stress-strain response of OM3950.

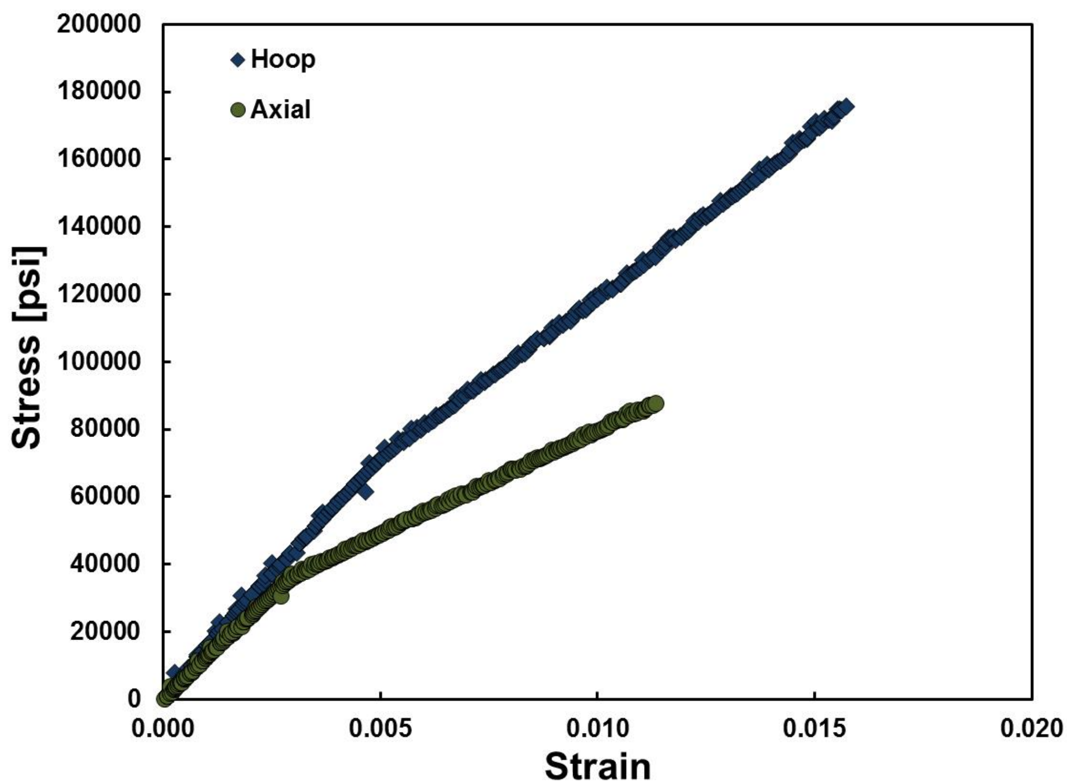

Figure A. 34 - Stress-strain response of IH1271.

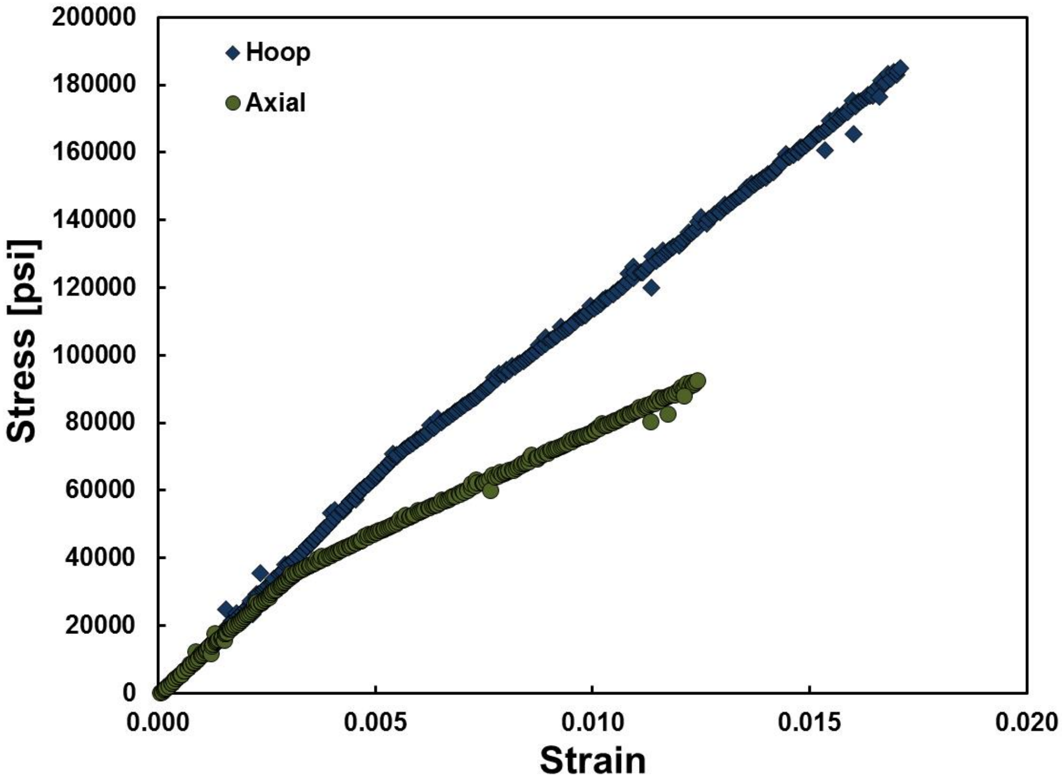

Figure A. 35 - Stress-strain response of IH2483.

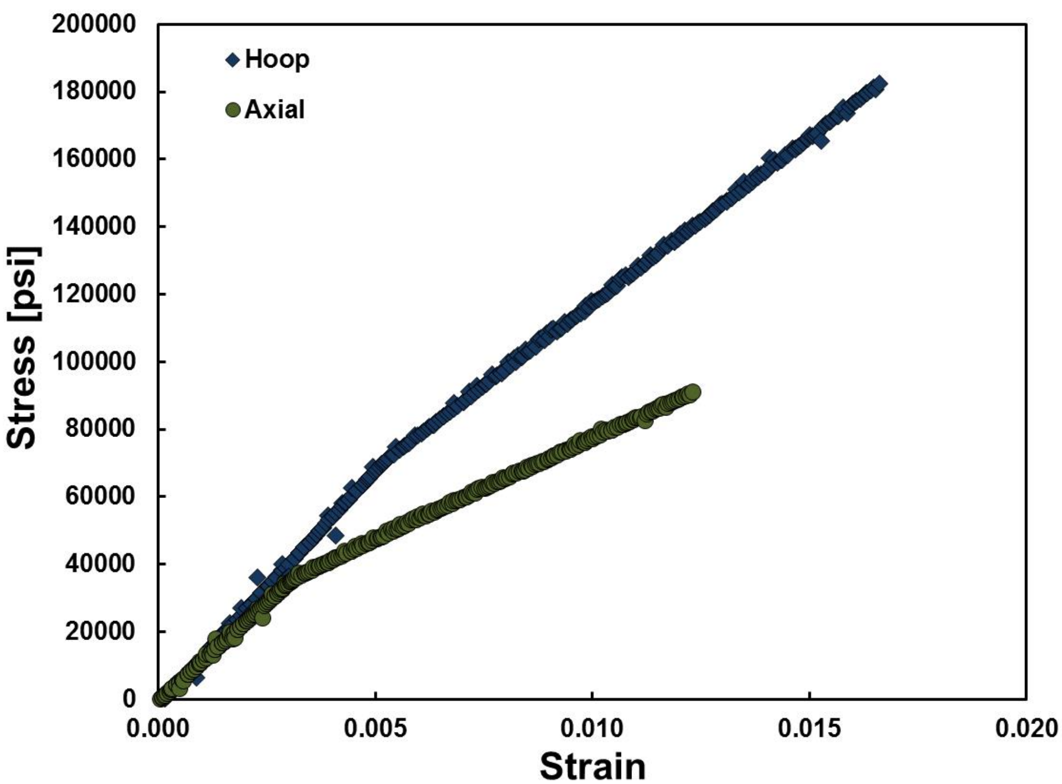

Figure A. 36 - Stress-strain response of IH1748.

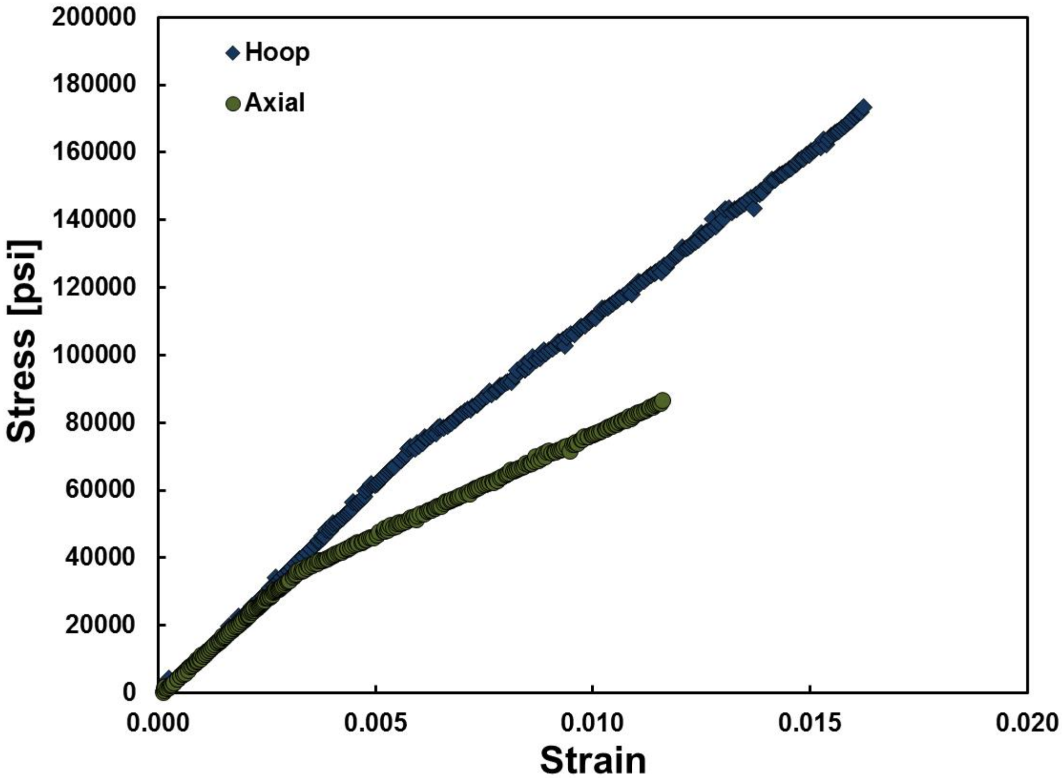

Figure A. 37 - Stress-strain response of IH1820.

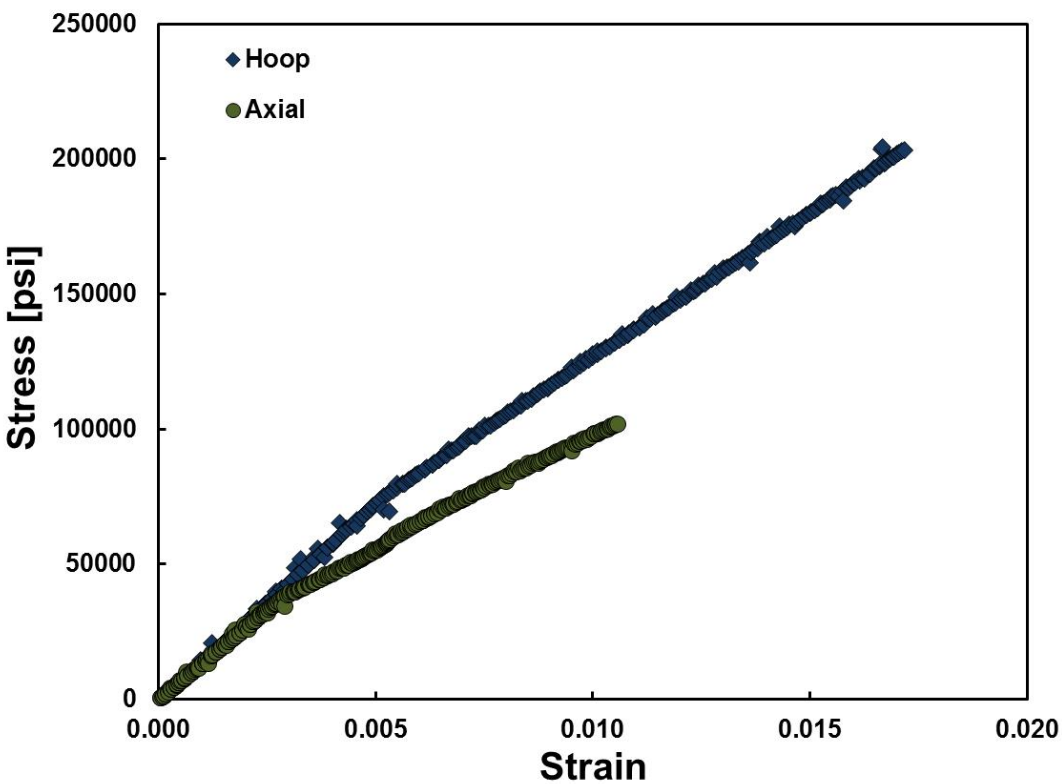

Figure A. 38 - Stress-strain response of ALT639 - 18974.

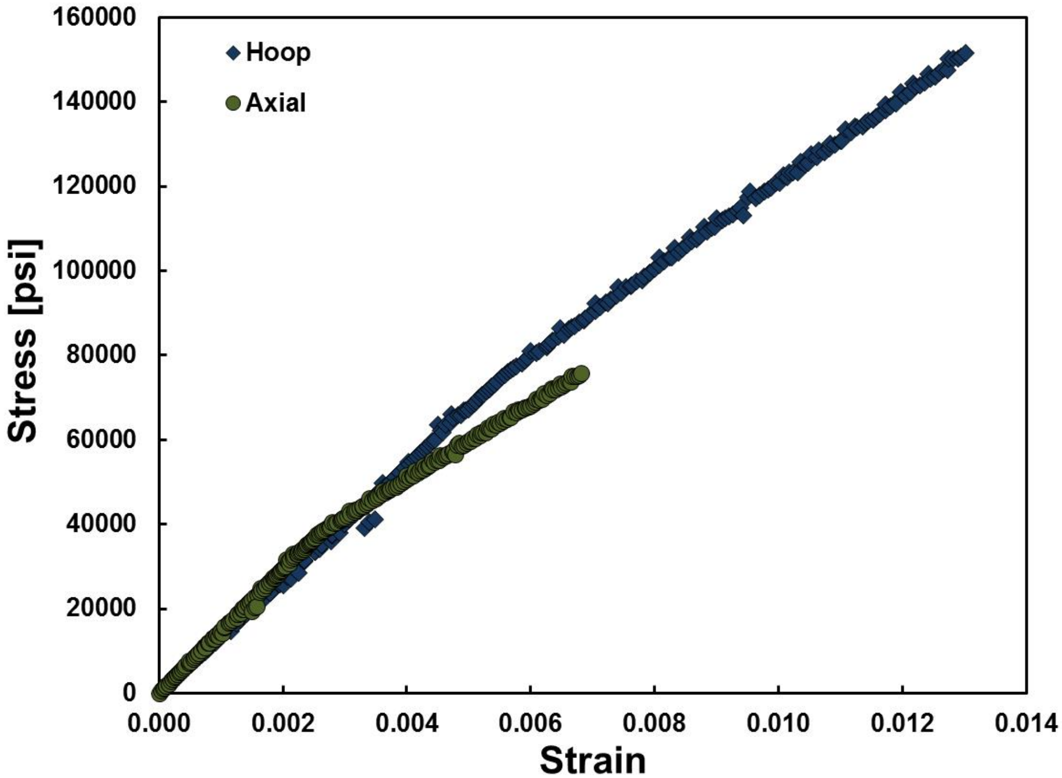

Figure A. 39 - Stress-strain response of ALT639 - 18799.

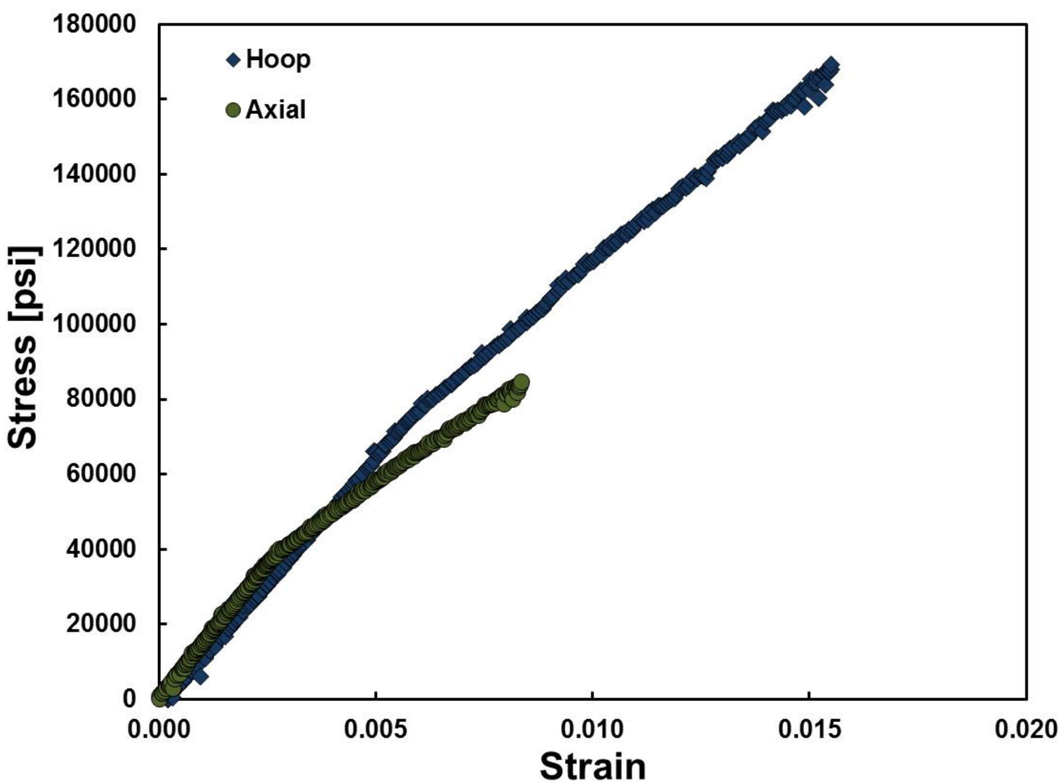

Figure A. 40 - Stress-strain response of ALT639 - 18799.

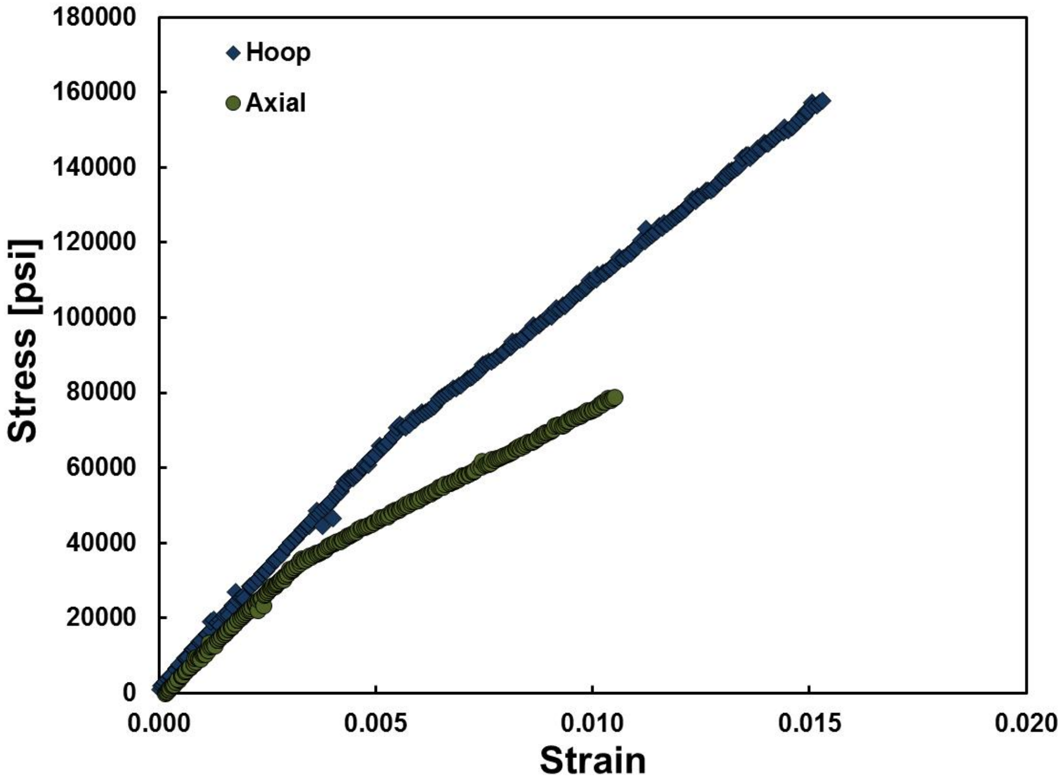

Figure A. 41 - Stress-strain response of ALT695 - 1653.

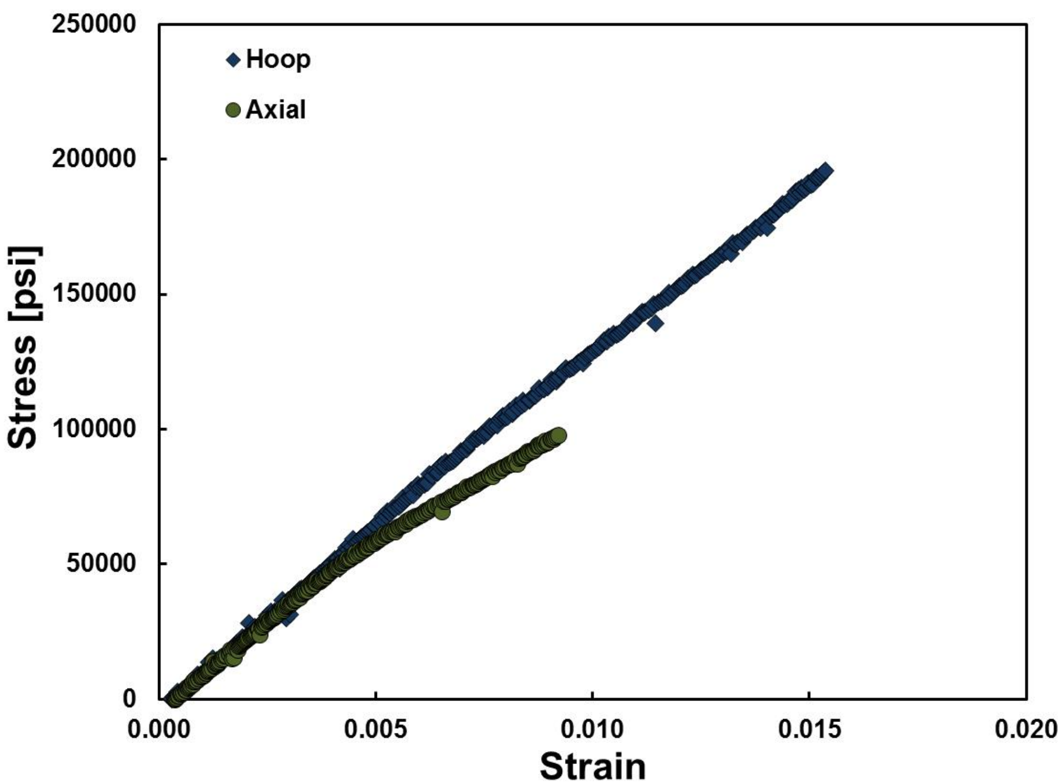

Figure A. 42 - Stress-strain response of ALT604 - 4342.

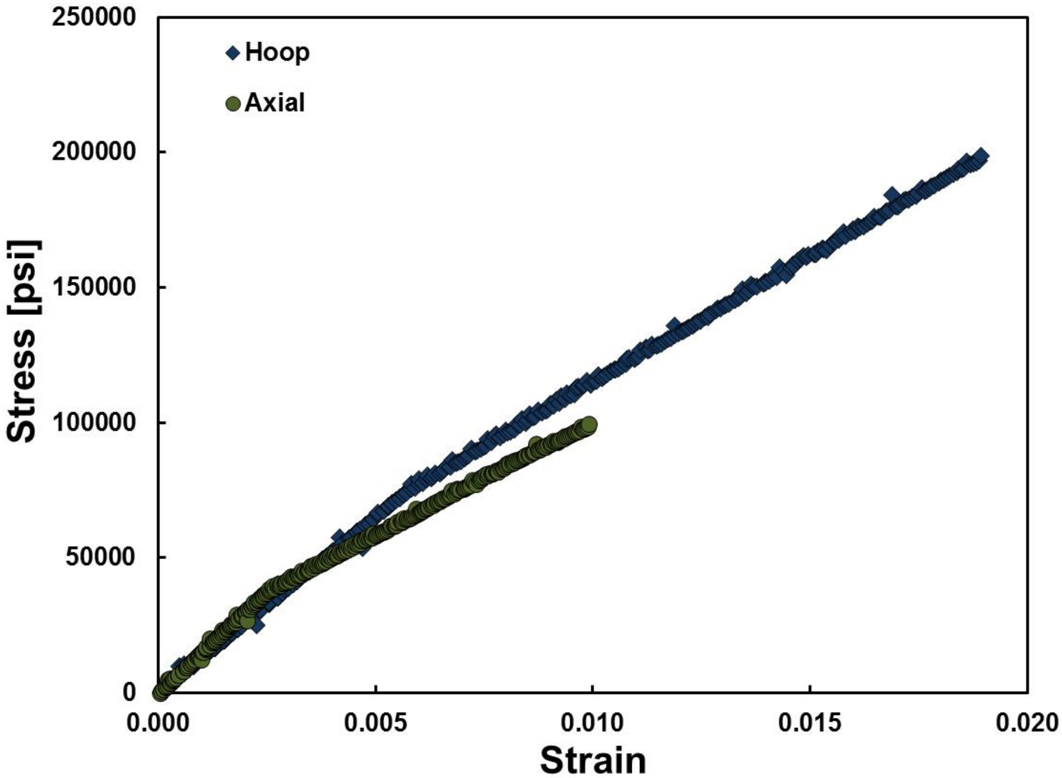

Figure A. 43 - Stress-strain response of ALT639 - 39764.

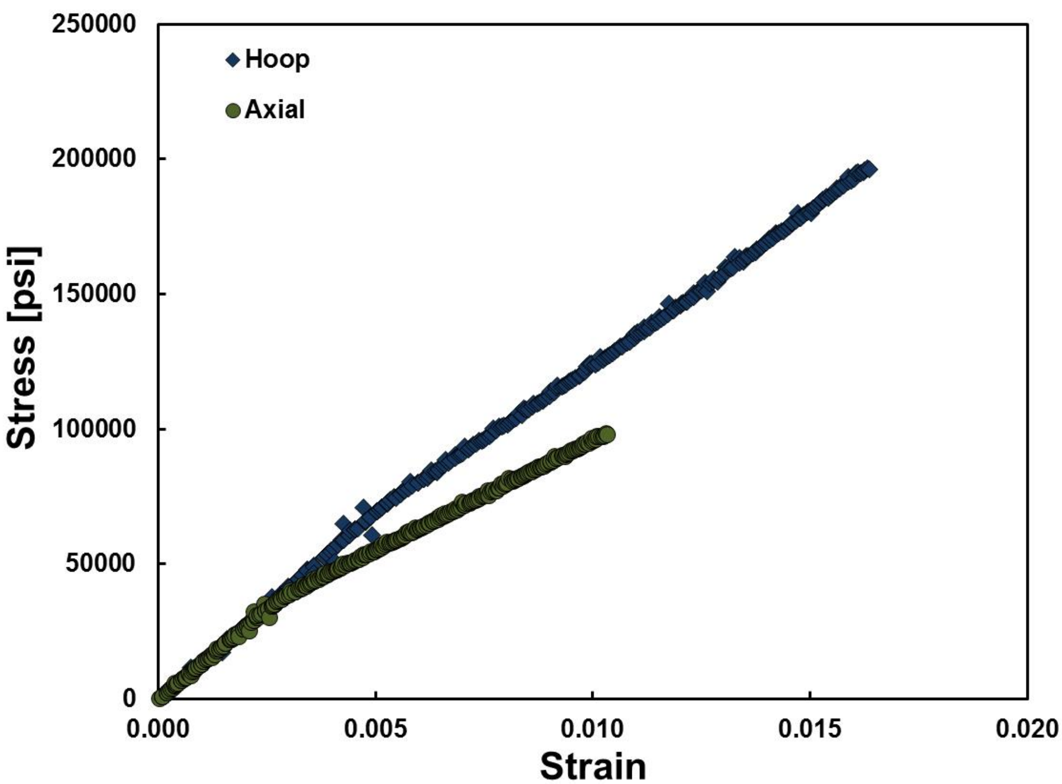

Figure A. 44 - Stress-strain response of ALT639 - 18435.

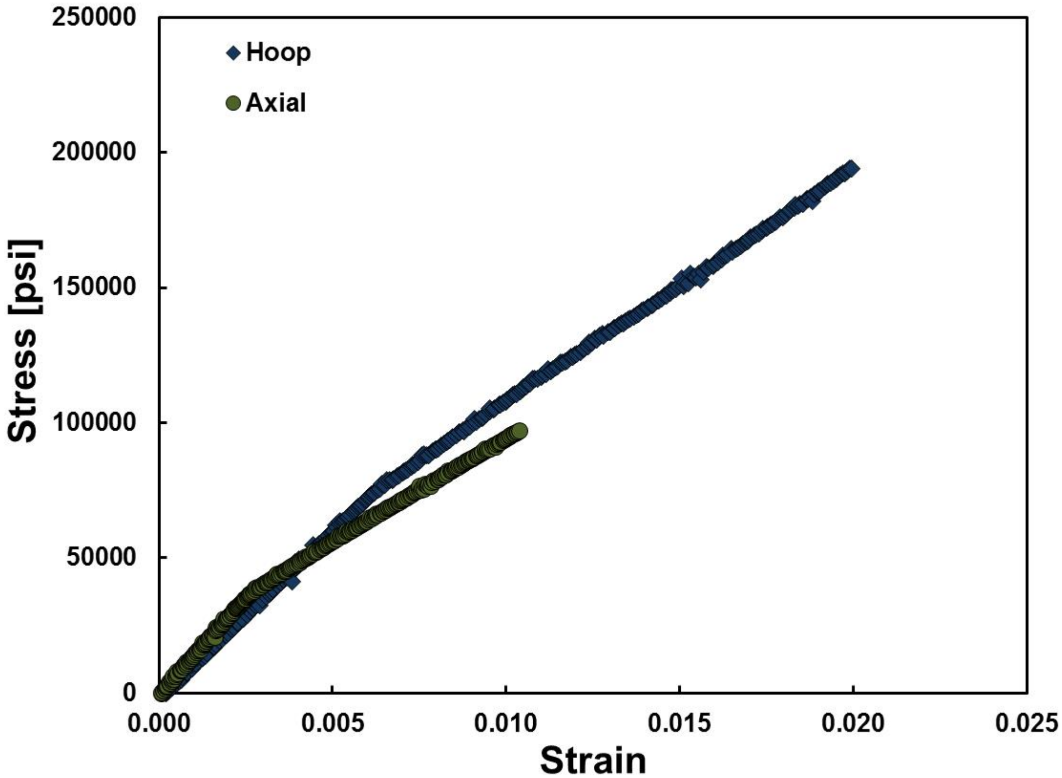

Figure A. 45 - Stress-strain response of ALT639 - 39694.

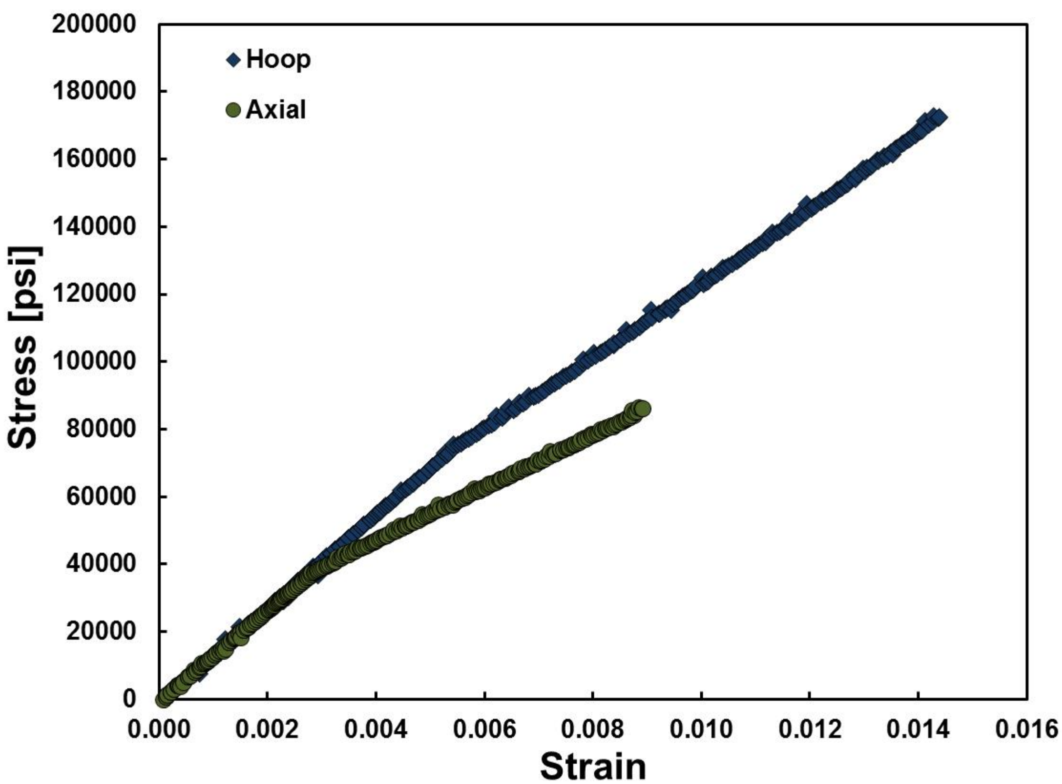

Figure A. 46 - tress-strain response of ALT639 – 18683.

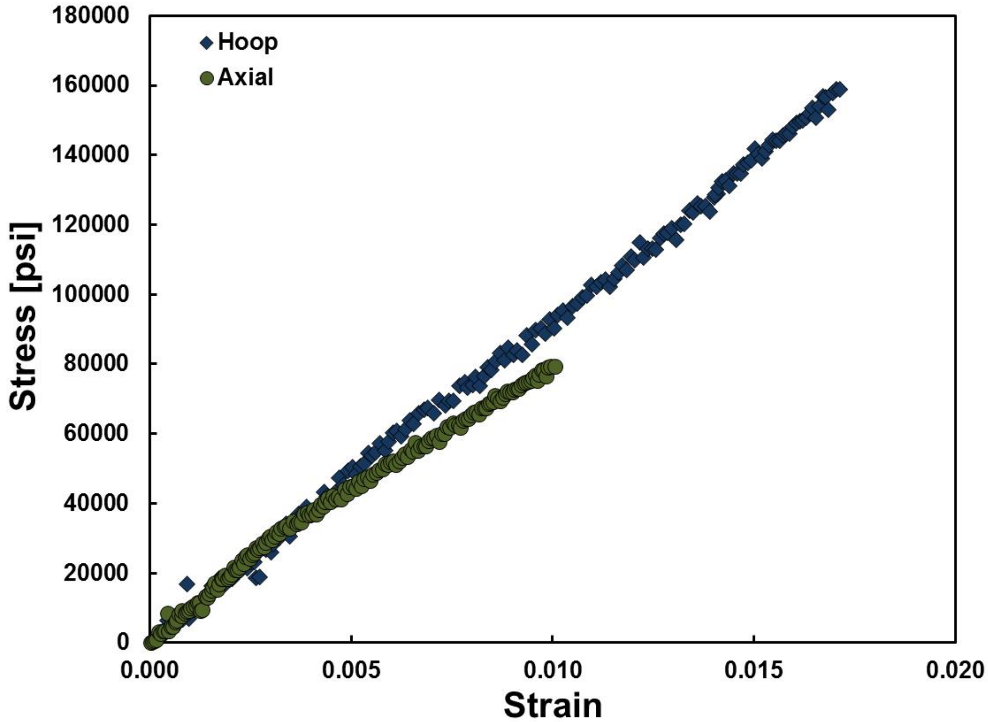

Figure A. 47 - Stress-strain response of ALT604 – 3567.

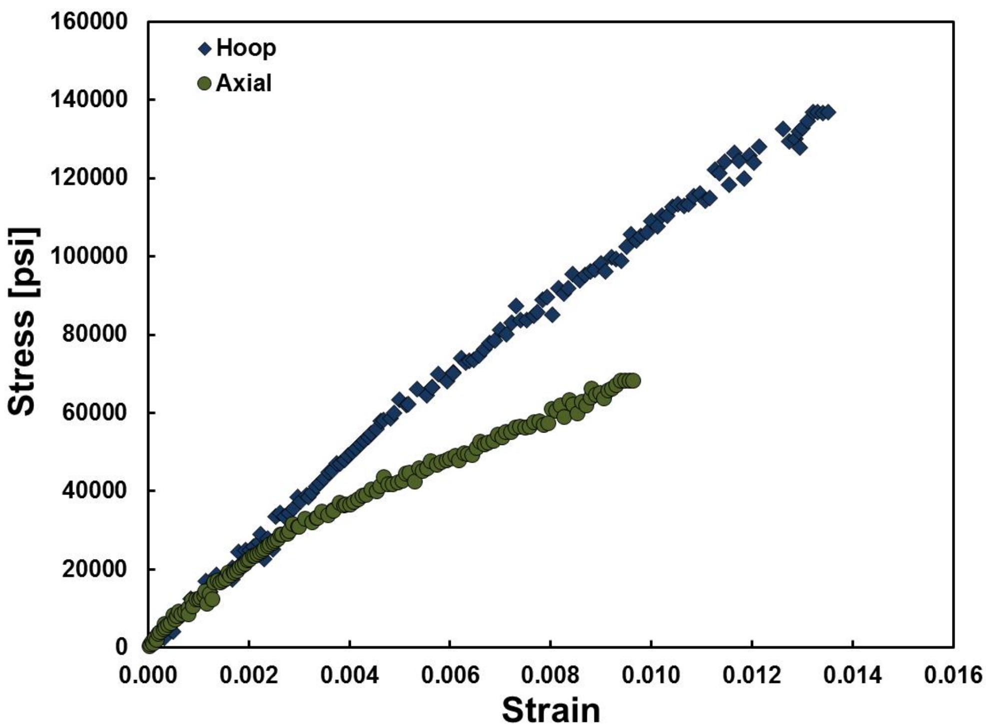

Figure A. 48 - Stress-strain response of ALT695 – 3794.

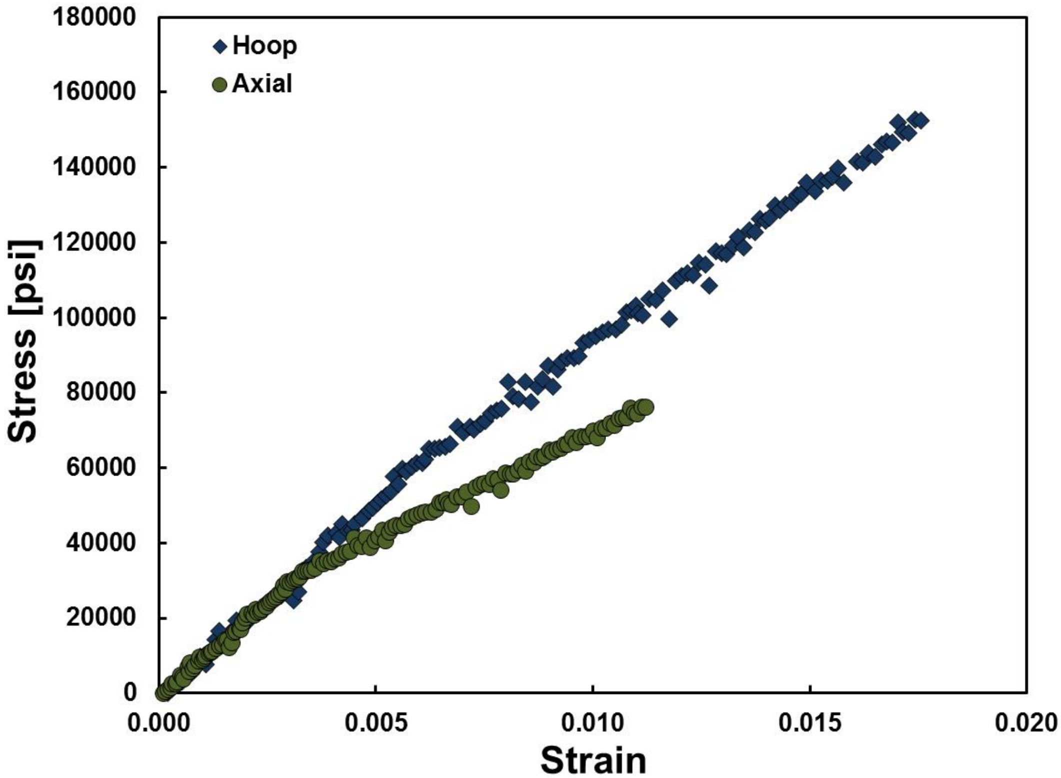

Figure A. 49 – Stress-strain response of OM3983.

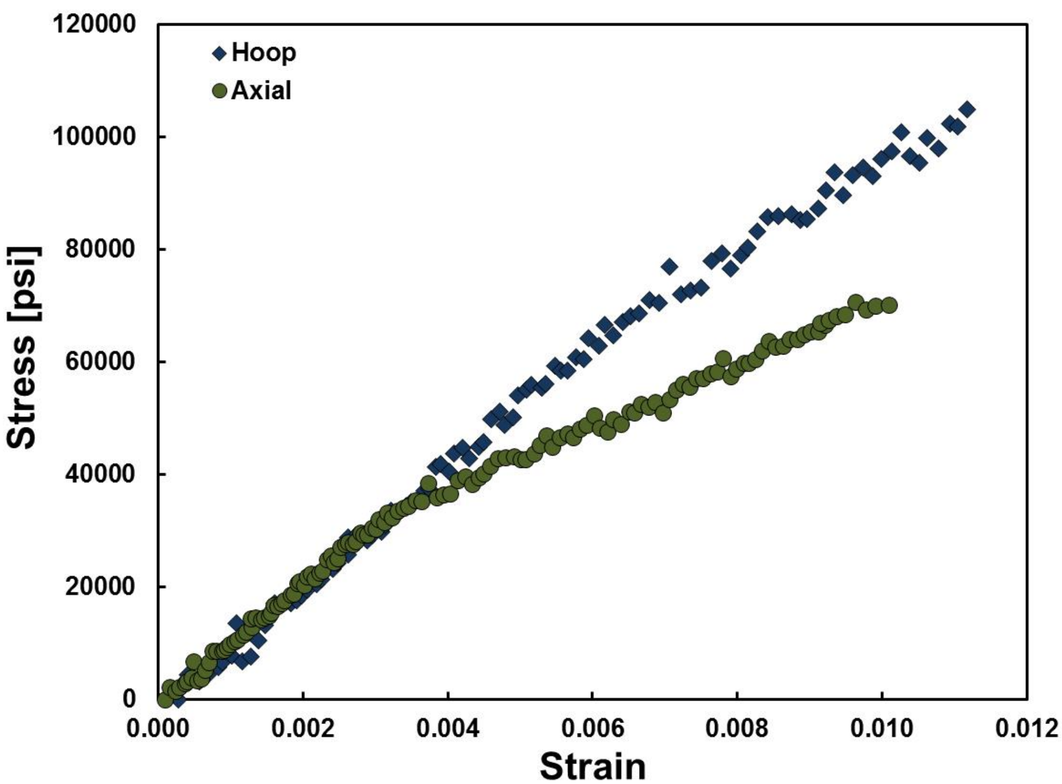

Figure A. 50 – Stress-strain response of OM3948.

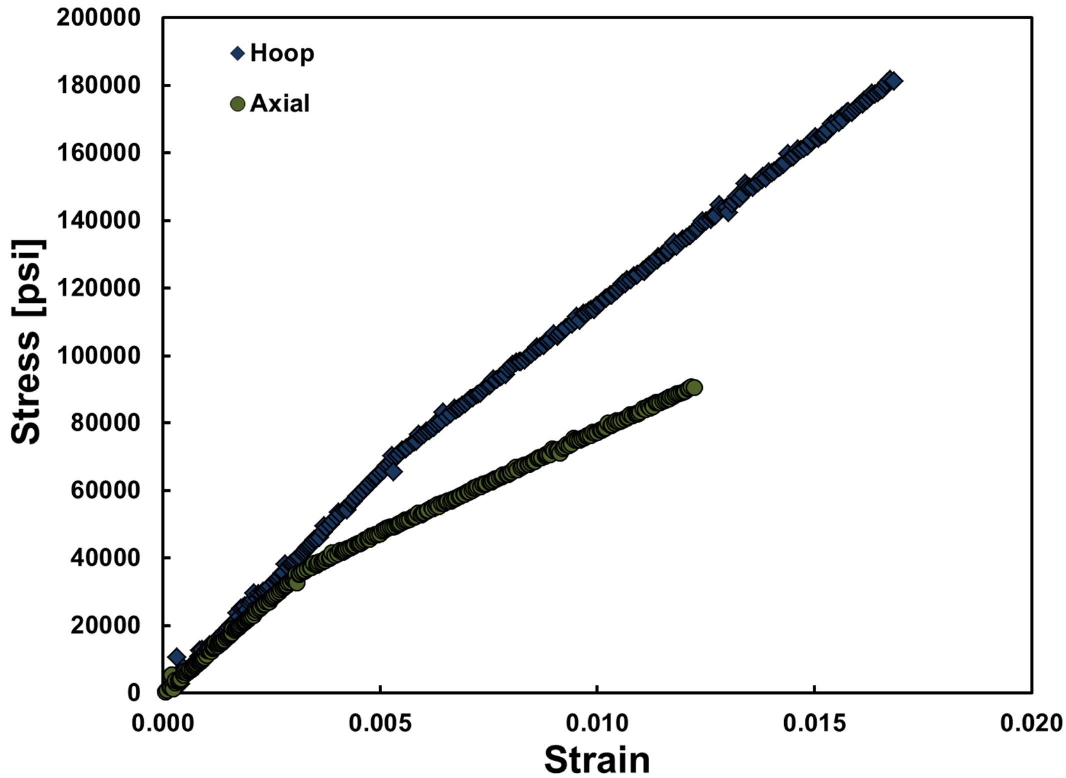

Figure A. 51 – Axial stress-strain response of IH2482.

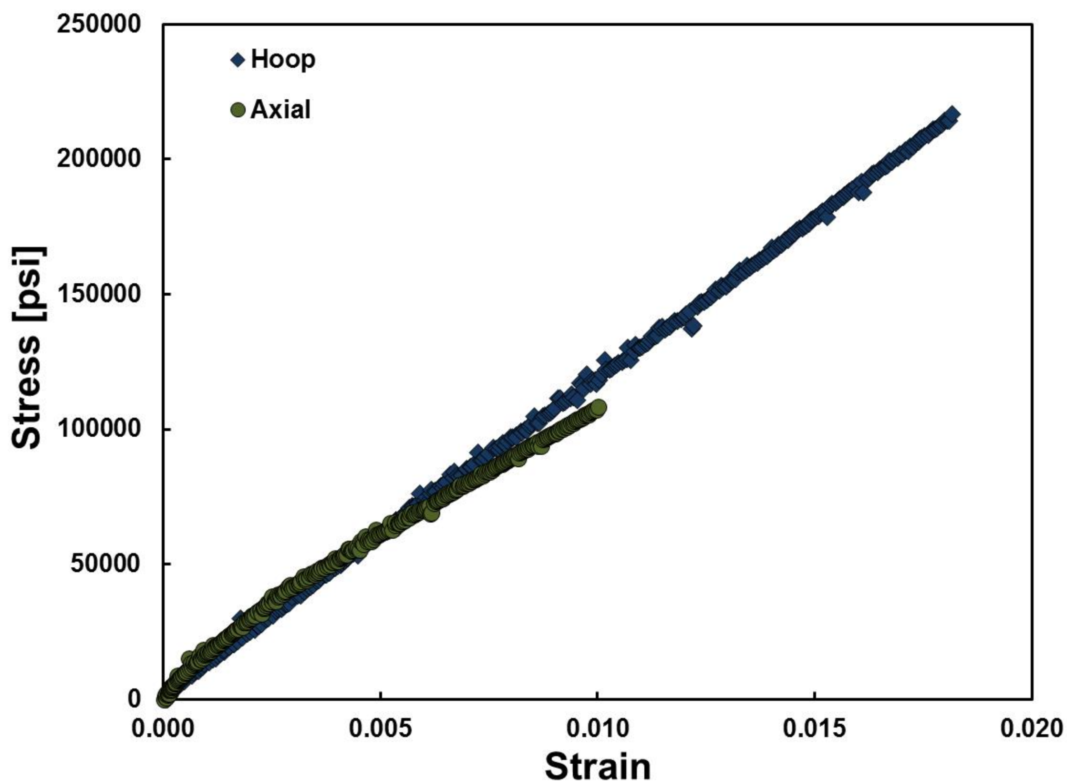

Figure A. 52 – Stress-strain response of ALT604 - 4371.

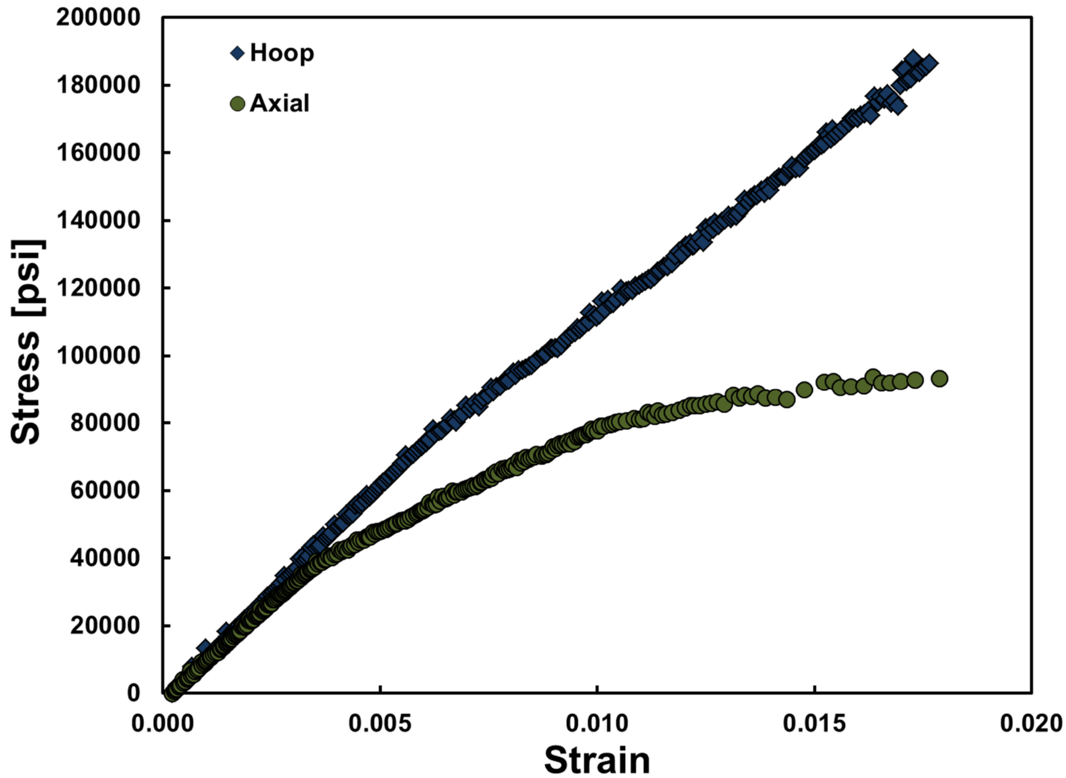

Figure A. 53 – Stress-strain response of OP11769.

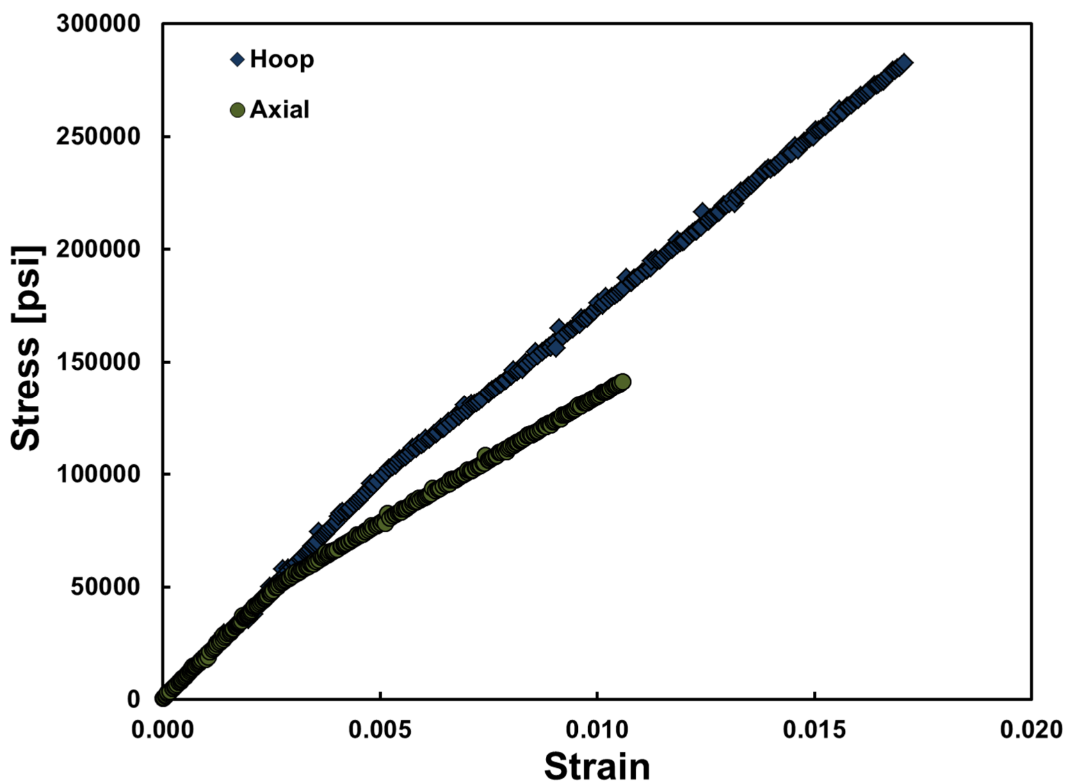

Figure A. 54 - Stress-strain response of ALT639 - 18722.

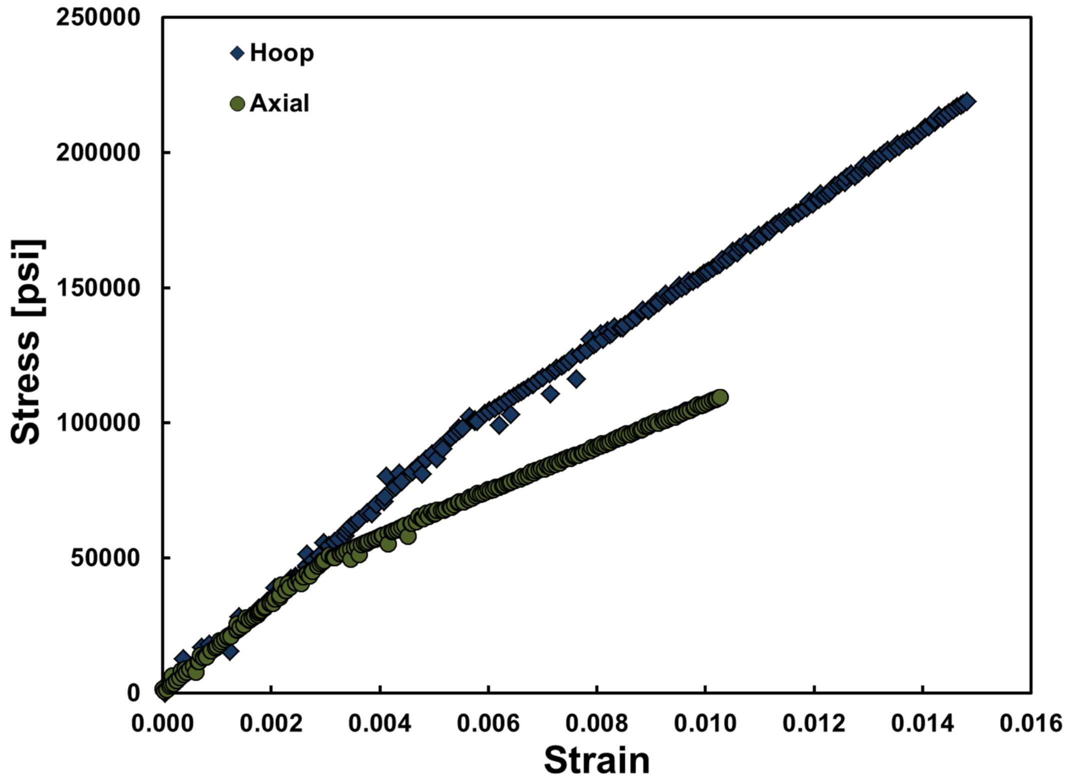

Figure A. 55 - Stress-strain response of IH2533.

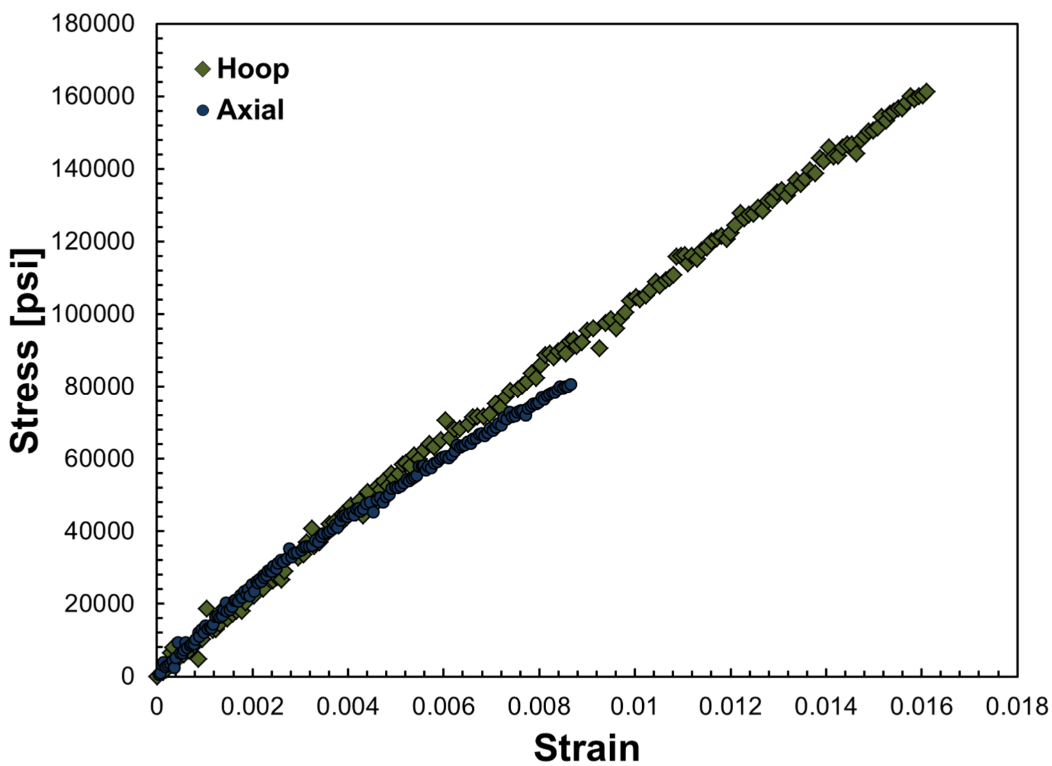

Figure A. 56 - Stress-strain response of ALT604 - 6021.

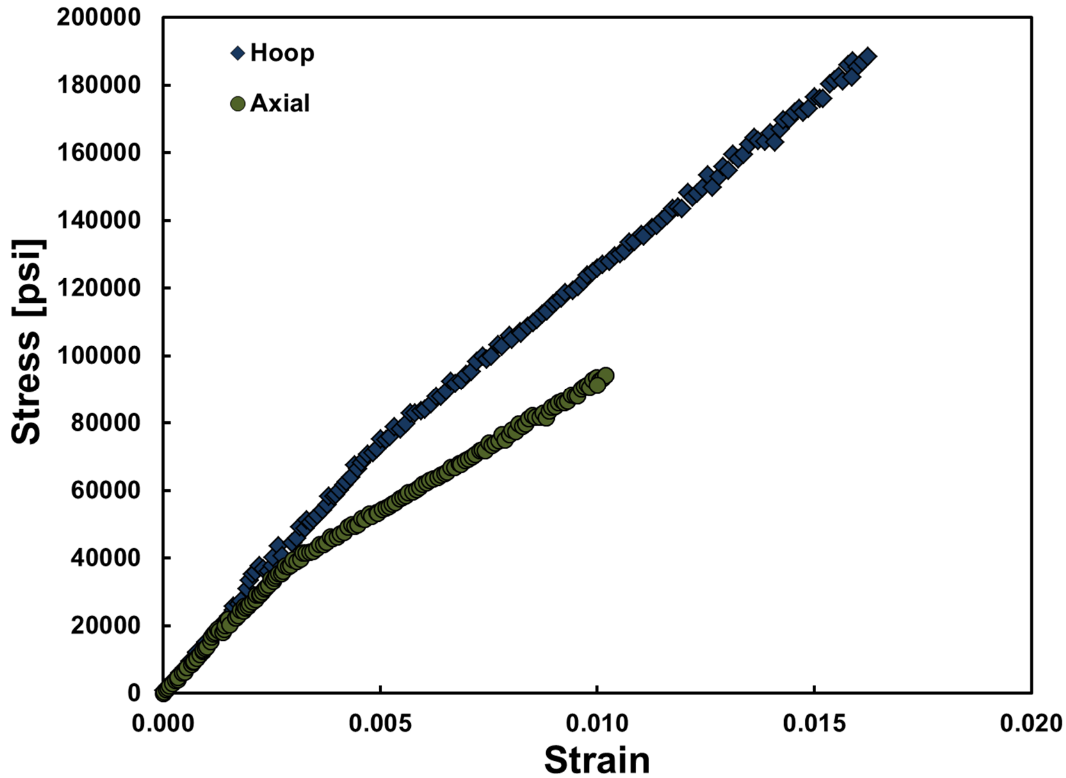

Figure A. 57 - Stress-strain response of ALT639 - 18699.

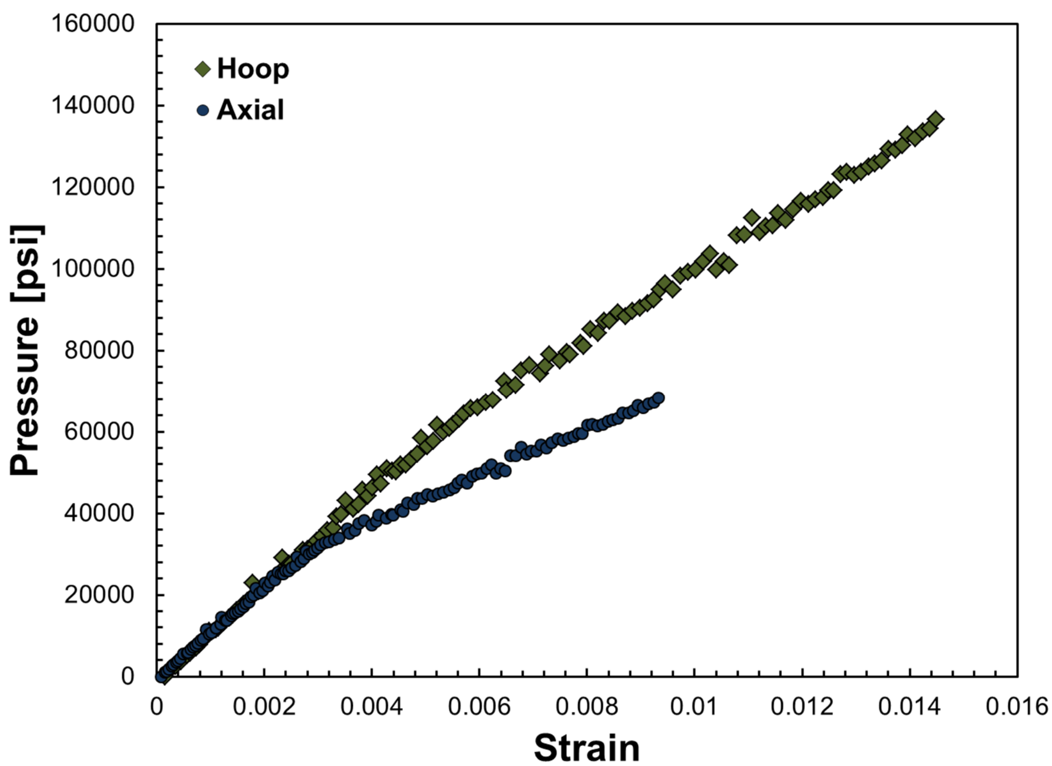

Figure A. 58 - Stress-strain response of OM3938.

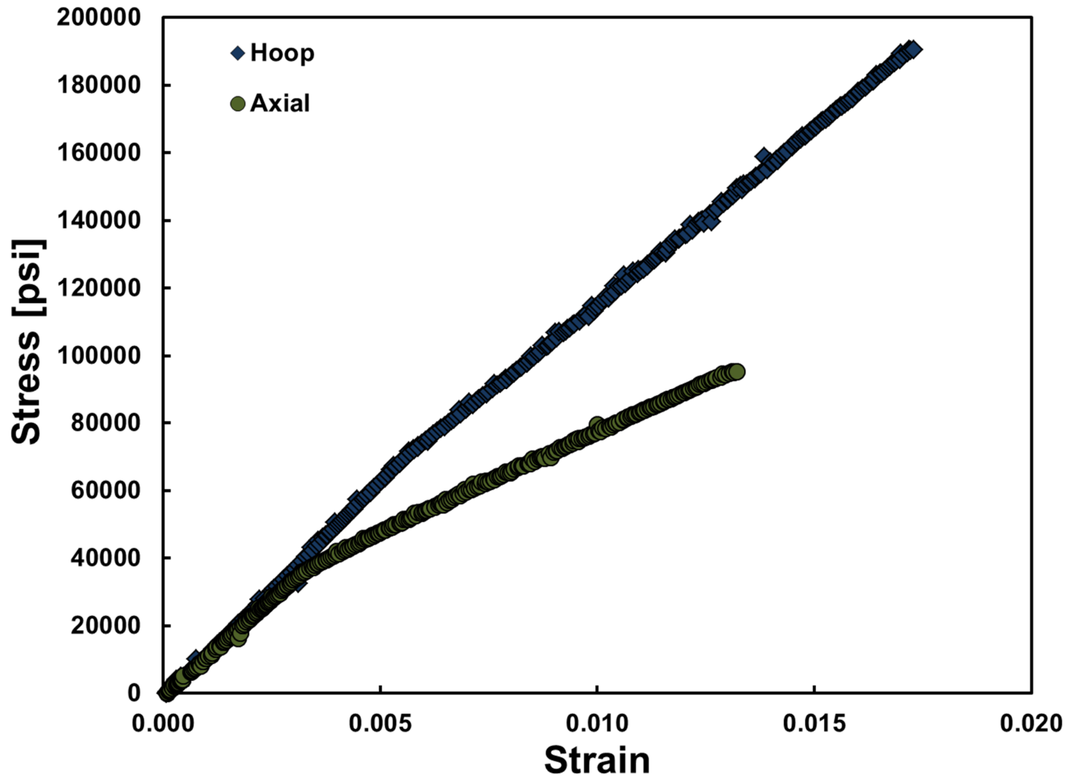

Figure A. 59 - Stress-strain response of IH2036.

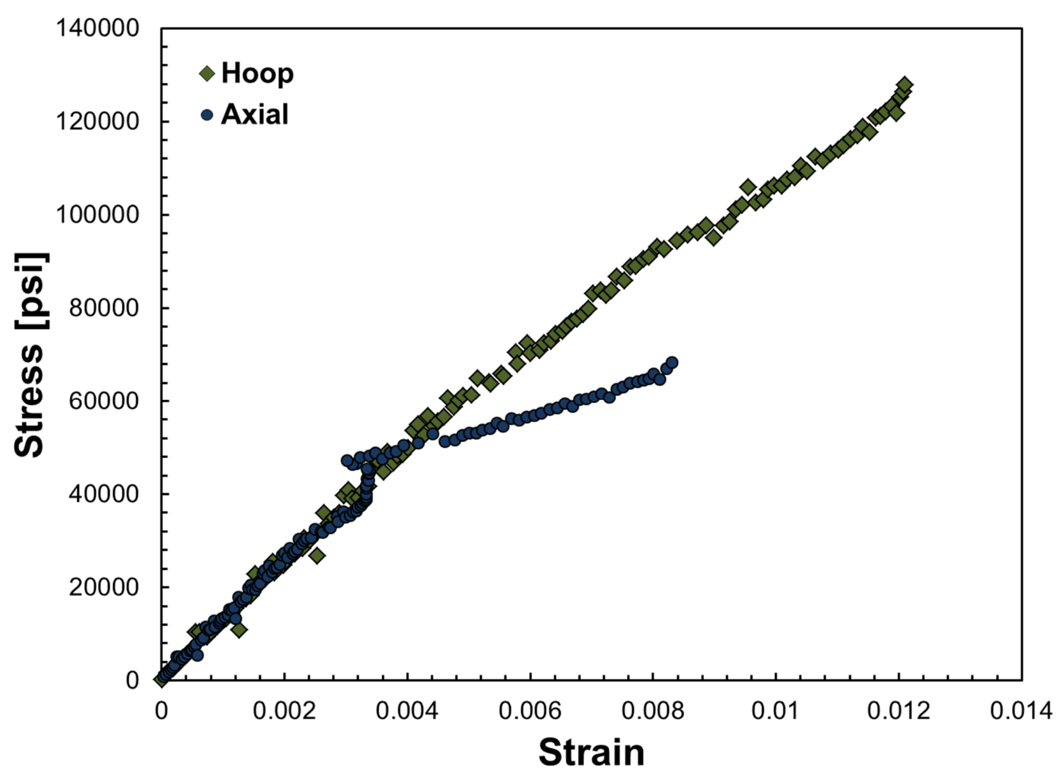

Figure A. 60 - Stress-strain response of ALT695 - 3929.

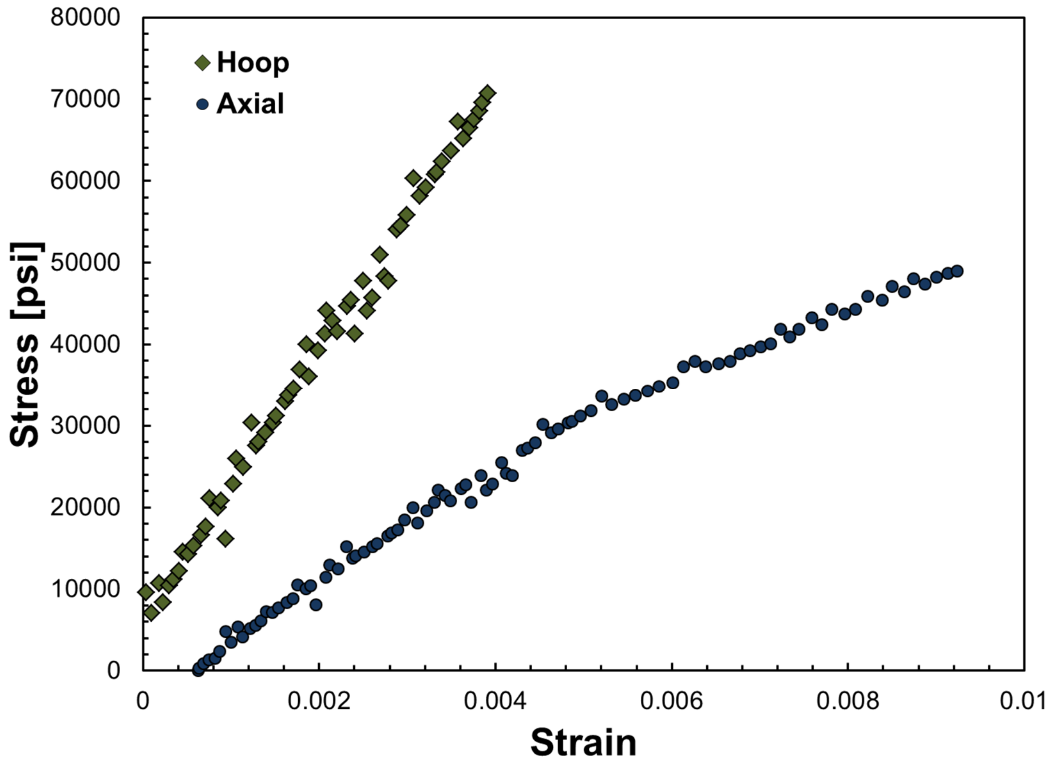

Figure A. 61 - Stress-strain response of OM3984.

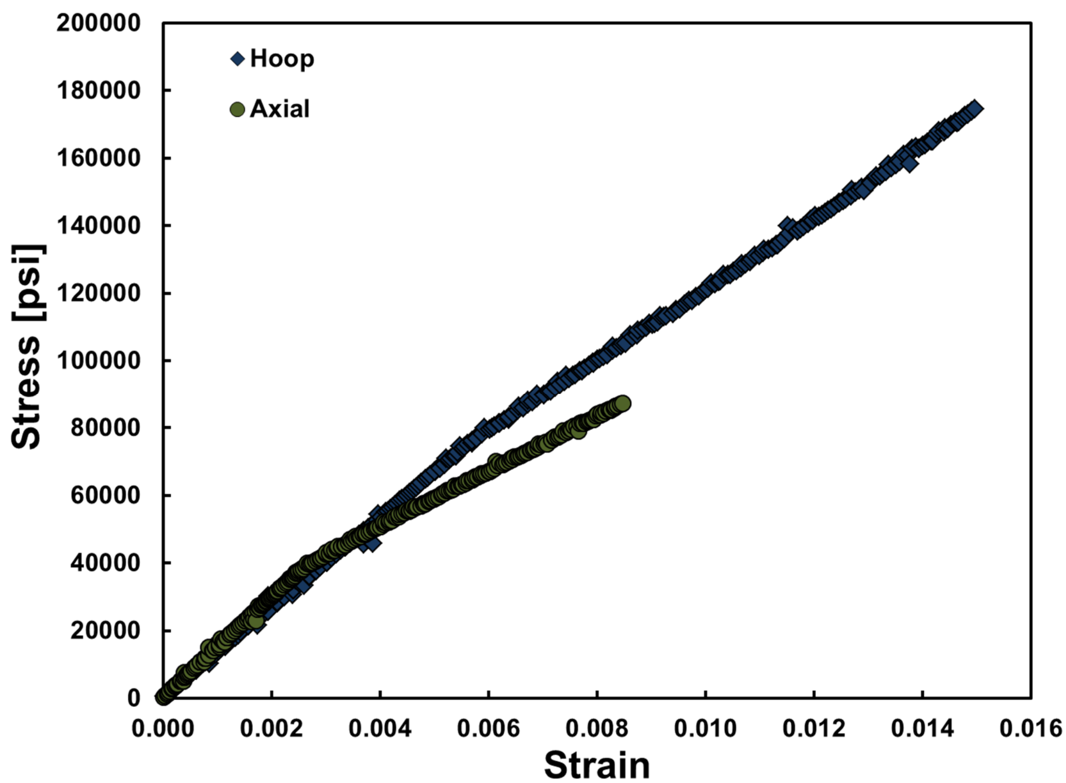

Figure A. 62 – Stress-strain response of ALT639 - 17732.

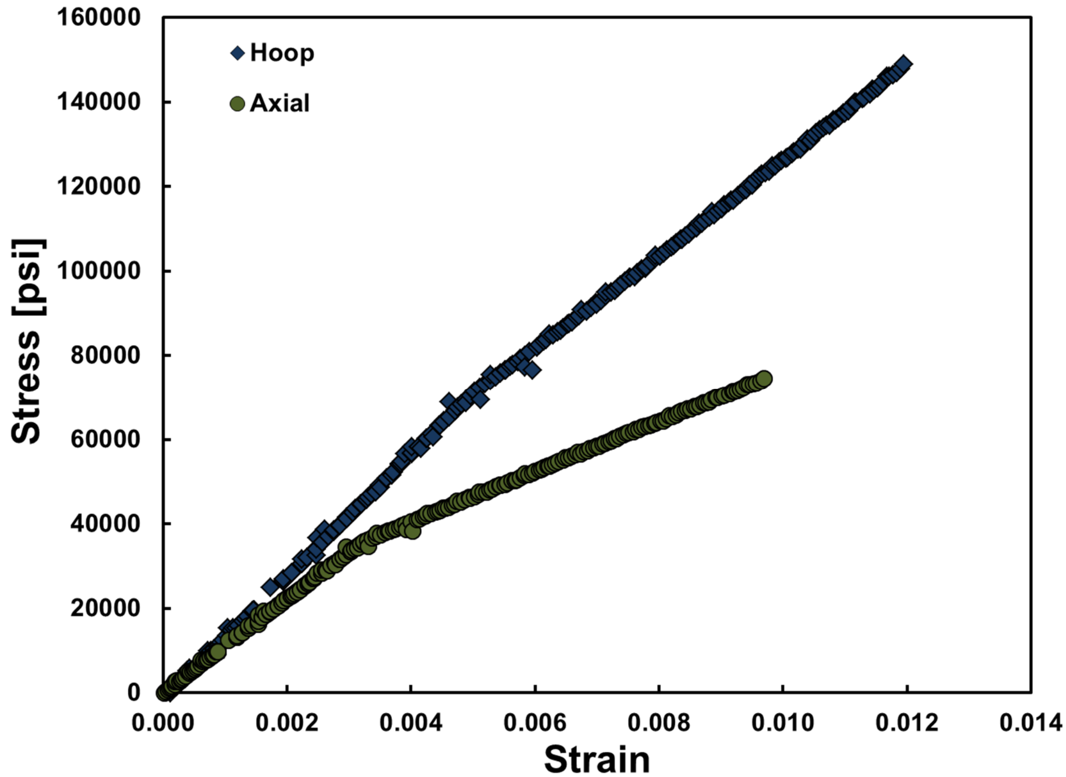

Figure A. 63 – Stress-strain response of IH2554.

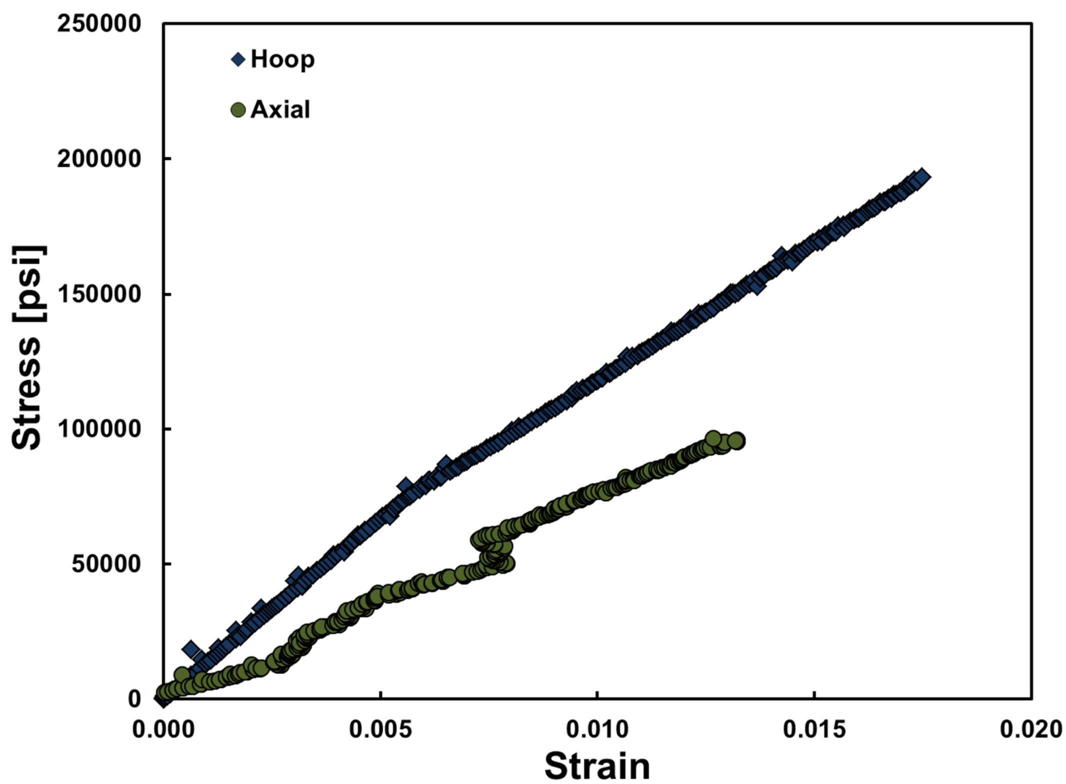

Figure A. 64 – Axial stress-strain response of ALT639 - 69925.

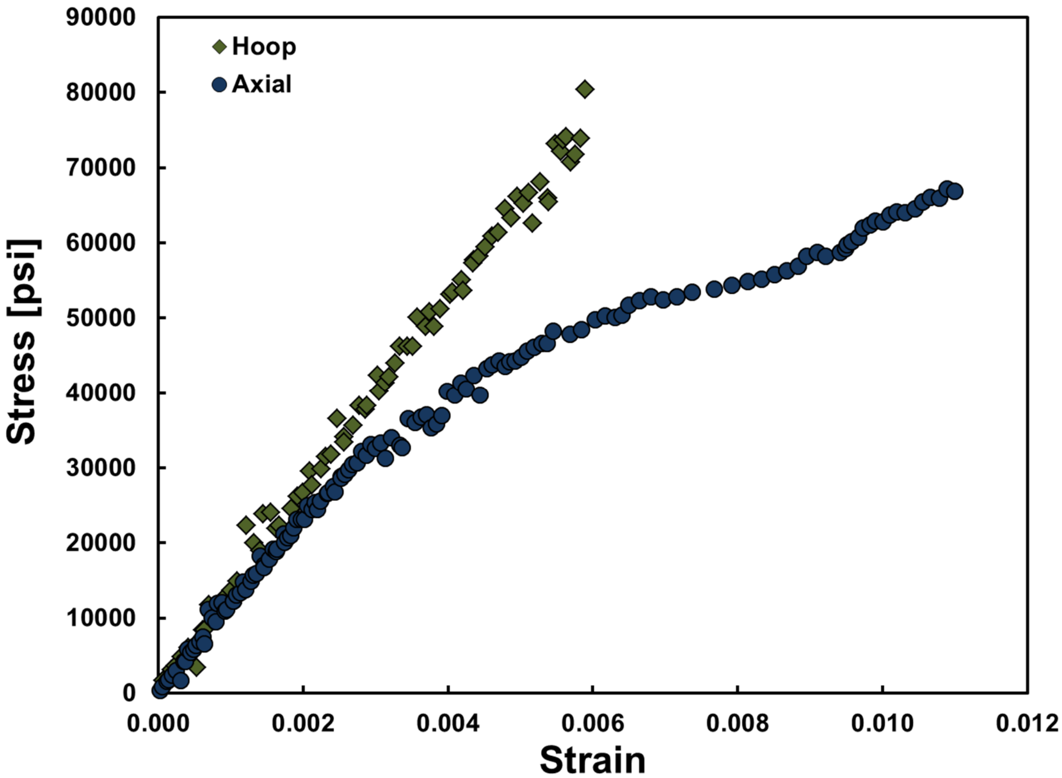

Figure A. 65 – Stress-strain response of ALT695 - 4304.

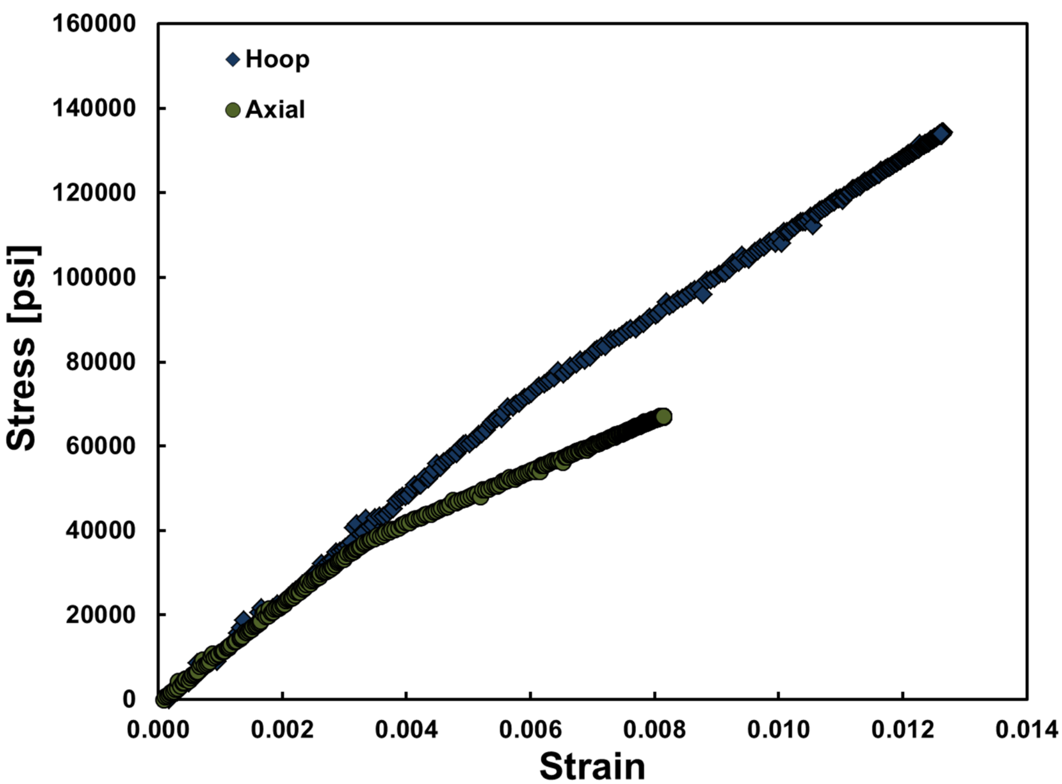

Figure A. 66 – Stress-strain response of OP11129.

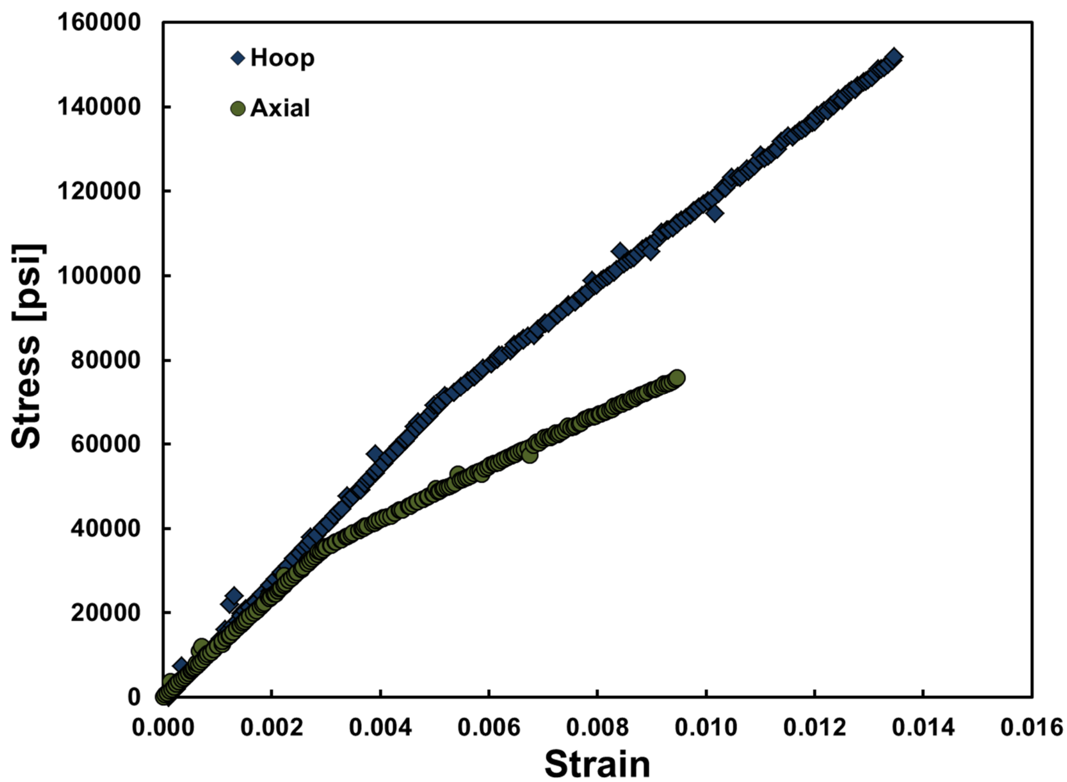

Figure A. 67 - Stress-strain response of IH1251.

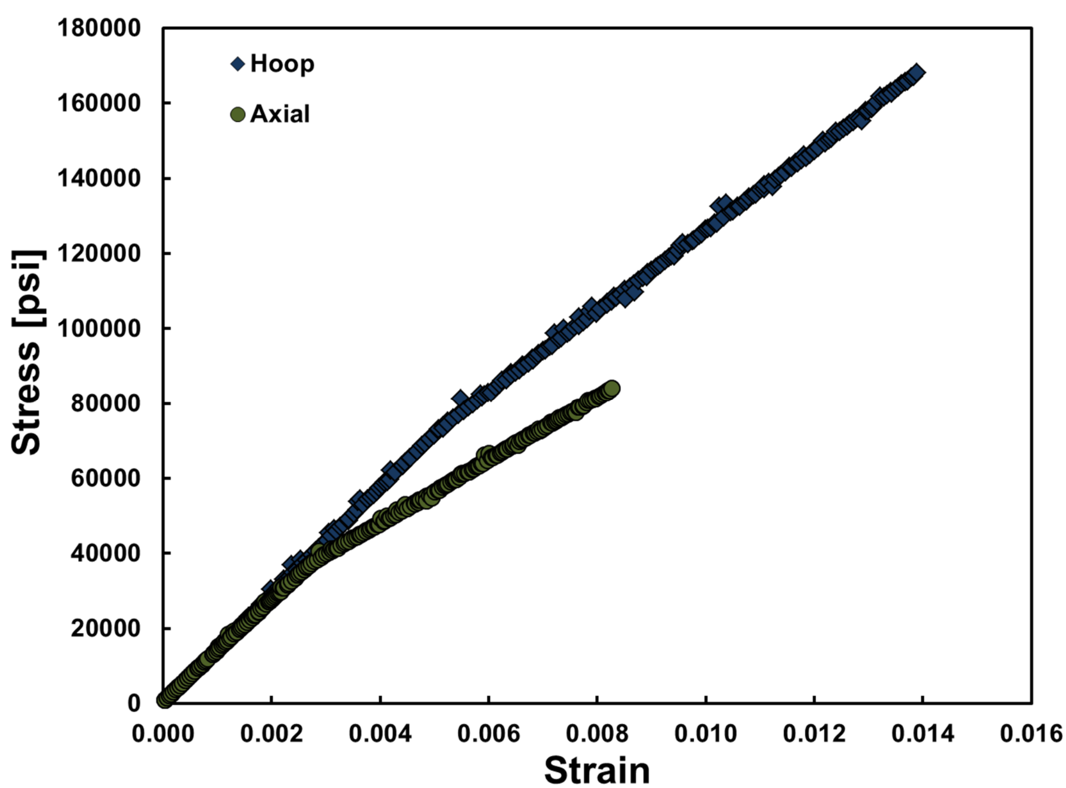

Figure A. 68 - Stress-strain response of ALT639 - 17827.

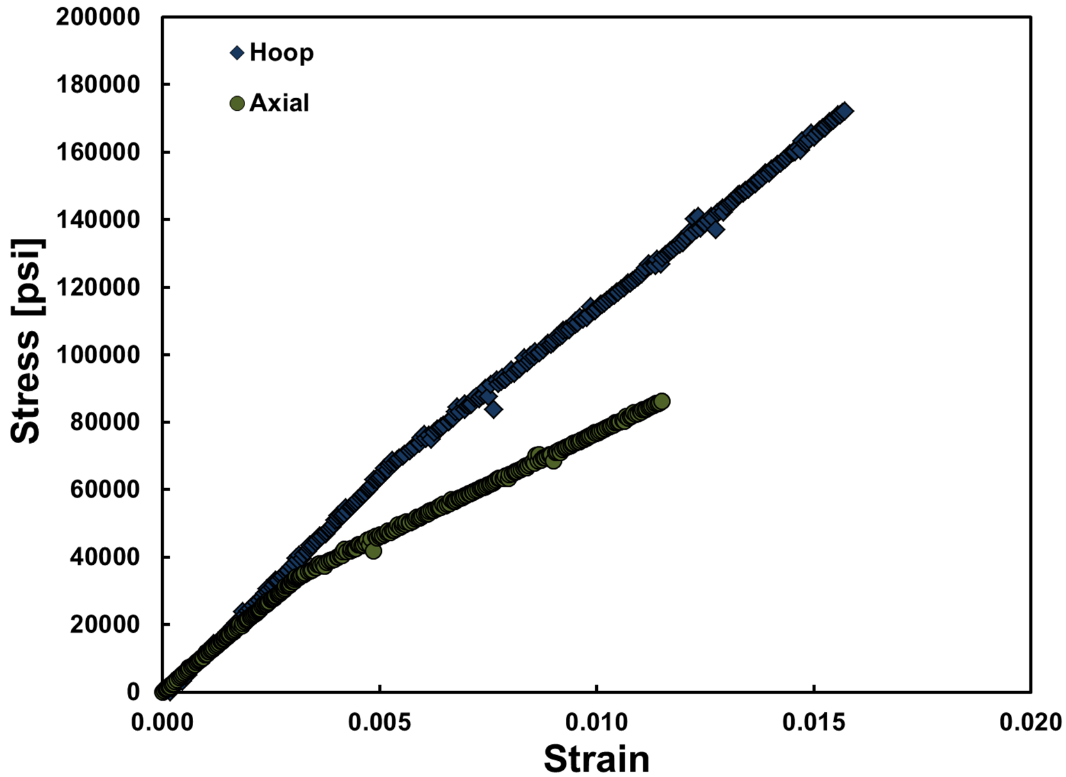

Figure A. 69 - Stress-strain response of ALT695-4333.

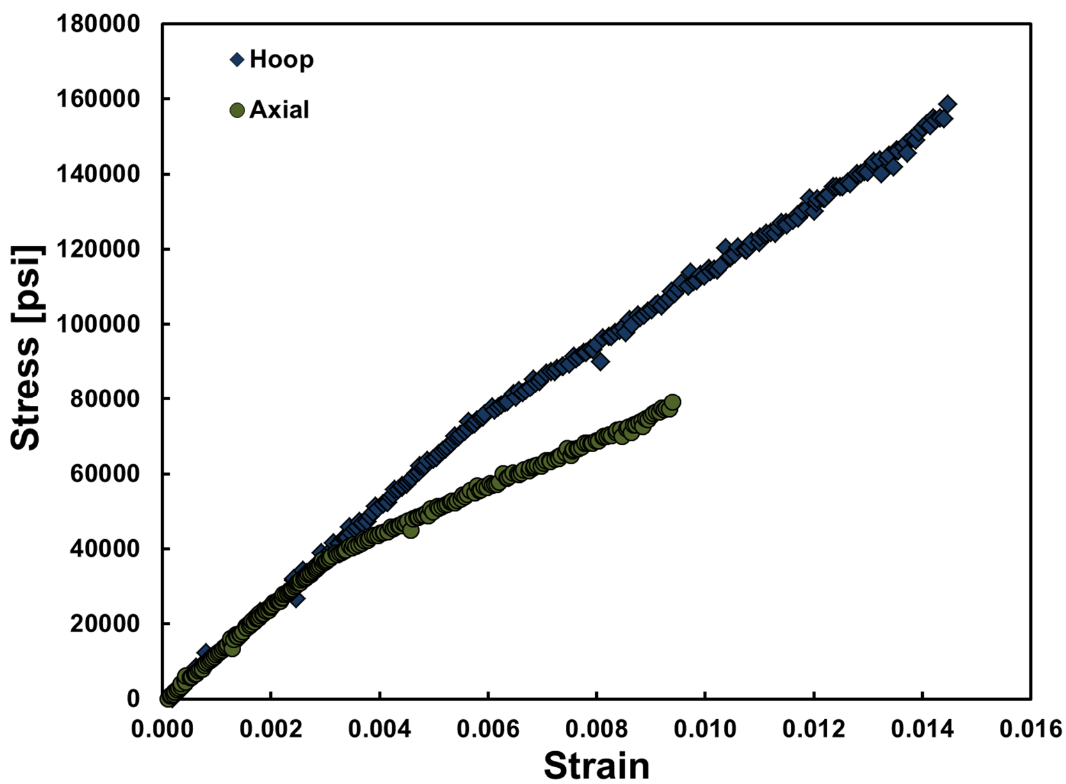

Figure A. 70 - Stress-strain response of OM3918.

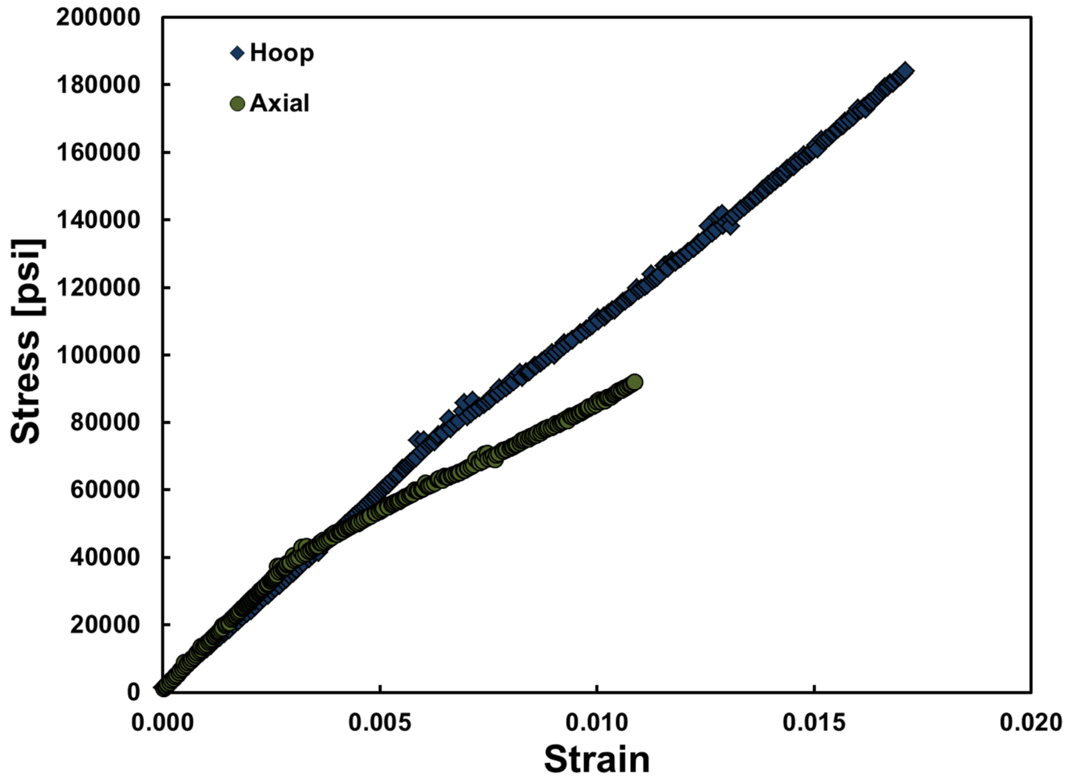

Figure A. 71 - Stress-strain response of ALT639-18800.

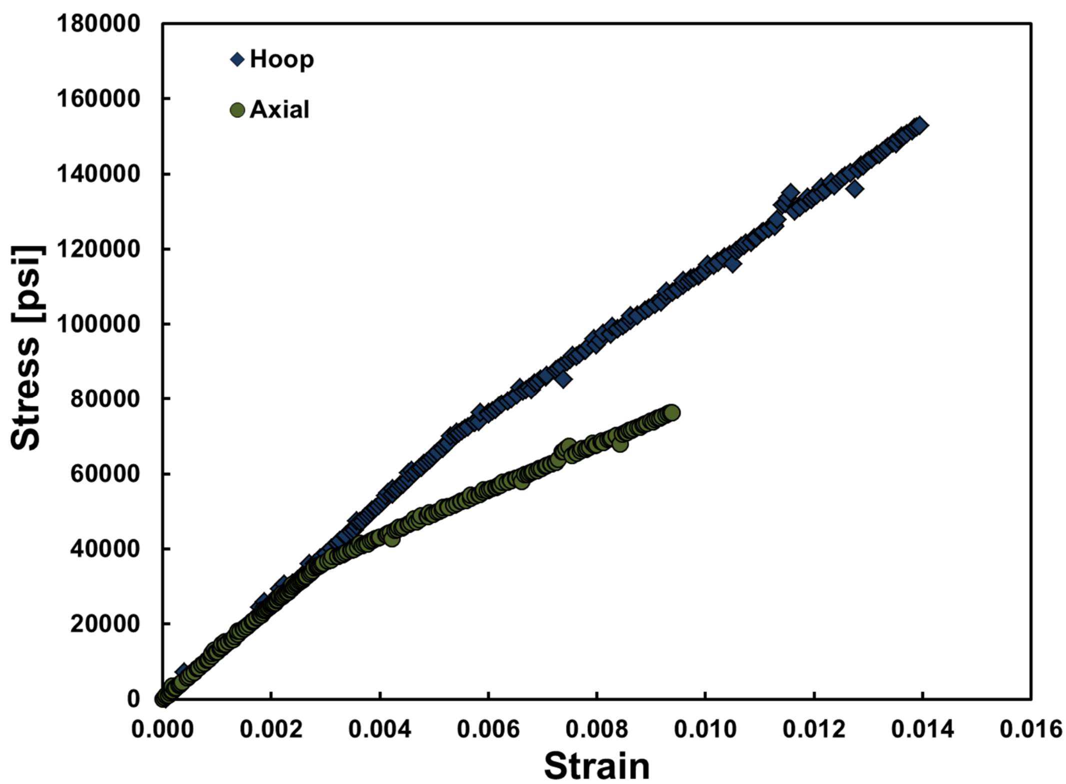

Figure A. 72 - Stress-strain response of IH1750.

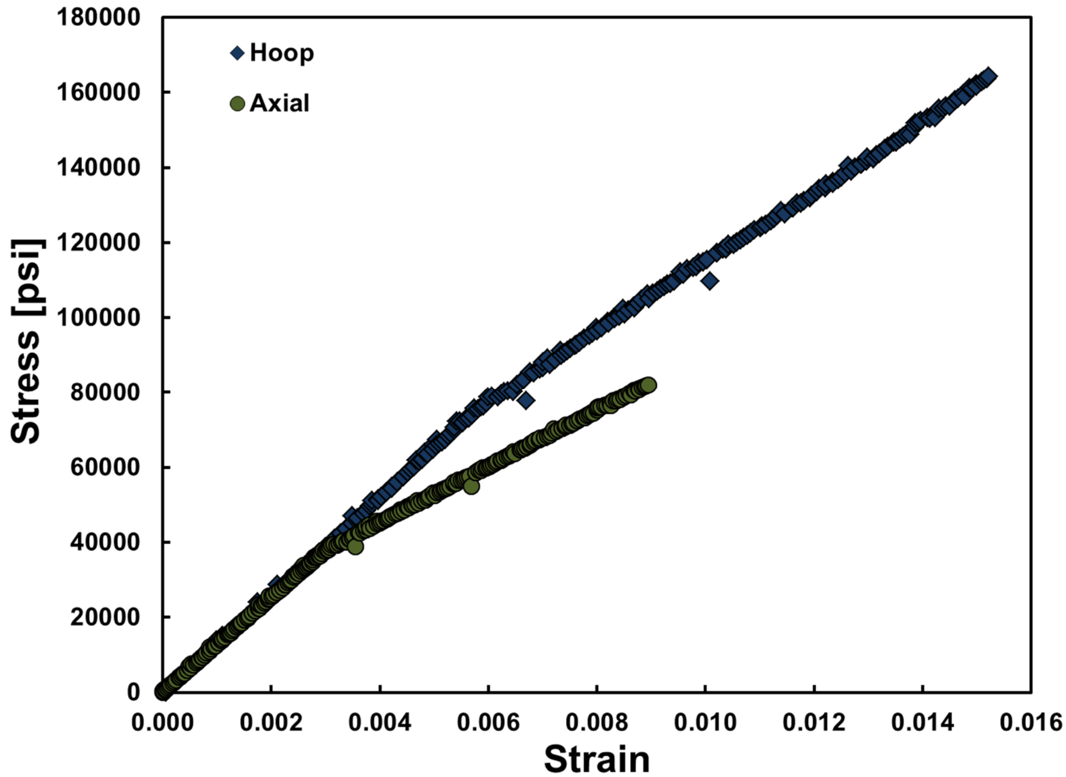

Figure A. 73 - Stress-strain response of ALT639-18713.

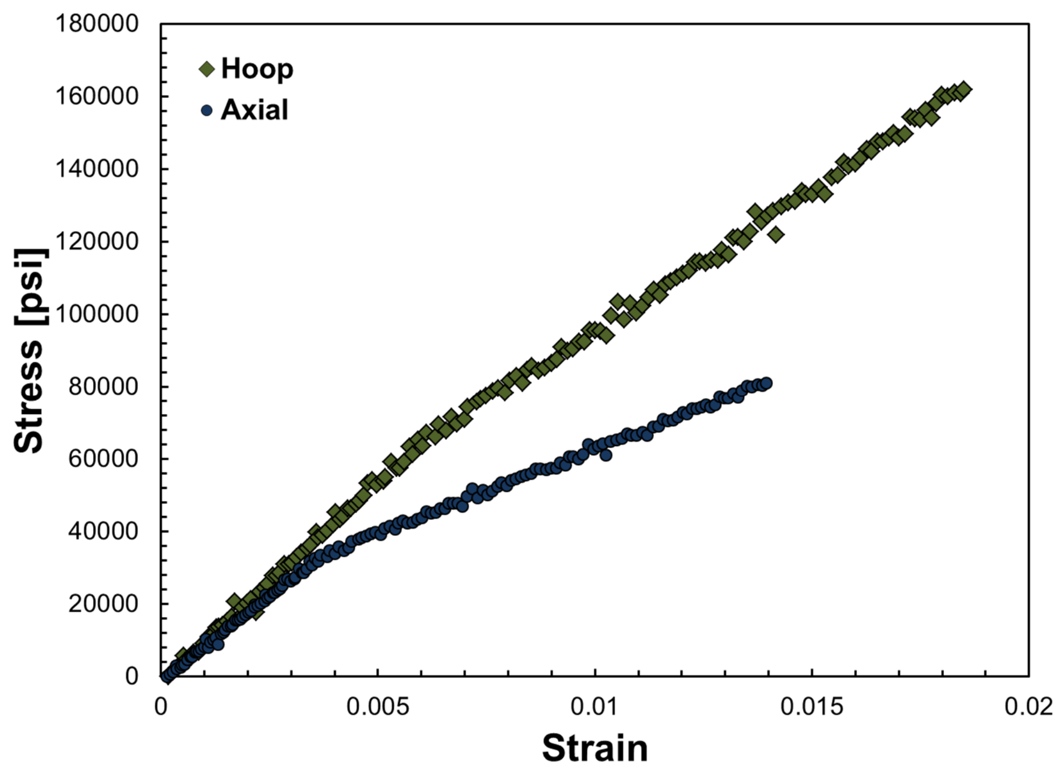

Figure A. 74 - Stress-strain response of OM4045.

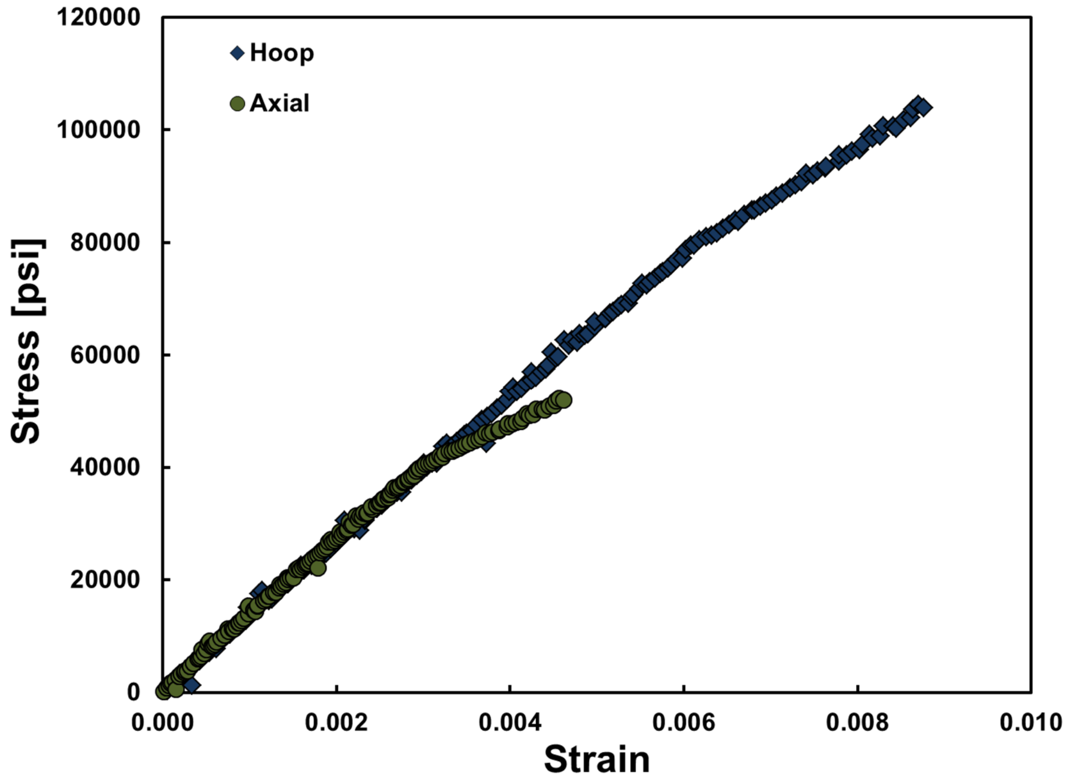

Figure A. 75 - Stress-strain response of OM3957.

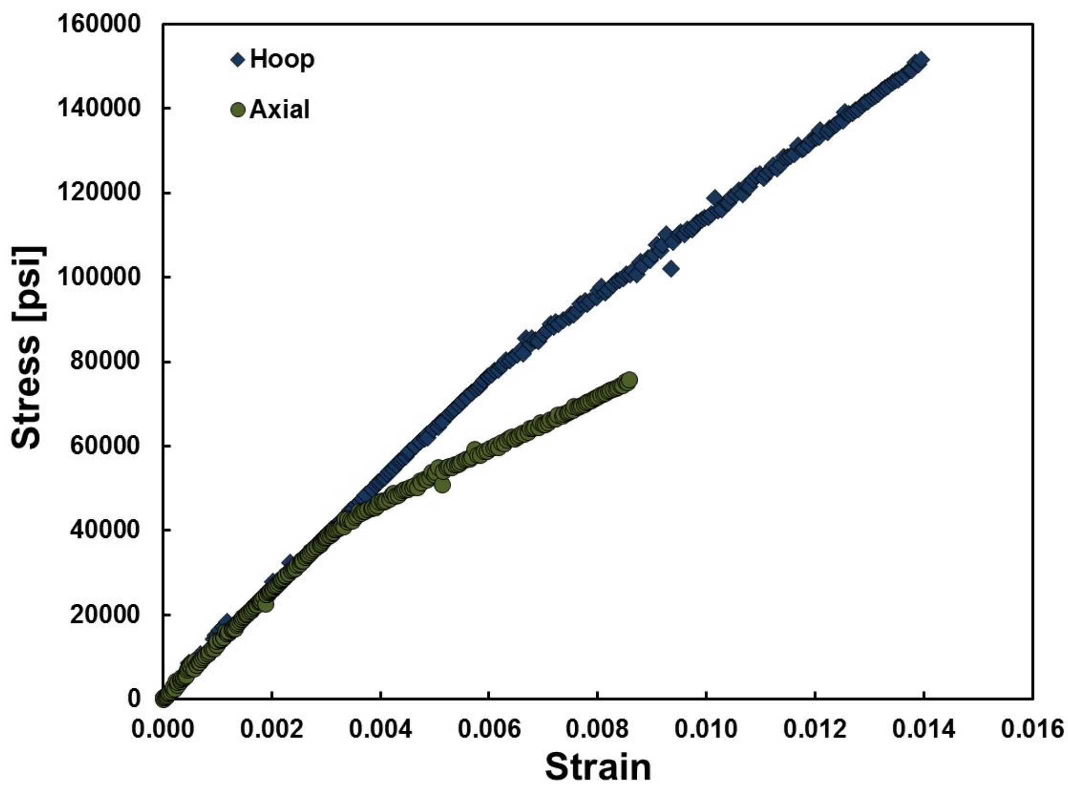

Figure A. 76 - Stress-strain response of OM3914.

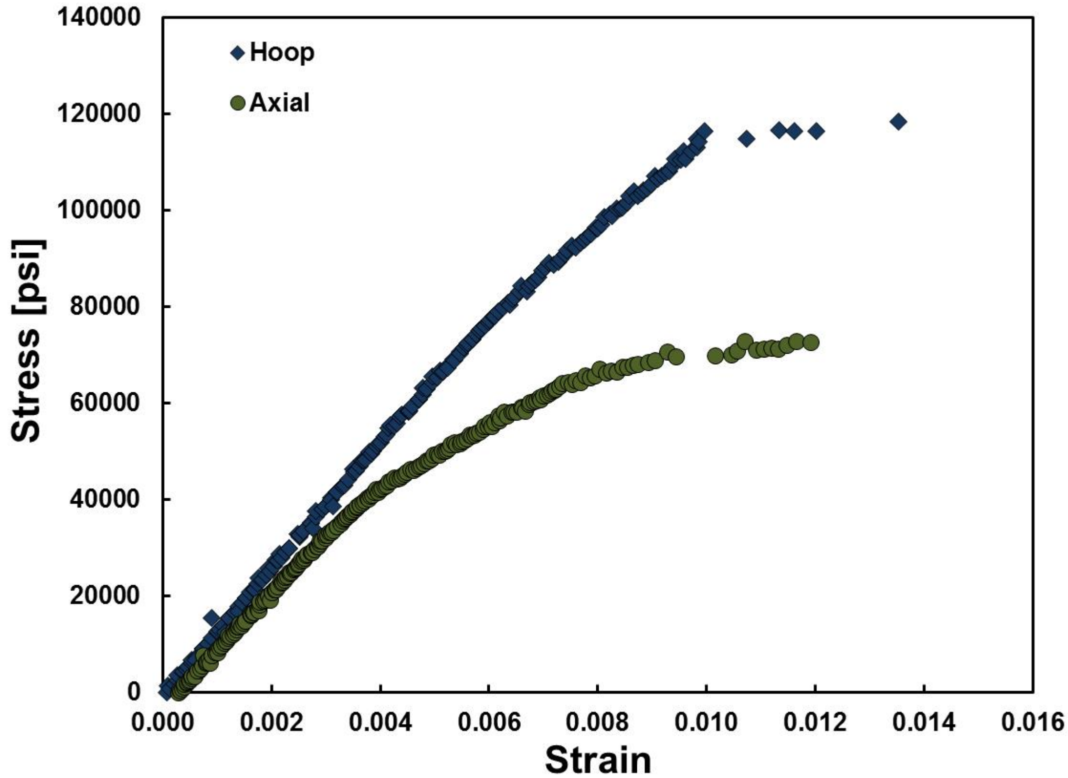

Figure A. 77 - Stress-strain response of OM3912.

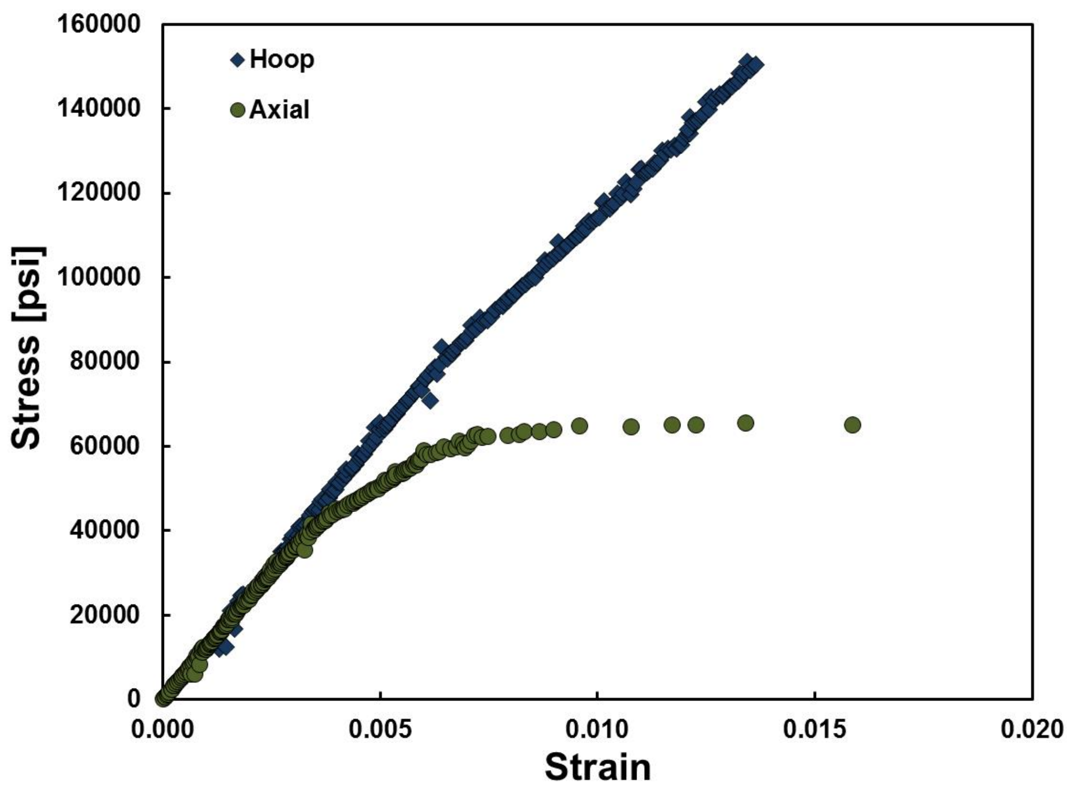

Figure A.78 - Stress-strain response of OM3954.

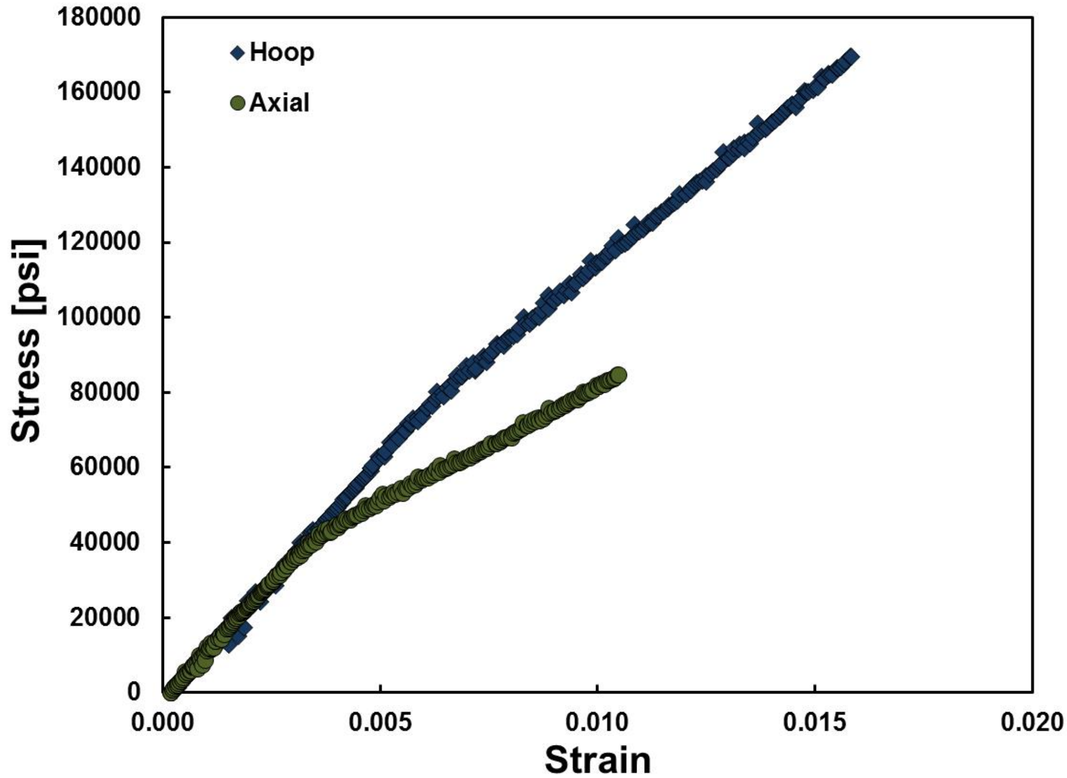

Figure A. 79 - Stress-strain response of OM3925.

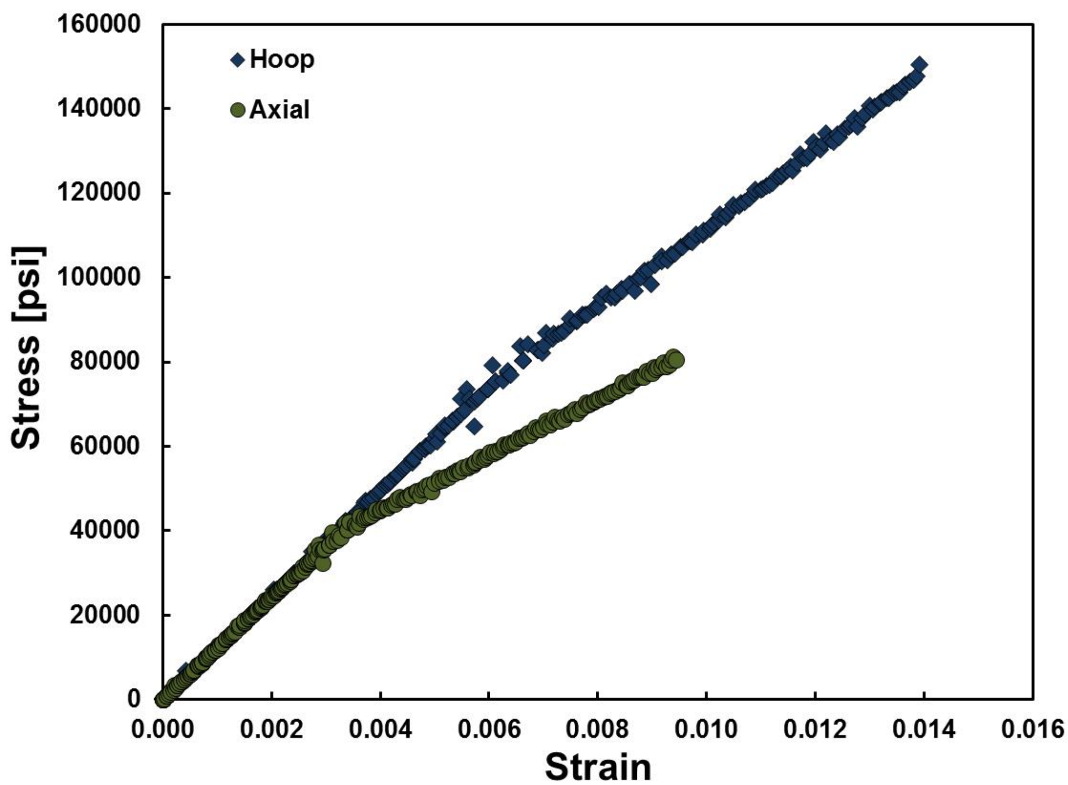

Figure A.80 - Stress-strain response of OM3982.

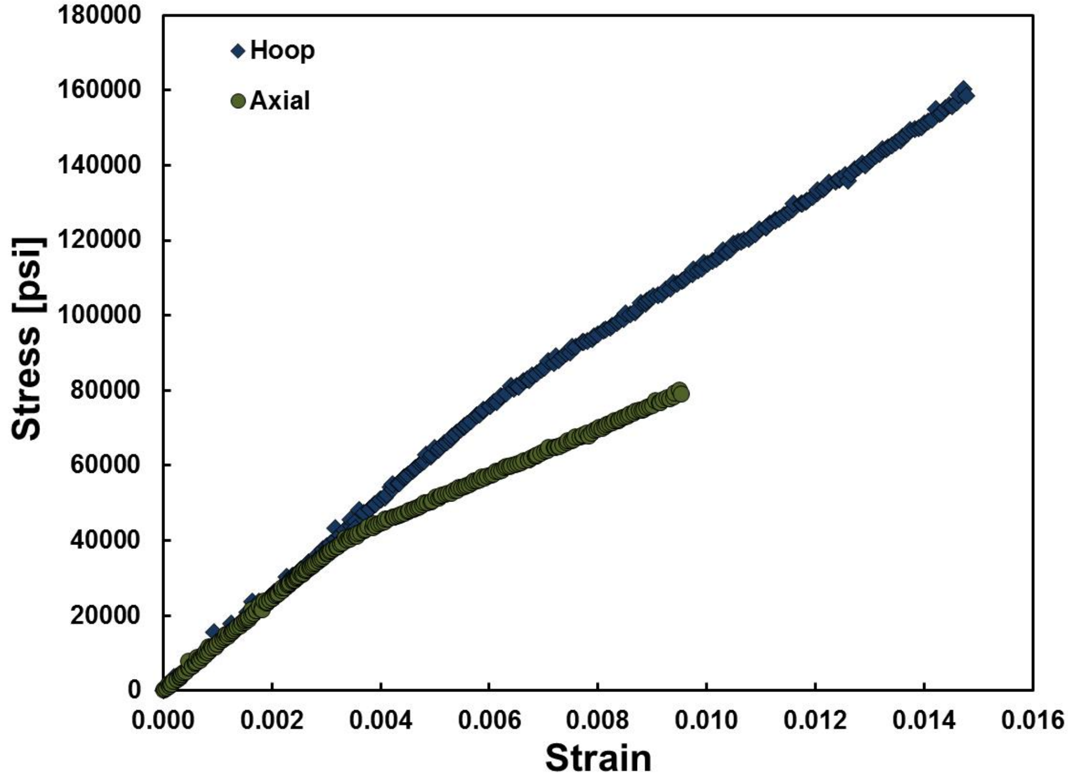

Figure A.81 - Stress-strain response of OM3917.

12.0 Appendix B – Background Energy Oscillation Curves

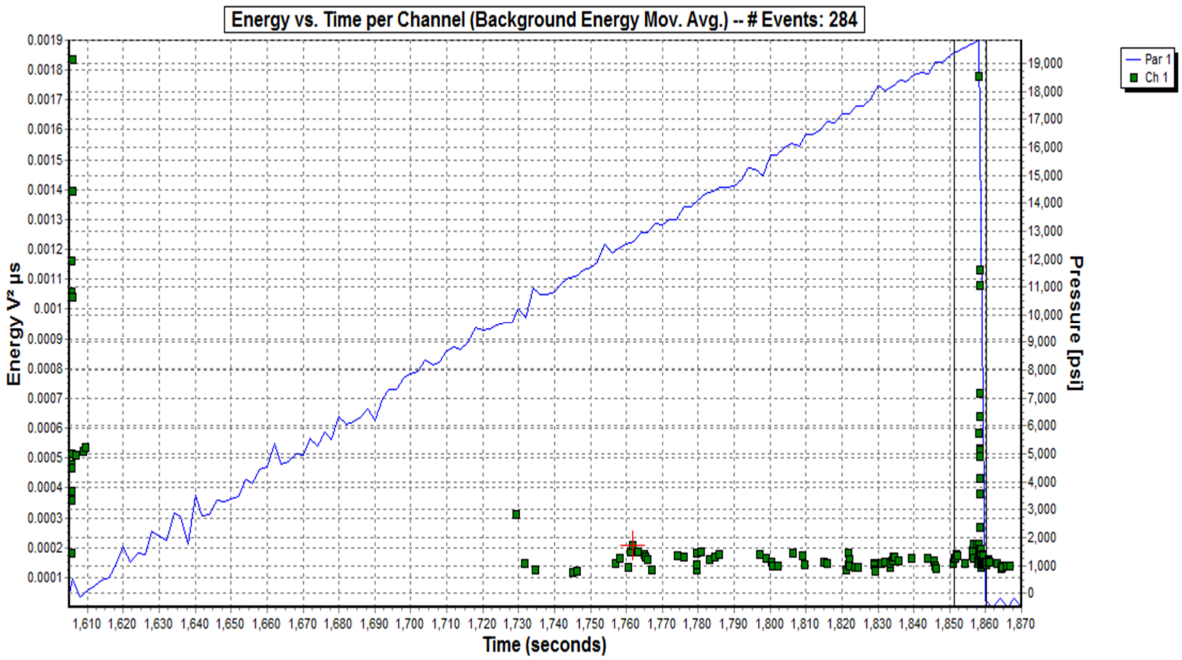

Figure B. 1 – Background Energy Oscillation for ALT604 – 4962.

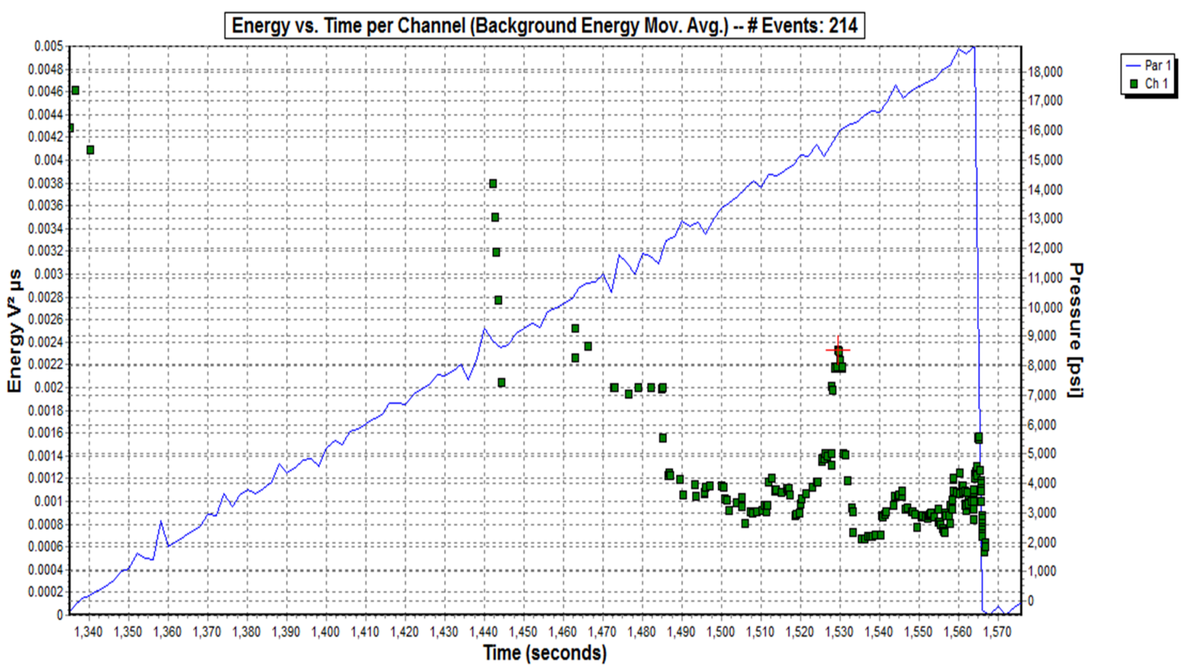

Figure B. 2 - Background Energy Oscillation for ALT695-3650.

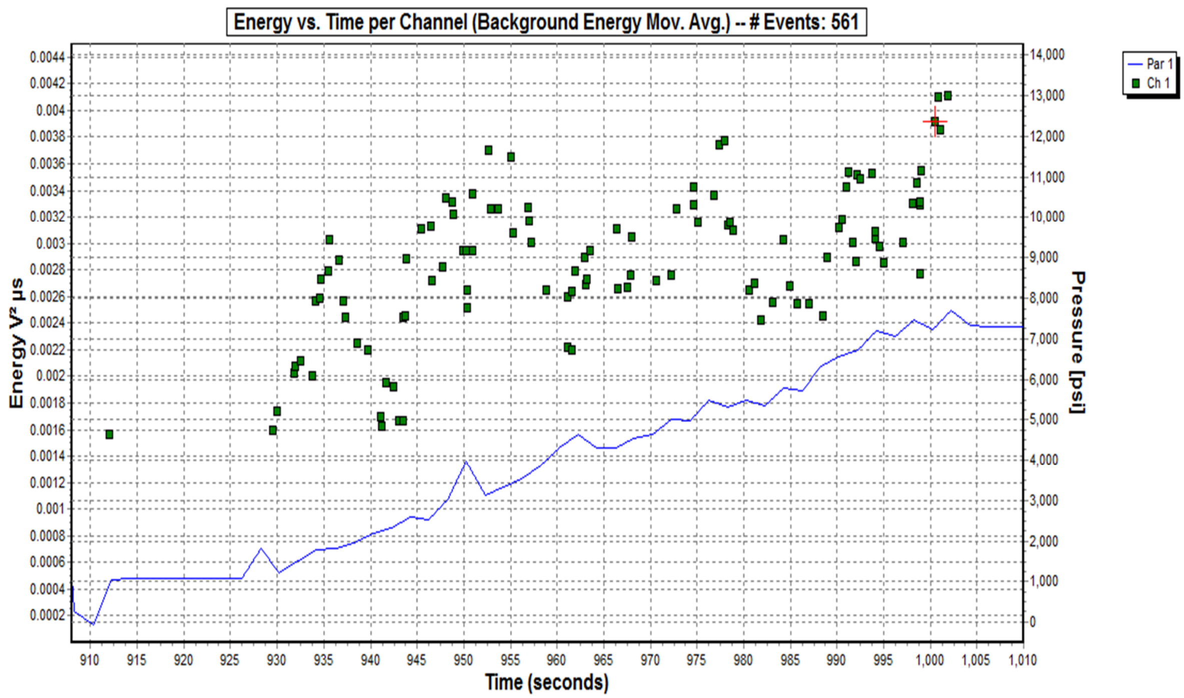

Figure B. 3 - Background Energy Oscillation for ALT604-3742.

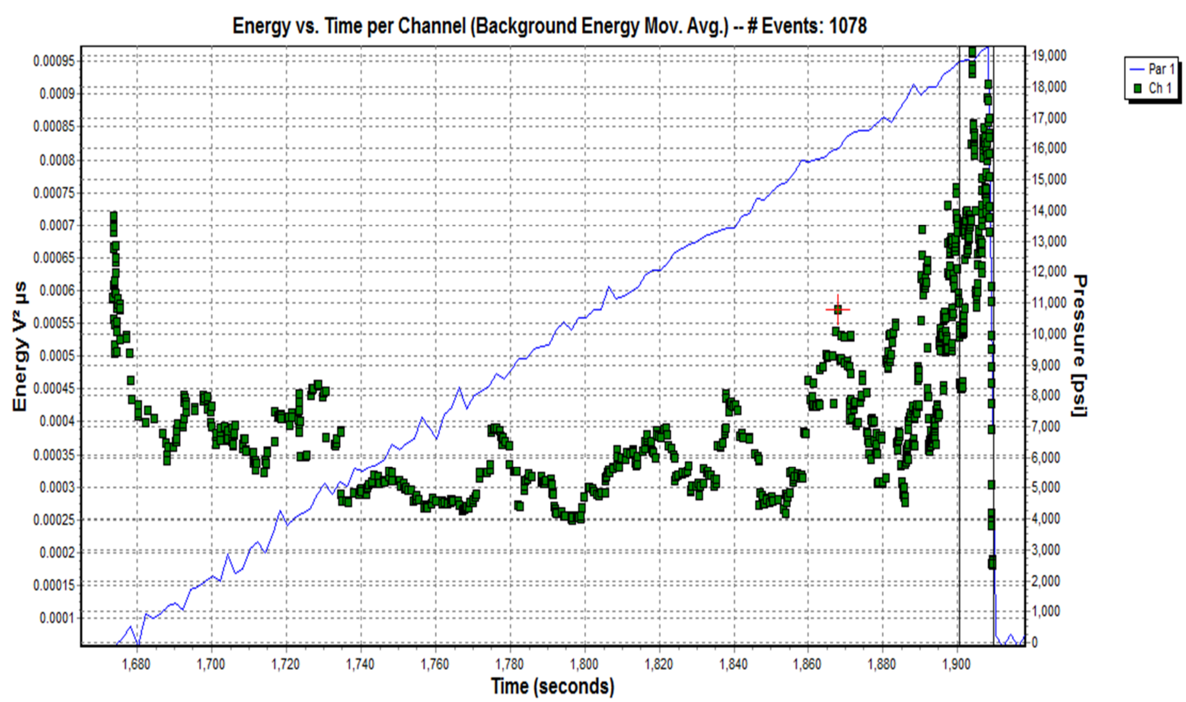

Figure B. 4 - Background Energy Oscillation for ALT695-4494.

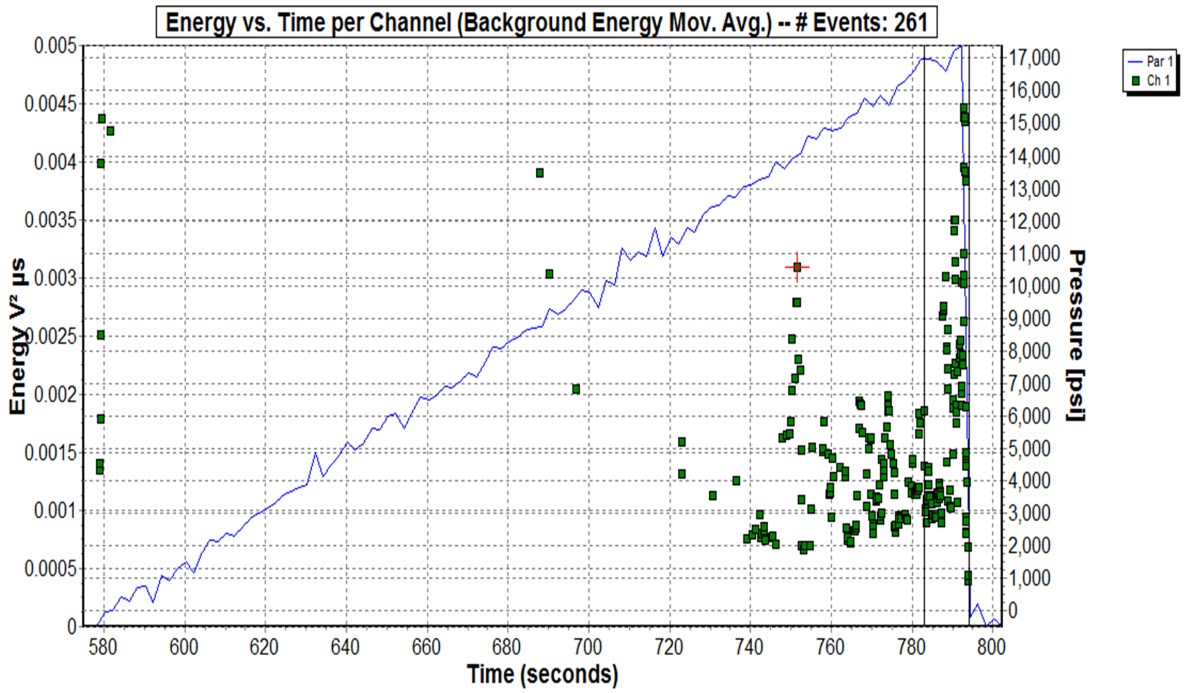

Figure B. 5 - Background Energy Oscillation for ALT695-4436.

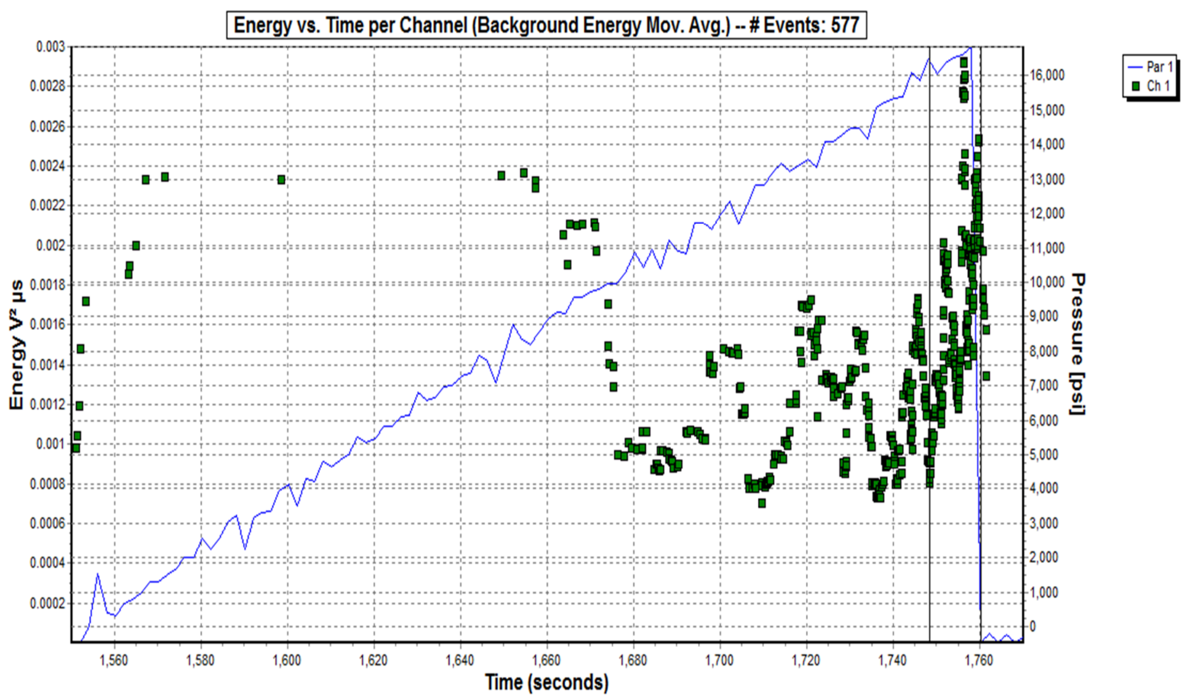

Figure B. 6 - Background Energy Oscillation for OM3915.

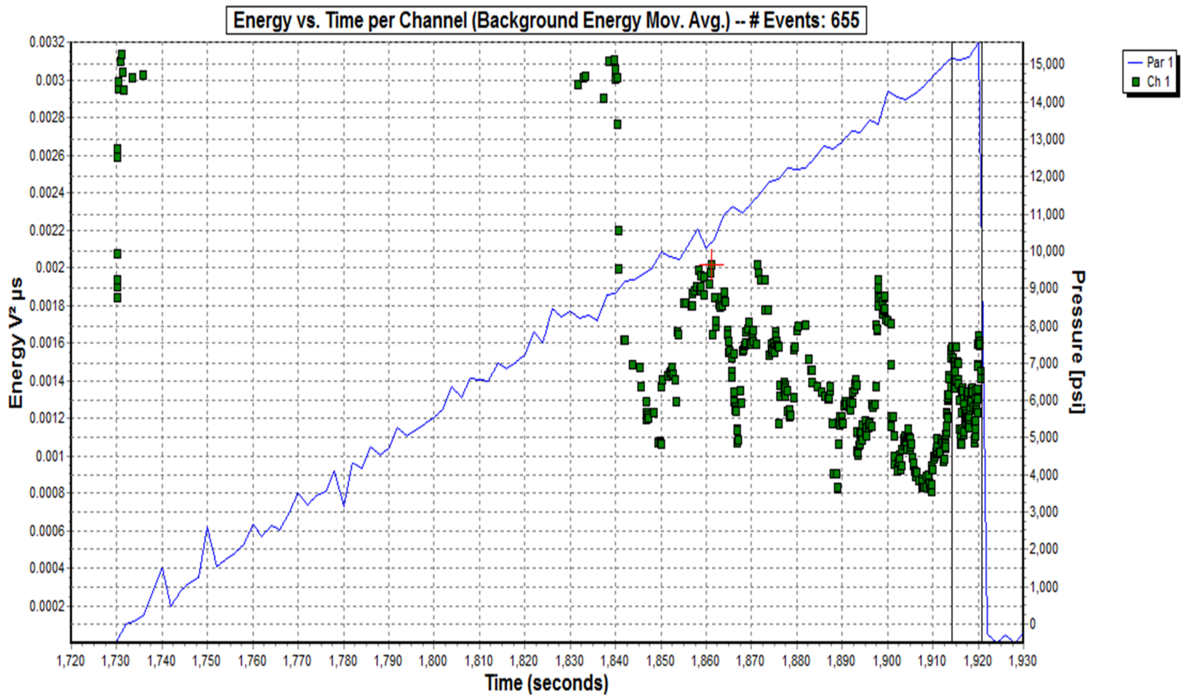

Figure B. 7 - Background Energy Oscillation for OM3934.

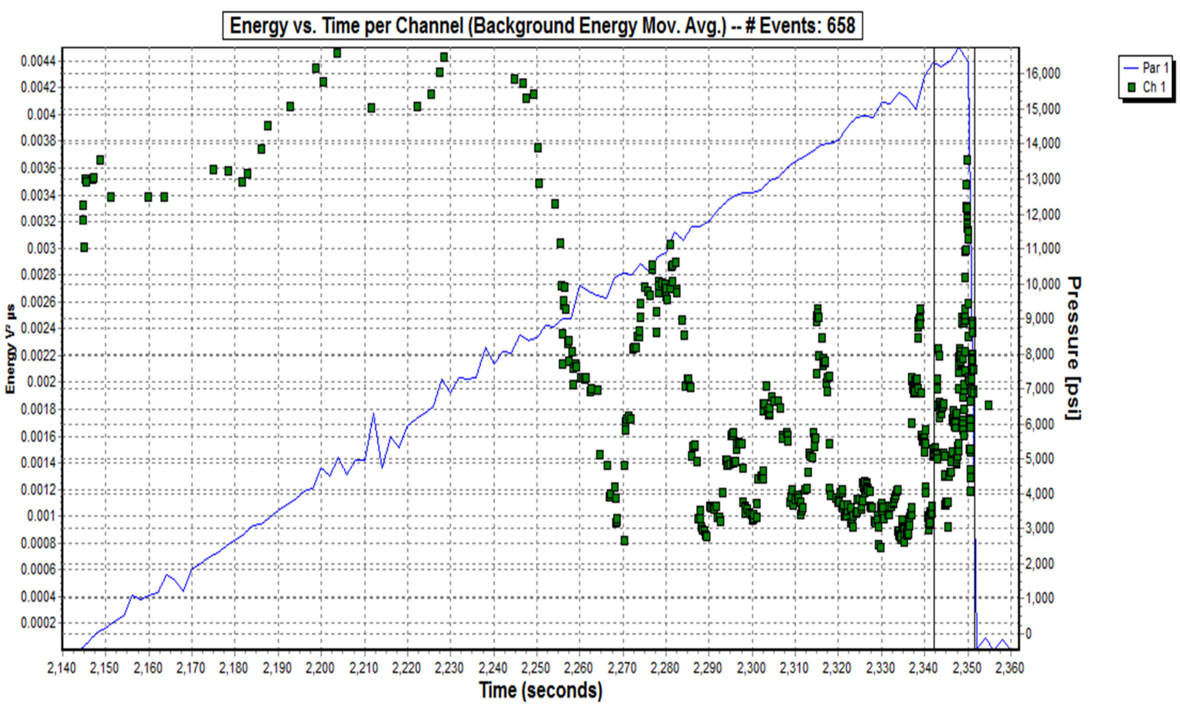

Figure B. 8 - Background Energy Oscillation for OM3941.

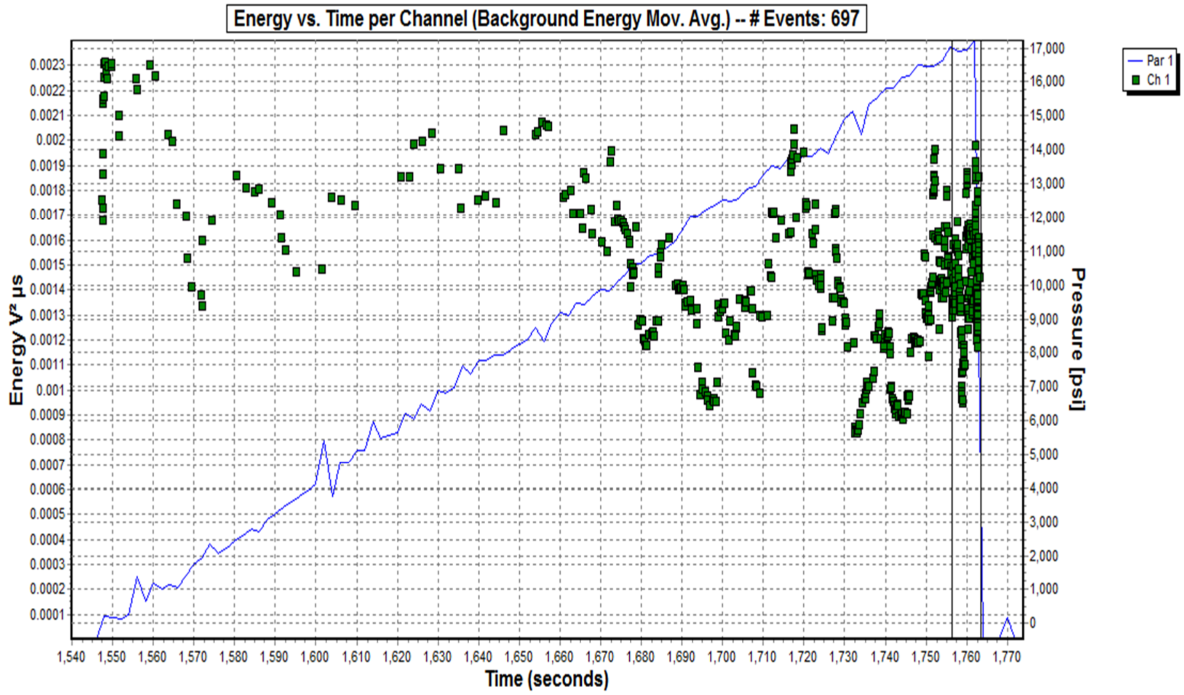

Figure B. 9 - Background Energy Oscillation for OM3962.

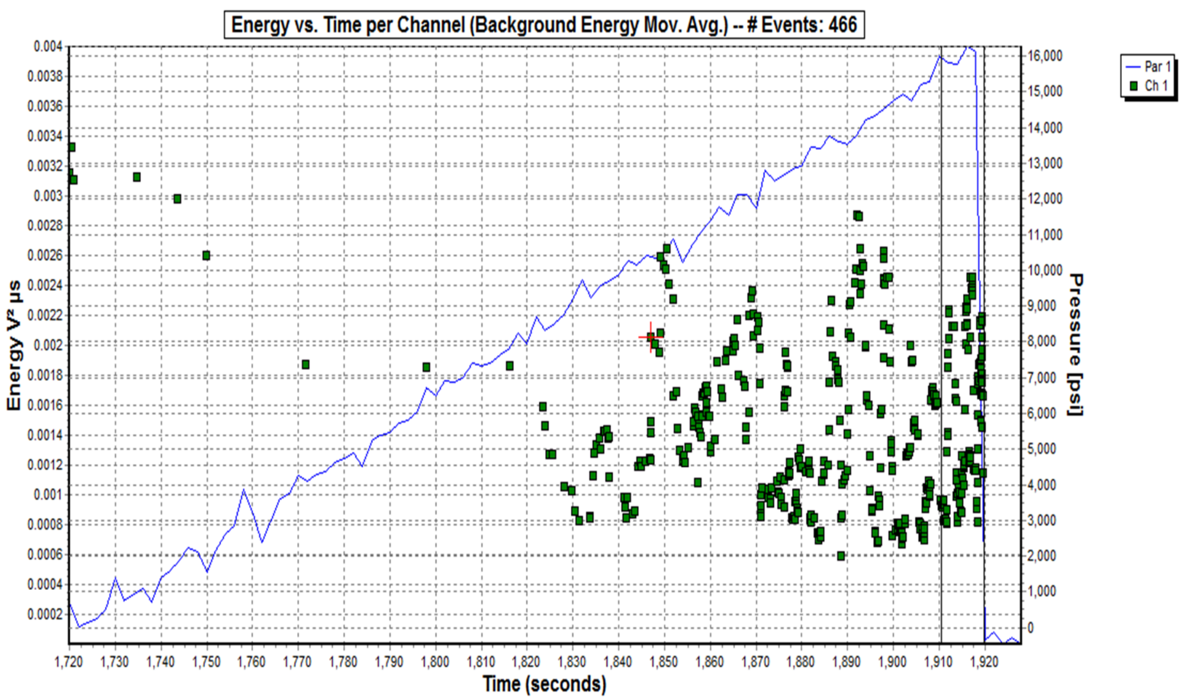

Figure B. 10 - Background Energy Oscillation for OM3990.

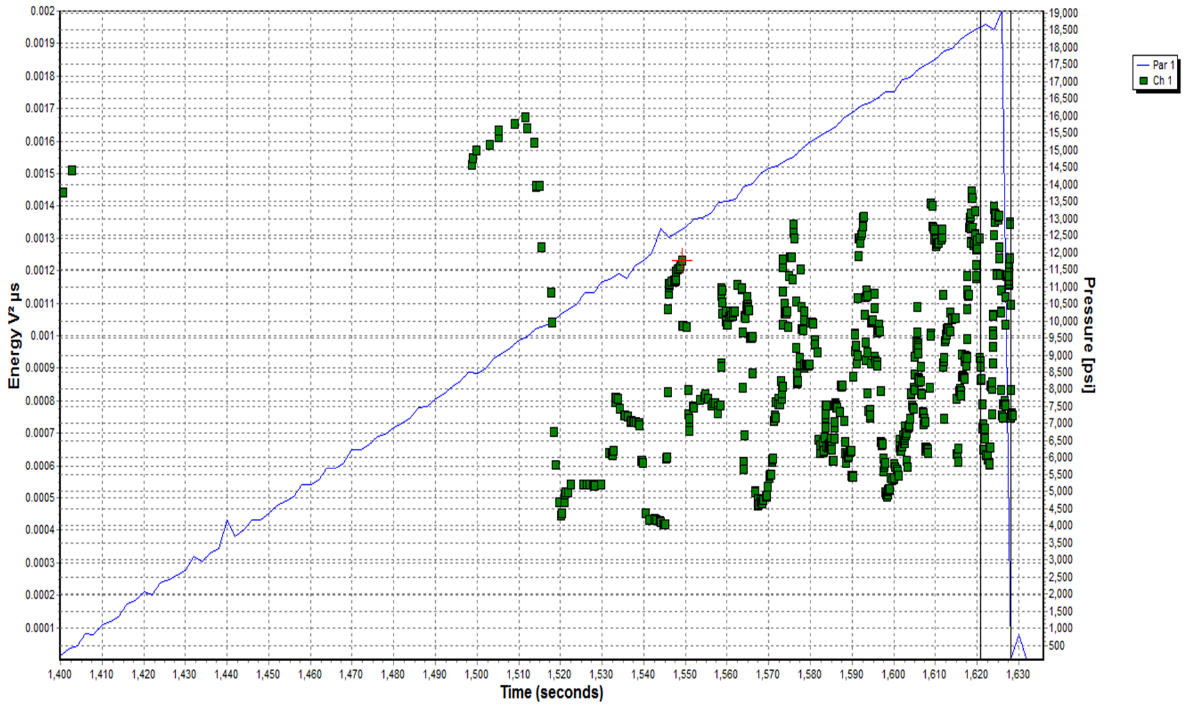

Figure B. 11 - Background Energy Oscillation for ALT639 - 14969.

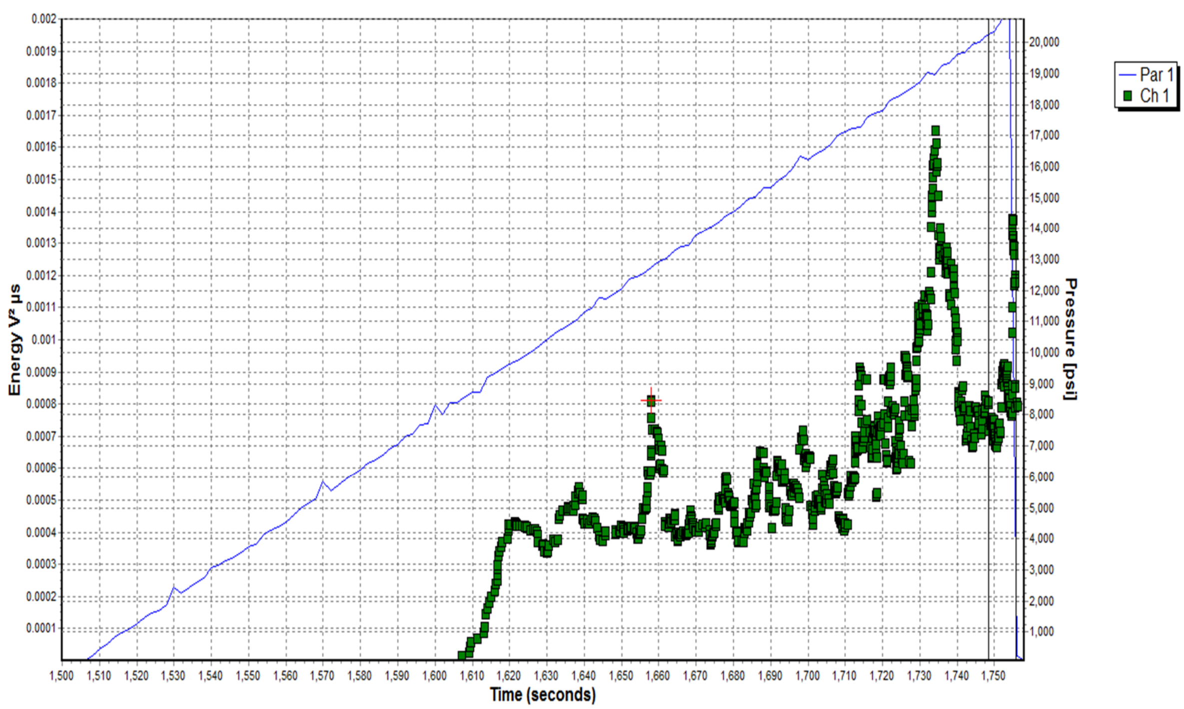

Figure B. 12 - Background Energy Oscillation for ALT639 - 17663.

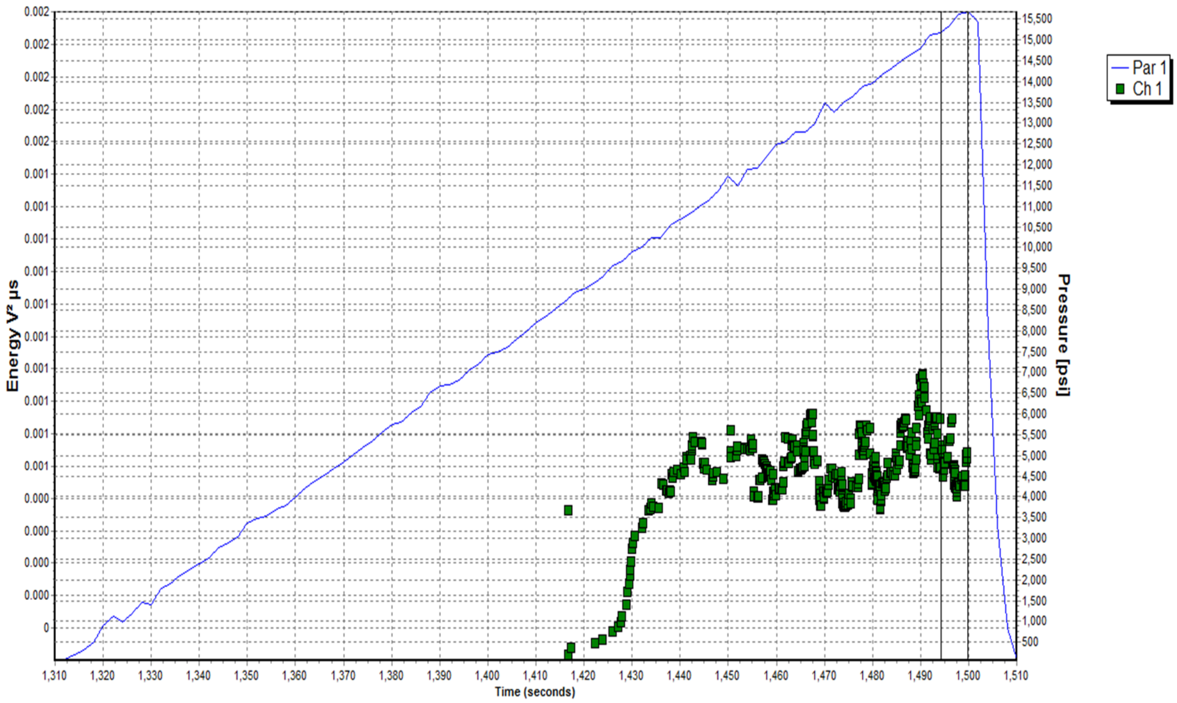

Figure B. 13 - Background Energy Oscillation for ALT639 - 18023.

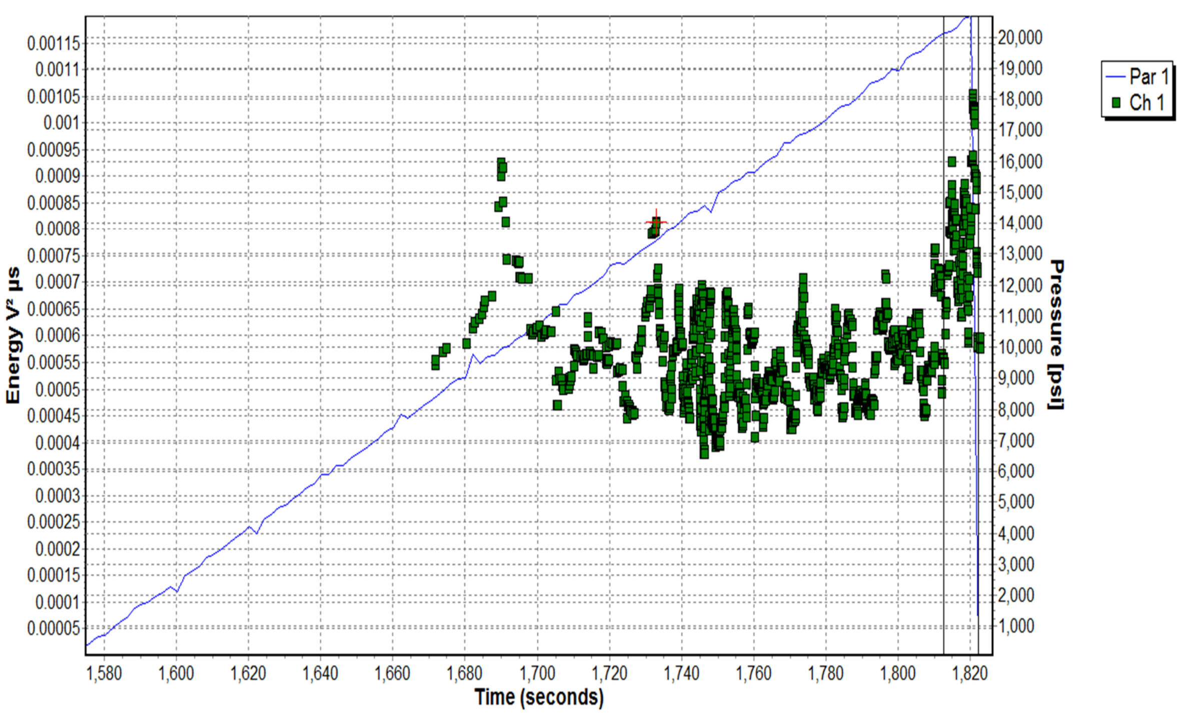

Figure B. 14 - Background Energy Oscillation for ALT639 - 69216.

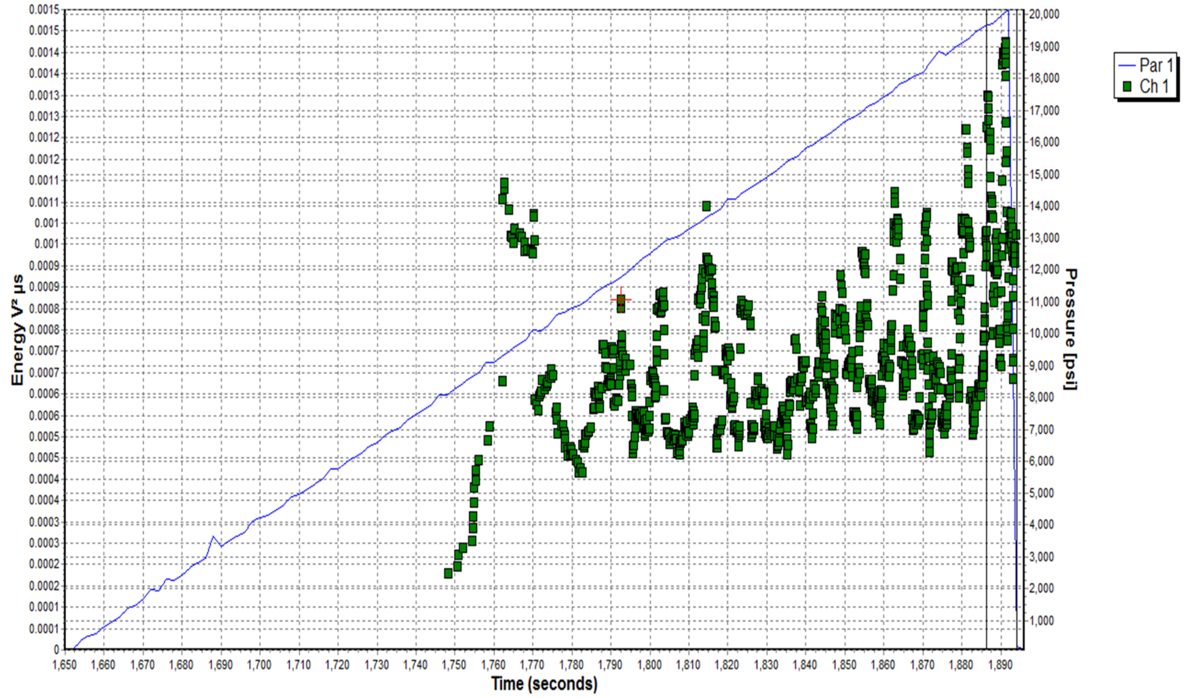

Figure B. 15 - Background Energy Oscillation for ALT639 - 18629.

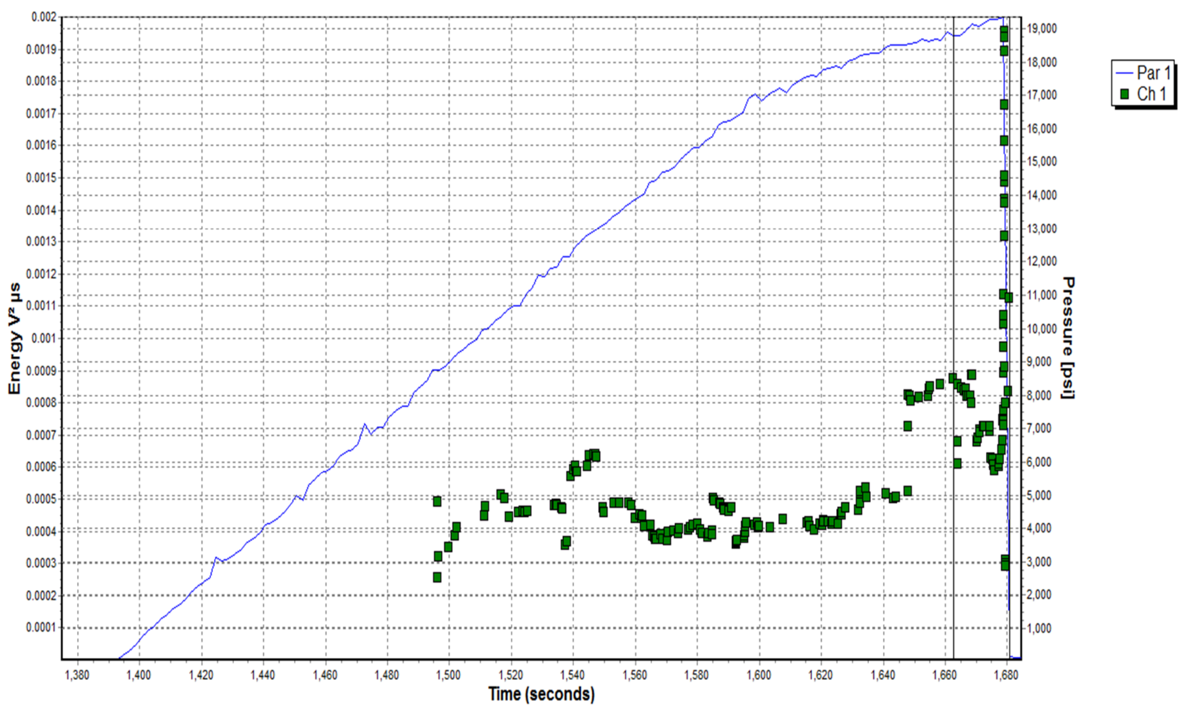

Figure B. 16 - Background Energy Oscillation for IH1740.

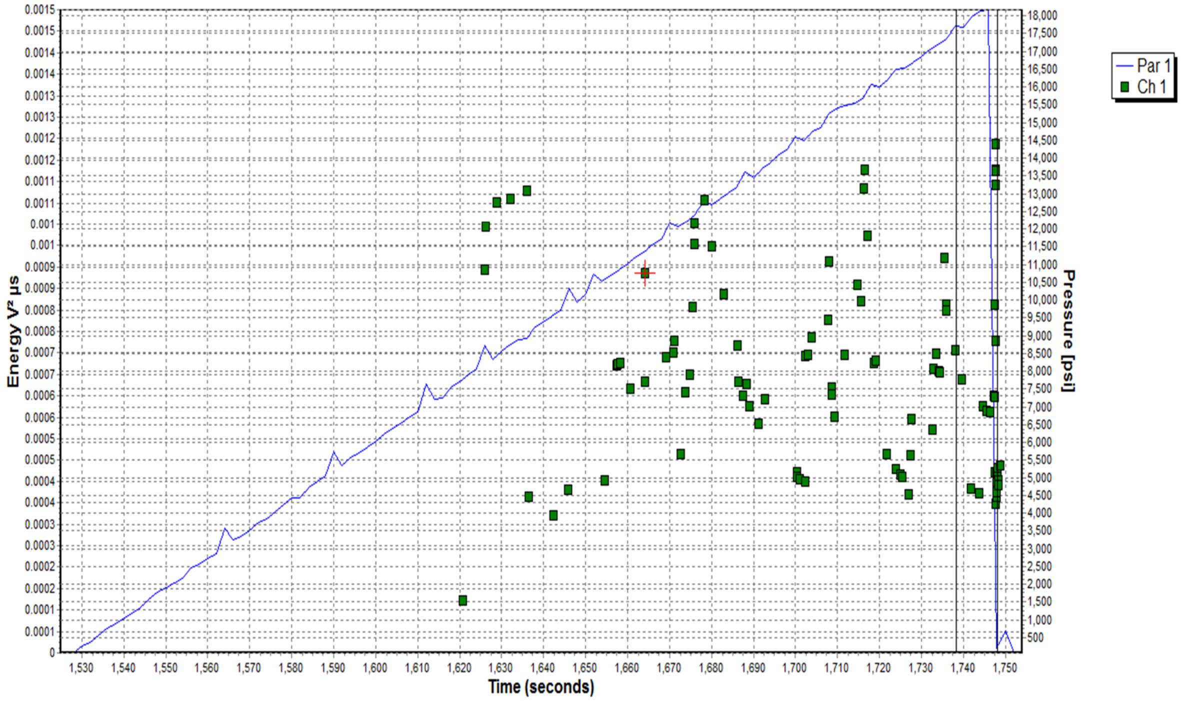

Figure B. 17 - Background Energy Oscillation for IH1855.

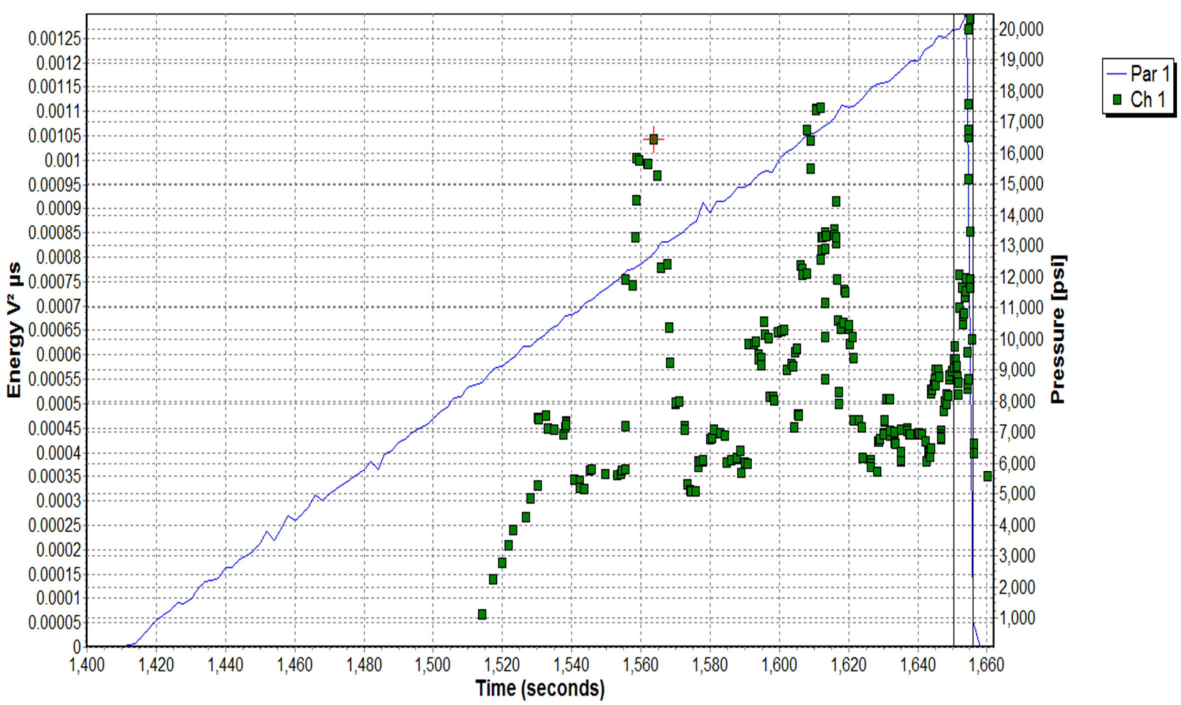

Figure B. 18 - Background Energy Oscillation for IH1763.

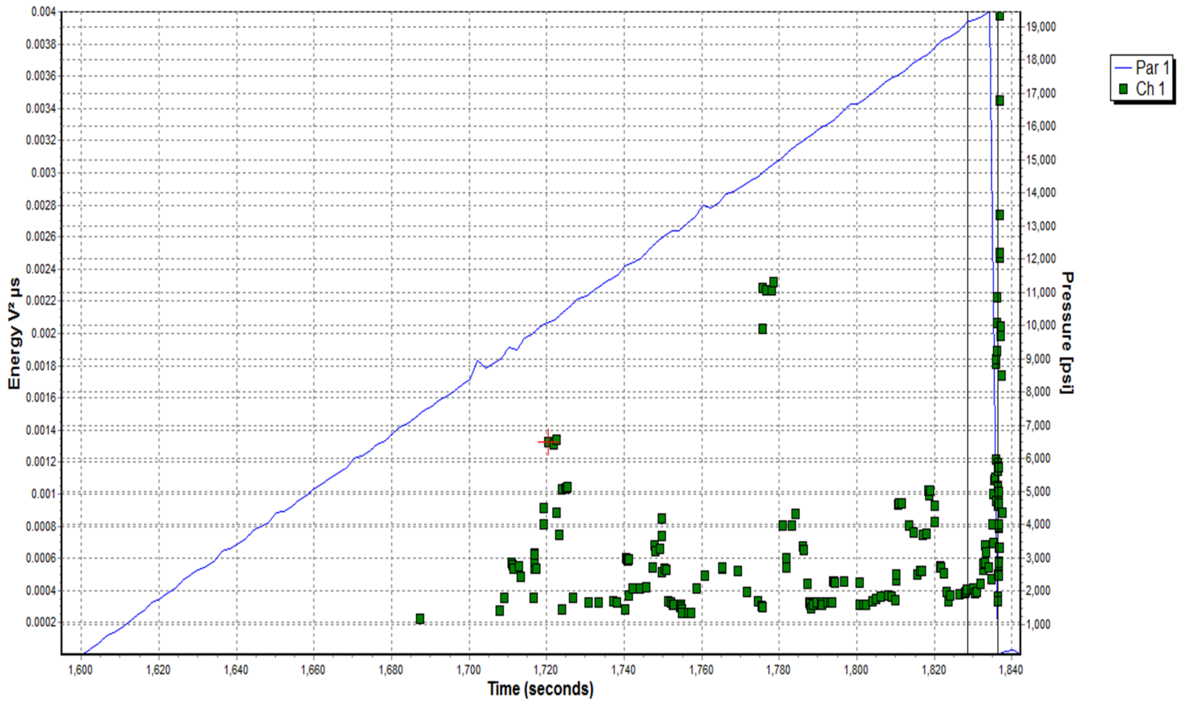

Figure B. 19 - Background Energy Oscillation for IH1135.

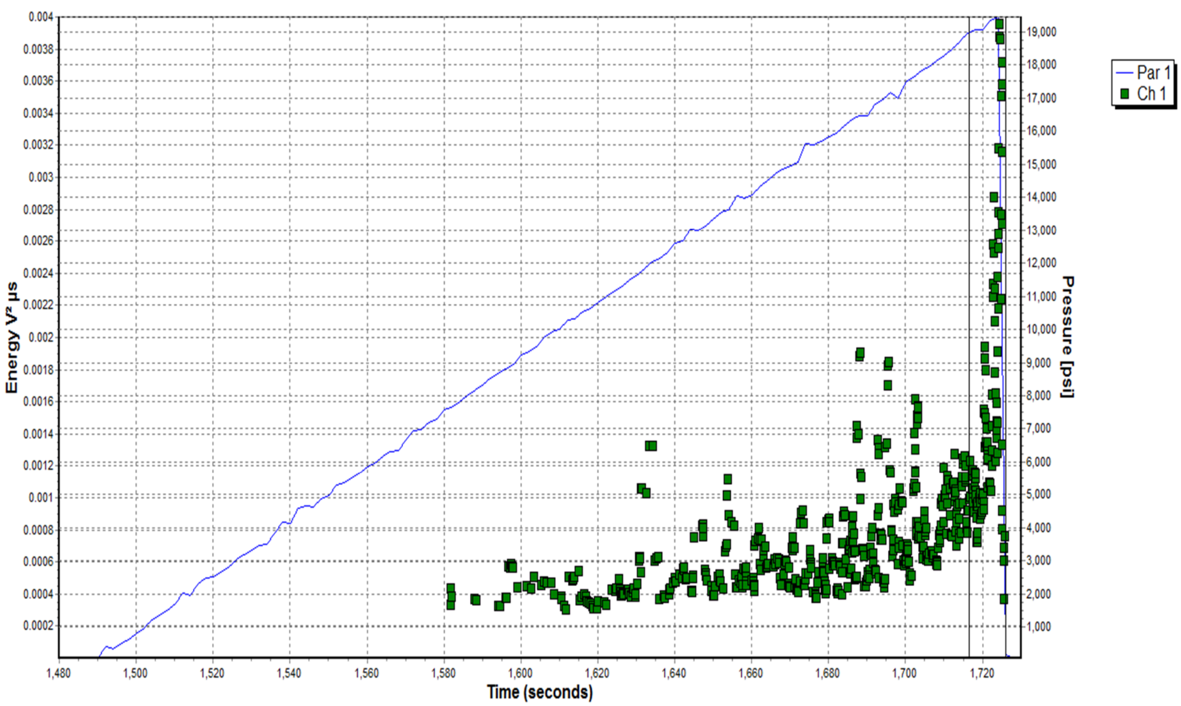

Figure B. 20 - Background Energy Oscillation for IH1929.

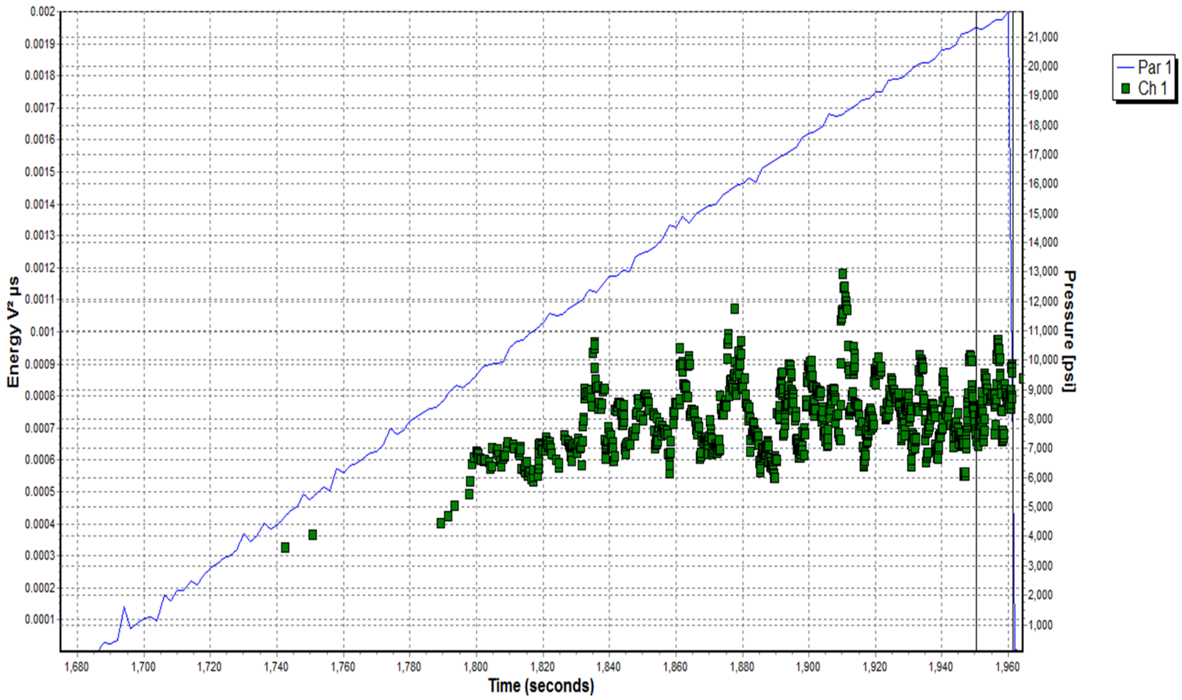

Figure B. 21 - Background Energy Oscillation for ALT604 - 6739.

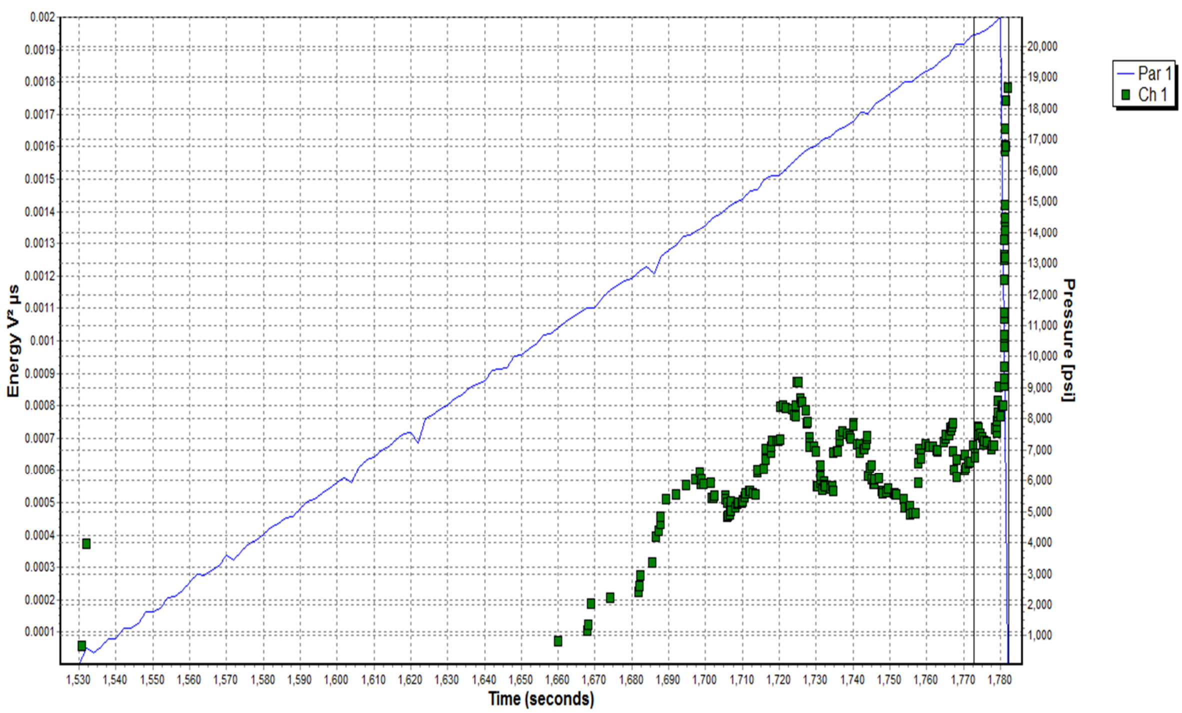

Figure B. 22 - Background Energy Oscillation for ALT639 - 17688.

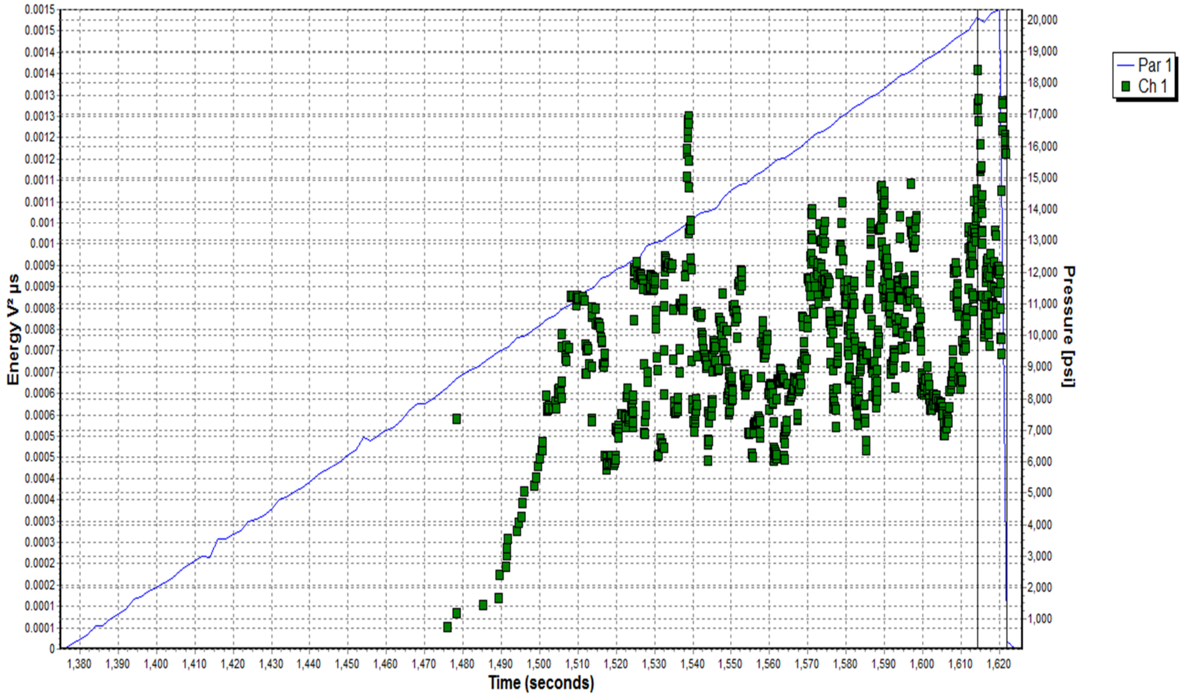

Figure B. 23 - Background Energy Oscillation for ALT639 - 18862.

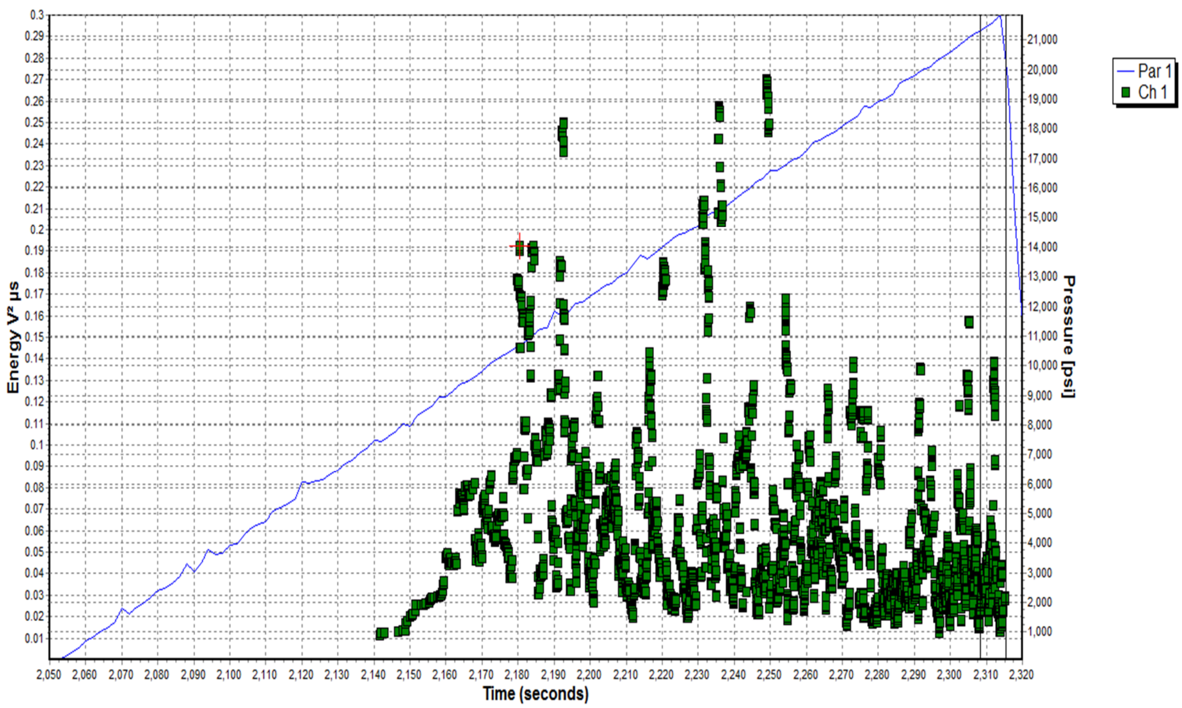

Figure B. 24 - Background Energy Oscillation for ALT639 - 18507.

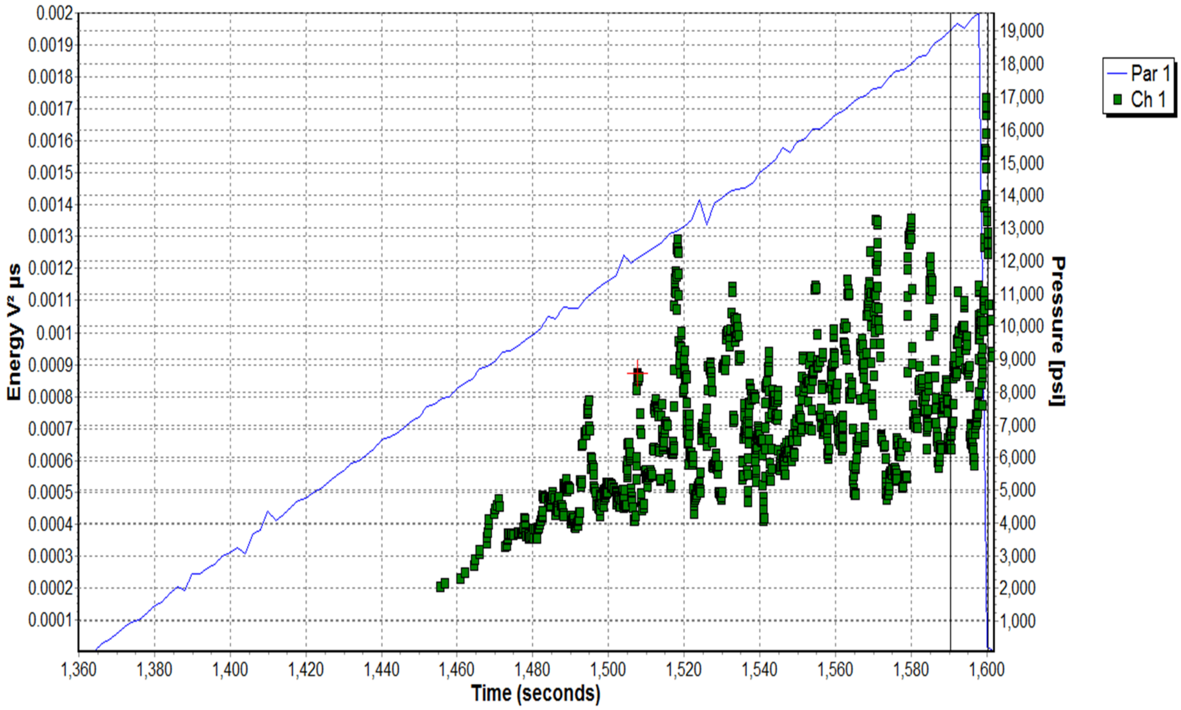

Figure B. 25 - Background Energy Oscillation for ALT639 - 18793.

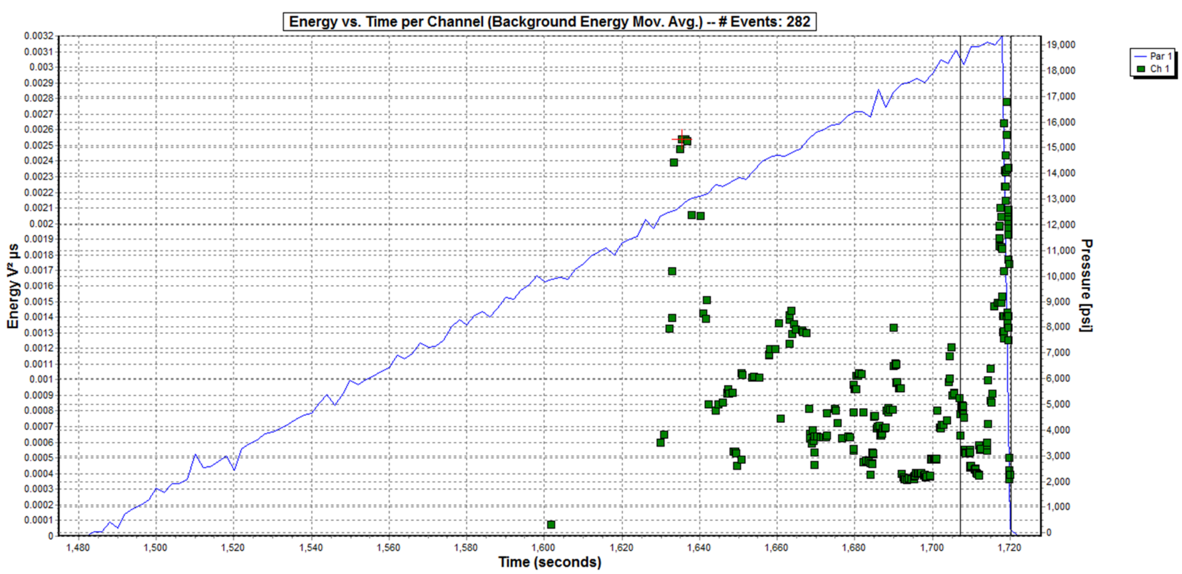

Figure B.26 – Background Energy Oscillation for ALT695 – 1700.

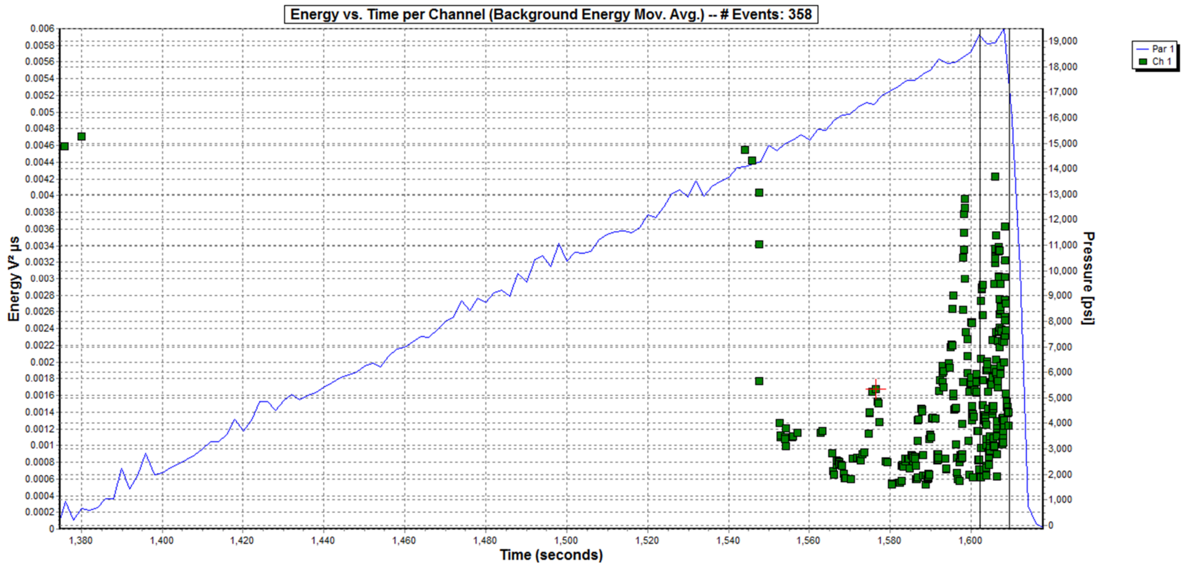

Figure B.27 - Background Energy Oscillation for ALT695-4745.

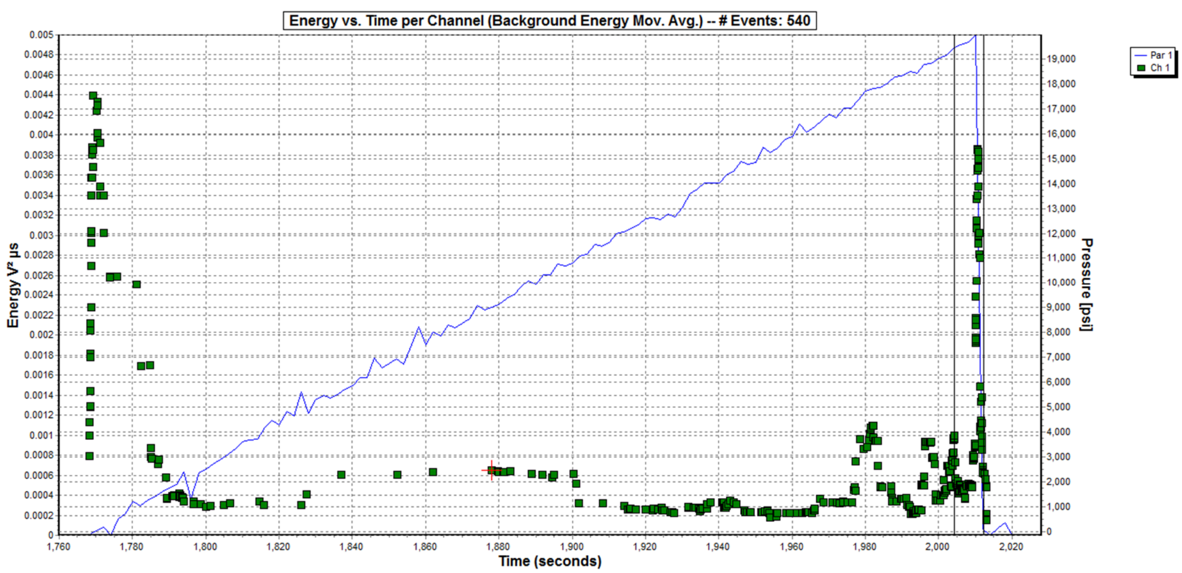

Figure B.28 - Background Energy Oscillation for ALT695-6058.

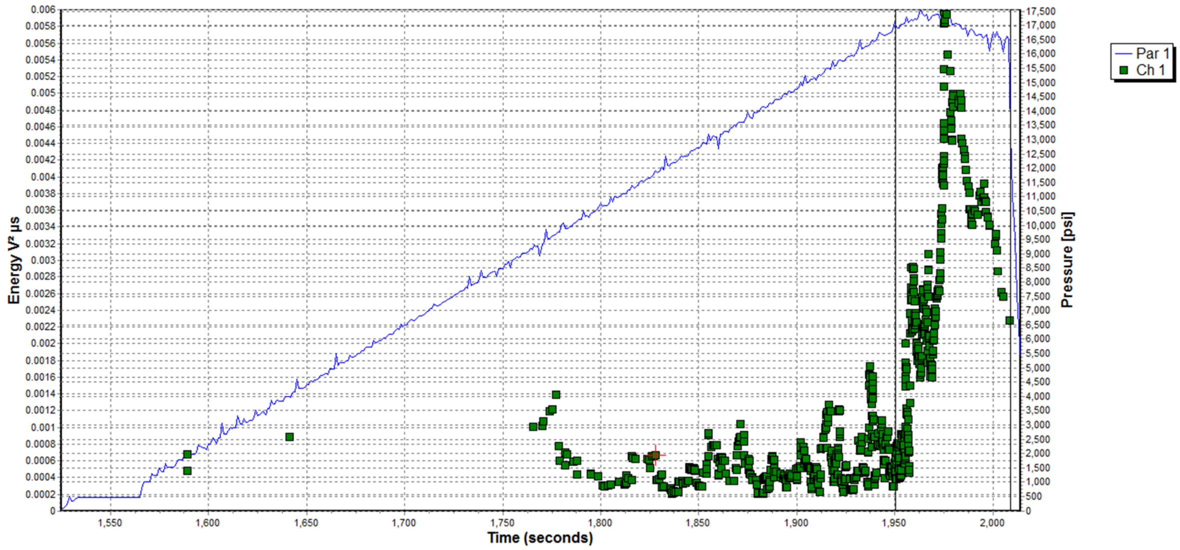

Figure B. 29 - Background Energy Oscillation for ALT695-1668.

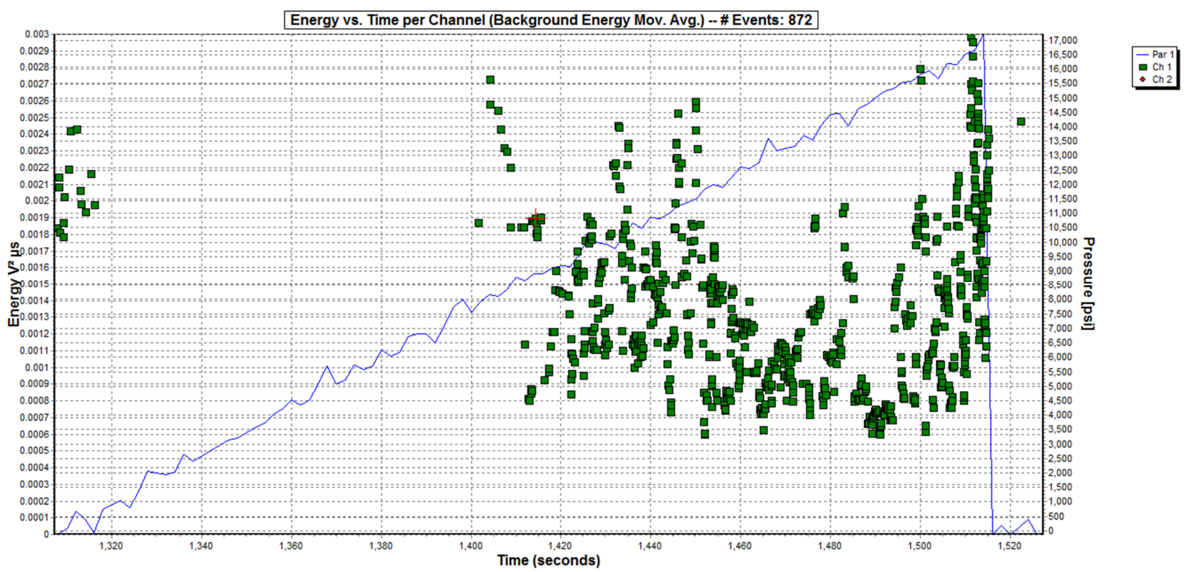

Figure B.30 - Background Energy Oscillation for OM3913.

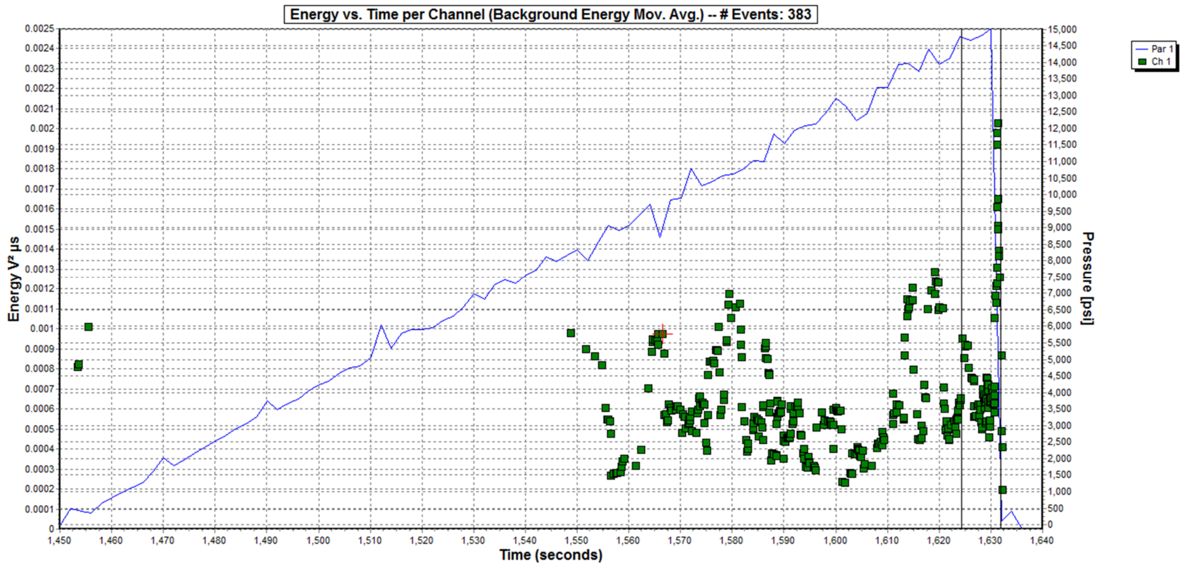

Figure B.31 - Background Energy Oscillation for OM3928.

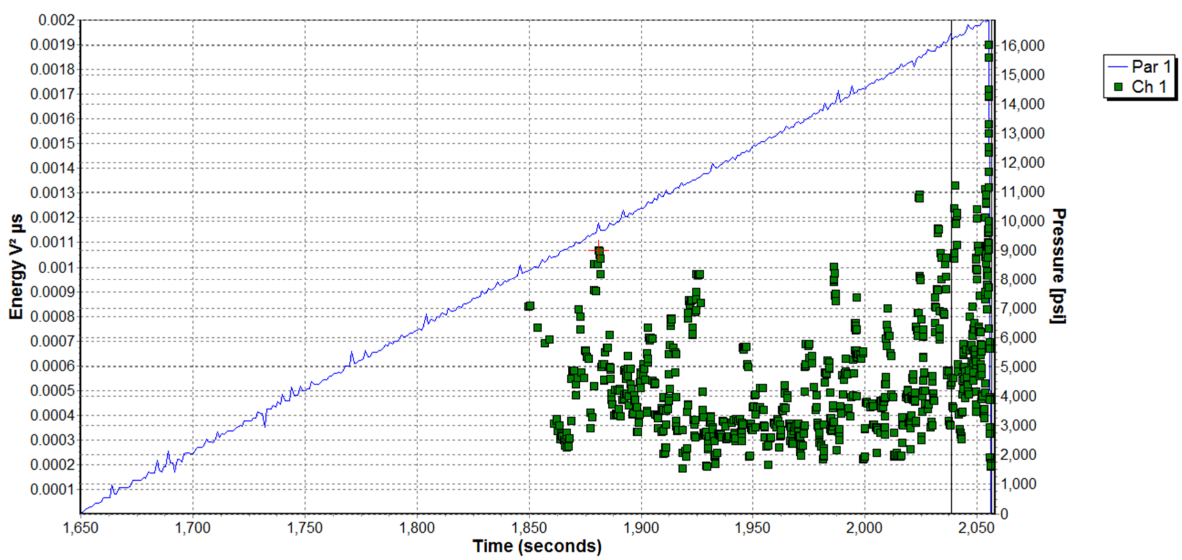

Figure B. 32 - Background Energy Oscillation for OM3950.

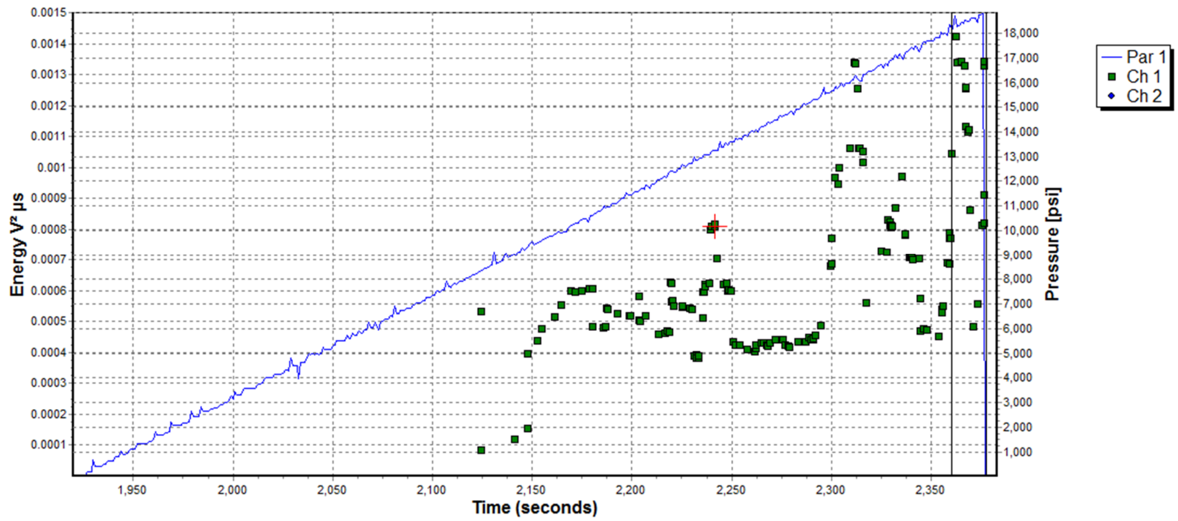

Figure B. 33 - Background Energy Oscillation for IH1271.

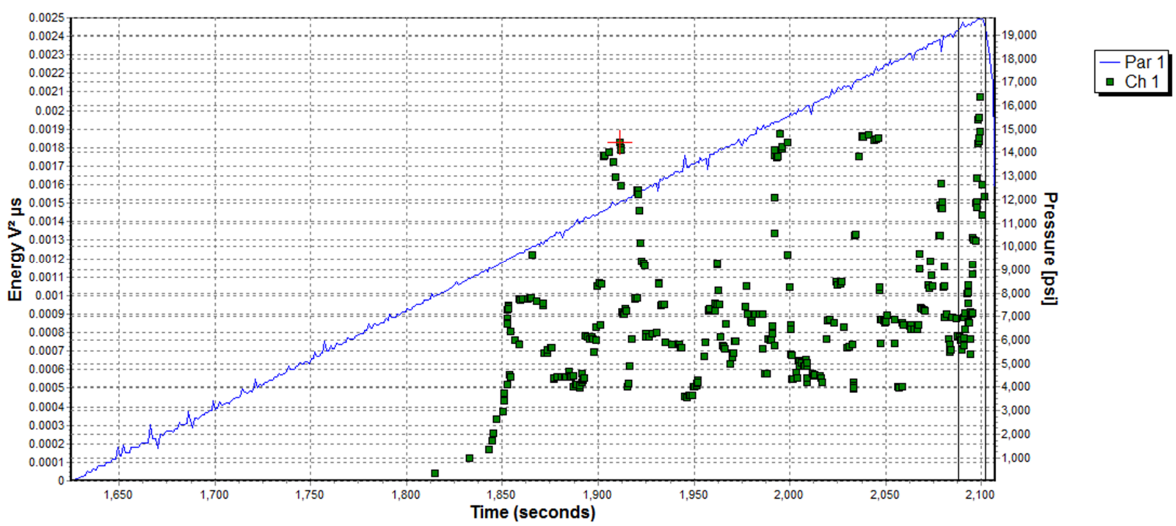

Figure B. 34 - Background Energy Oscillation for IH12483.

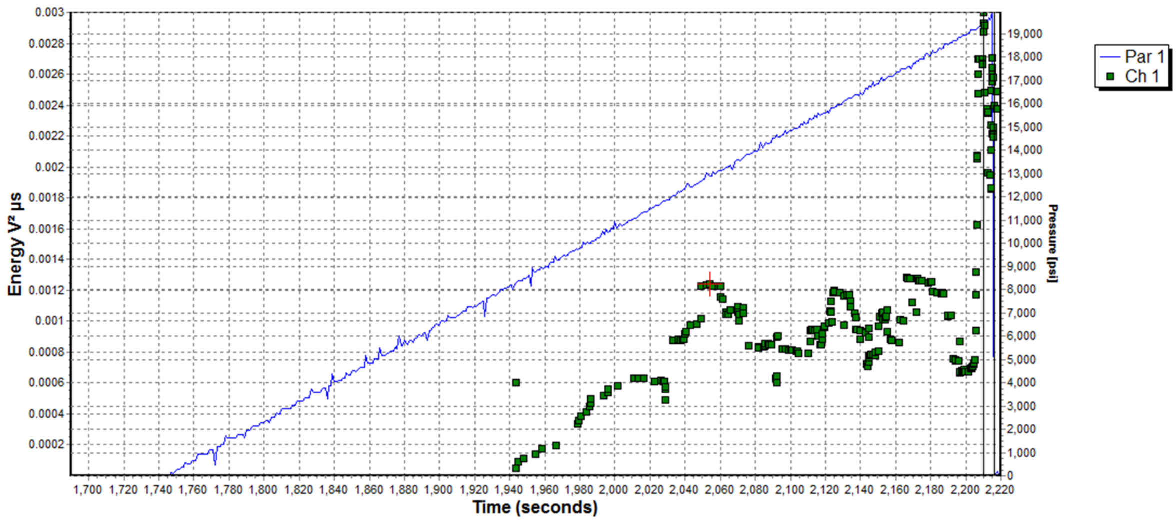

Figure B. 35 - Background Energy Oscillation for IH1748.

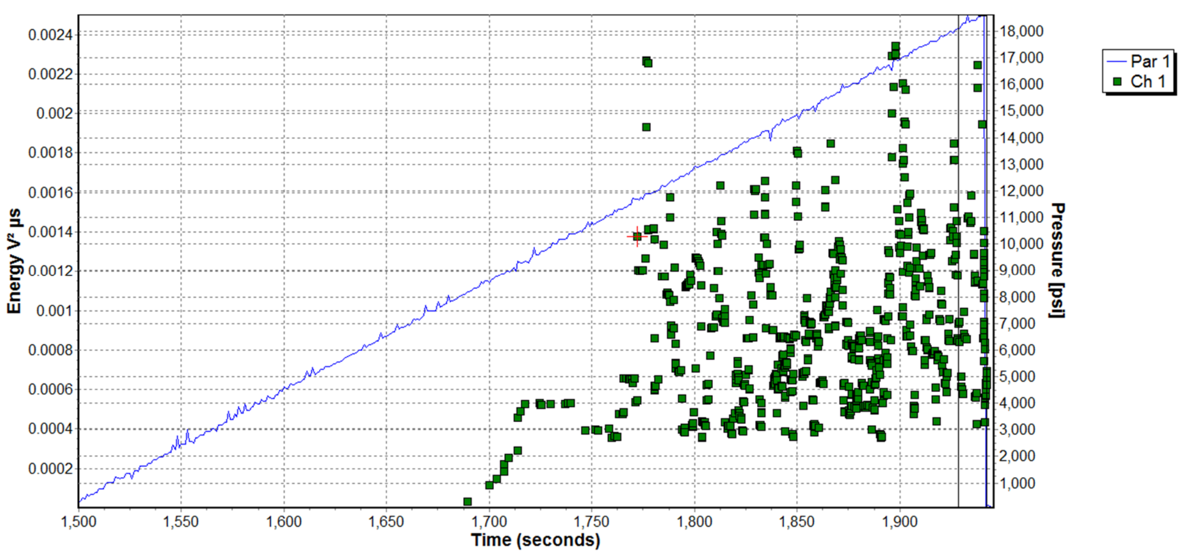

Figure B. 36 - Background Energy Oscillation for IH1820.

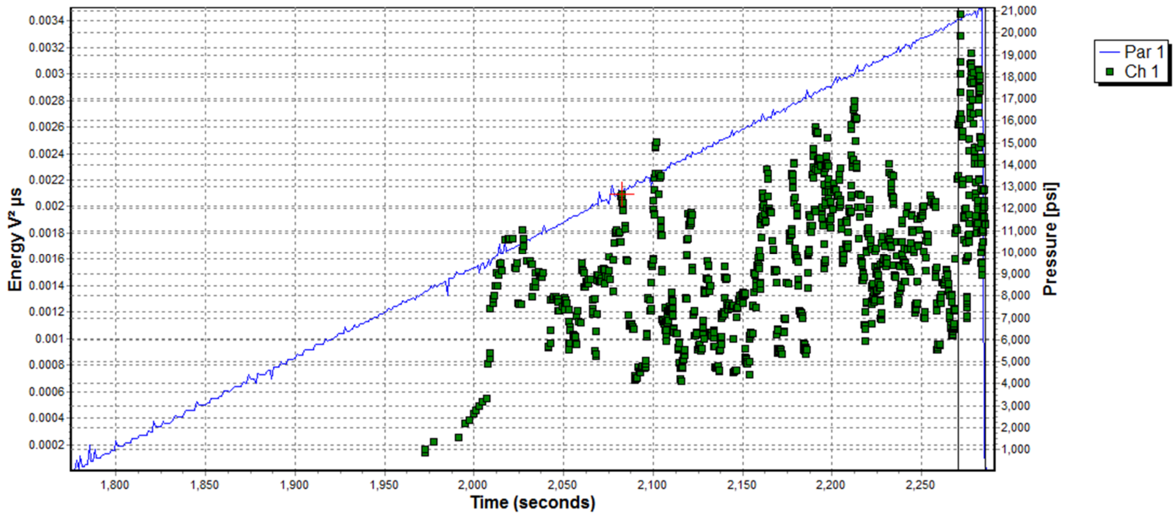

Figure B. 37 - Background Energy Oscillation for ALT639 - 18974.

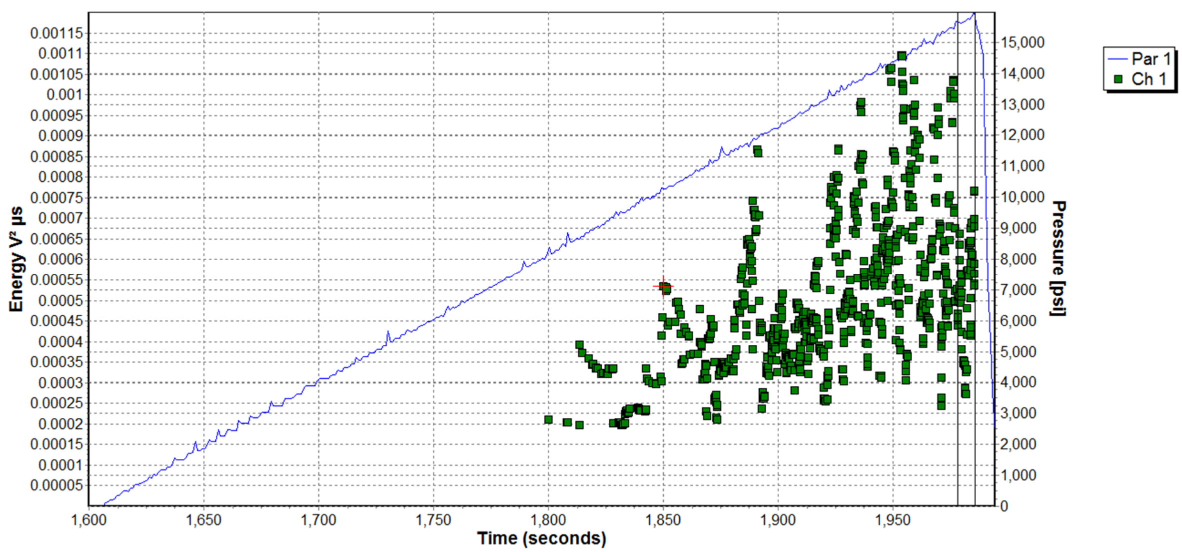

Figure B. 38 - Background Energy Oscillation for ALT639 - 18799.

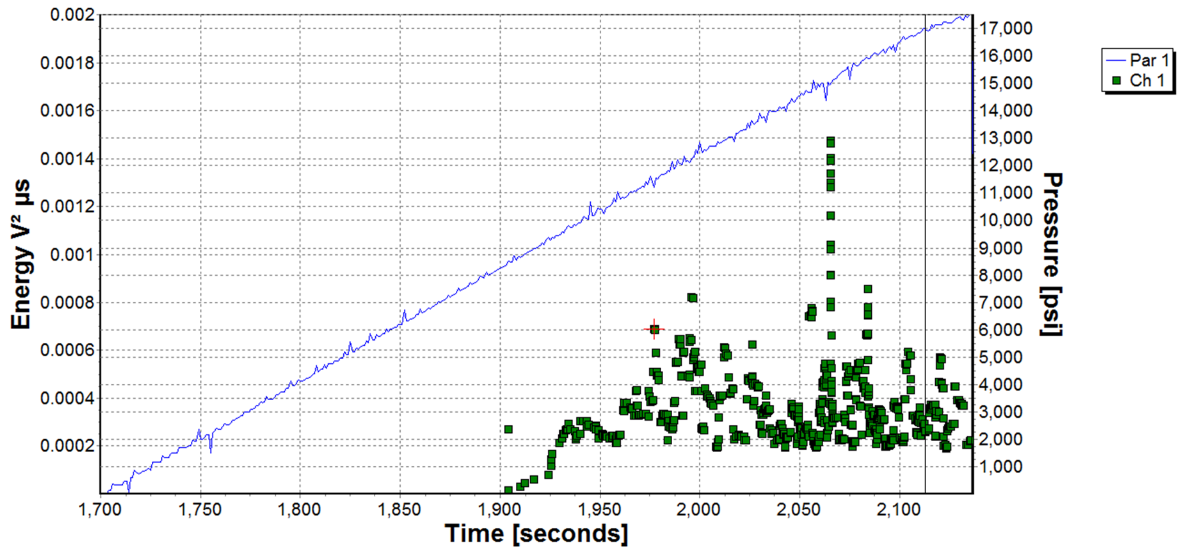

Figure B. 39 - Background Energy Oscillation for ALT639 - 18790.

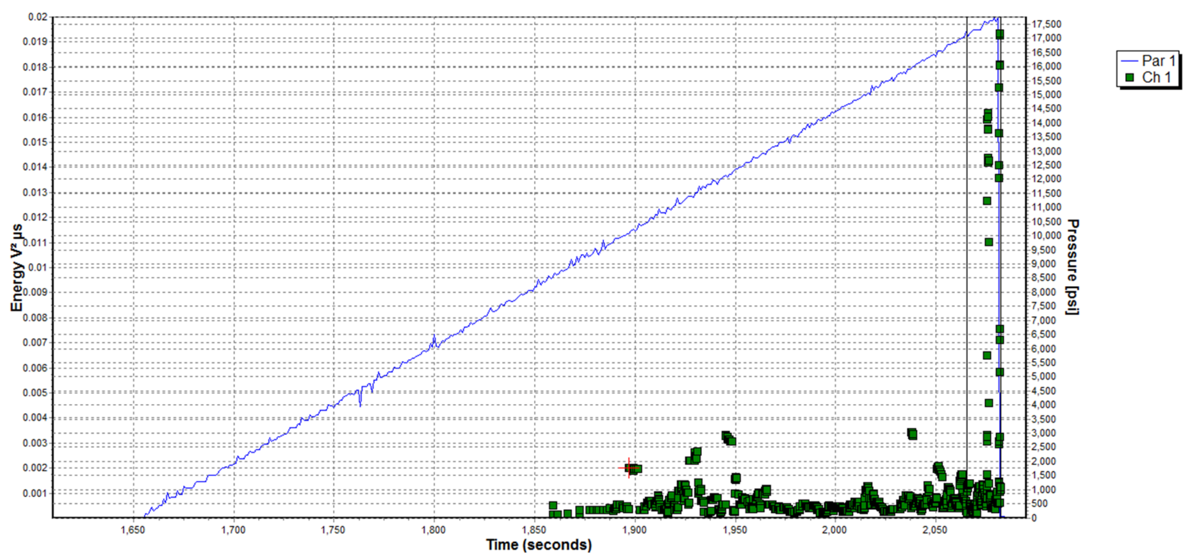

Figure B. 40 - Background Energy Oscillation for ALT695 - 1653.

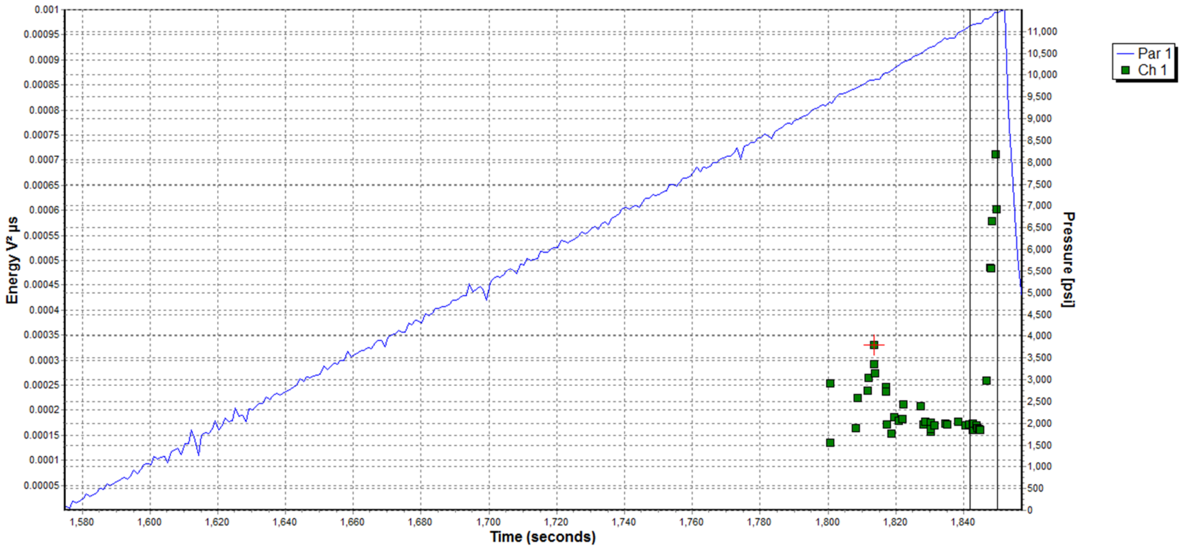

Figure B. 41 - Background Energy Oscillation for ALT604 - 4342.

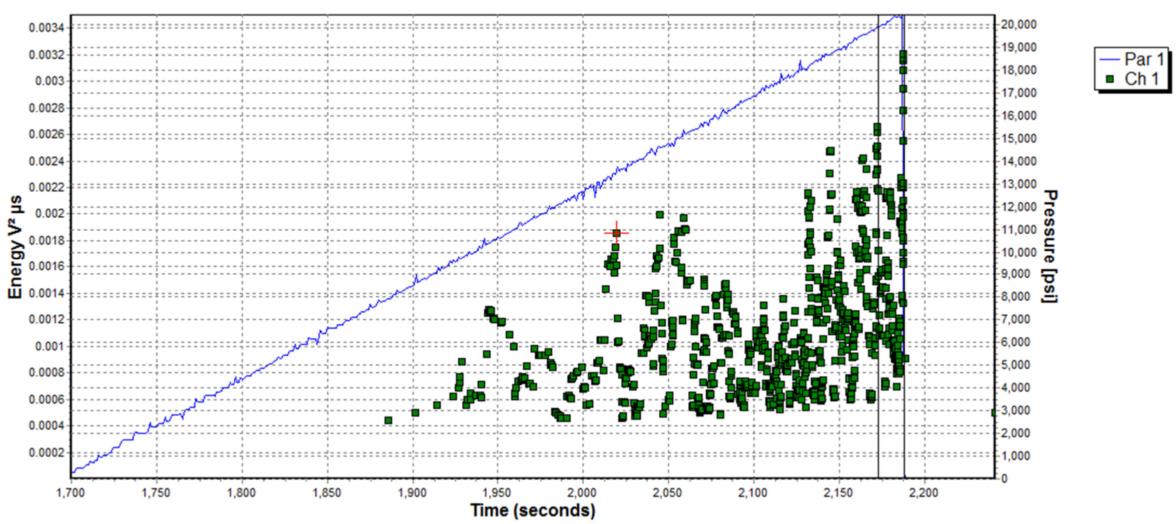

Figure B. 42 - Background Energy Oscillation for ALT639 - 39764.

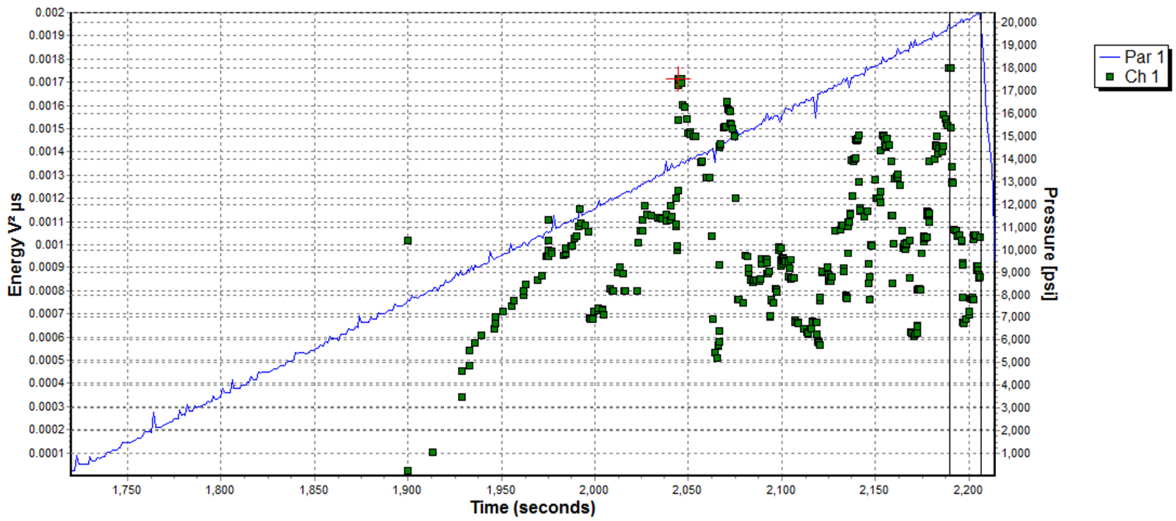

Figure B. 43- Background Energy Oscillation for ALT639 - 18435.

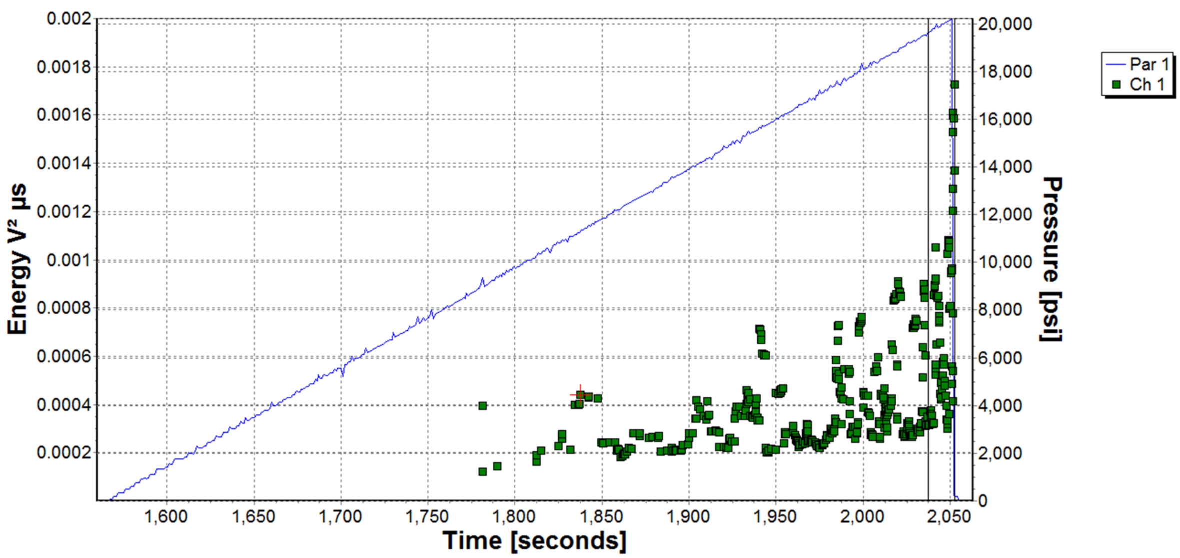

Figure B. 44 - Background Energy Oscillation for ALT639 - 39694.

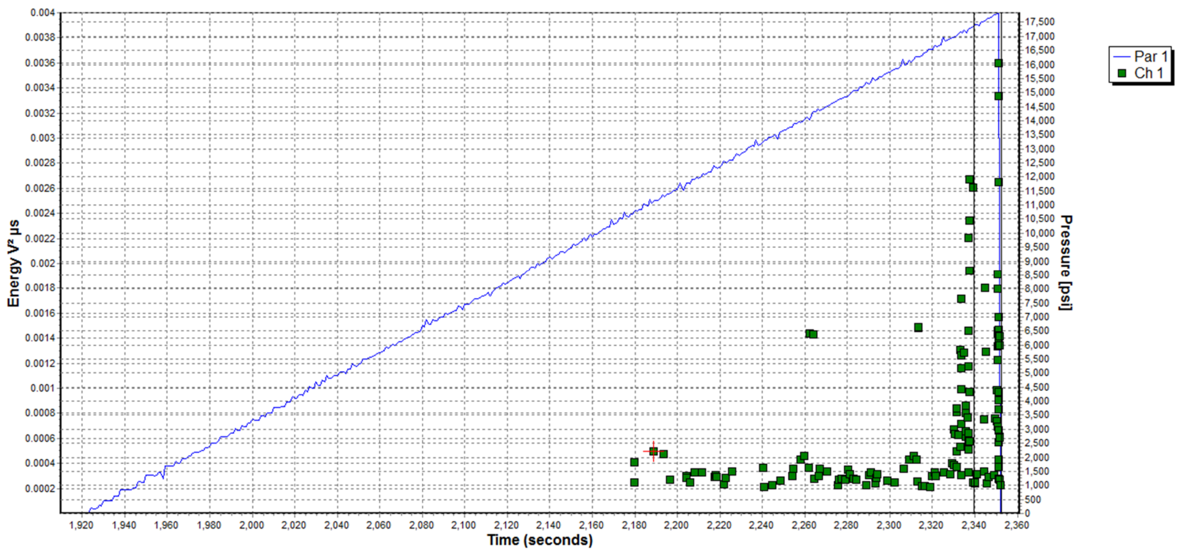

Figure B. 45 - Background Energy Oscillation for ALT639 - 18683.

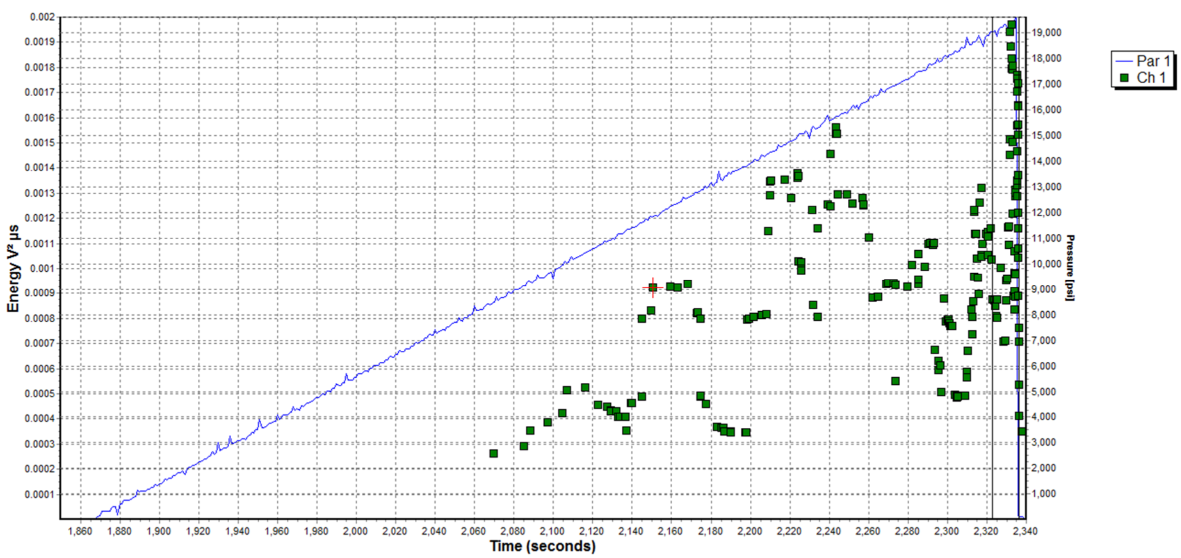

Figure B.46 – Background Energy Oscillation for IH2482.

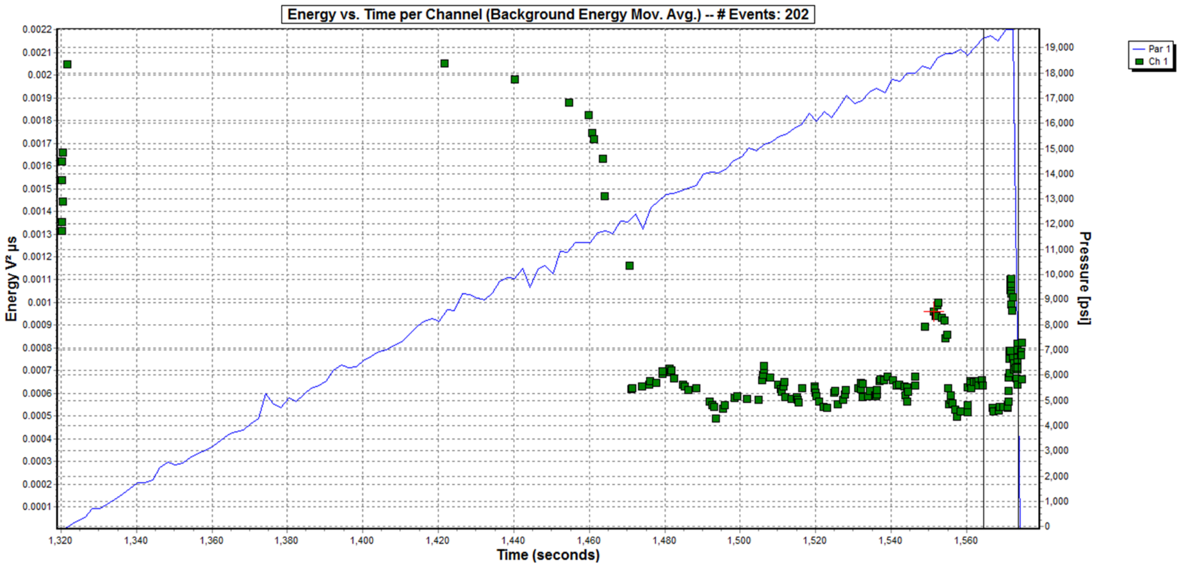

Figure B.47 - Background Energy Oscillation for ALT604 – 3567.

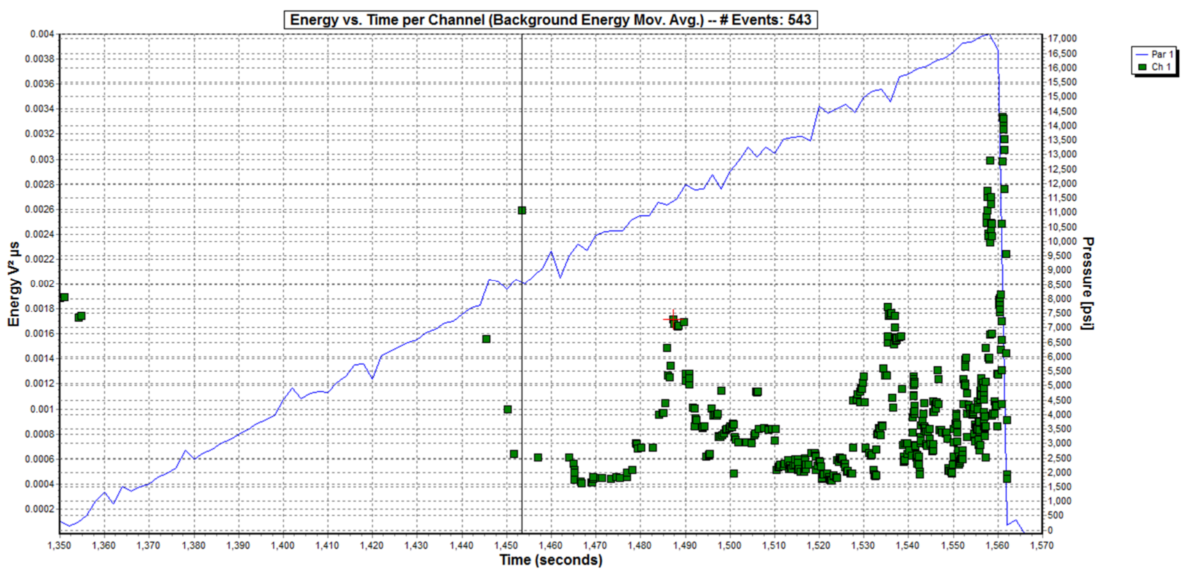

Figure B.48 - Background Energy Oscillation for ALT695-3794.

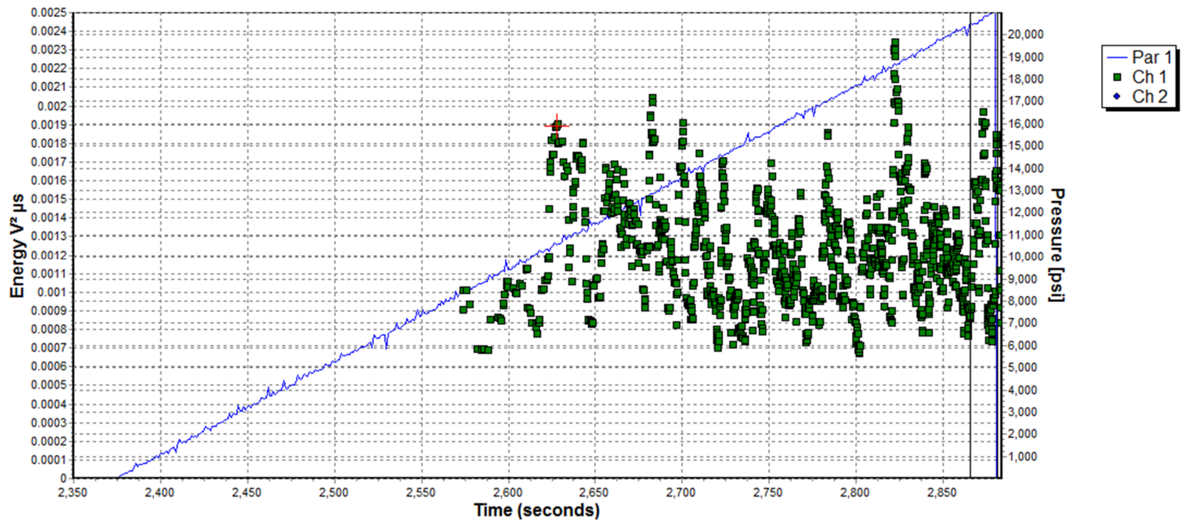

Figure B.49 - Background Energy Oscillation for ALT604-4371.

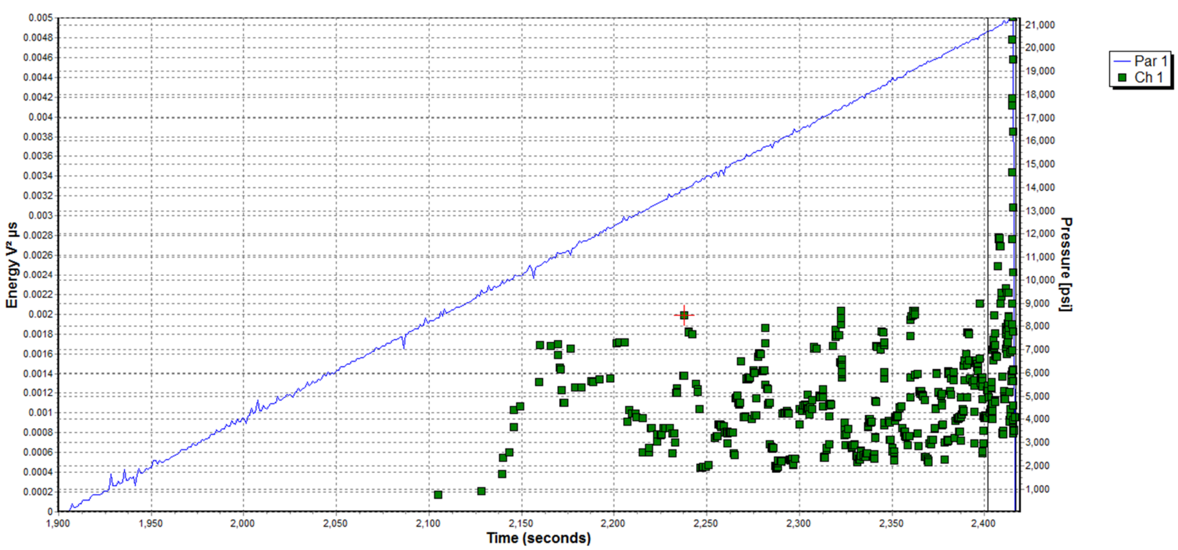

Figure B.50 - Background Energy Oscillation for ALT639 - 18722.

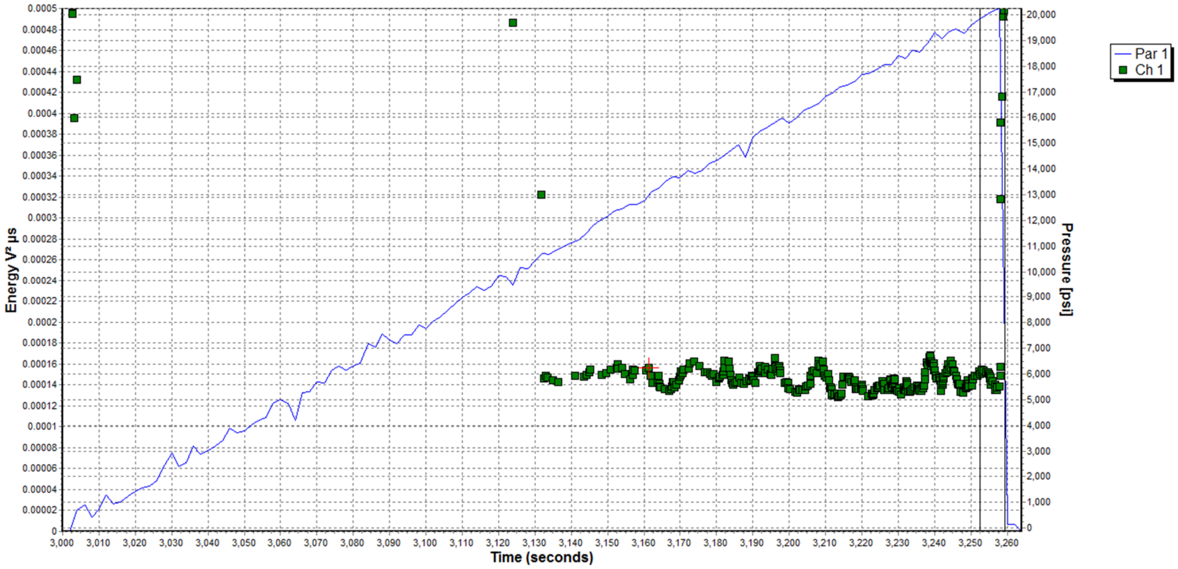

Figure B.51 - Background Energy Oscillation for ALT604-6021.

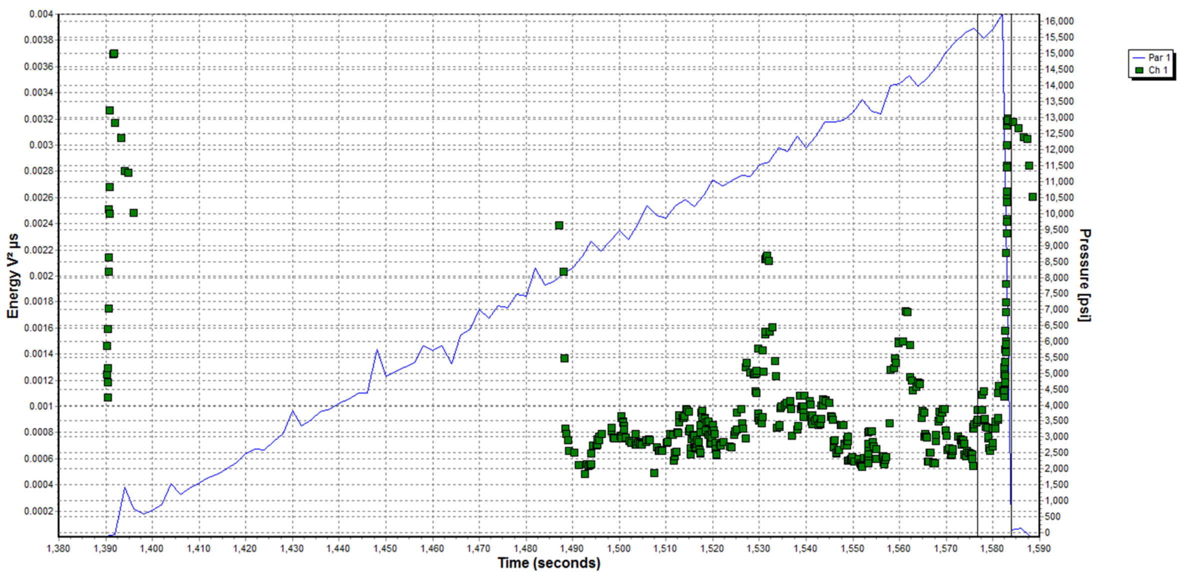

Figure B.52 - Background Energy Oscillation for OM3938.

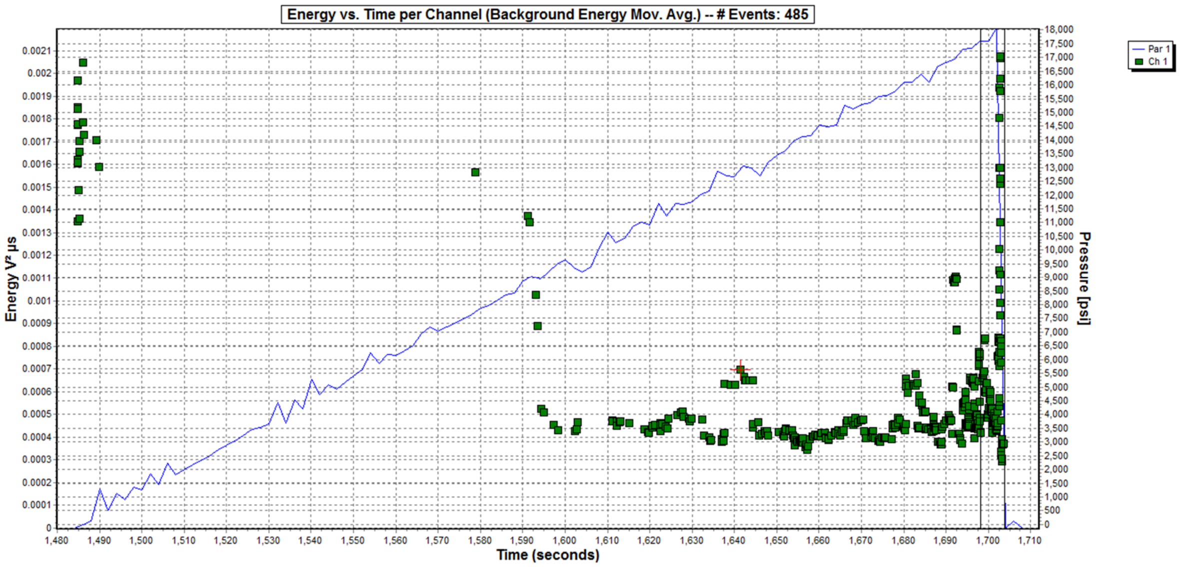

Figure B.53 - Background Energy Oscillation for OM3983.

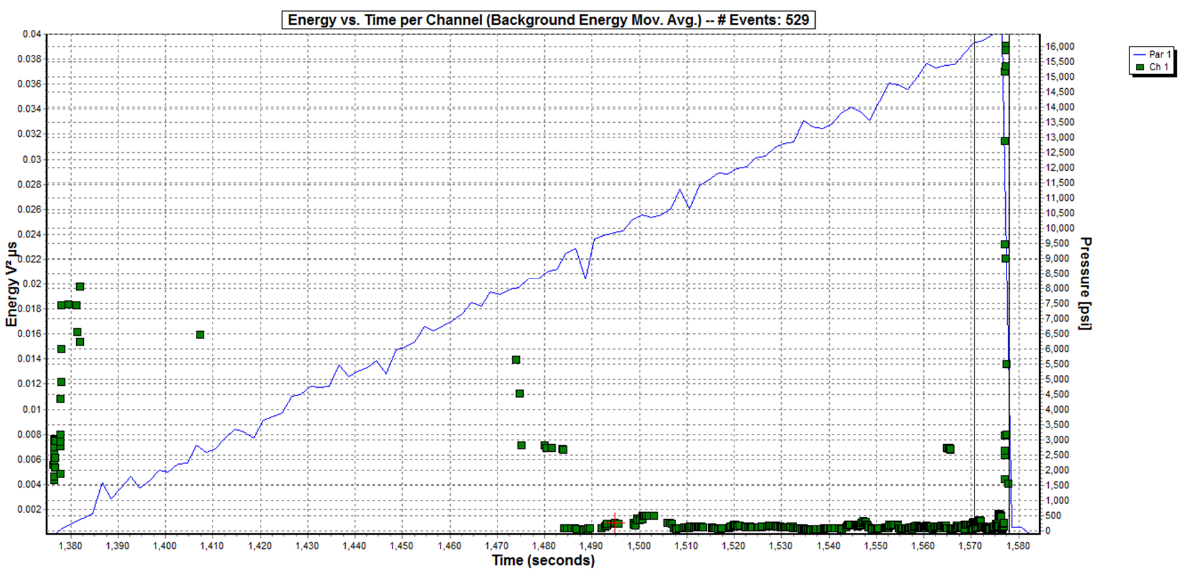

Figure B.54 - Background Energy Oscillation for OM3948.

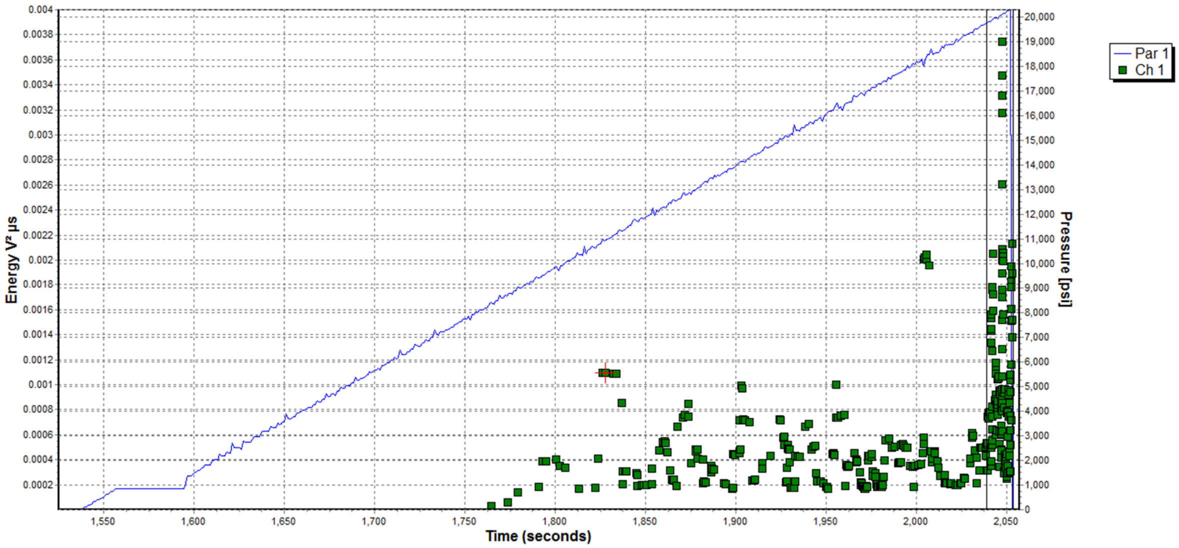

Figure B. 55 - Background Energy Oscillation for IH2036.

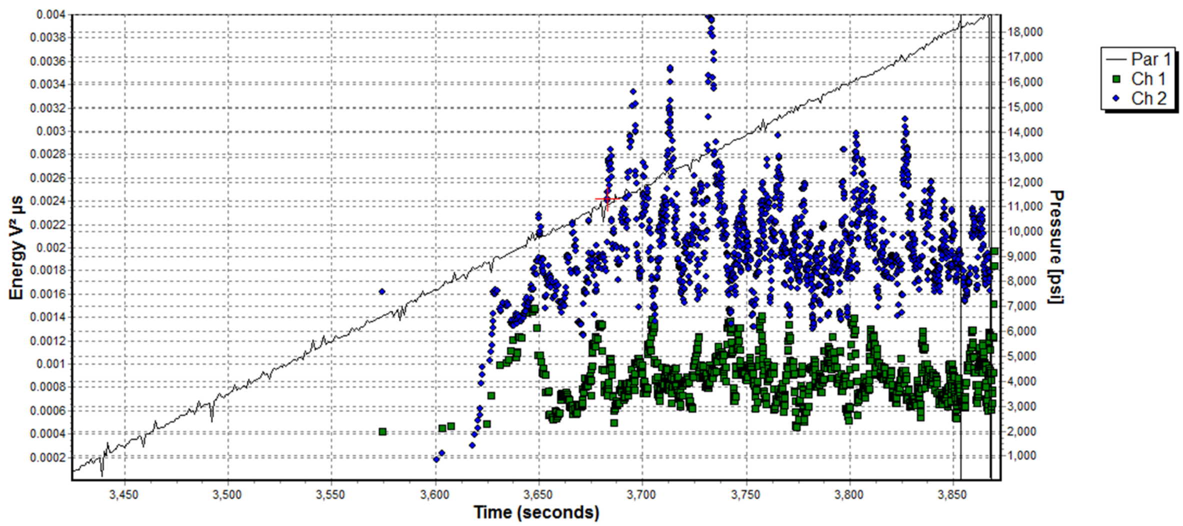

Figure B. 56 - Background Energy Oscillation for OP11769.

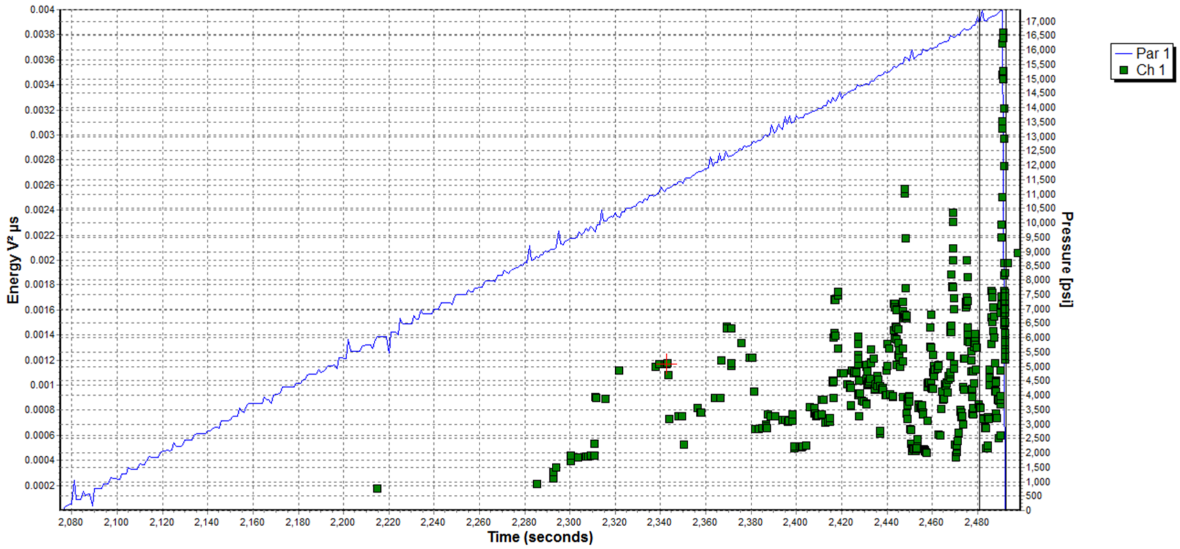

Figure B. 57 - Background Energy Oscillation for IH2533.

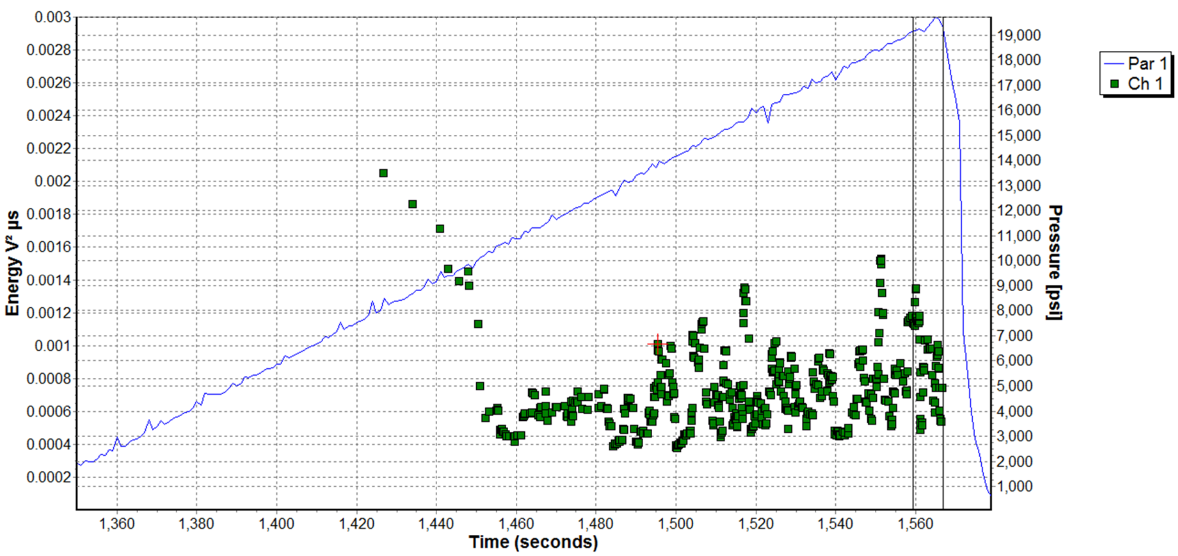

Figure B. 58 - Background Energy Oscillation for ALT639 - 18699.

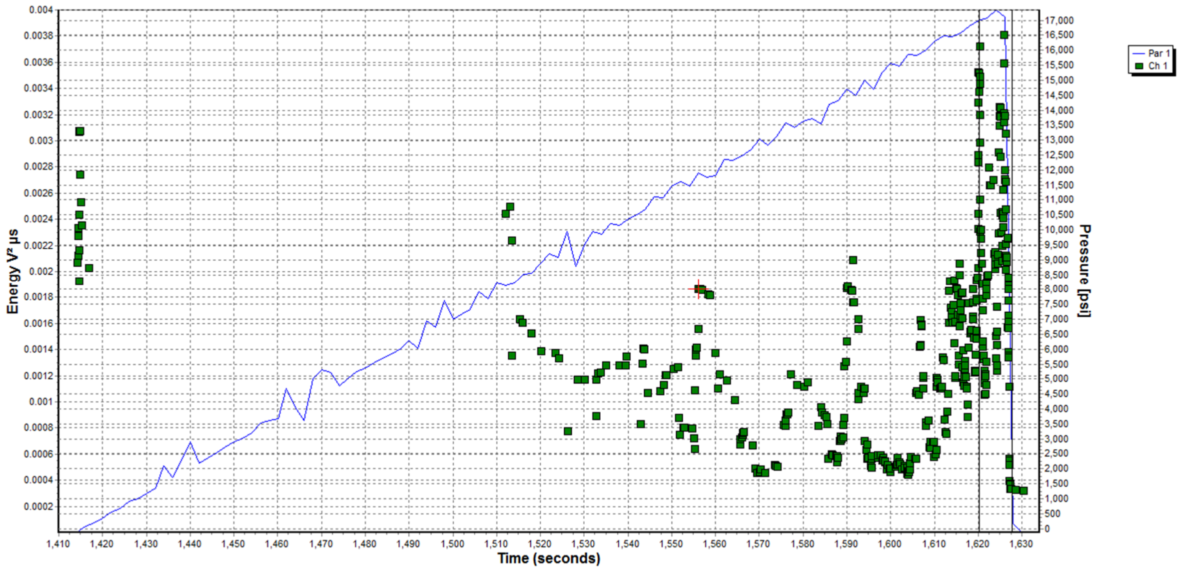

Figure B.59 – Background Energy Oscillation for ALT695 - 3929.

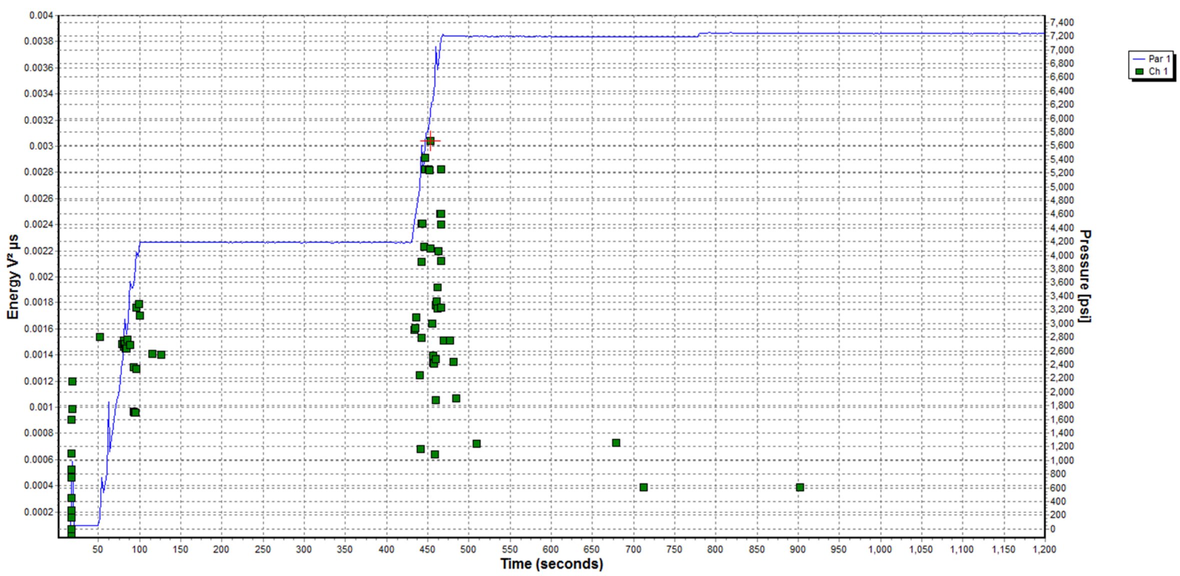

Figure B.60 - Background Energy Oscillation for OM3984.

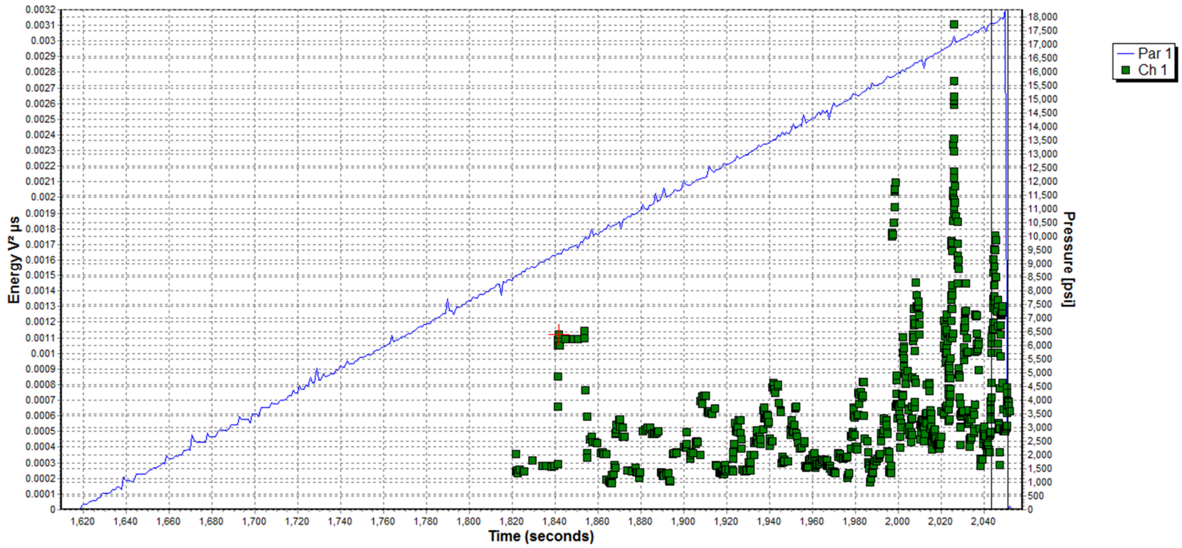

Figure B.61 - Background Energy Oscillation for ALT639 - 17732.

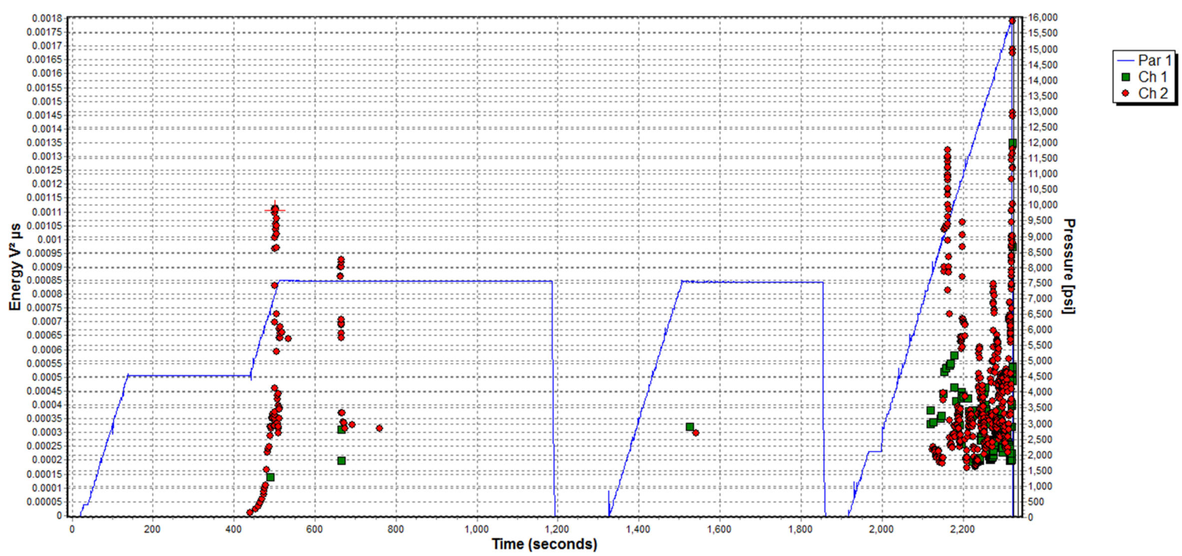

Figure B.62 - Background Energy Oscillation for IH2554.

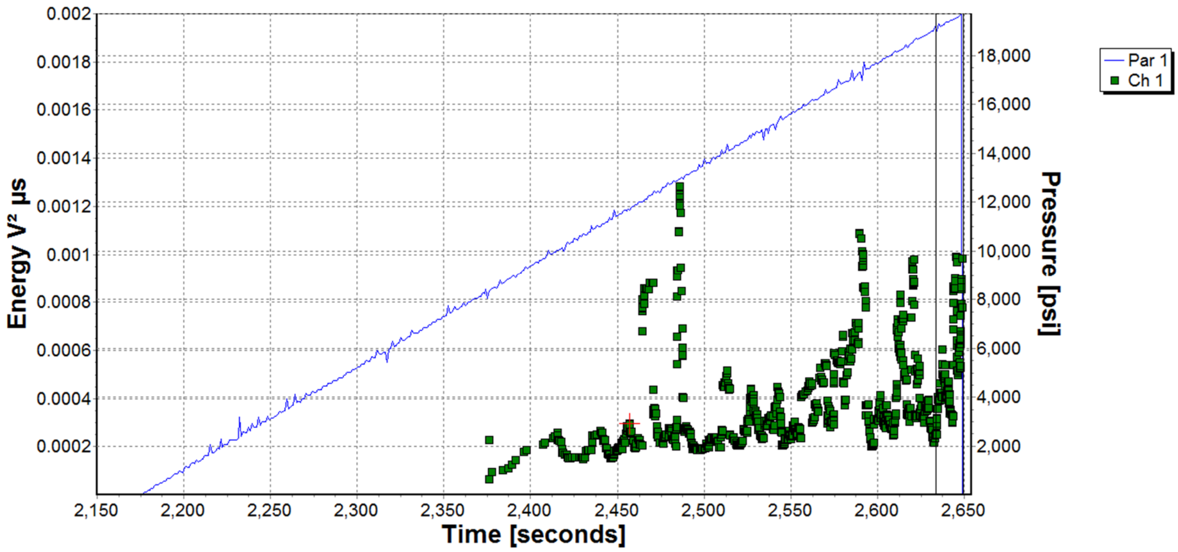

Figure B.63 - Background Energy Oscillation for ALT639 - 69925.

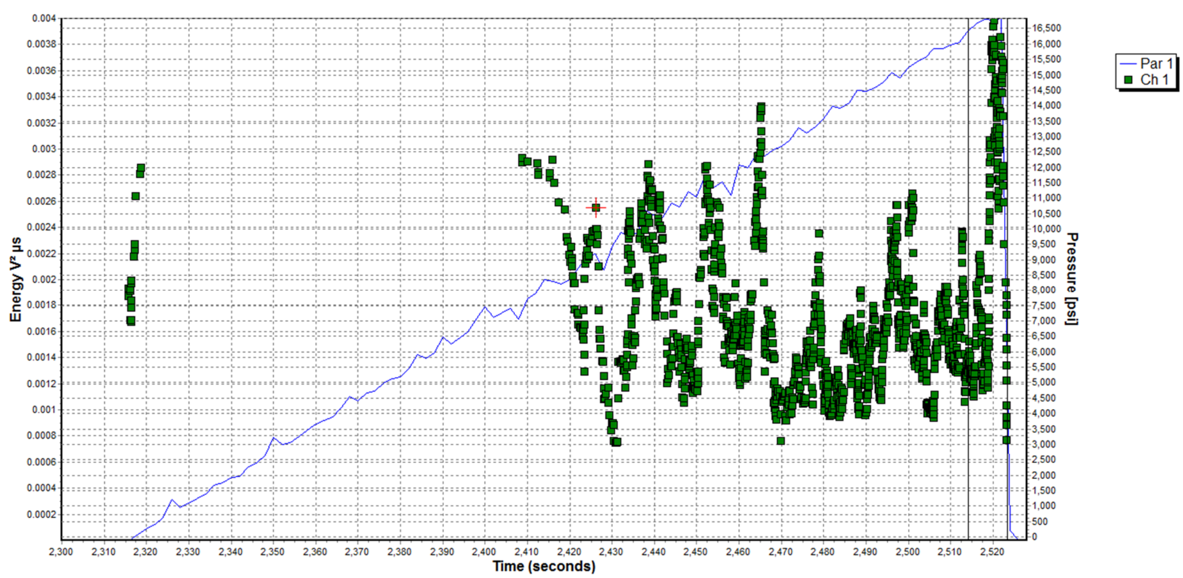

Figure B.64 - Background Energy Oscillation for ALT695 - 4304.

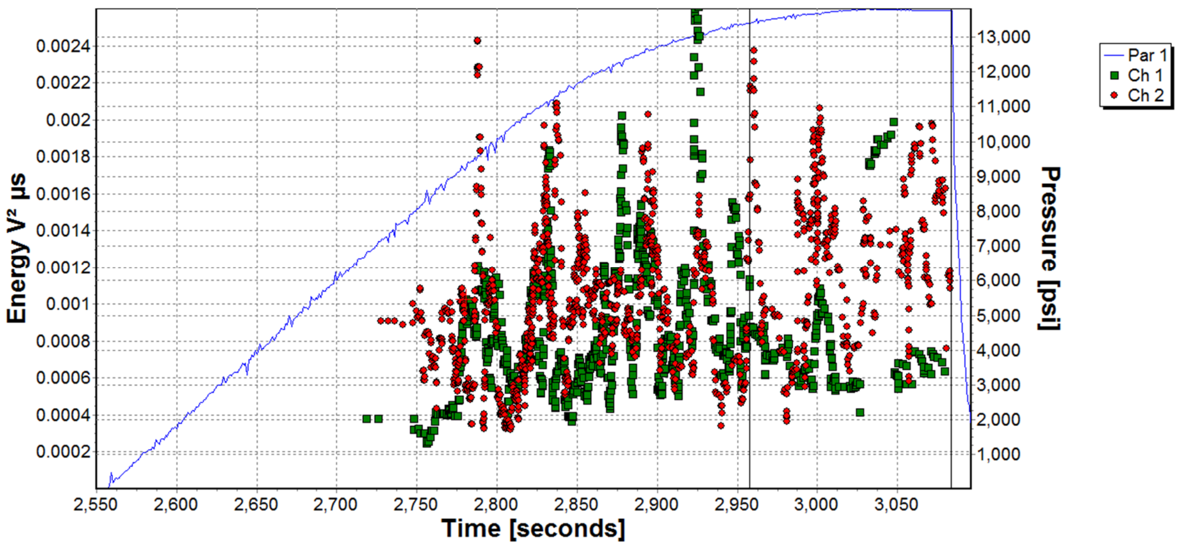

Figure B.65 - Background Energy Oscillation for OP11129.

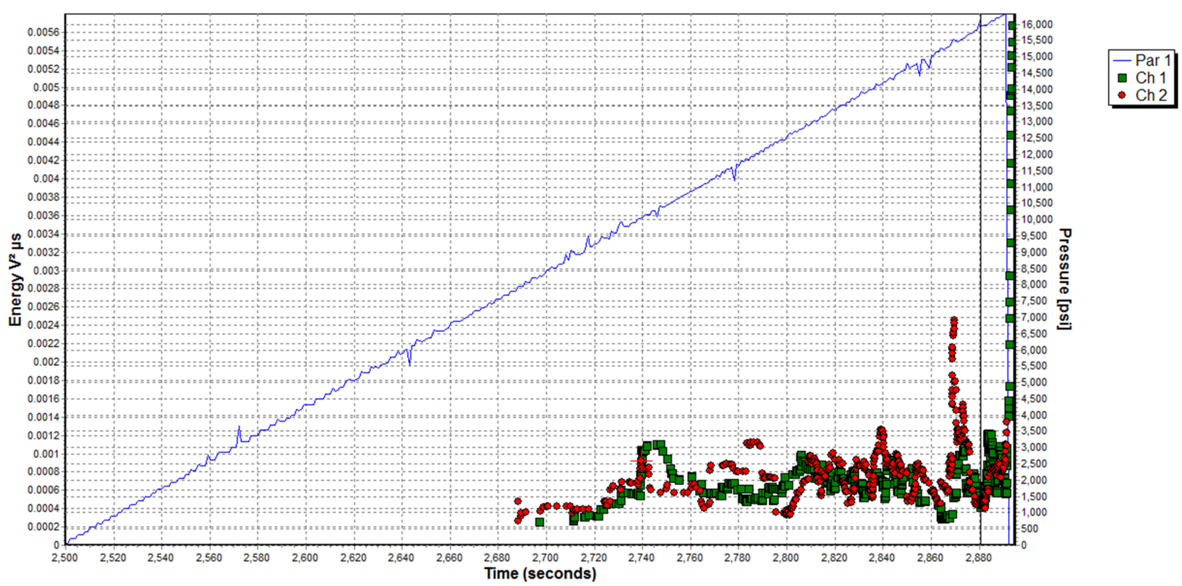

Figure B.66 - Background Energy Oscillation for IH1251.

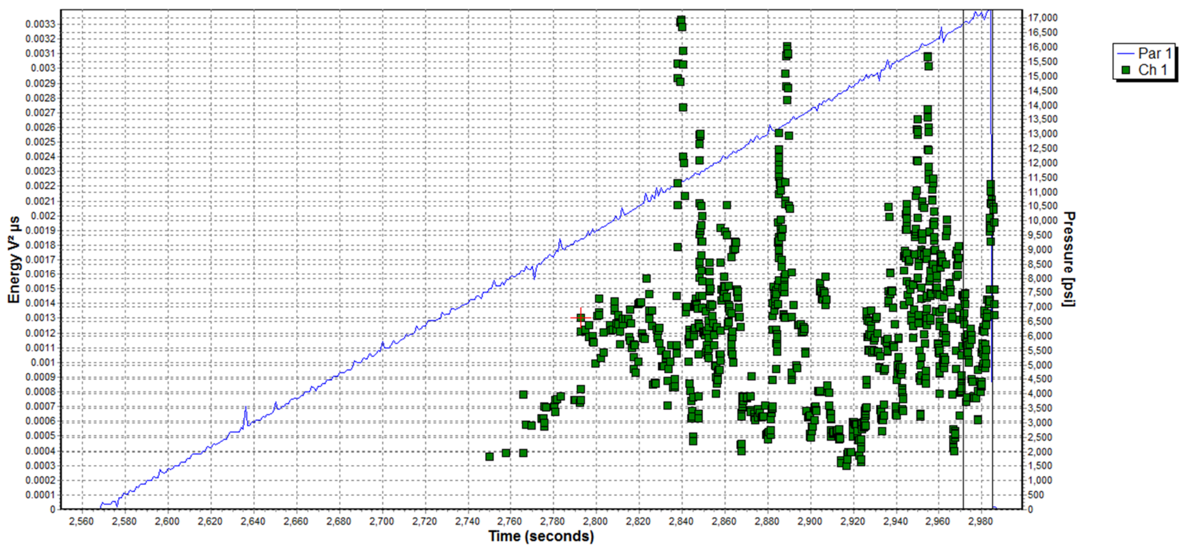

Figure B.67 - Background Energy Oscillation for ALT639 - 17827.

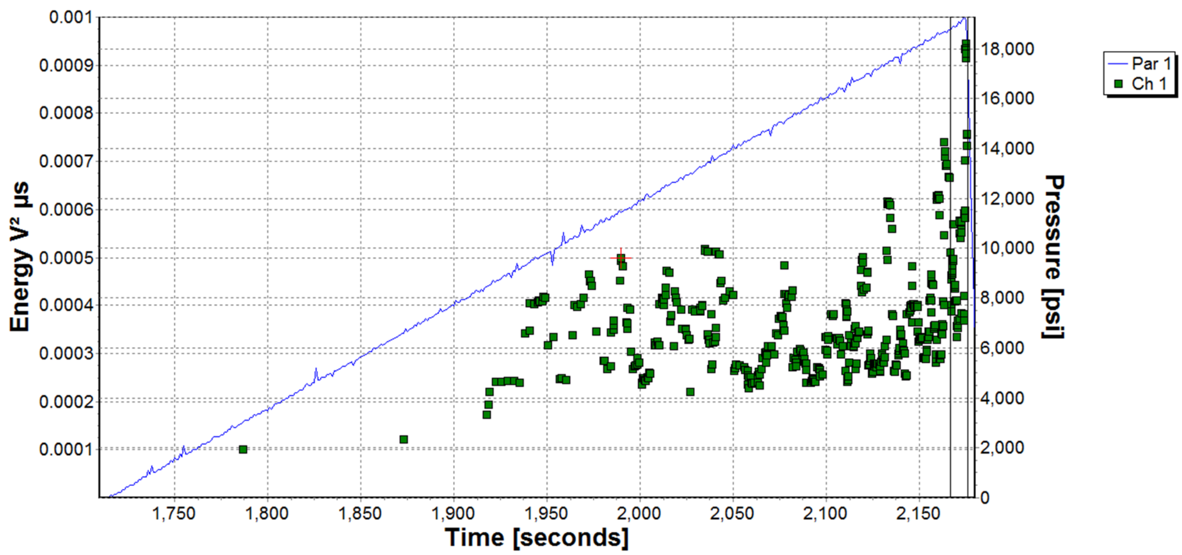

Figure B. 68 - Background Energy Oscillation for ALT695-4333.

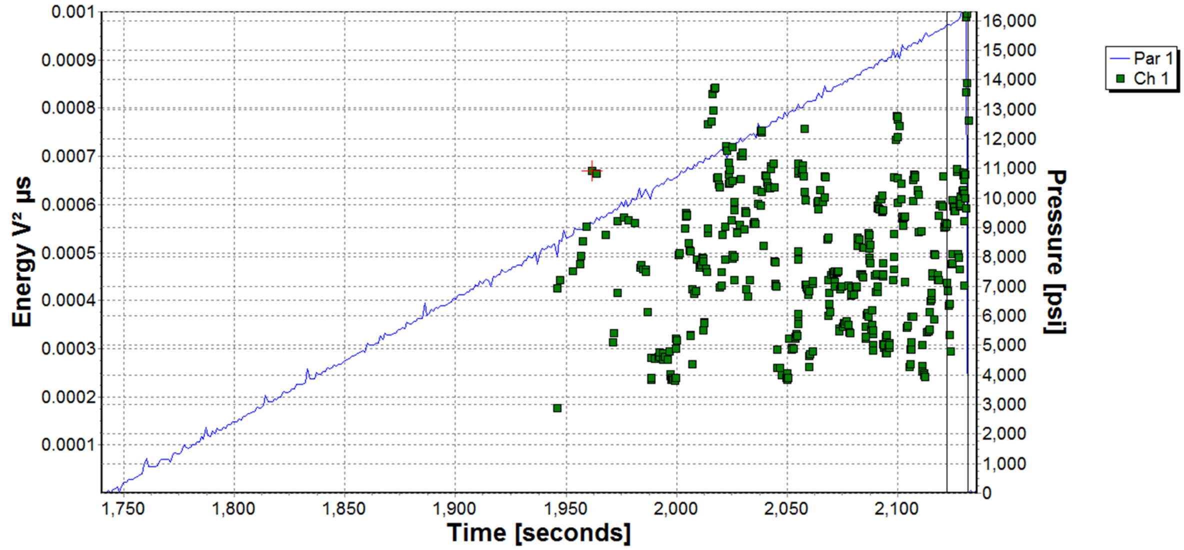

Figure B. 69 - Background Energy Oscillation for OM3918.

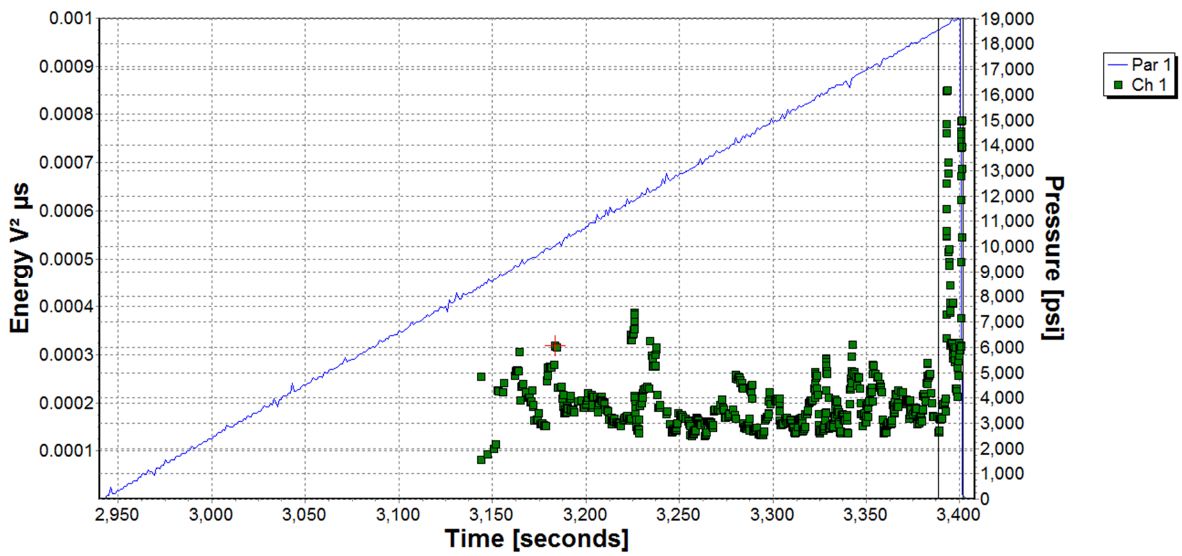

Figure B. 70 - Background Energy Oscillation for ALT639 - 18800.

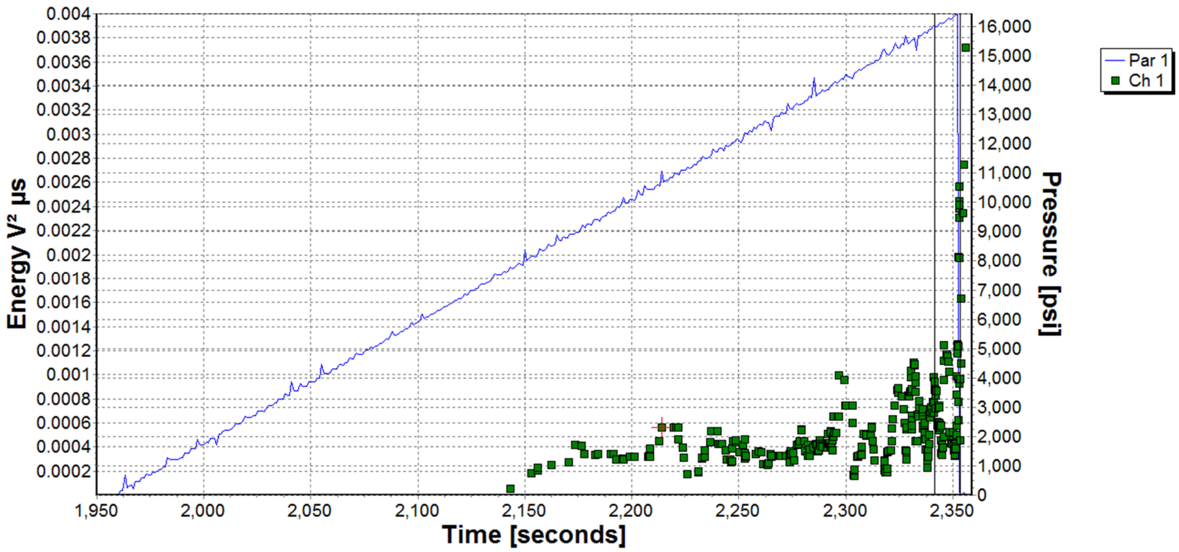

Figure B. 71 - Background Energy Oscillation for IH1750.

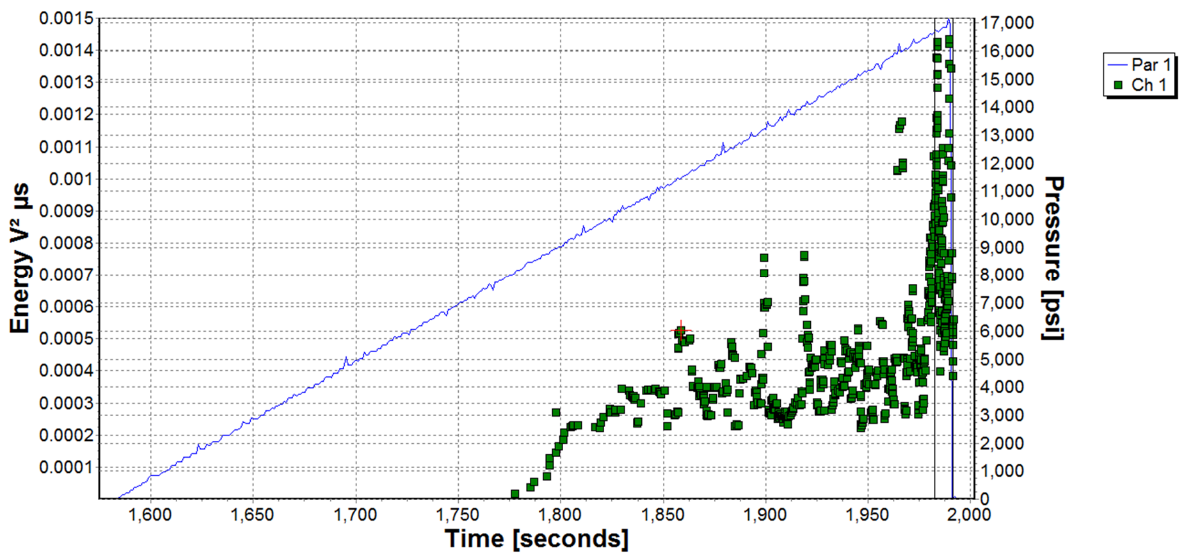

Figure B. 72 - Background Energy Oscillation for ALT639 - 18713.

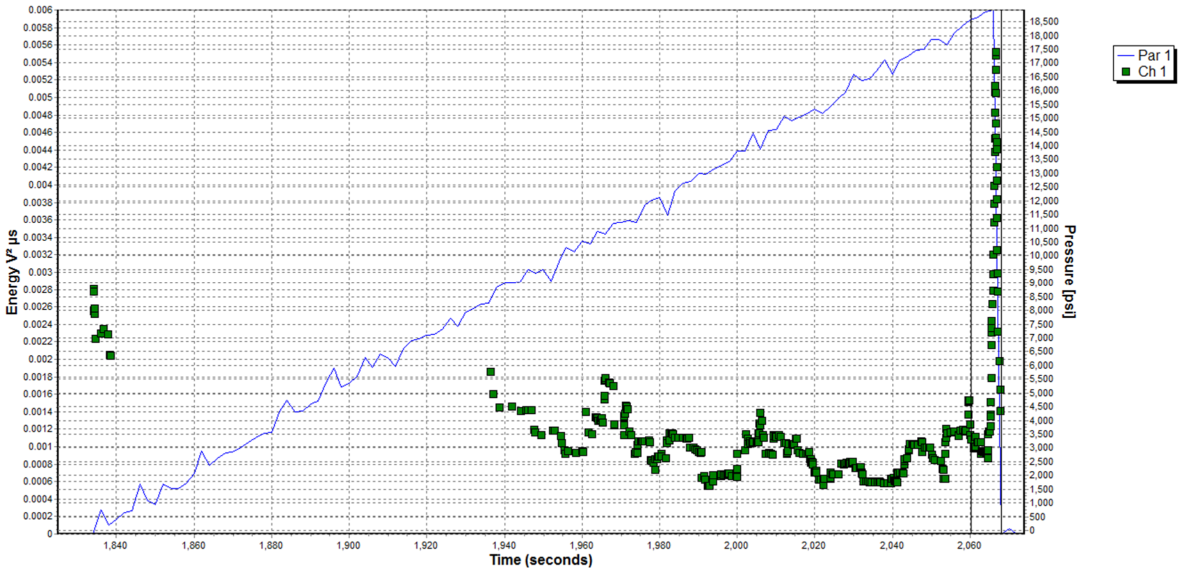

Figure B. 73 - Background Energy Oscillation for OM4045.

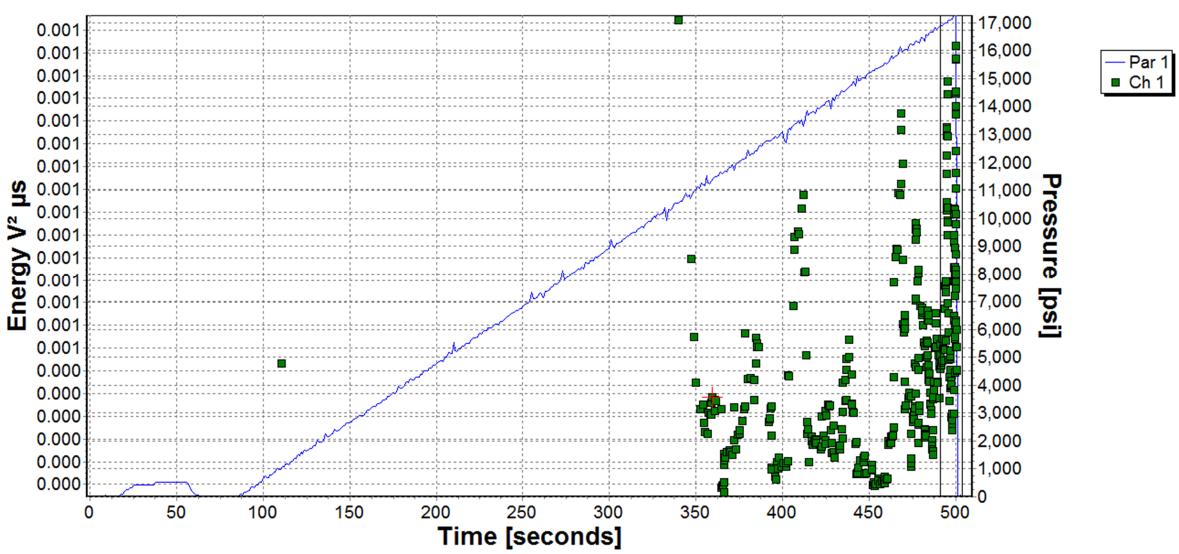

Figure B. 74 - Background Energy Oscillation for OM3957.

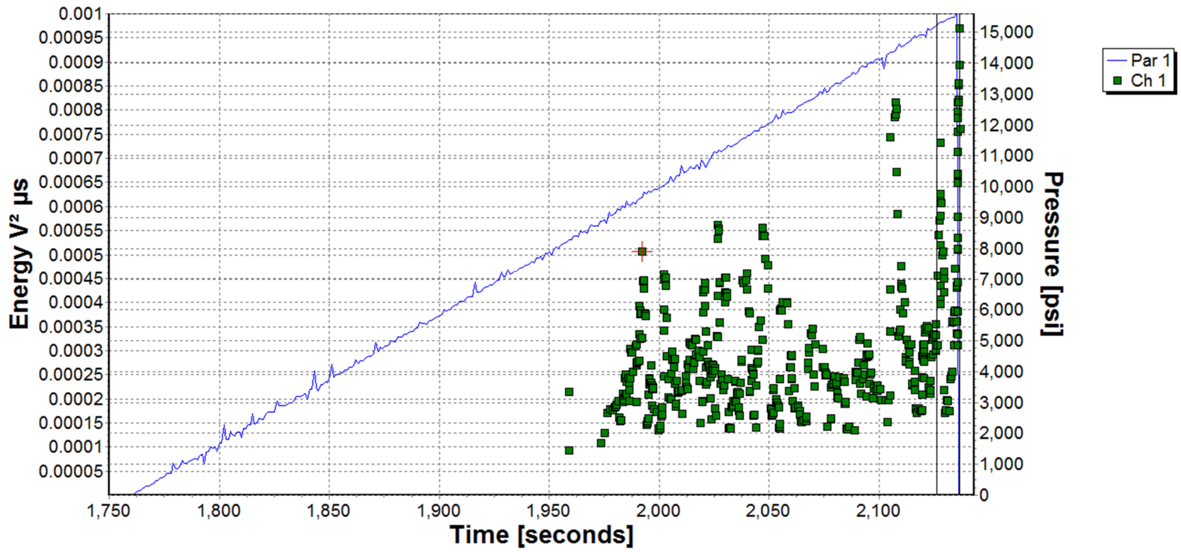

Figure B. 75 - Background Energy Oscillation for OM3914.

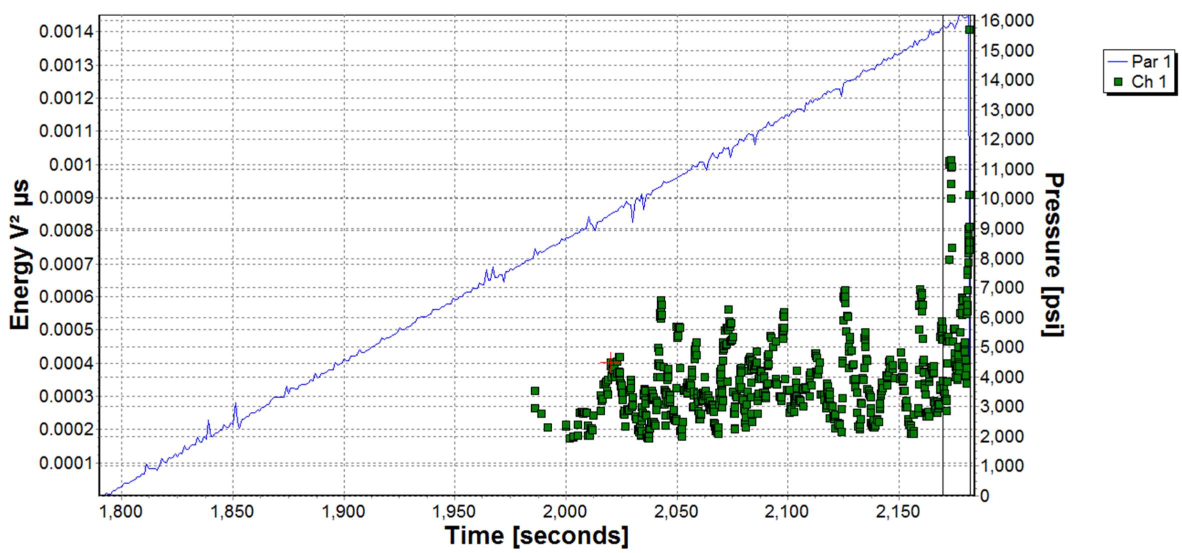

Figure B. 76 - Background Energy Oscillation for OM3912.

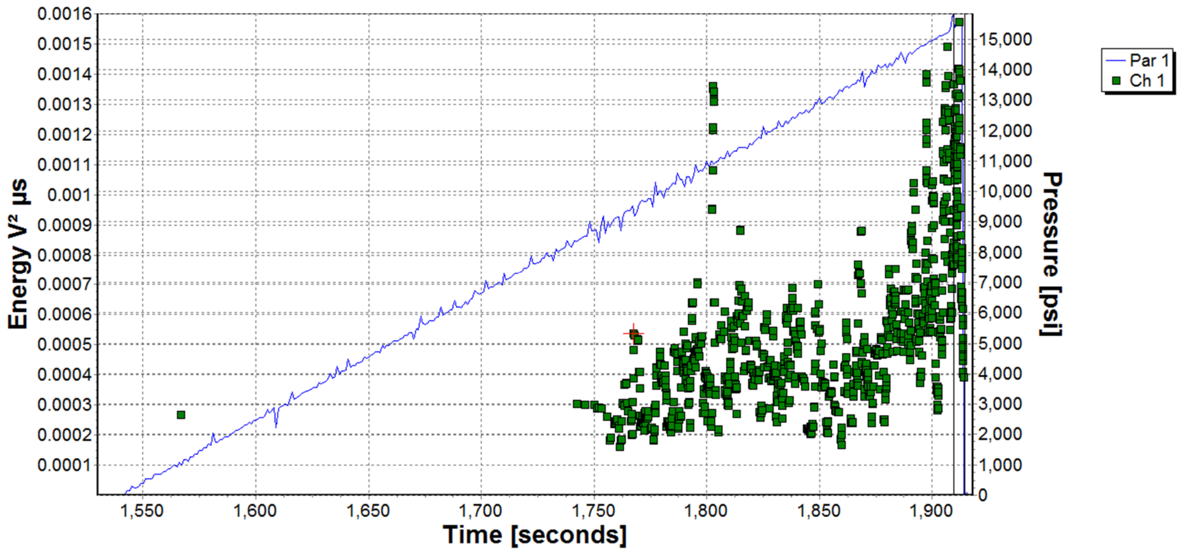

Figure B. 77 - Background Energy Oscillation for OM3954.

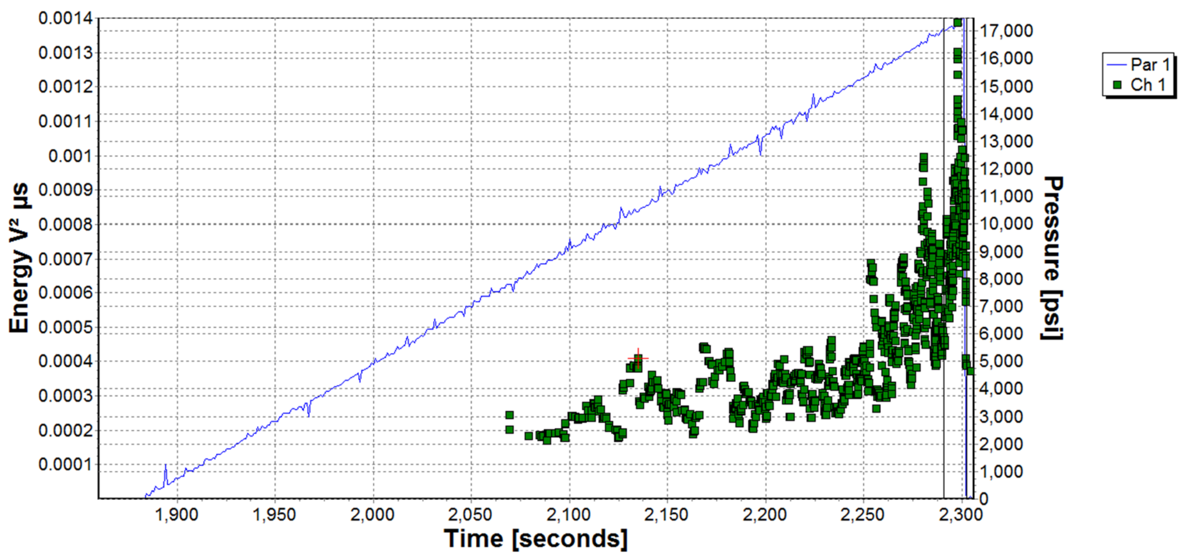

Figure B. 78 - Background Energy Oscillation for OM3925.

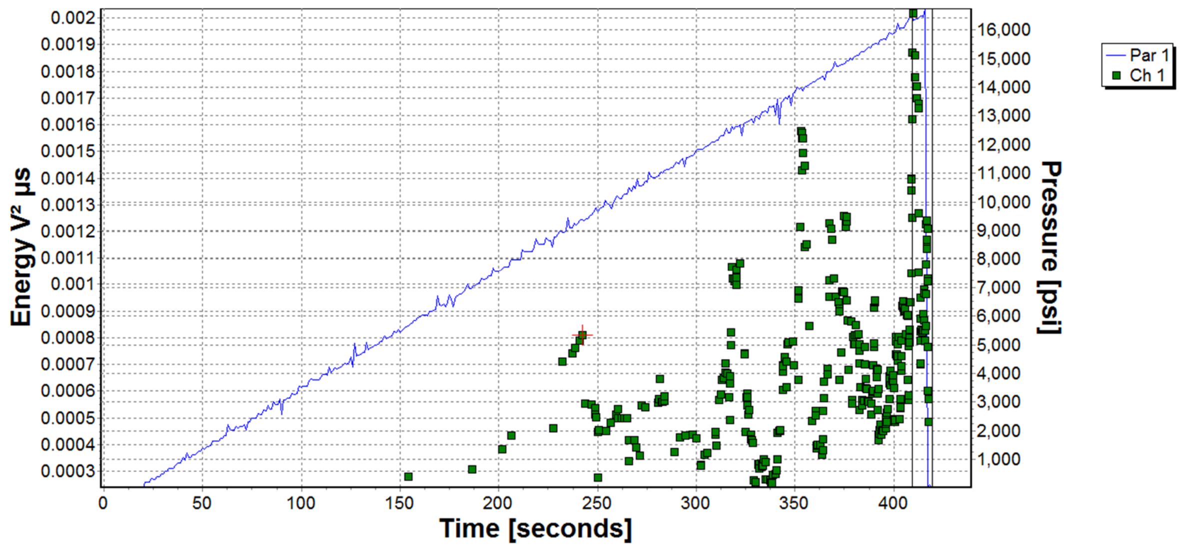

Figure B. 79 - Background Energy Oscillation for OM3982.

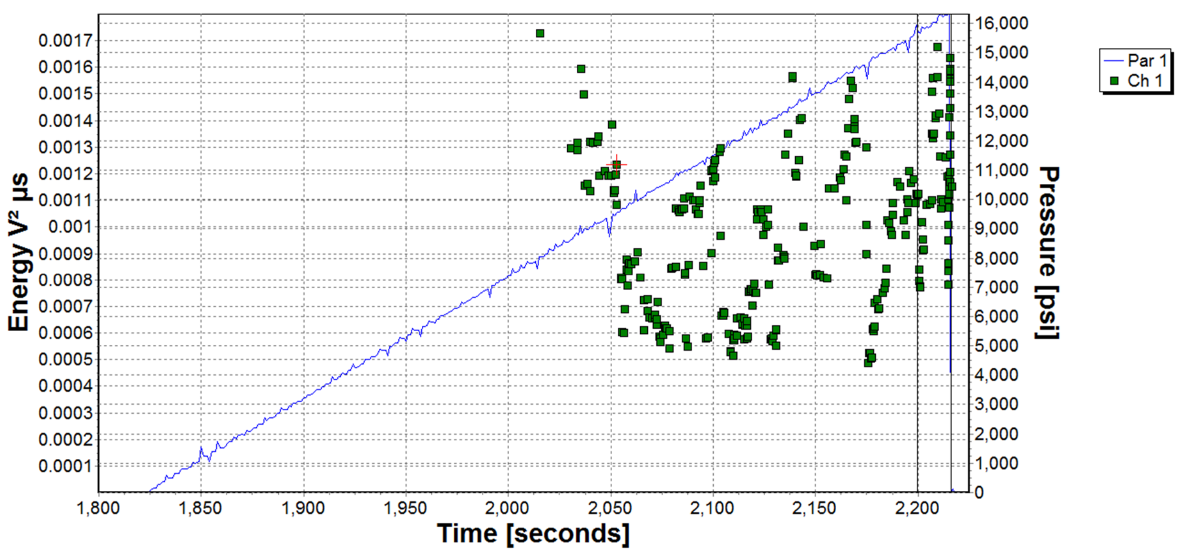

Figure B.80 - Background Energy Oscillation for OM3917.